Report DISS_23 (www.diss-co.it)

SHM METHODOLOGY, BY SOIL-COLOSSEUM INTERACTION

Rearrangement of memories already processed in no. 6 international Workshops DISS

Gianfranco Valente

EDITORS
Pierluigi De Berardinis, Francesco D'Annibale, Donatella Dominici, Angelo Luongo, Yutaka Nakamura

Report DISS_23 (www.diss-co.it)

SHM METHODOLOGY, BY SOIL-COLOSSEUM INTERACTION

Rearrangement of memories already processed in no. 6 international Workshops DISS

Gianfranco Valente

EDITORS
Pierluigi De Berardinis, Francesco D'Annibale, Donatella Dominici, Angelo Luongo, Yutaka Nakamura

DISS_*Edition* - via Alceste Trionfi, 25
00172 Roma - +39.6.2414640
www.diss-co.it – info@diss-co.it

1st edition: Rome, July 4th, 2023
Revised: November 20th, 2023

Secretary support: Massimo Valente Edos.

ISBN 978-88-940114-5-6

In the front covering, a free assembling appears of the original drawing by Prof. Arch. Mario Docci, in the volume published in 2016 by the Order of Architects: 50 Years of the Profession, VI, 1961-1965, Figure 9 on p. 132.

In the same collection
Proceedings of the International Workshops
"*Dynamic Interaction of Soil and Structure*":

1st DISS_**10**, L'Aquila 19 March 2010, D'Ovidio G., Nakamura Y., Rovelli A., Valente G., Aracne, ISBN 978-88-548-3693-8.

2nd DISS_**12**, L'Aquila 29-30 March 2012, Clemente P., D'Ovidio G., Nakamura Y., Rovelli A., Tallini M., Totani G., Valente G., DISS_*Edition*, ISBN 978-88-94011-0-1.

3rd DISS_**13**, Rome 12-13 December 2013, Carlo Baggio, Paolo Clemente, Yutaka Nakamura, Luciana Orlando, Antonio Rovelli, Gianfranco Valente, DISS_*Edition*, ISBN 978-88-94011418.

4th DISS_**15**, Rome 12-13 November 2015, Giorgio Monti, Gianfranco Valente, DISS_*Edition*, ISBN 978-88-94011425.

5th DISS_17, Rome 19-20 October 2017, Carlo Baggio, Giorgio Monti, Camillo Nuti, Silvia Santini, Gianfranco Valente, DISS_*Edition*, ISBN 978-88-94011432.

6th DISS_19, L'Aquila 28 november 2019, Angelo Luongo, Dante Galeota, Maria Alicandro, Donatella Dominici, Gino D'Ovidio, Marco Tallini, Gianfranco Totani, Gianfranco Valente, Carlo Baggio, Giorgio Monti, Yutaka Nakamura, Camillo Nuti, Silvia Santini, DISS_Edition, *ISBN 978-88-94011449.*

INTRODUCTION

A full 3D DISS FE model was developed for the Colosseum area, with a 600x600x80 m sod of soil having the anthropogenic, Holocene, Pleistocene, Gravel and Pliocene stratigraphies, with station, Metro B and C tunnels, Arch of Constantine.

The sure notices about monument damages by earthquakes are on the years 422, 443, 508, 801, 1349, 1703 and 1812, and the past maximum intensity happened in 1349, with a very long probabilistic return period.

Researchers show interest in recordings of monument vibrations because they consider them indispensable for SHM control.

Just as a musical instrument emits a series of sound frequencies that change if its structure is deformed, so from the random vibrations of the monument subjected to environmental actions, a series of dynamic frequencies can be extracted, which are independent of actions and change only if the masonry undergoes damage or structural modification; they are always frequencies, sound or dynamic.

Well, wanting to check the production of any masonry damage, from the comparison of recordings before and after a certain action, the unique reliable tool is the "SHM Monitoring" which can locate the non-visible damage, is highly advocated but non-trivial because very precise experimental and numerical modal analysis must be performed.

To achieve SHM, great care must be taken: the processing of frequency domain recordings to ascertain the damage, the numerical model to locate the damage.

The SHM methodology can control every structural problem, even like the past: c) Stern, Valadier and Canina reinforcements, d) differential foundation failures, e) vibration amplification in the south above the Holocene, f) near excavations, g) reinforcement with epoxy resins in the south-east pillars, h) environmental vibrations, i) seismic prevention and protection, l) conservation and restoration.

The natural evolution to today's artificial intelligence makes it likely that this SHM methodology is fully feasible, reliable, and even automatable.

The state of the art relative to the object shows a certain dispersion for: the positioning of the instruments, the types of instruments, the processing methods in the frequency domain, the conclusive results of the relative analyses.

For the indispensable comparison of the modal analyses before and after the event, we would need:

1) a permanent measuring station with measuring points in optimal geometric positions, and spread over the entire monument, to control every part of it,

2) fixed instruments with constant characteristics, also for thermal and rainfall control to purify the effects on the experimental data.

3) a numerical model and numerical and experimental modal analyses all with minimum deviations not exceeding 5%, to handle even small modal variations, to control the effects of both environmental vibrations over time and non-intense seismic events,

4) start with an experimental investigation like carried out by Nakamura between 1998 and 2013, which would seem to me to be the only example that meets all the previous requirements.

I declare that I am interested in the realization of such a measuring station, for the sole purpose of research and without financial interests.

The present document is a simple rearrangement of the material already published and shown in www.diss-co.it.

The DICEAA Department is thanked for organizing No. 6 DISS Workshops, and for all the opportunities it has given, as documented in www.diss-co.it.

Thanks to Prof. Nakamura which attended all the Workshops.

For their kind supports, many thanks are expressed to the Society Roma Metropolitane, the Society Metro C, the Institute CREA (Research Centre for Food and Nutrition), the Society ATAC.

Gianfranco Valente
Rome, November 20th, 2023

INDEX

History of damages and restorations for Colosseum structure

Abstract

Over two millennia, structural damages have been caused to the Colosseum by burnings, earthquakes, robberies, collapses, weathering, restorations, excavations for the metro, differential viscous subsidence, and environmental vibrations, resulting in a severe shrinkage of the monument.

But in the present age of smartphones, this damage could be controlled and even avoided with an analytical model of soil-monument interaction, based on tests, with engineering accuracy.

1. Introduction

The principal damagings in the past are summarized in Table 1.

***Table 1**. The principal historical happenings in Colosseum. [25]*

Year A.C.	Happenings	Notices
71-72	Works start	By Vespasiano
80	Inauguration	
217	Burning	23 August. Due to a thunderbolt
217-223	Restoration	Upper side in stones
250 and 320	Burning	Few damages
422	Earthquake	Collapse of senators floor
429	Earthquake	24 August
439	Earthquake	No exact notices of damages
443	Earthquake	New collapse as on 422
508	Earthquake	Decio Mario Venanzio Basilio *"abominandi terrae motus"*
610	Alarico invasion	Stones' metallic connections for weapons
614-617	Earthquake	No exact notices of damages
VIII century		By Beda: integer monument
801	Earthquake	Collapse of two arches orders in the upper porticos
847-855	Earthquake	No exact notices of damages
1044-1073	Earthquake	No exact notices of damages
1231	Earthquake	1st June
1349	Earthquake	Petrarca "*cecidit aedificarum veterum neglecta civibus, stupenda peregrinis moles",* 7-10 September, VIII MM.
1700	Repair Clemente XI	Stop salnitrum production for explosives.
1703	Earthquake	Arches fall, used for Ripetta harbour later
1714	Restoration	
1803	Escavations	Pio VII
1812	Earthquake	Fall of three arches orders
1805-1807	West buttress	Stern, Pio VII
1824	East buttress	Valadier, Leone XII
1844-1846	Restoration	Gregorio XVI
1846	Restoration	Pio IX
1912		n. 33 arches rest in the external ring
1915	Earthquake	Fucino epicentre. No damages
1946-1950	Restoration	With injections

The sure notices about monument damages by earthquakes are on the years 422, 443, 508, 801, 1349, 1703 and 1812, as in Table 1. Subsequent robberies happened, and other damages are connected to burnings.

2. Principal restoring works

The actual Colosseum is the result of damages from natural events in the past (earthquakes, burnings, vegetation, abandon, etc.) robberies by men, consolidations to save the monument against imminent risks. The greatest damages are concentrated in the period between IX and XV centuries, by the following witnesses:

1) Beda (*"collettanee",* 745):

2) Petrarca (epistola II del libro X, 7-10 September 1349, VIII M.M.) *"cecidit aedificarum veterum neglecta civibus, stupenda peregrinis moles"*,

3) Luigi Canina (Sul ristabilimento e riparazione della parte media verso l'Esquilino dell'Anfiteatro Flavio", letta nell'adunanza dell'accademia di archeologia in Roma il 7 aprile 1857), "….*io ora non voglio stare a ricercare quando e come siano accadute le rovine principali del monumento medesimo, per esserne occupati dotti scrittori e principalmente il Marangoni nelle sue Memorie sacre e profane dell'Anfiteatro Flavio, ed il Fea nella sua dissertazione sulle rovine di Roma: ma mi limiterò ad osservare che sino dal principio del secolo decimo sesto l'edificio si trovava in circa nel medesimo stato di rovina, cui ora vedesi ridotto, come ne servono di autorevole documento le vedute prospettiche, che ci furono conservate per cura del Marliano, del Kock e del Du Perac; e perciò la rovina maggiore deve essere accaduta tra il nono ed il decimo quinto secolo,…."*

4) Rodolfo Lanciani (" Segni di terremoti negli edifici di Roma antica " – Tipografia della R. accademia dei Lincei, 1895) "*Non è possibile ammettere una disintegrazione spontanea per vecchiezza, perché, se volgiamo lo sguardo alla metà dell' Anfiteatro superstite, dalla parte dell' Oppio, e ne consideriamo la prodigiosa solidità dobbiamo respingere qualunque congettura di disfacimento su larga scala, prodotto da agenti atmosferici o tellurici: ma al tempo stesso può darsi che*

il terremoto del 508, o qualcun altro del quale non rimane notizia, abbiano prodotta una fenditura, simile a quella che spacca il cilindro del Pantheon dalla parte di via della Palombella, e che in questa fenditura abbiano messo radici piante arborescenti. Una volta rotto l'equilibrio nessuna forza umana avrebbe potuto arrestare la rovina dell'Anfiteatro…, in questa maniera avrà avuto principio la caduta dei blocchi dell'orlo superiore dell'anfiteatro. Ma, al tempo stesso, non si può negare che, a un dato momento, in un'epoca che non è stata ancora determinata, tutta la parte dell'ellisse dalla parte del Celio cadde a terra, sulla profondità di due ambulacri, creando una montagna di blocchi, che ha servito da cava di materiale per circa sei secoli. La catastrofe è posteriore al secolo VIII, quando il ven. Beda scrisse il famoso proverbio. Forse avvenne nel terremoto del 1° giugno 1231, forse nel terremoto del Petrarca".

3. The construction place

The Colosseum is a huge amphitheatre which Roman Emperor Vespasian built to amuse common people on a reclaimed artificial lake at the garden of Nero's Domus Aurea as if to wipe away the memory of nightmare caused by Nero a tyrant from common people [22], [23], [24].

Figure 1 shows a geologic map around Colosseum [10]. According to this figure, the ground supporting Colosseum is rather stiff in the northern half. On the other hand, that of the southern half is on the comparatively soft soil deposit [9].

Figure 1 is a map to show the physical location of Domus Aurea, Golden House of Nero, three hills and the artificial lake on the present satellite image to indicate the relationship between the past artificial lake and current Colosseum.

It can be seen that Colosseum is enclosed in the artificial lake [5]
The foundation was constructed strong enough to support huge Colosseum on the disposal weak site of the artificial lake.
Colosseum is thought standing on the filled artificial lake of Domus Aurea and the knowledge of the ground under the foundation has changed

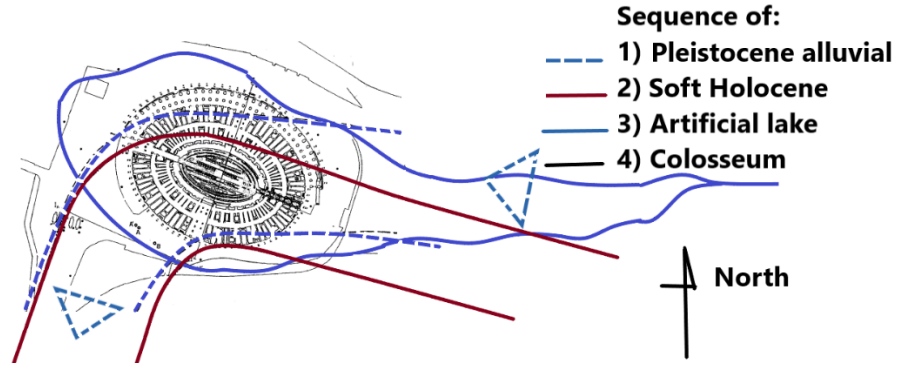

Figure 1. From Bozzano [8], Benevolo [5]

4. Earthquake on 1349

The national seismic catalogues report the most disastrous event in Rome on September 9th, 1349, with 7.5÷8 MCS (Figure 2 from [21], [19]); from which in the outer southern ring derived:

1) a first breach contained in the South, already documented in the fifteenth century, referred to in Figures 3 and 4 in the documents [19], [21].

2) subsequent damage up to the reduction to half circumference.

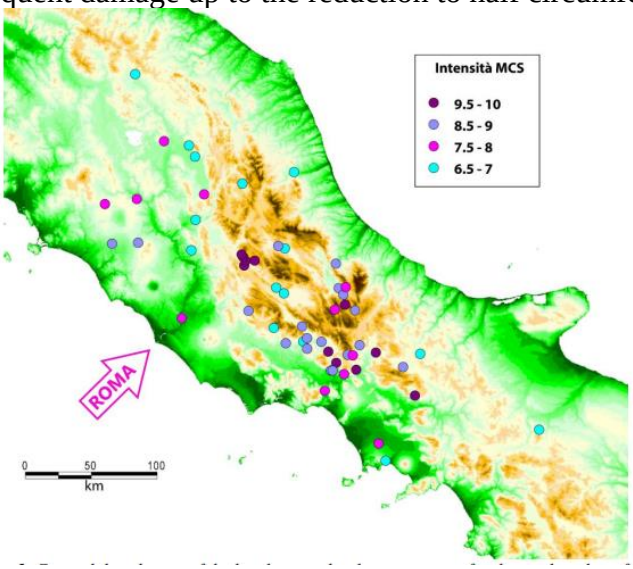

***Figure 2**. General distribution of the localities with relative intensity for the earthquakes of 1349. Data reported by DBMI04 [1], [8] for the INGV Catalogue.*

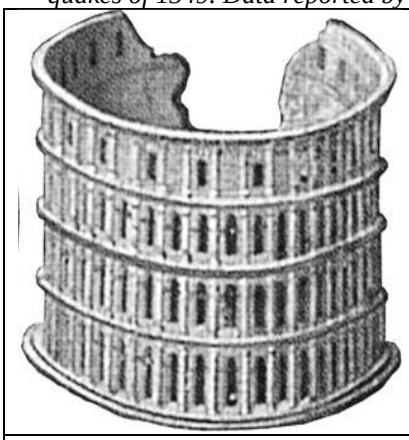

***Figure 3a.** Detail of Colosseum from a copy of a lost view attributed to Francesco Roselli (second half of fifteenth century) in the Mantua Ducal Palace [1].*

***Figure 3b.** The Colosseum crack due to earthquakes, 1600, Matheo Florimj formis [2].*

5. Restorings on outer northern wall

5.1 Buttresses

Buttresses Stern (1806) and Valadier (1823). Cracks over arcades XXVIII e XLVII, almost symmetric; stresses concentration due to sudden curvature change from a policentric plan.

The actual monument is more vulnerable with respect to the initial integer one, and that the buttresses are the weakest parts, as by following Authors:

A) Nakamura [14]: *"For 1349 earthquake the reported modified Mercalli intensity is VIII which correspond to an acceleration of 175 Gal. These values show that, MM VI-VII earthquake which correspond to acceleration about 67 Gal will be enough to cause more damage in vulnerable points of Colosseum".*

B) Pau, Vestroni [33] "*The most vulnerable areas of the monument, are the vaults of the second order near Stern's buttress, and the pillars of the third order near Valadier's buttress. At these points, the Fourier*

transforms of the maximum principal stress, exhibit the same pattern and confirm that the first and second modes are mainly responsible for the maximum stress".

a) *Stern*

b) *Valadier*

Figure 4. *Buttresses **r**estorations.*

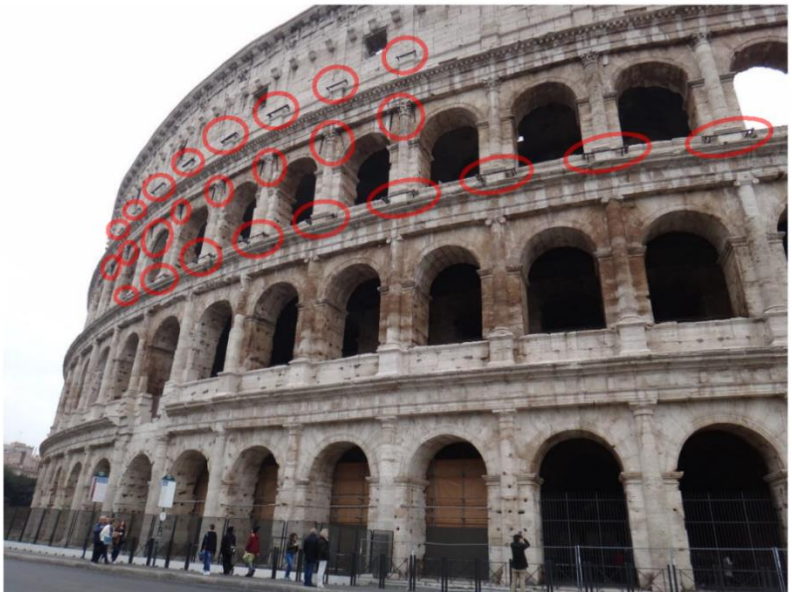

Figure 5. *Fasteners by Canina.*

5.2 Salvi and Canina intervention for 60 CM out plumb on inner side (1830-1850)

5.3 Escavation of Metro B (1939).

It happened close to Colosseum foundations, the ground, Constantine arch.

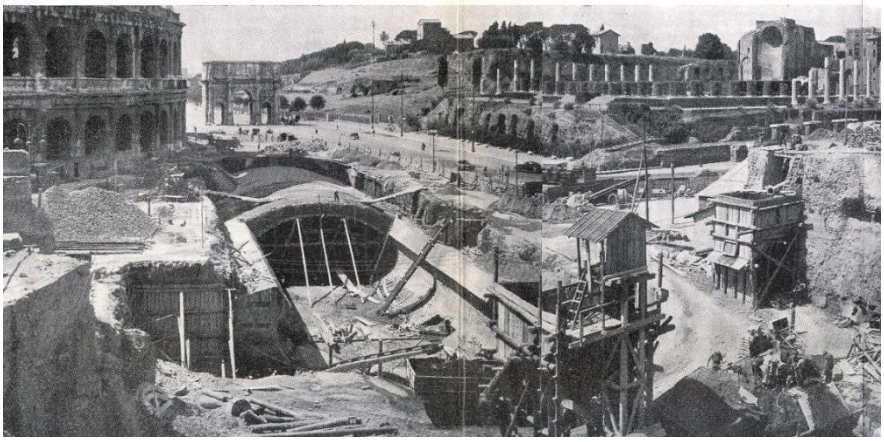

Figure 6. *Metro B excavation **b**y Perrone [3].*

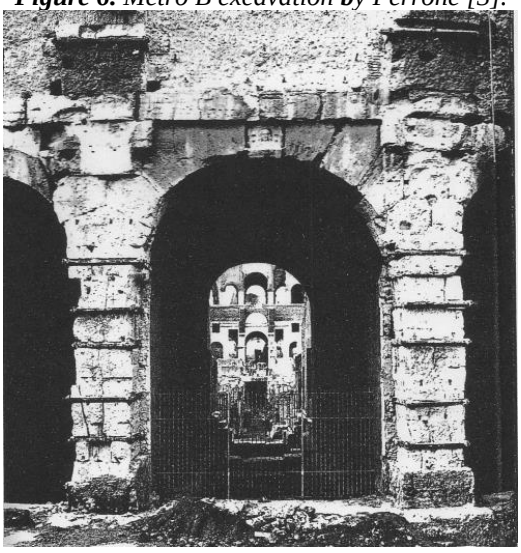

Figure 7a. The pillars #18 and #19 before restoration and after the travertine cladding has been taken away.

5.4 Six pillars strengthened with steel bars and epoxy resins injections (1979) [4]

The reinforcement of six pillars on the south sector of the Flavian Amphitheatre begun in 1978 and completed in 1979. Before the work was carried out, the travertine facing was stripped and the pillars shored. The decision of reinforcing the pillars was taken both investigations on the fall of the pilaster strips capital oi the nineteenth century travertine facing of pillar #18, which took place when the iron c1amps became completely rusted and snapped. Then the whole lacing was stripped, and the pillar was seen to be seriously damaged: large widespread cracks could be seen, due to crushing, and the section was considerably smaller than the original one. The same situation applied to the five adjacent pillars from #16 to #21.

Figure 7b. *Support of the arcades: the seven masonry pillars [4]. Reinforcement of pillars with steel and Epoxy resin injections through holes*

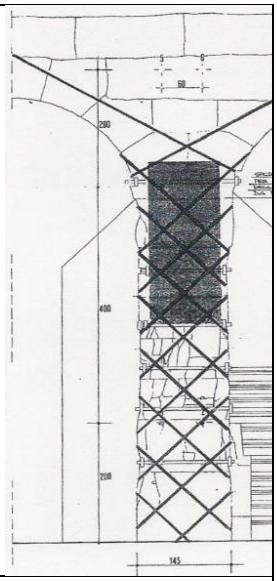

Figure 7c. *Single pillar.*

6. Influence of walls' disconnections

***Table 2**. Principal observed disconnections; Left/Right from outside; 1° and 2° levels*

#	Cylindrical vertical surface						#	Cylindrical vertical surface					
	11	10	9	8	7	6		11	10	9	8	7	6
2	2		2				41	2					
3	1L/2						42	2					
4	½	1	1	1			43	2					
5	1/L				1R		44			2			
6					1L		45		2	½			
7	2						46		½	1L/2R			
8	½						47	½	1/2L				
9	½						48	1L	1L/2R				1
10	½						49	2D					1
11	1/2			1L			50	1/2L					
12	½	1					51	½	1L	1L	1		
13	2						52	½					
14	½						53	1					
15	½			1			54	1L/2L					
17	2						57	1	1R/2L	1R/2L			
18	1						58	1/2R					
19	1						59	½					
21	1						61	2					
26	2						63	1					
27	½						64	2					
28	½						65	1					
29	1/2						67	1					
30							68	1					
31	½					1	69	1					
32	½						70	1					
35	1L				1		72	2				1	1
36	2				1		73	1	1	1	1		
38	2	2					77	2					

For the sake of simplicity, the roman numbering of Figure 8 was translated in the Arabian numbering of Table 2.

In the Table 2; the evident principal cracks between radial walls and annular walls are obtained by [12] and are defined by the level, by the cylindrical vertical surface and the possible left or right disconnection looking from outside, or full disconnection.

The Figure 9 shows the pillar #51, looking from left side, there two disconnections exist:

a) regular on vertical cylinder n.11 for human interview,

b) irregular for natural assessment on vertical cylinder n.10 for different behaviour of different materials, for the passage from travertine to tuff walls.

The two FE models of "soil-structure interaction" with Colosseo having continue and disconnected structures are prepared, the latter is obtained by introducing new nodes coincident with those existing, in order to obtain the real disconnections of Table 2; the train actions are applied to the two aforementioned models.

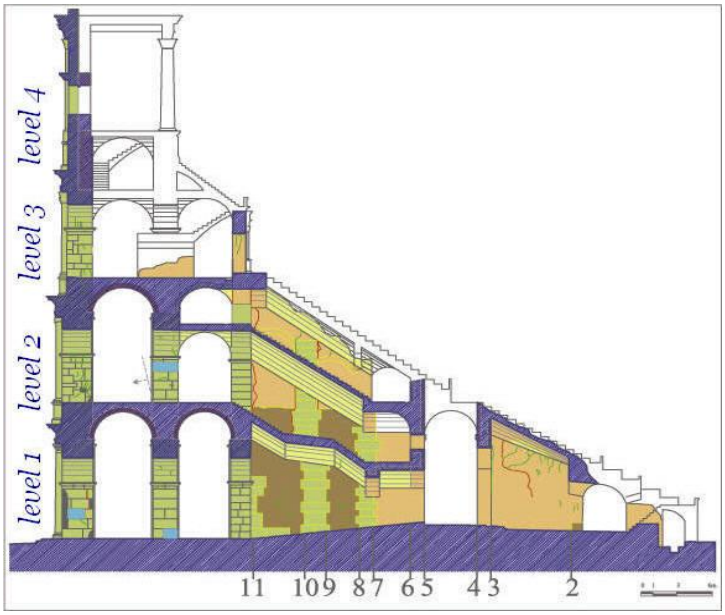

Figure 8*. The pillar # 49. N.13 rings and n. 4 levels.*

As example, in the disconnected structure, a new node is introduced, coincident with original node 365077 which rests in the annular wall, the new one belongs to the corresponding radial wall.

By CISTEC [15] for elevation; for cryptoportici and hypogea by Beste, Mertens, Schingo, Rea [6], [12], [13], [16], [17], [18].

We have the luck to know the geometry with accuracy, and all the densities are around 1.8÷2.2 t/mc.

About 70 disconnections between walls were performed, by CIS-TEC drawings [15], and the help by Maurizio Cerone, Figures 8 and 9.

Figure 9. *Pillar # 49, left, 1st level, disconnections 10 irregular and 11 regulars.*

7. 40 cm of lowering between northern and southern foundations

Da Maria Egizia Fiaschetti, in Cronaca di Roma sul Corriere della Sera 29 luglio 2012:

PLATEA DI FONDAZIONE FRATTURATA «La platea di fondazione in calcestruzzo su cui poggia il Colosseo, una "ciambella" ovoidale di circa 13 metri di spessore potrebbe presentare al suo interno una frattura accentuata».

GEORADAR E CAROTAGGI - «Dovremo verificare con strumenti ad hoc .Se i dubbi fossero confermati, avremmo a che fare con due monumenti strutturalmente diversi: a quel punto, sarebbe necessario ricollegarli».

RILEVARE LE VIBRAZIONI «Rilevare l'impatto delle vibrazioni dinamiche sul monumento e sul terreno»

AUTO PEGGIO DEL METRO' «Le auto producono più danni della subway. Il lato sud, il più vulnerabile anche per i movimenti sismici.

MAPPARE I RISCHI - Lo screening servirà, dunque, a mappare i rischi e a prevenirli:

8. Pillar #40 comparing the results of microtremor measurement in 1998 and 2013 [26]

Our first extensive microtremor measurement at Colosseum was in 1998, and we had an opportunity to measure again near the pillar #40 in 2013 at almost the same point of the past measurement.
Here, the results of the measurement in 1998 and 2013 at the pillar #40 can be compared. As a result, both spectral shapes basically agree well in wide frequency range.
But with confirming the detail of the predominant frequency and the amplification factor, they slightly differ for each other.
The result of measurement in 2013 shows that the peaks shift to a little higher for the radial direction and lower for the tangential direction, and the amplification factor becomes larger for each direction.
And the mode changing the phase for 180 degrees between 3F and 4F can be commonly observed in 1998 but not in 2013.
There seems to be something structural difference between 3F and 4F, for example the affection of the 2009 L'Aquila earthquake or the work of the floors and the fences of 4F and 3F in 2010.
If the degradation of the structure can be grasped quantitatively with periodic microtremor measurement, it is possible to maintain rationally and is not impossible to take a countermeasure as reinforcement of maintenance prophylactically and properly. It is necessary for establishing the application method to confirm the accuracy of the microtremor measurement, and to make clear the reason of changing the dynamic characteristics at pillar #40 quantitatively.

9. Uncontrolled effects of new interventions

Luca 5: 33-39, parable. "*No one tears a piece from a new cloak to patch an old one. Otherwise, he will tear the new and the piece from it will not match the old cloak*".

The risk of damages produced by uncontrolled different elasticities coupling was known in the last 2000 years. Generally, all new interventions would have to be controlled, and it would be allowed since the third millennium.

10. Conclusions

Certain reports of damage to monuments caused by earthquakes date back to the years 422, 443, 508, 801, 1349, 1703 and 1812.

The present Colosseum is the result of damage caused by natural events in the past (earthquakes, fires, vegetation, abandonment, etc.), spoliation, dynamic pollution, consolidation to save the monument from imminent danger, with empirical control.

The greatest damage was concentrated in the period between the 9th and 15th centuries. The principal restoring works were done by the following architects: Beda, Canina, Lanciani, Stern, Valadier.

Petrarca was an eyewitness to the great earthquake "cecidit aedificarum veterum neglecta civibus, stupenda peregrinis moles", (Epistle II in Book X, 7-10 September 1349).

For the elevation, the current condition is represented by CISTEC [15]; and for the cryptoporticus and hypogea by [6], [12], [16], [17], [18], [22], [23], [24].

References

[1] Copia di un disegno perduto attribuito a Francesco Roselli (seconda metà XV secolo) nel Palazzo Ducale di Mantova.

[2] 1600, Matheo Florimj formis.

[3] Perrone, V., “la ferrovia Metropolitana a Roma”, Trasporti pubblici, nn. 4…10 1952, nn. 1-2, 9, 11 1953, nn. 5, 7-8 1954.

[4] G. Bulian, “*Resine epossidiche per il consolidamento di sei pilastri dell’Anfiteatro Flavio*”, L'industria tecnica delle costruzioni, A. N. C. E, 1980, n° 99.

[5] L.Benevolo: The History of the City, MIT press, 1980.

[6] Schingo G., Rea R., "Il progetto di restauro del Colosseo. I sotterranei: assetto idraulico e interventi strutturali tra XIX e XX secolo", *Bollettino di archeologia*, 23-24 Settembre-Dicembre 1993.

[7] Funiciello, R., Lombardi, L., Marra, F., Parotto, M. (1995) "Seismic damage and geological heterogeneity in Rome's Colosseum area: are they related?", *Annali di Geofisica*, 927-937.

[8] Bozzano, F., Funiciello, R., Marra, F., Rovelli, A., Valentini, G. (1995) "*Il sottosuolo dell'area dell'anfiteatro Flavio in Roma*", 405÷422.

[9] Memorie Descrittive Della Carta Geologica D'Italia, La Geologia Di Roma, Istituto Poligrafico e Zecca Dello Stato, 1995.

[10] Moczo, P., Rovelli, A., Labàk, P., Malagnini, L., (1995) Seismic response of the geologic structure underlying the Roman Colosseum and a 2-D resonance of a sediment valley, *Annali di geofisica,* pp. 939÷956.

[11] Nakamura, Y. (1996). "Seismic response of roman Colosseum and its foundation by using micro-tremor measurements", *The 10th Japan Earthquake Engineering Symposium*, pp. 2625-2630, 1998.

[12] Mertens D., Rea R., Schingo G., Beste H.J., Piraino C., (1998) Il Colosseo: lo studio degli ipogei, *"Sonderdruck aus Mittelungen des deutschen archaeologischen instituts roemische abteilung*", Vol. 105, 1998, ISBN 3-8053-2459-6.

[13] Coarelli F., Gregori G.L., Lombardi L., Orlandi S., Rea R., Vismara C., "*Il Colosseo*", Electa, Milano, 1999.

[14] Nakamura, Y., Gurler, E.D., Saita, J., Rovelli, A., Donati, S., (2000) Vulnerability investigation of roman Collisseum using ambient vibration, *12WCEE2000*, paper 2660.

[15] CISTEC (2000), "*Analisi e documentazione dei dissesti strutturali ed individuazione delle situazioni a rischio*", le tre Università di Roma.

[16] Pensabene P., Panella C., "*Arco di Costantino tra archeologia e archeomentria*", "L'Erma" di Bretschneider, Roma, 2001.

[17] Schingo G., "*Gli sterri del 1939 per la costruzione della metropolitana. Dati archeologici inediti dalla valle del Colosseo*", "L'Erma" di Bretschneider, Roma, 2001.

[18] Jappelli R., Rea R., Schingo G., "Artificial openings in the foundation of the Colosseum", *AITES-ITA 2001 World Tunnel Congress, Milano*, June 2001.

[19] Stucchi et alii.; 2007: "*DBMI04, il database delle osservazioni macrosismiche dei terremoti italiani utilizzate per la compilazione del catalogo parametrico CPTI04"*. Quaderni di Geofisica, Vol 49, pp.38.

[20] Nakamura, Y. (2011)," The H/V Technique and Example of its Application for L'Aquila and Rome Area", *Proceedings of the workshop DISS_10, L'Aquila, 19 March 2010,* Aracne, ISBN 978-88-548-3693-8.

[21] A. Tertulliani, A. Rossi, V. Castelli, C. Meletti, V. D'Amico, "*Spunti e contrappunti di sismologia storica: 1349 annus horribilis*", INGV, GNGTS 2011

[22] Anna Maria Liberati and Fabio Bourbon: Ancient Rome, White Star, Italy, 1996, pp.74-75.

[23] Leonardo B. Dal Maso: Rome of the Caesars, Italy.

[24] Roberto Luciani: "The Colosseum", DeAgostini, Italy, 1990.

[25] A. Caserta, P. Clemente, C. Conti, G. D'Ovidio , Y. Nakamura , R. Rea , A. Rovelli , G. Valente, "A methodology to analyse ambient vibrations in the Colosseum", DISS13

[26] Yutaka Nakamura, Jun Saita, Tsutomu Sato, "Dynamic characteristics of the Colosseum at the pillar #40 comparing the results of microtremor measurement in 1998 and 2013", DISS15.

Inescapable soil Colosseum interaction

Abstract

Through the soil, the transit of trains produces vibrations in the monument, and seismic action reaches the monument from distant epicentres. The elasticity moduli of the soil and the monument are very similar, so it is necessary to study the complete soil-structure interaction. If we analyse the analytical dynamic response of the geological structure under the Colosseum, for a plane SH incident wave, it turns out that the southern part of the monument may be exposed to a ground motion with significantly greater amplitude and duration than the northern part. The southern foundations are 40 cm lower than the northern ones, which could be due to different viscous effects at the Holocene-Pleistocene boundary. During the construction of the tunnel, a small part of the soil is lost; this produces a movement of the ground around the tunnel with a lowering of the green field.

1. Introduction

Some researchers, from the geophysical area, have proposed a preliminary reconstruction of the stratigraphy beneath the Colosseum: while the northern part of the monument rests on a more rigid Pleistocene stratum, in its southern area there is a softer alluvial deposit, in a well-bounded depression of fluvial origin, already transformed from palaeo-tever to Labic ditch until the Holocene.

Then, they perform the 2-D analysis on the N-S diameter, applying only a vertically incident plane shear wave as a harmonic forcing and discretizing, with finite differences, the space consisting of only the soil without the monument.

They find a significant amplification of the motion and its duration at the surface, and attribute the greatest damage, in the southern area of the Colosseum, to past earthquakes.

2. The interaction of soil and Colosseum

The importance of this interaction is related to the masses and stiffnesses involved and is generally much greater for soft soils and tall structures.

Therefore, the entire structural system consisting of the soil and the elevated structure should be modelled in finite elements.

The soil-structure interaction is derived from the literature of the disciplines of Geophysics;

The ground is represented as a semi-indefinite continuum confined to a sufficient distance from the structure, where tension and/or deformation changes due to loads become negligible.

The ambient vibrations of Colosseum are due to external random dynamic actions as:

a) trains' transit,
b) ground traffic,
c) the wind,
d) the people on the steps of arena, especially 2000 years ago.

The true place level is +23.26 m o.s.l.

2.1 The model by structural engineering

Usually, the structural engineers assume the hypothesis of elastic monument fixed at the basis as in Figure 1 [3], [4], which is unsatisfactory for our purpose.

It is equivalent to admit the presence of a rigid plate between monument and soil, the respective actions cannot be transmitted between them, and the dynamic actions are reflected by this plate.

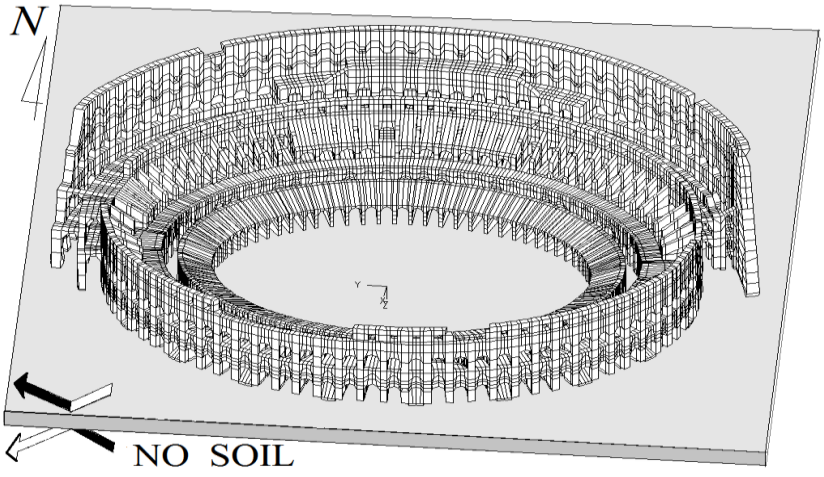

Figure 1. *Model fixed at the basis, by Structural Engineers. No soil? Fixed basis? No Colosseum vibrations, for traffic and microtremors.*

2.2 The model by geophysics

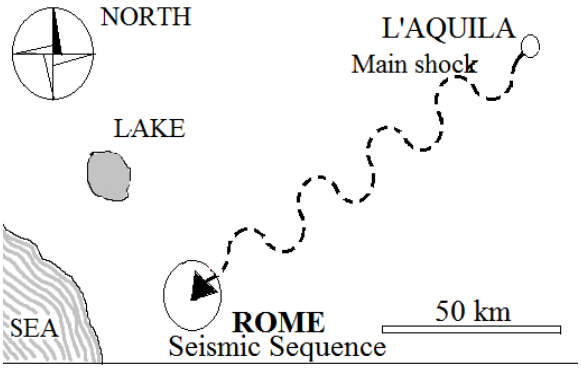

Figure 2. *The earthquake travel on April 2009 seismic, from L'Aquila to Rome, for 90 km.*

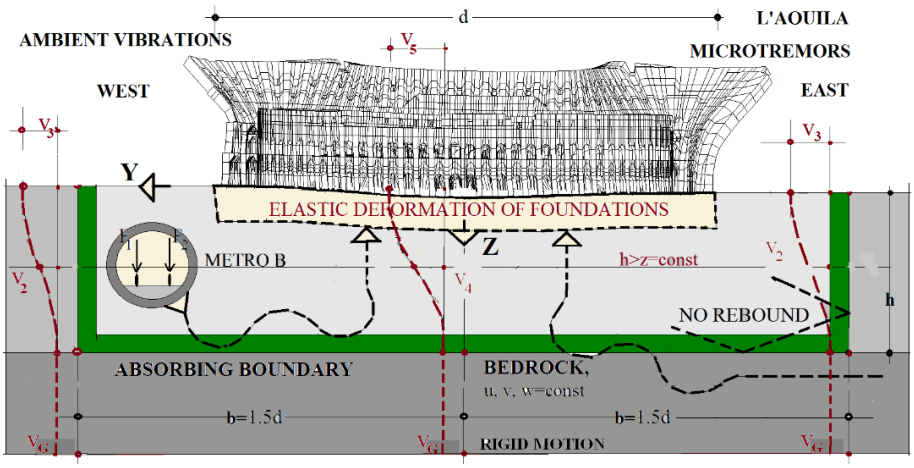

Figure 3. *Geophysical model. Vibrations from soil to monument.*

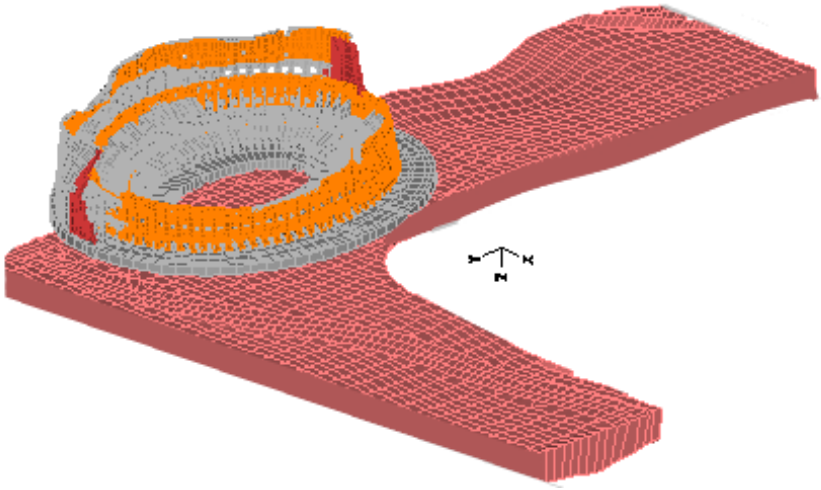

Figure 4. *Vibrations of Holocene and monument (mode n. 140).*

At 3.32 a.m. on 6th April 2009, the main shock of L'Aquila earthquake travelled through the soil, and INGV recorded a seismic sequence in Rome, in underlying soil and Colosseum as in Figure 3.

Since 2000 years, the soil transmits all the vibrations to the monument, by ambient vibrations too.

Figure 4 shows the mode shape n. 140 with deformations of both monument and soil.

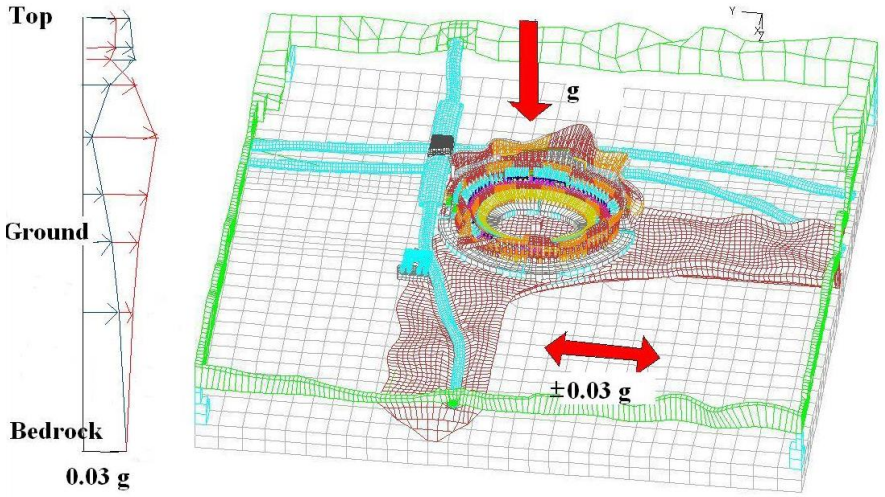

Figure 5*. The Colosseum vibrations for input 0.03g at bedrock in the vertical line of pillar #51.*

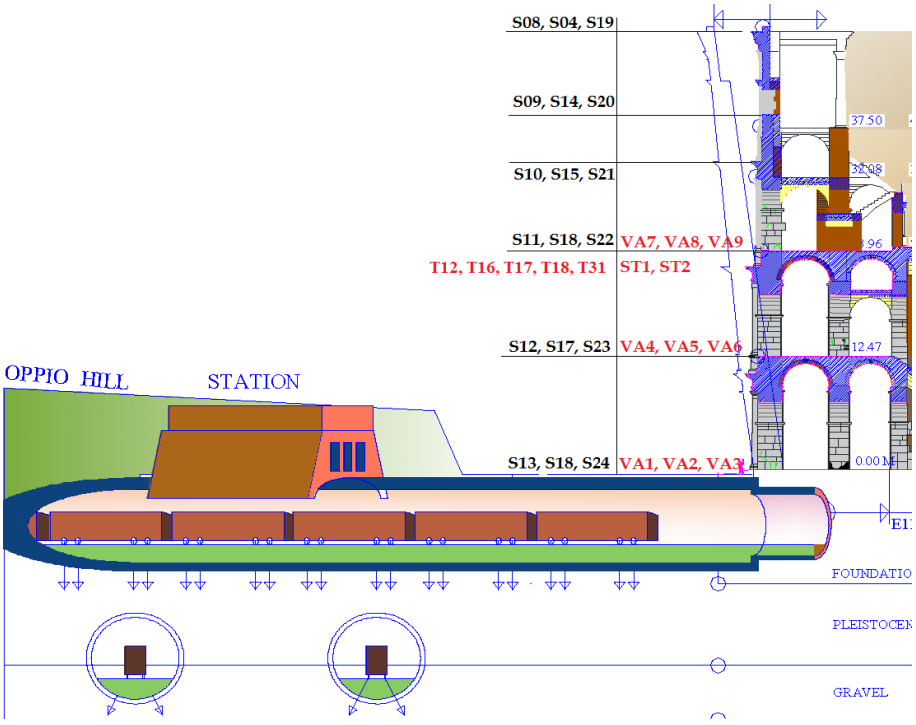

Figure 6. *Vertical section on pillar #51.*

The proposed model of dynamic interaction between soil and structure is represented in Figure 5; for a natural dynamic action, different points at bedrock have the same acceleration (±0.03 g), but ascending along a vertical line the accelerations change for different inertial actions.

3. Actual large uncertainties for Holocene

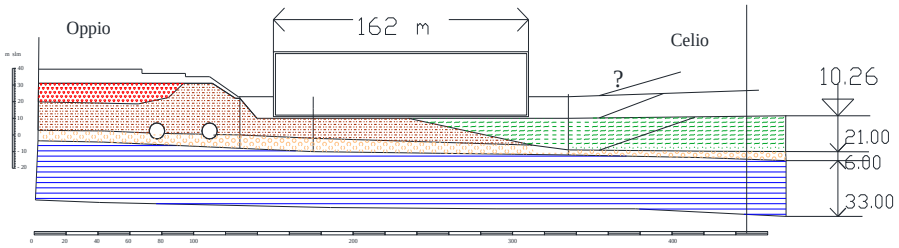

Figure 7. *Cross section along the minimum diameter:the new proposal [2].*

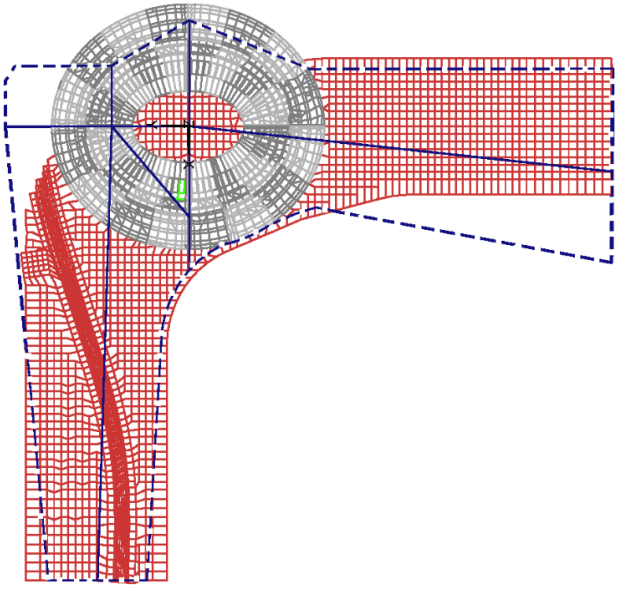

Figure 8. *Holocene plan uncertainties: c) d_1=21 m [2], d) d_2=45 m (---) [2].*

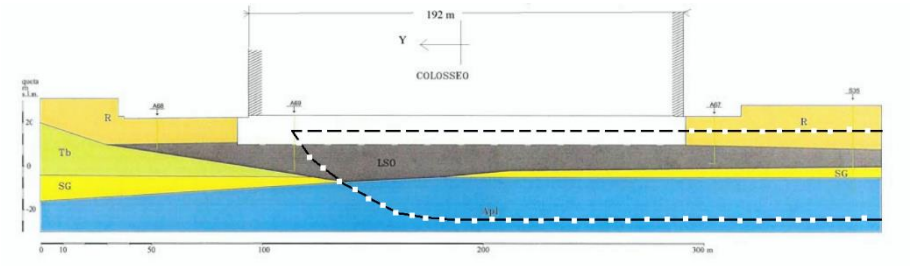

Figure 9. *Vertical section on L2 Holocene: a) (--) Bozzano [1], b) Sciotti [2].*

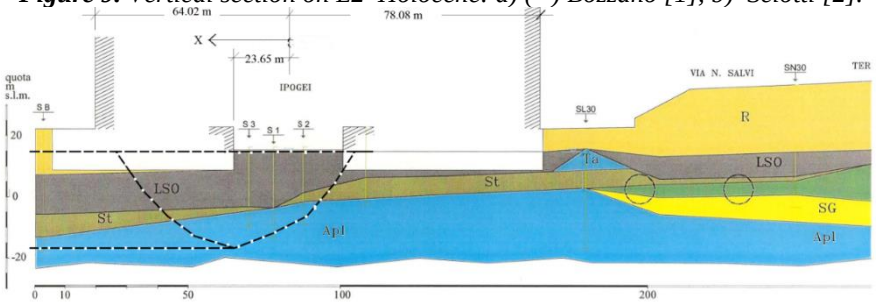

Figure 10. *Vertical section on T1 Holocene: a) (--) Bozzano [1], b) Sciotti [2].*

Actually, we have large uncertainties for Holocene:

the last tests for Metro C construction by Sciotti [2] proposed a depth of 21 m;

instead, the geological tests by Bozzano [1] proposed a depth of 45 m, as in Figures 7÷10.

The Ipogei zone is surrounded by the foundation ring. This latter is an around 13 m thick concrete layer.

4. 40 cm of southern foundations lowering

"La platea di fondazione ..potrebbe presentare al suo interno una frattura accentuata.. Quaranta centimetri di dislivello nella parte sud del Colosseo" (Corriere della Sera **29 luglio 2012**).

The incremental static analysis is performed, as in Figure 11.

$$M({}^{t+\Delta t}\ddot{u} - {}^{t}\ddot{u}) + {}^{t}K({}^{t+\Delta t}u - {}^{t}u) = ({}^{t+\Delta t}P - {}^{t}P)$$

with C=0, M=const, ${}^{t}K$=variable.

We believe that this phenomenon is due to differential viscosity actions between different soils, Holocene and Pleistocene.

In fact a long fracture of the foundations appears along the northern Holocene boundary, from:

Tests, in Figure 11;

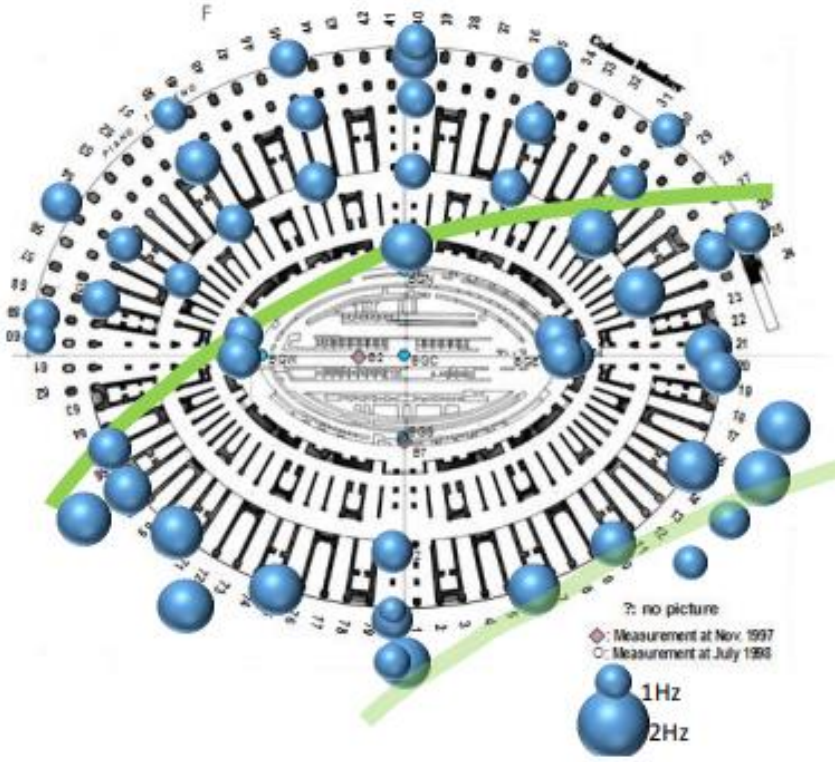

Figure 11. *Lower predominanat frequencies*

5. Ground vibrations

About the vibrations on the ground, the lower limit of vibrations perceptible to people is set by observation and experiment at approximately 0.00lg or l cm/sec (from National Information Service for Earthquake Engineering, University of California, Berkeley, *"The Nature of Ground Motion and its Effect on Buildings*", Christopher Arnold, A.I.A., 1982).

Whole-body vibrations in the range of 3-10 Hz are particularly critical because large body organs within the rib cage and abdomen resonate within this frequency range and it is within this general

range that the inherent vibration isolation capability of the body is least effective (Grether, W. F., *"Vibration and Human Performance,"* Human Factors, Vol.13, No. 3, 1971, pp. 203-216).

Man is sensitive to mechanical oscillations ranging in frequency from well below 1 Hz up to at least 100 kHz. Guignard, J. C., Journal of Sound and Vibration, Volume 15, Issue 1, 03/1971.

The maximum accelerations overcome this threshold of human perceptibility; instead the maximum velocities are near the limit of perceptibility for pedestrians.

For the proposed 3D model consisting of the monument and the underlying terrain, it is necessary to reduce uncertainties related to the knowledge of the stratigraphy of the ground, the collaboration between the various structural elements, the map of the modulus of elasticity and the average dynamic dissipation coefficients for the elevation and the ground.

Fig. 3. Pseudo-impulse responses of the MI and M2 models — time-domain responses to a relatively short «delta-like» I1 signal ~ at the free surface sites. The irregularity in trace spacing to the left of A edge, and to the right of D edge is connected with the irregularity of the computational grid. Amplitude scale: 0.8 cm in the figure corresponds to the actual surface displacement of 2.649 cm for a maximum basement displacement of 1 cm.

6. Tunnel excavation

The tunnel has: internal diameter 10. m, external 11. m, depth of the axis 20.76 m, it is developed parallel to greater axis of the monument, at North side, the distance between the tunnel axis and the monument axis is 120. m.

The excavation happens with a TBM shield having depth 10.0 m and weight 10000 kN and excavation pressure of 225 kPa; from Est to West. The following phases are repeated 116 times on depths of 5.0 m:

a) excavation,
b) advancing of TBM shield,
c) contraction,
d) concrete covering.

7. Conclusions

It is essential to use a soil-structure interaction model and carry out static and dynamic tests that provide comprehensive information on mechanical characteristics, such as those derived from:

1) stratigraphic investigation of the soil,

2) in situ tests with vertical holes,

3) monitoring along the current metro tunnel, in a sod measuring approximately 600x600x80 m, with simultaneous measurement of train actions and vibrations of the monument and the ground,

4) the installation of a permanent monitoring system of the Colosseum and the ground.

References

[1] Bozzano, F., Funiciello, R., Marra, F., Rovelli, A., Valentini, G. (1995) "*Il sottosuolo dell'area dell'anfiteatro Flavio in Roma*", 405÷422.

[2] Burghignoli A., Desortis A., Lacarbonara W., Soccodato F.M., Vestroni F., Viggiani G., (2003), "*Studio tecnico-scientifico dei problemi di interazione tra le Opere di linea e l'ambito monumentale circostante lungo la tratta S. Giovanni-P.za Venezia della Linea C della Metropolitana di Roma",* Convenzione di ricerca tra la S.T.A. e il Dpt. DISG, Università di Roma "la Sapienza".

[3] Pau, A., De Sortis, A., Marzellotta, R., Vestroni, F., *"Health monitoring of cultural heritage using ambient vibrations. In Safety and Security Engineering",* Brebbia CA, Bucciarelli T, Garzia F, Guarascio M (eds). WIT Press: Southampton, 2005; 331÷340.

[4] Pau, A., Vestroni, F., (2008) Vibration analysis and dynamic characterization of the Colosseum, *Structural Control and Health monitoring,* Journal of Structural control, Ed. J. Wiley & Sons, Febr.

Scientific method for monument analysis

Abstract

The 'International Scientific Committee for the Analysis and Restoration of Architectural Heritage Structures' (ISCARSAH) is a technical committee of the 'International Council on Monuments and Sites' (ICOMOS).

Everyone agrees with the structural prescriptions of ICOMOS, but until the second millennium, the permissible methods were intuition, the empirical method, the scale model, the shaking table, transfer functions, the model fixed to the base, the limit equilibrium method, and 2D analysis; none of these could guarantee the analysis recalled by ISCARSAH in an objective and verifiable manner.

Analytical tools capable of solving with an engineering accuracy have only been available since the third millennium.

Developments have now occurred: a) research into material behaviour, b) dynamic and static analysis, the FFEE method, c) test procedures, d) DISS Workshops, e) binary algebra by Boole, f) the Turing machine during the Second World War, g) today's powerful computers.

Today, structural problems can be solved by the scientific method through tests, correlation, physical-mathematical model, verification and assurance of the results with the best accuracy.

1. Introduction

In 1984 [4] it was said "*nel campo della ingegneria strutturale, il modello è diventato numerico…Purtroppo per le ossature murarie si sa tanto poco da rasentare il nulla….non sembri citata a sproposito una raccomandazione messa in bocca a Leonard Euler [1], probabilmente da Voltaire....qu'il n'omploiera plus soixante pages de calcul pour arriver à une conclusion qu'on peut établir par un raisonnement de dix lignes".*

The approximate methods for structural analysis enclose the above 10 lines reasoning and 60 pages of analysis, and about them:

1) they were the unique tools up to 1970s, for the inquiry of masonry walls;

2) their main flaw is the lack of objective control for the analytical tolerance;

3) our scientific field of interest is grateful to them and studied deeply them, as shown in § 2.

Up today, Colosseum suffered different earthquakes, with the stronger one in the 14th century, the actual stone masonry is the same since two millenniums, with a seismic probabilistic return period of many centuries, which we want to preserve from damage, without invasive devices.

We should need a scientific method based on physical mathematical demonstration, with objective assurance of accuracy from the test analysis comparison, within the engineering value of 5%, indispensable for safety of people and money.

Wonderful research could start from the lacerating feeling of helplessness, due to the contrast between the Colosseum problem and the approximate methods.

Since the 1970s [3], the FFEE method was available with reliable solutions of real small problems; and only in the third millennium, there are at disposal enough powerful and cheap PCs.

Two new doubts appear, they are wonderful from the scientific research viewpoint, and they are about the effective possibility to obtain a reliable solution of Colosseum problem with such powerful tools of the third millennium.

2. Recommendations by ISCARSAH [8]

Everybody agrees with the chapter "*Research and diagnosis"*, and its following points:

2.1 Usually a multidisciplinary team,

2.2 Data and information should first be processed approximately,

2.3 A full understanding of the structural and material characteristics is required in conservation practice,

2.4 In archaeological sites specific problems may be posed,

2.5 Diagnosis is based on historical, qualitative and quantitative approaches,

2.6 Before making a structural intervention it is indispensable to determine the causes of damage,

2.7 The safety evaluation, where the need for treatment measures is determined,

2.8 The required safety levels for buildings are different from monuments.

2.9 The diagnosis includes the safety evaluation, the decision to intervene in an "explanatory report".

The problem is governed by Mathematics and Physics, which are hard Sciences, and which must consent the solution by the rigorous "Scientific Method".

Surely, the solution is engaging and complicated, but is it reliable?

3. Approximate methods

About approximate methods:

a) they are model fixed at the basis, Limit Equilibrium Method (LEM), shaking table, transfer of functions through the soil, intuition in structural design, rules that allow personal discretion;

b) they shy away from any objective dialectic; they are not looking for the assurance of objective control for errors;

c) they are comprised between the first three not scientific methods;

d) for our problem, the analytical approximations are so rough that the comparisons with tests cannot be used at all; then the tests would be abandoned.

3.1 The intuition

The intuition method is the true ten-line reasoning [1], [2]; it is the more brilliant; it is the best for speed and economy; it does not rest confused from many simplifying hypotheses; it was the unique opportunity before seventies of the last millennium, and so it is still today for the majority of monuments.
But anyone can have an intuition, even non-graduate. Which is the best intuition? All the other approximate methods correspond to sixty-pages of long and expensive analyses.

3.2. Scale models and shaking table

On 1937, P.L. Nervi declared the physical model to be the best solution for himself [4]; at that time, he was right. For these choices, the Author recall that in 1996, for a two-storey unreinforced masonry (URM) building [6], a full-scale prototype was subjected to static actions, in Pavia, Italy.

The same structure in a $3/8^{th}$ model, for bricks and mortar too, was tested on a shaking table at Urbana in Illinois [6], with 22 kN of additional weight added at each storey level because the mass density is not properly proportional between prototype and model, subjected to the Nahanni earthquake which occurred in NW Canada on December 23rd 1985, recorded at a time interval of dt=0.005 sec, applied with the same amplitude and scaled time interval dt=0.0031 sec.

It is impossible to reproduce the existing damages in the model, as cracks' system.
On between approximate methods with few elasticity modules, with respect to analytical model fixed at the basis (§ 3.3.1.1.), the shaking table introduces further errors due to the use of too many scales: geometric, time, dynamic, mechanical, granulometric (logarithmic too).

Besides this, in [9] the research for an analytical model started with n. 4 different elasticity modules; after a first unsuccessful characterization trial, all the elasticity modules were reduced by a constant coefficient 4. If the same would be happened with a physical scale model, it was needed to destroy and to rebuild the model. All those above

produce the incommunicability between physical models and reality. But intuition does it better, almost always.

3.3. Hazards with Limit Equilibrium Method (LEM) [7], [10]

In the 18th century, the LEM was proposed which consists in imposing limit equilibrium conditions for rigid rotations of portions of wall obtained with selected planes. These parts of the wall are connected to each other by plastic hinges in their corners; the designer selects some cutting plan systems, and he evaluates the minimum collapse multiplier.
It seems a metaphysical method [7], because it considers too many hypotheses, which are (the real problem is shown in brackets):

1. horizontal static loads, (dynamic);
2. monotone horizontal loads (alternating);
3. constant horizontal acceleration along the height, (increasing);
4. null tensile strength, (cannot be neglected to guarantee the shape only by gravity);
5. structure fixed to the base (interaction of the soil structure);
6. generation of macro elements by cutting planes;
7. transformation of the problem from 3D to 2D, practically as in Figures 1÷4 the designer considers an arc with four hinges in 2D;
8. the only conditions of equilibrium are imposed (the characteristics of the material are not used, why are there always tests?);
9. introduction of plastic hinges (impossible stress concentrations).

Each of them is a rough hypothesis, adopted without any errors' control; their use all together may lead to the missing errors' control.
The following section will examine the behavior of the Colosseum's structures with LEM [10], [11]. The ring walls can be represented by a series of single cells, together with the adjacent circumferential arcades, the architraves, and the arches below, all taken along the piers' half-spans as in Figures 2a and 2b.

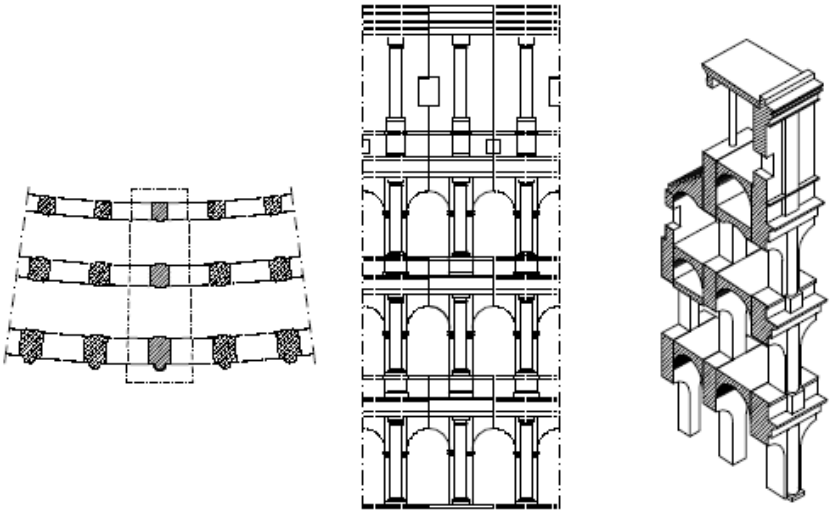

Figure 1. *Structural cell: a) plan; b) front; c) axonometry.*

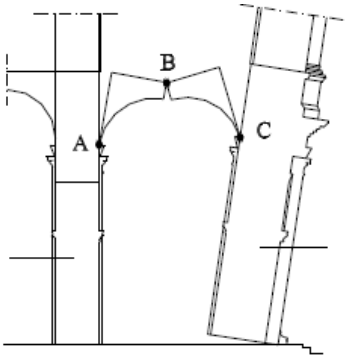

Figure 2a. *Radial displacements in the curvilinear vault.*

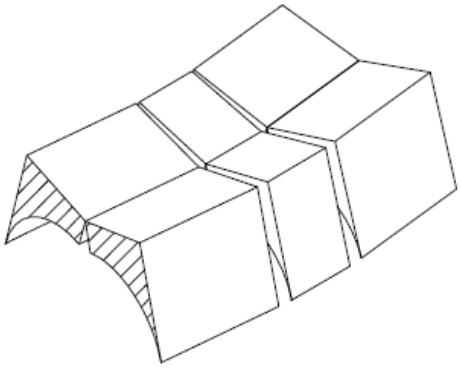

Figure 2b. *Compatible mechanism of the curvilinear vault.*

This type of mechanism regards only the outer wall and the circumferential vault. Three external wall rotates outwards, while the internal and central walls do not move.

The Figure 3 illustrates the vertical and horizontal components of the displacement field. The mostly downward displacement of the circumferential arcades as the mechanism develops highlights the destabilizing

effect of the loads acting on these vaults. All the displacements can be linked to parameter θ, that is, the rotation of the external wall.
The relation between the displacements and rotation θ can be inferred from Figures 3a, 3b and 3c. Figure 4 shows the broadening of the wall at collapse, like a quiet night flower in front of a disordered earthquake. But intuition does it better, almost always.

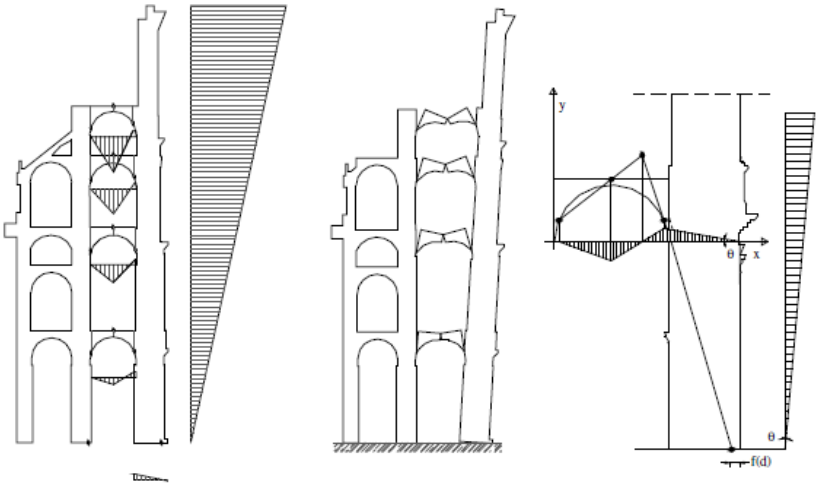

Figure 3. *Radial section: a) loading; b) displacements; c) centers of rotation.*

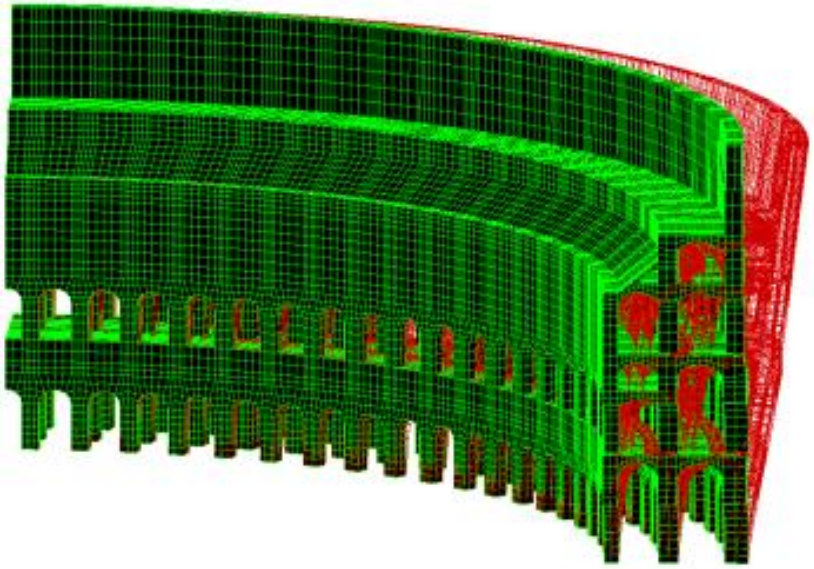

Figure 4. *Broadening of the outer wall at collapse [4], λ=0.122.*

3.4 The monument fixed at the base

Usually, the structural engineers assume the hypothesis of elastic monument fixed at the basis as in Figure 5 [10], which is unsatisfactory for our initial purpose.
It is equivalent to admit the presence of a rigid plate between monument and soil, the respective actions cannot be transmitted between them, and the dynamic actions are reflected by this plate.

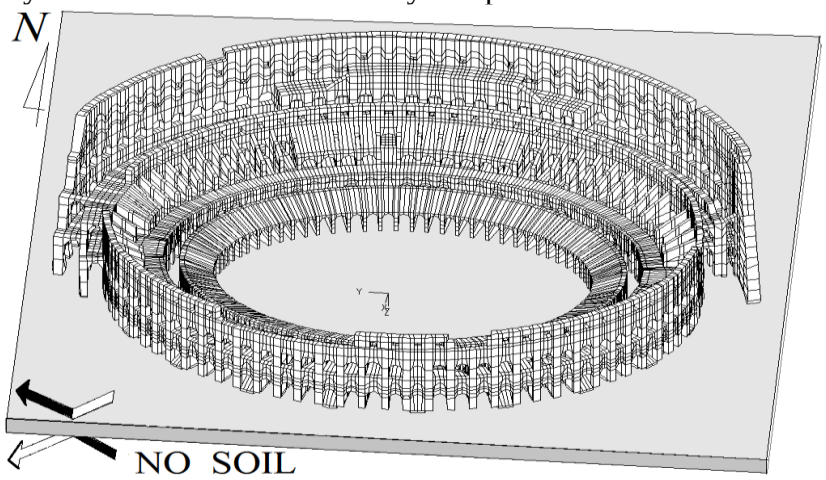

Figure 5. *Model fixed at the basis, by Structural Engineers.*

3.5 The transferring functions

We use constant coefficients for the actions between different levels [5].

4. the scientific method

The scientific method for natural sciences (hard sciences), is the typical way in which science proceeds to reach a knowledge of objective, reliable, verifiable and shareable reality; the principle of reproducibility of the experiments is clearly applicable.

Experimental studies and philosophical reflections on this have roots also in antiquity, in the Middle Ages and in the Renaissance by: Aristotile (384-322 BC), Ruggero Bacone (1214-1274), Tommaso d'Aquino (1225-1274), Leonardo (1452–1919), Galileo Galilei (1564-1642), René Descartes (1596-1650), Emmanuele Kant (1724-1804), Bertrand Russell (1872-1970), Albert Einstein (1879-1955), Alfred Tarski (1902-1983), Karl Popper (1902-1994), Charles Sanders *Peirce* (1839 –1914), Lee Smolin (born on 1955).

Only the scientific method can accept correction and therefore accepts the **fallibilism** and **falsificationism** of any initial conjecture, in order to arrive at the true objective solution.

It requests pleasure of scientific research, because it is a more tiring and tearing method than the others, in fact:

I) it consists of a struggle to move from an irritating and inhibitory doubt born of surprise of an inexplicable phenomenon;

II) it can produce anger and frustration;

III) it requires work on all possible conjectures and refutations;

IV) it achieves objectively demonstrated belief up to an acceptable numerical tolerance regarding the test analysis comparison;

V) it encourages dissent and competition between different hypotheses, without any pretense to establish a solution prematurely;

VI) it tests those parts that seem more doubtful, even with independent double blind tests.

We must proceed with the following steps, repeated cyclically:

a) **Observation**, is the starting (and finishing) point of the cycle of acquiring knowledge in the sense that constitutes the stimulus for the search for a methodology that governs the observed phenomenon;

b) **Experiment**, is programmed by the observer who measures the monument vibrations produced by natural environmental vibrations;

c) **Correlation**, data processing consists in the construction of functions and graphs invariant with the forcing, but which depend on the geometric and mechanical characteristics of the structure;

d) **Physical mathematical model**, is constructed with EEFF, which is supposed apt to represent the overall phenomenon to be studied, with appropriate mechanical characteristics,

e) **Verification and assurance**, the mechanical characteristics are changed to reproduce the invariants of the previous steps with the best accuracy.

4.1 Numerical analysis, with engineering accuracy

Our problem is not algebraic, and the solution is numerical with controlled accuracy, around 5%, evaluated in the dispersion between tests and analyses; so the reliable solution is obtained anywhere in the structure for the safety of people and financing.
Numerical analysis is the study of algorithms, within assigned tolerances. From the earliest civilizations, numerical analysis was considered important for surveying, buildings, ships, astronomy; and we observe the following developments:

a) around 1800 BC, the ancient Babylonians had already numerical system based on powers of 60, angle of rotation divided into 60 degrees, they knew how to calculate the hypotenuse of the right-angled triangle with a precision of nine significant digits, before Pythagoras (570 ÷ 495 BC), therefore they solved problems of trigonometry;

b) in the 19th century binary algebra was founded, with two numbers and two logical operators by Boole;

c) modern computers began to develop during the II World War;

d) In the early 1970s, finite element and nonlinear analysis codes were available [3].

So after this period an accurate calculation is possible, but the good accuracy is not always warranted, and the requested time for the research is long. Important researchers always knew that problems of numerical analysis were not simple to solve, in fact they engaged directly by themselves, like Boole, Coulomb, Euler, Fourier, Galileo, Gauss, Kepler, Lagrange, Laplace, von Leibniz, Napier, Newton, Touring; they are remembered with their algorithms.

4.2 The missing link is the reliable evaluation of K and C

The collapse analysis is impossible to perform, because for each material too many characteristics are requested, and they are impossible to obtain. But our unique interest is on monument preservation.
So we study the linear elastic behavior of the monument alone, from the initial elasticity modules alone.
The reliability of the analytical model of an ancient masonry structure is rarely attainable, it depends on analytical-experimental comparison of K and C. This condition is extremely interesting for the research, we wish to analyze: a) the actual static condition, b) seismic vulnerability, c) subsidence produced from close excavations, d) seismic actions, e) effects of ambient vibrations.
The classical dynamic equation will be used, or its equivalent for static problems:

$$M \ddot{u} + C \dot{u} + K u = -M \ddot{u}_G \quad (2)$$

$$K u = F \quad (3)$$

Where the dynamic strength ($-M \ddot{u}_G$) is random, while the monument characteristics (M, C, K) are deterministic. In these equations, the true original characteristics must be used (M, C, K).
M is easily evaluable, but a problem exists for C and K of original monument; then the accuracy of the model is depending on these last two characteristics. If C and K are rough, in the evaluations a)..e).

5. Geotechnical characteristics

We know initial elasticity modules for soil.
We hypotize different geotechnical models: Drucker-Prager, Cam-Clay, Mohr-Coulomb, etc.
For each model we hypotize a fork analysis, with maximum and minimum mechanical characteristics.

6. The scientific progress

Scientific progress is not linked to the mechanical application of a method, but to the existence of a community of specialists guided by common ethical principles, in which:

a) tell the truth and argue rationally on the basis of publicly available data;

b) when the available data are insufficient for a binding argument, encourage dissent and competition between different hypotheses, without prematurely claiming to establish new paradigms.

The proposed method aims to solve a real problem of many monuments, e.g. that of the Colosseum:

c) it suffered major earthquakes in the 14th century,

d) today we want to preserve the remaining masonry, with the structural philology of two thousand years ago, without intervening with modern reinforcements.

Let us look at some excellent solutions using the scientific method:

1) gravitational waves are perturbations of the curvature of spacetime, generated by accelerated masses, which propagate as waves outwards from their source at the speed of light; they were predicted in 1916 by Albert Einstein, and in 2016 Virgo announced the first direct observation, from measurements of the rupture of two black holes;

2) habitable rocky planets require conditions roughly comparable to Earth's; Ross 128 b is the closest exoplanet around a quiet red dwarf Ross 128, at a distance of about 11 light-years from Earth; it has these characteristics and was discovered in 2017, indirectly from the star's periodic vibrations;

3) the curvature of starlight, is an unexplained exception to Newton's laws and has predicted and explained other observations such as the deflection of light by gravity, evidence that mass and energy are bent by observing the solar eclipse of 29 May 1919 on the West African island of Príncipe.

The above three examples have the same scientific approach as the proposed problem, but ours are much less demanding, in fact we can observe that:

I) all are based on the classical comparison of analysis with tests, with an engineering accuracy;

II) our proposed method uses high school Physics and Mathematics, and the analysis test comparison with accuracy around 5%.

7. Conclusions

For the proposed problem, approximate methods have been shown to produce more than 100 per cent error; they introduce many simplifying assumptions and do not evaluate the approximation; they rely on subjective and qualitative reasoning.

In the third millennium, smartphones perform extremely complicated operations and have software that is so simple that it can easily be used by a five-year-old through icons and touch controls. With thorough research, the structural problems of monuments could be handled just as well in the third millennium.

References

[1] Voltaire?, "*Maupertuisiana"*, Hamburg 1753, Traitè de paix, pag. 13.

[2] Croci, G., "*Intuizione e calcolo nella progettazione delle strutture*", 1970, Tipolitografia Pioda.

[3] Zienkiewicz, O. C., *The finite element method*, McGraw Hill, 1971.

[4] Di Pasquale S., "*L'uso dei modelli nella costruzione della cupola di S. Maria del Fiore*", Università di Firenze, Facoltà di Architettura, Pubblicazione 26/1984.

[5] Pasquali, C., (1994) "*Esperienze e risultati delle campagne di misura per la Metropolitana di Roma*", Giornate Impatto vibro-acustico e ambientale delle ferrovie Metropolitane.

[6] Costley A.C., Abrams D. P., Calvi G. M.: *Shaking table of an unreinforced brick masonry building*, Proceedings of the 5th National Conference on Earthquake Engineering, Chicago, pages 127-135, 1994.

[7] Giuffrè A., Carocci C., Ceradini V., De Benedictis R., De Felice G., Pugliano A., Zampilli M.; e con Baggio C., Boschi E., Guidoboni E., Mariotti D., Trovalusci P., *Sicurezza e conservazione dei Centri Storici - Il Caso Ortigia*, Laterza, 1999.

[8] Recommendations ICOMOS/ISCARSAH, 20/05/2007

[9] Pau, A., Vestroni, F., (2008) "*Vibration analysis and dynamic characterization of the Colosseum*", Structural Control and Health monitoring, Ed. J. Wiley & Sons.

[10] Como, M., "*Statics of Historic Masonry Constructions*", Springer, 2012.

[11] Ministero BBCC, Soprintendenza Archeologica di Roma, le tre Università di Roma, "*Omaggio al Colosseo*", Convenzione 1 Agosto 1995 Rep. N° 561 app. con D.M. 30 Gennaio 1996.

Existing tests for the elevation

Abstract

Using environmental vibration recordings, experimental mechanical characteristics were determined, invariant to external actions for elevation, the natural frequencies and mode shapes of the monument. These data will be used in the 3D model to evaluate the elasticity moduli in order to reproduce the same analytical shapes and frequencies. Similarly, numerical-experimental comparisons can be made for PSD diagrams.

1. Introduction

The tests were aimed at determining the natural frequencies and mode shapes of the structure.

For Colosseum, we were exceptionally lucky because the tests in many points are at disposal of researchers.

But further tests and analyses are needed for:

c) Constantine Arch, cryptoportici and tunnels of Metro B and C;

d) improvement of geometric and mechanical characteristics of foundations and soil;

e) the tests for the map of damping coefficients.

2. Measurement points

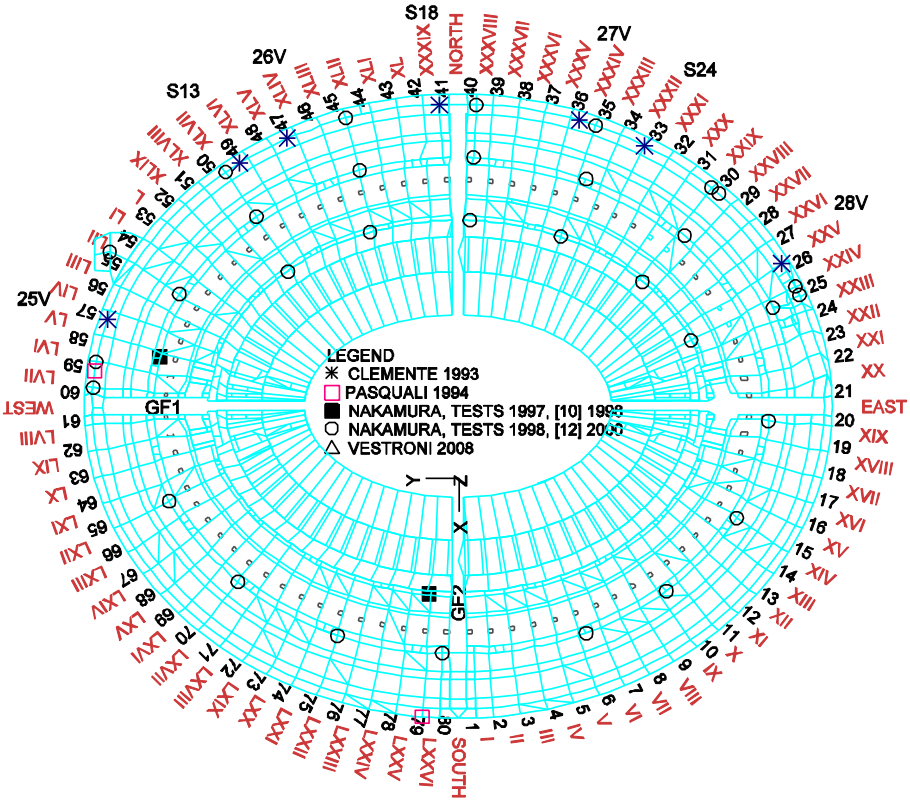

***Figure 1**. Measurement points on the ground at Z=0.0 m, a) radial wall RA with arabian numbers, b) radial access RA with roman numbers. (n.45 points).*

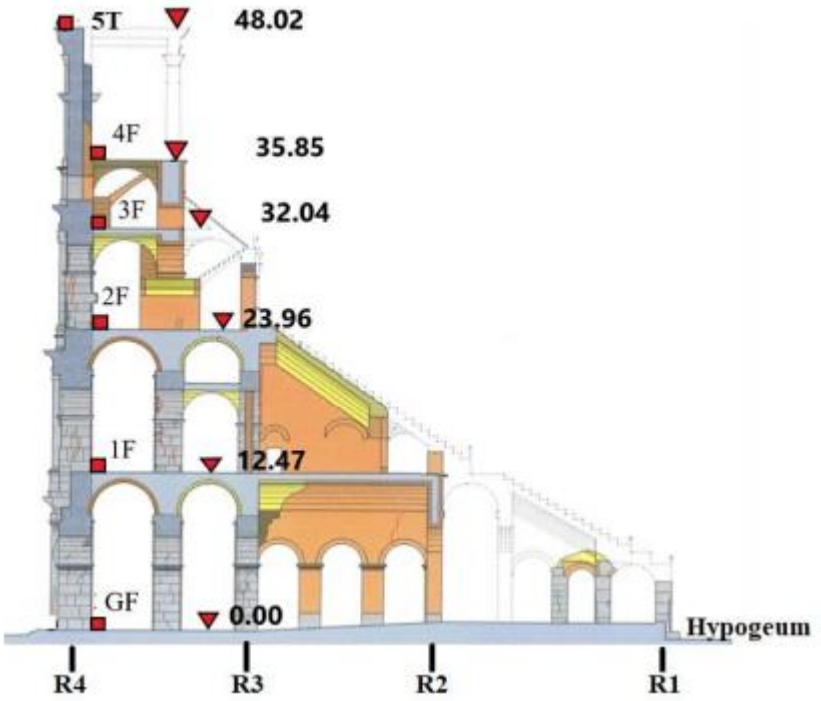

Figure 2. Floor levels (Hypogeum, GF, 1F, 2F, 3F, 4F, 5T) and elliptical rings (R1, R2, R3, R4).

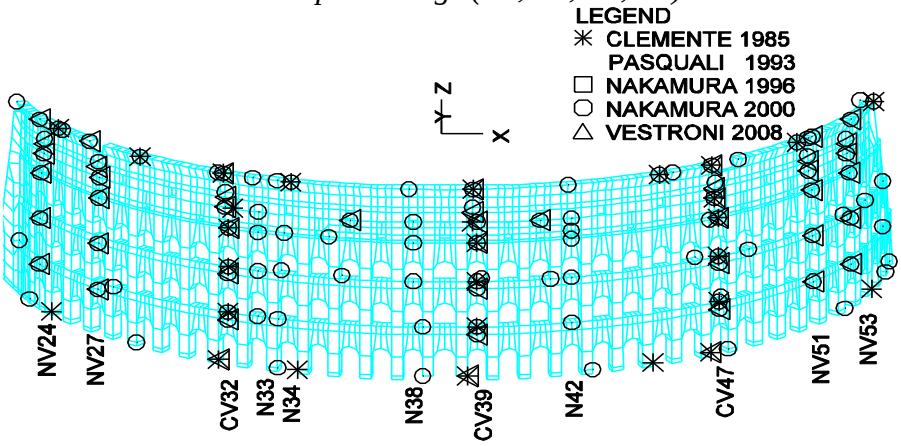

***Figure 3**. External façade of northern tallest wall, with buttresses; with n. 11 evident vertical alignments, with letters of Authors and number of arcades [1], [6], [9], [10].*

The existing tests are described in the Table 1÷3, and in all the following Figures, for a total about n. 200 measurement points, with multiple tests in the same point; the greatest number are on the northern travertine wall, the Table 4 define n. 119 existing tests points by many Authors.

Other tests are described in Table 1 of DISS_10 Proceedings.

The measurement points of Colosseum may be defined by three independent ordered indexes for:

1) the pillar (1 to 80 from the southern direction with anticlockwise rotation), or the radial access RA with sculptured roman numbers on external arches, except the cardinal directions, Fig. 1;

2) the level (ground, 1st floor, 2nd floor, 3rd floor, 4th floor, L1÷L6), as in Fig. 2;

3) the elliptical ring (R1 to R4, e.g.), as in Fig. 2 and Table 1.

In this way, GF1 in Figure 4b has three indexes, 56 for the pillar, 1 for the floor, 3 for the ring; so, its compact index is 5613.

Table 1*. Rings.*

Ring	R1	R2	R3	R4
Group		885	883	881
Rmin	23.65	48.28	64.26	75.46
Rmax	39.68	64.34	80.56	91.86

2.1. Tests by Nakamura

Table 2. *Couple of points for simultaneous measurement [5]*

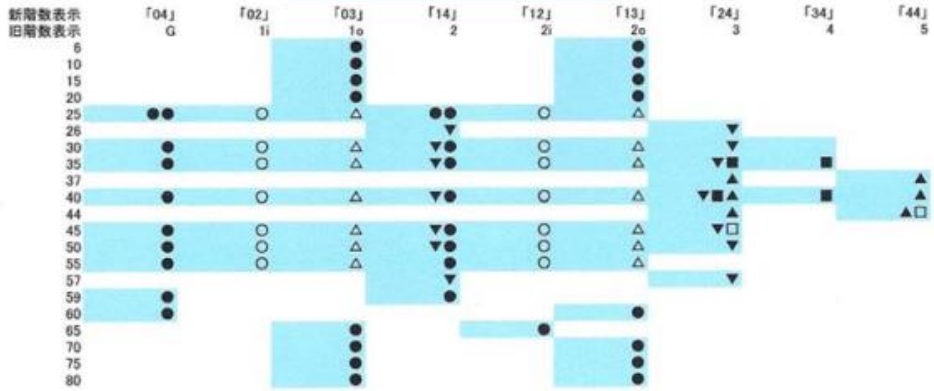

Table 3*. Measurement points [5]: a) o November 1997 [5]; b) • July 1998 [12]. H hypogeum, G ground, Floors 1, 2, 3, 4.*

Ring	**R4**					**R3**				**R2**			**R1**				
Level	**G**	**1**	**2**	**3**	**4**	**H**	**G**	**1**		**H**	**G**	**1**			**H**	**H**	
RW						**RW**				**R.W.**			**R.W.**				
1						1				1			1			•	BGC
2						2				2			2			o	B2
6						6	•	•		6			6				
10						10	•	•		10			10				
15						15	•	•		15			15				
20						20	•	•		20			20	B4	o	•	BGE
21						21		o	1F3I	21			21				
24						24		o	1F3	24			24				
25	•	•				25	•	•		25	•	•	25	B5	o		
26		•	•			26				26			26				
30	•	•	•			30	•	•		30	•	•	30				
35	•	•	•	•		35	•	•		35	•	•	35				
37			•		•	37				37			37				
40	•	•	•	•	•	40	•	•		40	•	•	40	B6	o	•	BGN
42						42		o	1F2	42			42				
44			•		•	44				44			44				
45	•	•	•	•		45	•	•		45	•	•	45				
50	•	•	•			50	•	•		50	•	•	50				
55	•	•				55	•	•		55	•	•	55				
56						56		o	1FI	56			56				
57		•	•			57				57			57				
58						58	o		GF1	58			58				
59	•	•				59				59			59	B3	o		
60	•					60		•		60			60	B1	o	•	BGW
65						65	•			65		•	65				
70						70	•	•		70			70				
75						75	•	•		75			75				
79						79		o	1F4I	79	o		79				GF2
80						80	•	•		80			80	B7	o	•	BGS
Level	**G**	**1**	**2**	**3**	**4**		**G**	**1**			**G**	**1**			**H**	**G**	

3. Dynamic tests for modal characterization of the monument

Table 4. E*xperimental natural frequencies, (--) [1], (--) [5], (--) [2]*

RA	XXIV	XXVII	XXXII	XXXIX	XLVII	LI	LIII	f_e
1	1.03	1.03						1.03
2						1.30	1.30	1.30
3	1.49	1.48	1.47, 1.46	1.46	1.49,1.46	1.49		1.49
4			1.59	1.62		1.60		1.60
5			1.65,1.70,1.70	1.70	1.67,1.70			1.66
6			1.75	1.73	1.76			1.75
7			2.75, 2.80	2.75	2.75			2.75

[4]: 1.05, 1.29, 1.46, 1.51, 1.61, 1.71, 1.78, 2.00, 2.22, 2.51, 2.76, 2.95

3.1 Measurement points for [4]

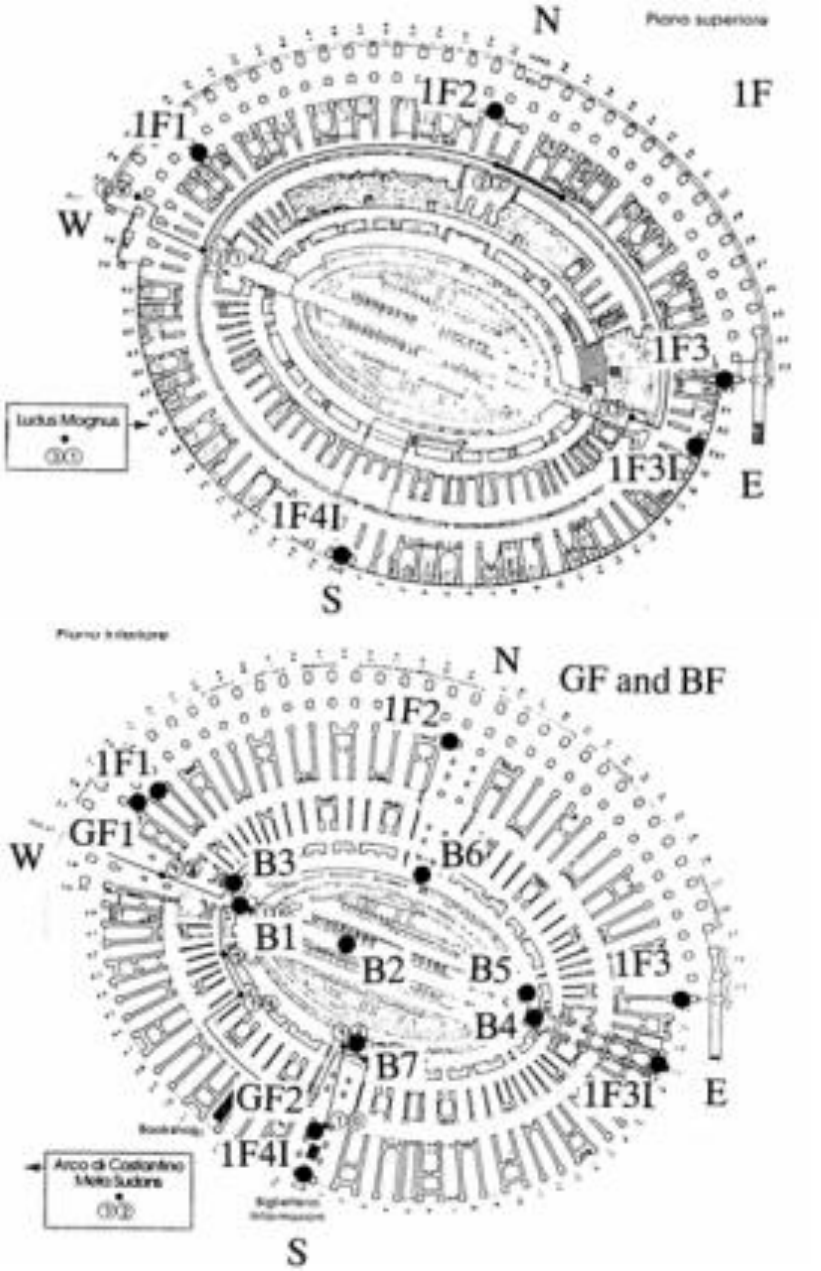

Figure 4*. Plan.*

3.2 Measurement points for [5]

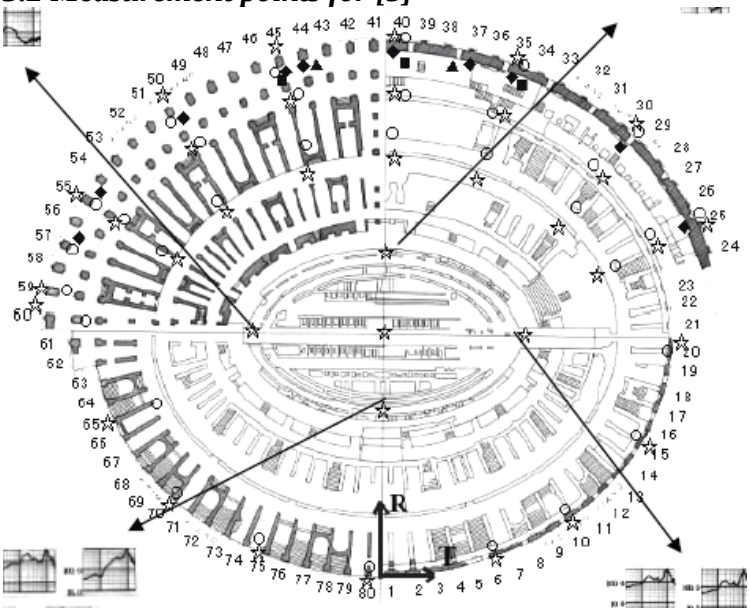

Figure 5*: Location of measurement points [5], at ground, 1st, 2nd, 3rd,4th floors with ☆,O,◆,,◙▲, respectively.*

Three components (two horizontal and one vertical) of microtremor are recorded at every measurement points. Sampling interval is 1/100 sec and the length of each record is 40.96 sec. Measurement was repeated three times at each observation point. Figures 4 and 5 show the location of measurements at ground, 1st, 2nd, 3rd,4th floors.

3.2 Results for [1] and [6]

In the Figures from 6 to 9, the check points monitored during the campaigns are represented: a) the first [1]; b) the second [6].
The effects of velocities are computed at the points:

a) the vertical alignments, each one with n. 6 points, C1 (S08÷S13) in the arcade XLVII, C2 (S04, S14÷S18) in the arcade XXXIX, C3 (S19÷S24) in the arcade XXXII;

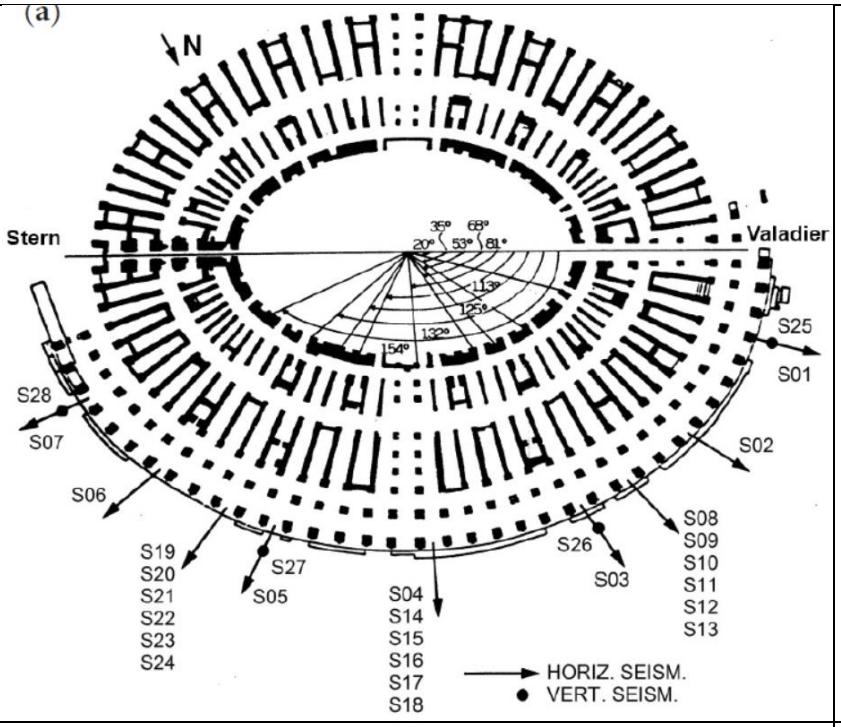

***Figure 6**. Plan of the first campaign [1].*

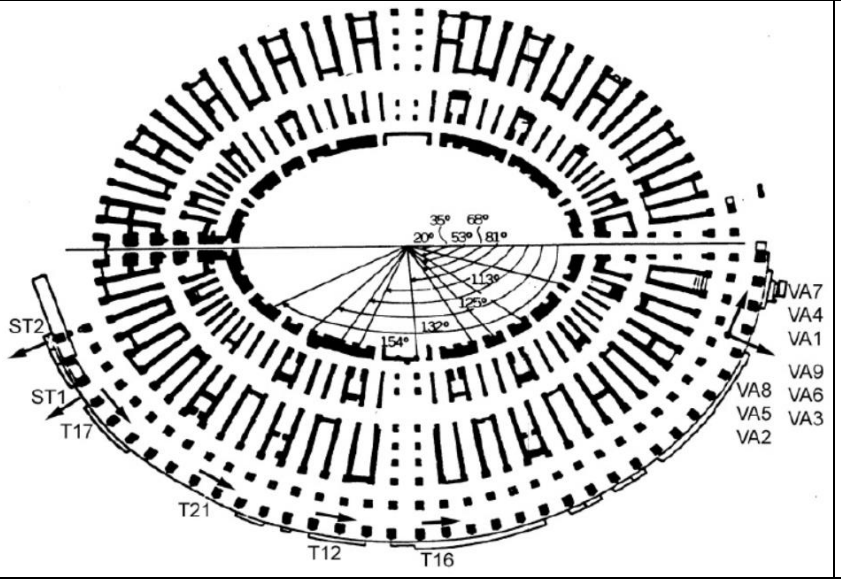

***Figure 7**. Plan of the second campaign [6].*

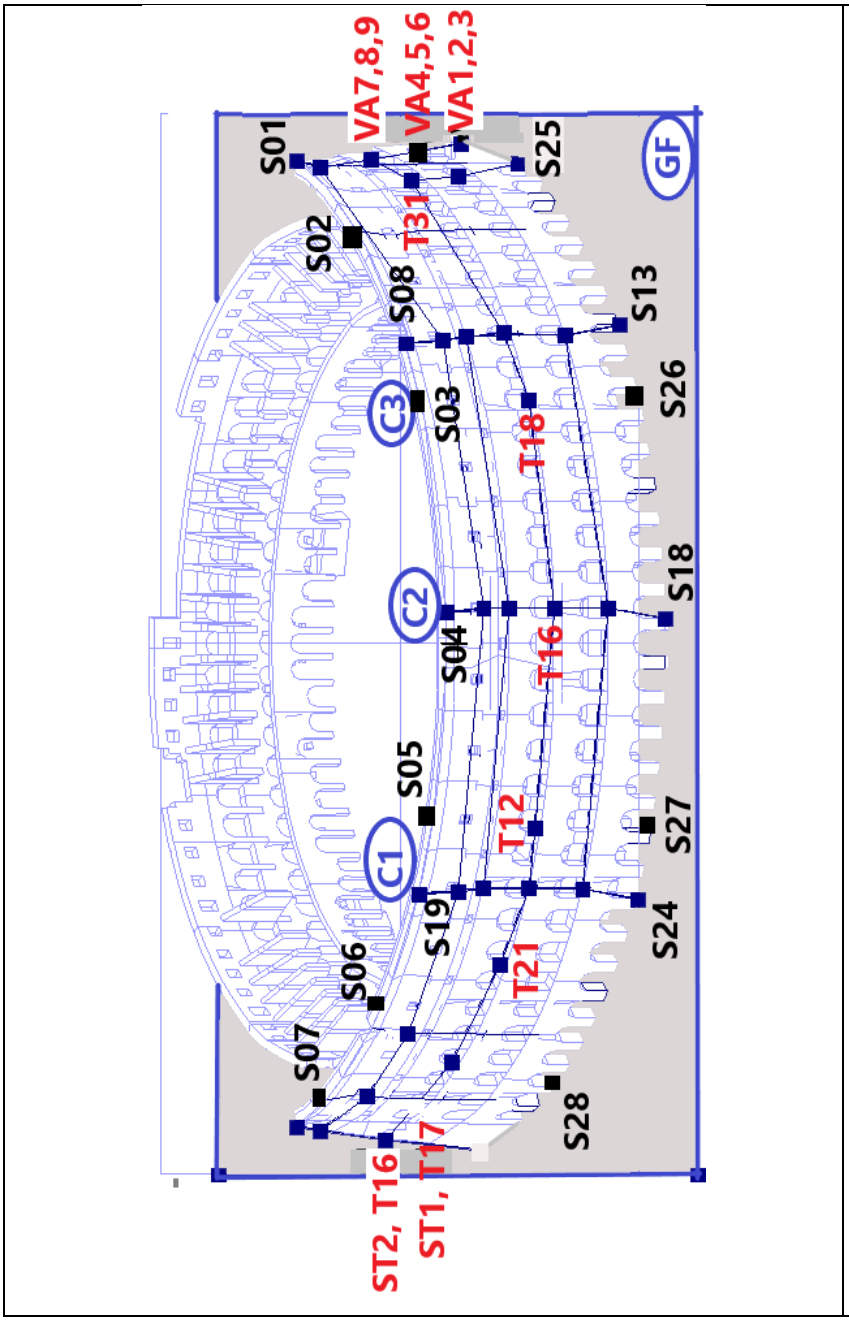

Figure 8 *Axonometry*

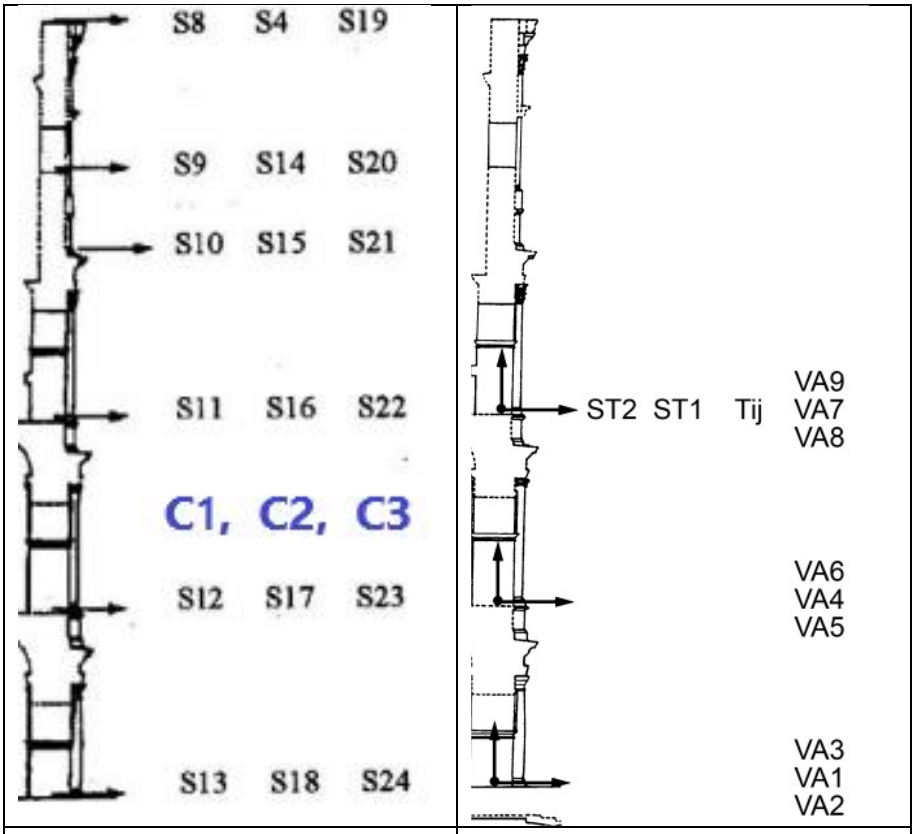

***Figure 9**. Check points in: a) the first campaign [1], b) second campaign [6].*

b) a fourth layout C4 regarded the measurement of the vertical vibrations, in four points of the basement, at locations S25 to S28, respectively in arcades LIV, XLV, XXXIV, XXV;

c) nine of them were kept in the horizontal radial directions at the top of the wall, S01÷S08 in the arcades LIV, L, XLV, XXXIX, XXXII, XXIX, XXV respectively, S19 in the arcade XXXII;

d) on the foundations, S13, S18, S24, VA1, VA2, VA3, S25÷S28;

e) on the middle height of the monument, S11, S18, S22, VA7, VA8, VA9;

f) on the middle height of the monument, in tangential directions

T12, T16, T17, T18, T31;

g) at Valadier buttress, T17, T18, T31; in the directions radial VA3, VA6, VA9; tangential VA1 VA4, VA7; vertical VA2, VA5, VA8;

h) at the middle height, on Stern buttress, ST1, ST2.

*3.3 D*ata acquisition and signal processing [5], [7]

Table 5*. Accelerometer tests.*

	Tests	*Arcades*	*Levels*	*Fig.*
1.1	*Triaxial*	*XXXVI, XLI*	*L4*	*10a, 10c*
1.2	*Triaxial*	*XXXII, XXXIX, XLVII*	*base, L1, L2*	*10a, 10c*
2	*Radial*	*XXIV, XXVII, XXXII, XXXIX, XLVII, LI, LIII*	*L1÷L6*	*10b, 10c*

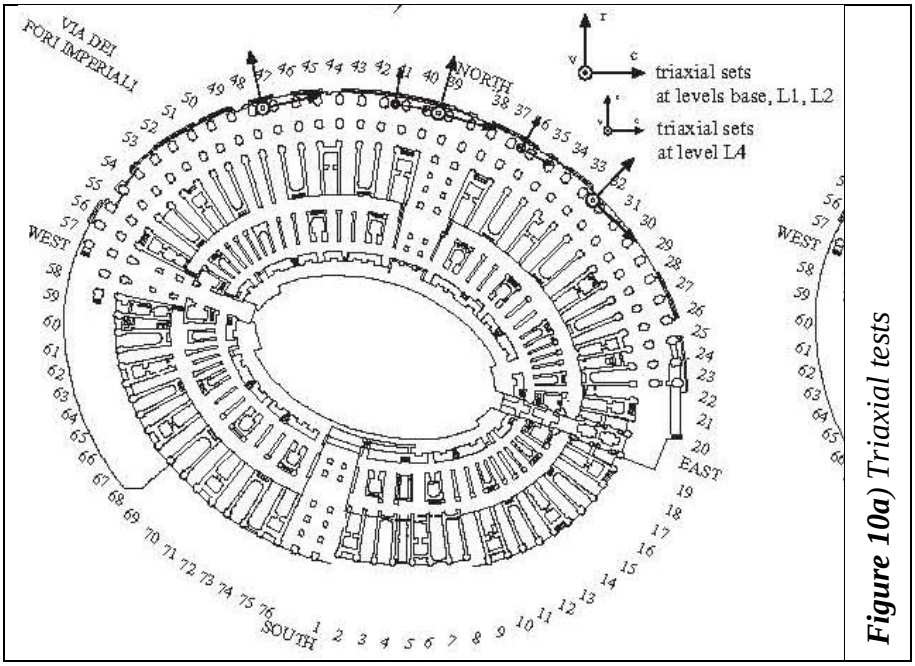

Figure 10a) *Triaxial tests*

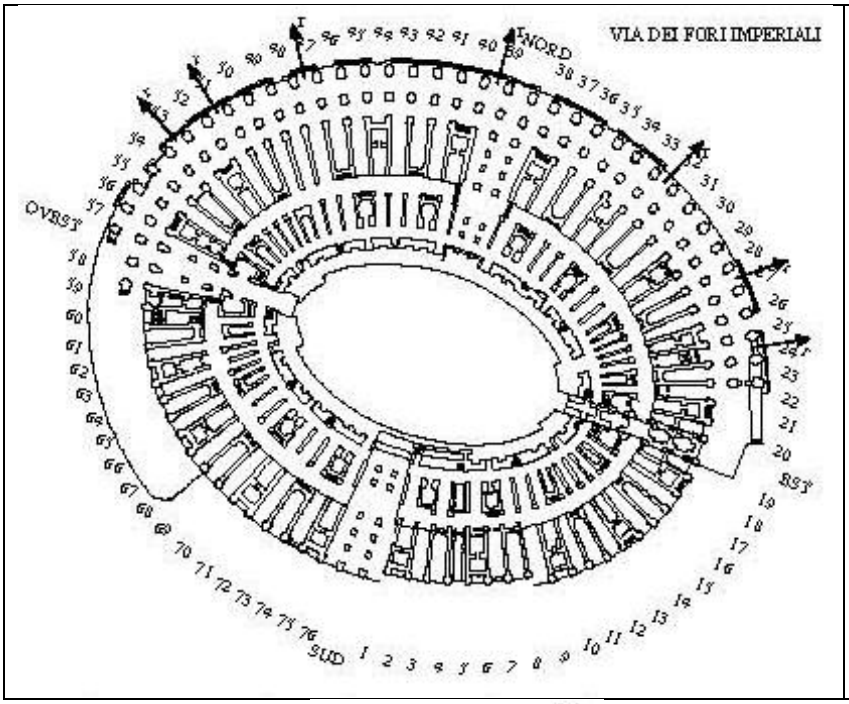

Figure 10b) *radial tests*

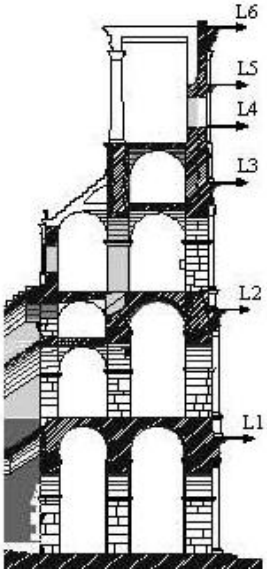

Figure 10c*. Position of accelerometers in section.*

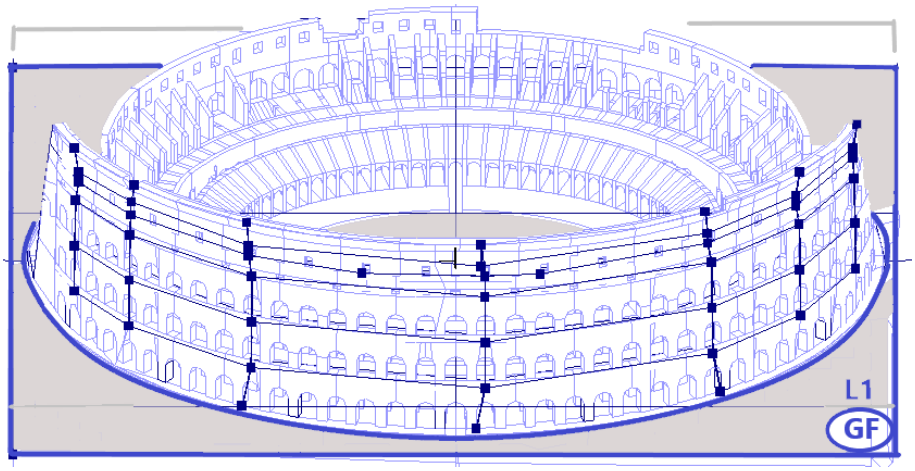

Figure 11a. *N. 47 measurement points. On arcades XXIV, XXVII, XXXII, XXXIX, XLVII, LI, LV. Level GF fixed points, Z=0., K=∞, GF with instruments.*

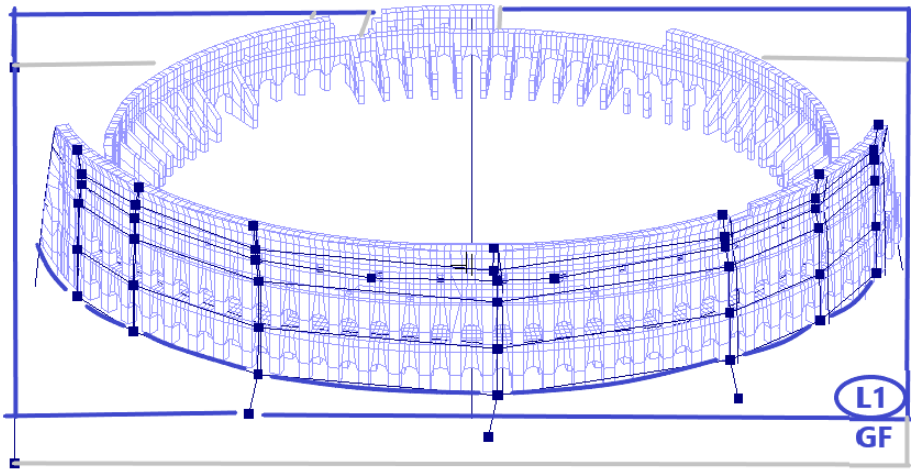

Figure 11b. *N. 47 measurement points. On arcades XXIV, XXVII, XXXII, XXXIX, XLVII, LI, LV. Level L1, Z=12.49, r=t=v=0. K=∞, the nodes are fixed.*

The recording points are summarized in Table 5, Figure 10a, b, c.
In Figure 11a appears that the tangential and vertical modal components are declared negligible with t=v=0.

The choice of the instruments used, their location and the parameters for data acquisition were based on the results obtained in the structure's finite element analysis, which indicates the frequency band where the significant modes are expected.

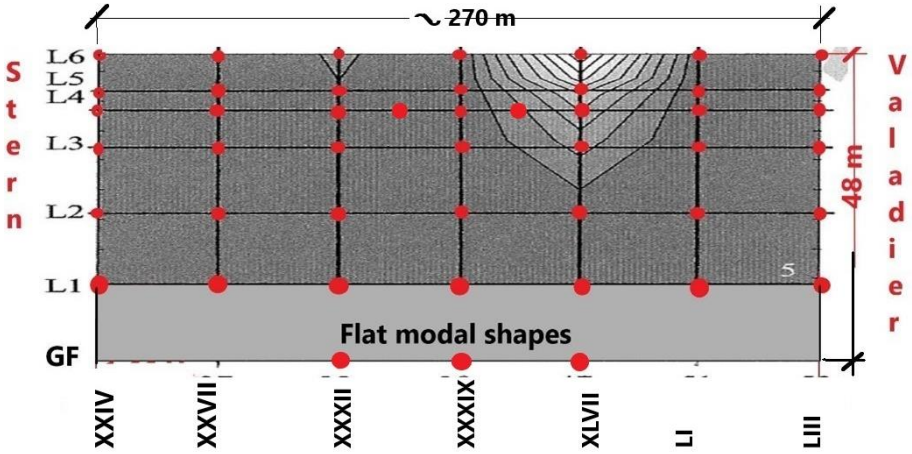

Figure 11c. *N. 47 measurement points, for the unrolled northern wall. None at GF with flat modal shapes between GF and L1 [6], [10].*

When moving from one vertical to another, one extra accelerometer was kept on the previous line to keep track of the phase.
All the modal components are explicitly declared r=t=v=0, at level GF, as in Figures 11a and 11b.
The model contains the outer ring and all the internal rings.
About figures 11c, it may be said flat modal shape appears only between levels GF and L1.
In [5], it is declared "*Traffic vibrations are induced by the stress waves generated by the vehicle–pavement interaction. Stress waves in the soil reach the foundations of buildings and cause them to vibrate ..Interaction with soil is not taken into account in this study and all degrees of freedom are restrained at the base … so that the soil–structure interaction is deemed of scant significance for the present analysis."*

4. Further problems

As a further problems, assuming that the current observation system is capable of measuring the level of micro-tremors, I would like to ask you to make the following measurements before stopping the observation:

(i) Vibrations when Metro B is running near the Colosseum.

(ii) Continuous observation of vibrations for at least six months (during periods of temperature differences and heavy rainfall)

The purpose of these measurements is to understand the impact of the circulation of the Metro trains to the Colosseum and to confirm the state of changes in the physical characteristics of the Colosseum. I would like to confirm if the above measurement (ii) is possible with the current observation system.

Data of temperatures are very important for considering a physical property.

5. Conclusions

We are interested on tests devoted to 3D DISS model, not to generic tests.

For such model, further dynamic tests are requested inside the monument too, for:

1) completing the map of elasticity modules;

2) producing the map of damping coefficients;

3) permanent recording in 50 points from the depth of 80 m under the place to the monument summit.

References

[1] Clemente, P., Bongiovanni, G., (1993) "*Ambient vibration effects on the Colosseum*", IABSE Symposium on Structural Preservation of the Architectural Heritage, Rome, pp. 107÷114.

[2] Bozzano, F., Funiciello, R., Marra, F., Rovelli, A., Valentini, G. (1995) "*Il sottosuolo dell'area dell'anfiteatro Flavio in Roma*", 405÷422.

[3] Nakamura, Y. (1998). "*Seismic response of roman Colosseum and its foundation by using micro-tremor measurements*", *The 10th Japan Earthquake Engineering Symposium*, pp 2625-2630 (Japanese).

[4] Nakamura, Y., Gurler, E.D., Saita, J., Rovelli, A., Donati, S., (2000) *Vulnerability investigation of roman Collisseum using ambient vibration, 12WCEE2000*, paper 2660.

[5] Pau, A., Vestroni, F., (2008) "*Vibration analysis and dynamic characterization of the Colosseum*", *Structural Control and Health monitoring*, Ed. J. Wiley & Sons.

[6] Bongiovanni G., Buffarini G., Clemente P., Rinaldis D., Saitta F., (2017). "*Dynamic characteristics of the Amphitheatrum Flavium northern wall from traffic-induced vibrations*", Annals of geophysics, 60, 4, S0439, doi: 10.4401/ag-7178

[7] Vestroni, Pau, De Sortis, "*Measurements of the Colosseum response to environmental actions*", Eurodyn Conference Paper · January 2020.

Modal analysis of Colosseum elevation

Abstract

Experimental dynamic recordings are analysed in the frequency domain, using the Fourier transform, power spectral density and cross spectral density to extract natural frequencies and modal shapes. The modal results by tests are compared with the analysis of the FFEE model to obtain the initial Young's modulus map. The target is to obtain the best fitting between tests and analyses, for modal results, for shapes and frequencies. The initial Young moduli alone may be obtained.

1. Introduction

The results obtained in many experimental campaigns, were analysed in the frequency domains and resonance frequencies, modal shapes and damping were extracted.
This information is fundamental for the mathematical modelling, which should allow the check of the structure in its present condition and the choice and design of a suitable intervention.
The results in frequency domain contain information regarding the intrinsic properties of the structure that can be used to produce its accurate FFEE model.
Periodical repetition of the measurements, to capture modifications in the dynamic response and possible reductions in structural integrity, is an important part of the monitoring procedure [7].

In 2013 the same measurement in 1998 was repeated, at almost same points with almost same instruments in the same procedure, and the difference of microtremor characteristics were obtained in a time span of 15 years.

2. ENEA, with two campaigns [1], [5]

2.1. Measurement points

A series of check points monitored during the first test campaign (in black), [1] and second test campaign (in red) [5], they were taken into account for our analyses.
The effects of velocities are computed at the points of Figures 1 and 2:

a) the vertical alignments, each one with n. 6 points, C1 (S08÷S13), C2 (S04, S14÷S18), C3, S19÷S24);

b) a fourth layout C4 regarded the measurement of the vertical vibrations, in four points of the basement, at locations S25 to S28;

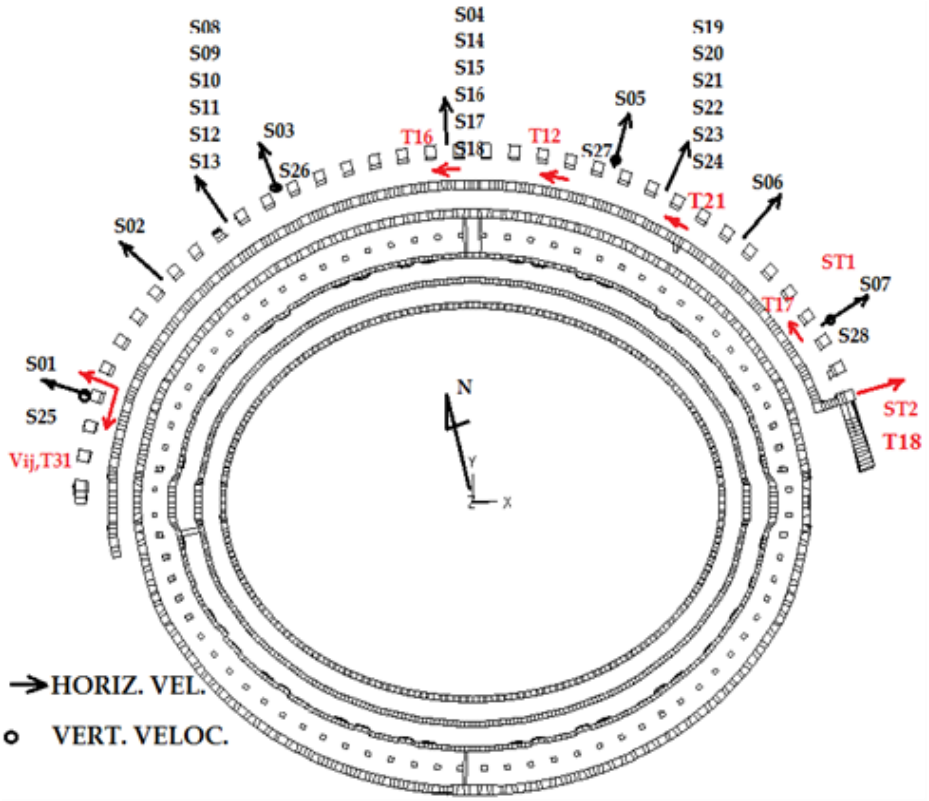

***Figure 1**. Plan Seismometers: 1st campaign (in black), 2nd campaign (in red).*

c) nine of them were kept in the horizontal radial directions at the top of the wall, S01÷S08, S19;

d) on the foundations, S13, S18, S24, VA1, VA2, VA3, S25÷S28;

e) on the middle height of the monument, S11, S18, S22, VA7, VA8, VA9;

f) on the middle height of the monument, in tangential directions T12, T16, T17, T18, T31;

g) at Valadier buttress, T17, T18, T31; in the directions radial VA3, VA6, VA9; tangential VA1, VA4, VA7; vertical VA2, VA5, VA8;

h) at the middle height, on Stern **buttress**, ST1, ST2.

The **buttress**es were built at different times respectively by the architect Valadier (West) and the architect Stern (East) in order to strengthen the existing structure damaged by seismic and historical events.

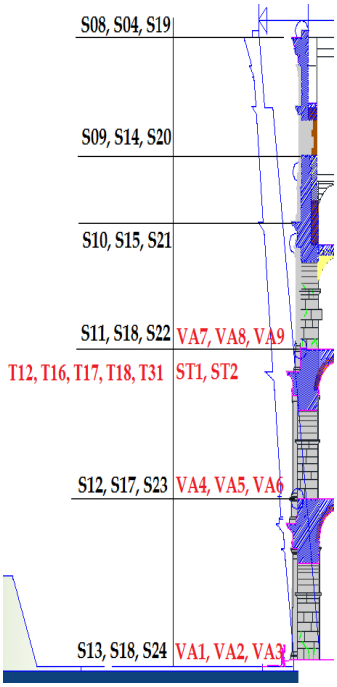

***Figure 2**. Section Seismometers: 1st campaign (in black), 2nd campaign (in red).*

2.2. Modal shapes

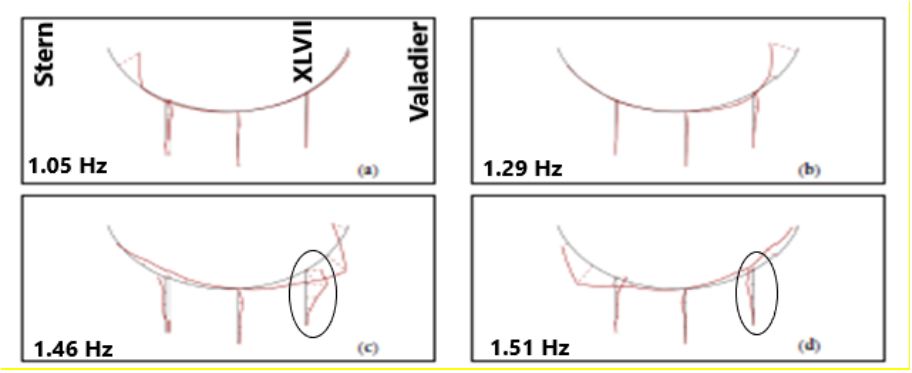

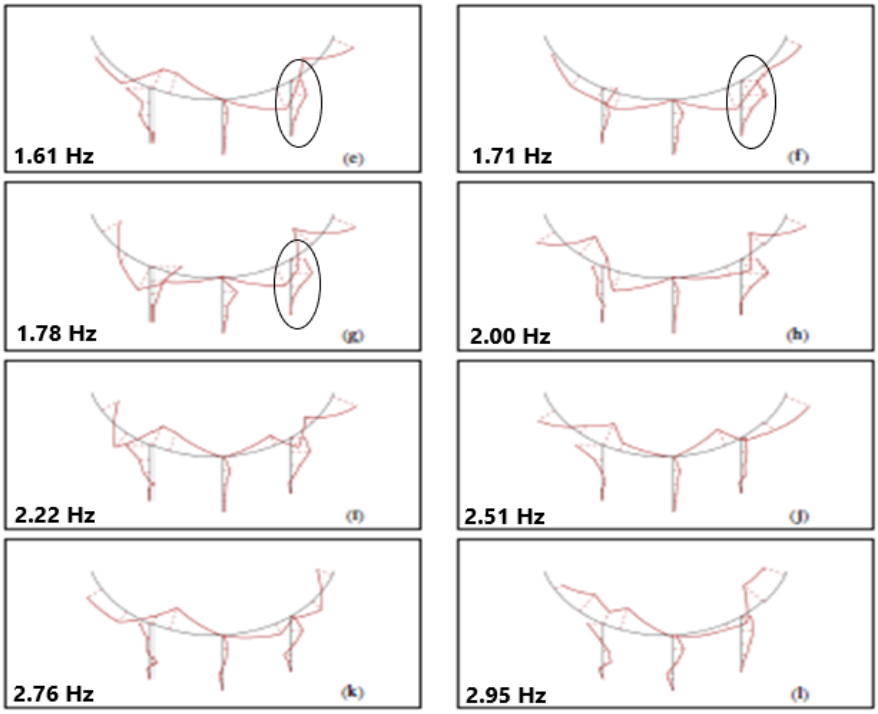

Figure 3. *Second campaign [5]. N. 12 Frequencies: 1.05, 1.29, 1.46, 1.51, 1.61, 1.71, 1.78, 2.00, 2.22, 2.51, 2.76, 2.95 Hz*

2.3. Power Spectral Density for velocities, from Metro B and C

The comparison between tests and analyses for PSD values are shown in the following Figures 4÷12 [(mm/sec)^2/Hz] x 10^{-4}:

4) radial values at top S01÷ S07;

5) radial values at vertical alignment C1, S08÷S13;

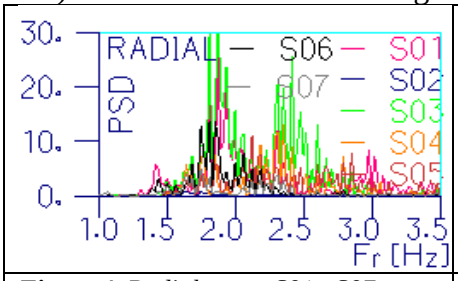

Figure 4. *Radial at top S01÷ S07*

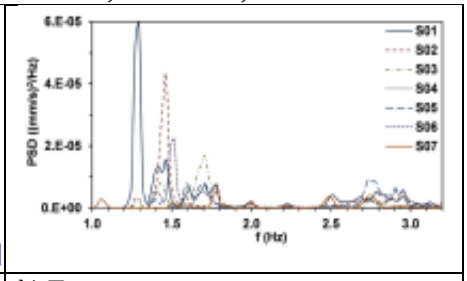

b) Tests.

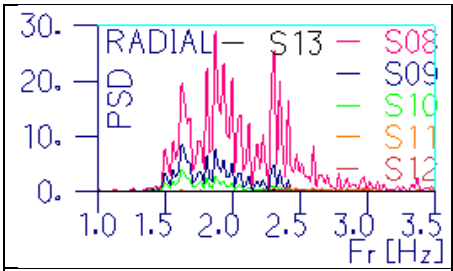

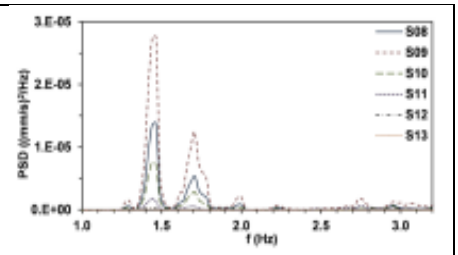

Figure 5. *Radial C1, S08÷S13.* b) Tests.

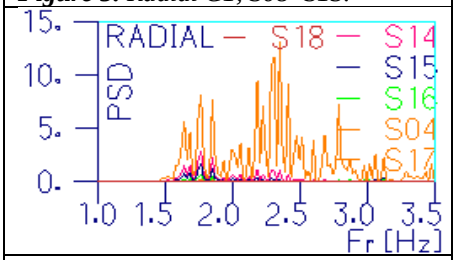

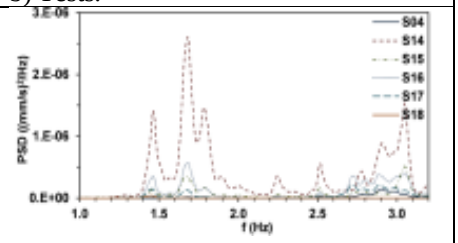

Figure 6. *Radial C2, S04, S14÷S18* b) Tests.

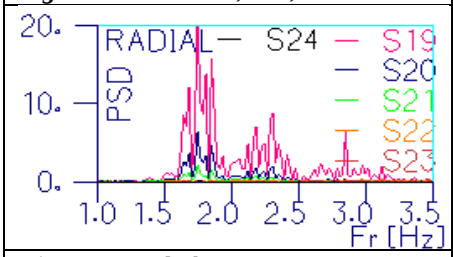

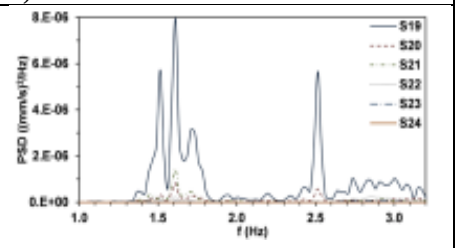

Figure 7. *Radial C3 S19÷S24* b) Tests.

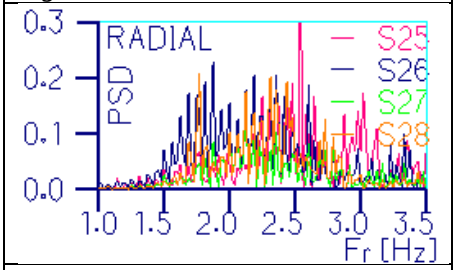

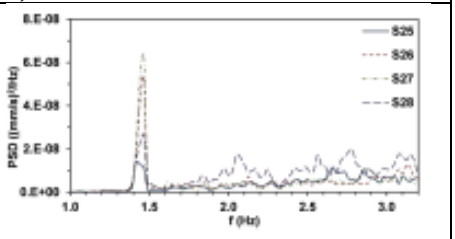

Figure 8. *Vertical basement S25÷S28.* b) Tests.

6) radial values at vertical alignment C2, S04, S14÷S18;
7) radial Values at vertical alignment C3 S19÷S24;

8) vertical values at basement S25÷S28; they show a very sharp peak at the frequency f1= 1.46 Hz is apparent at all the locations, while signals are much lower at the other components.

2.4. Vertical recordings at the wall basement

Furthermore, vertical values were much lower than the horizontal ones obtained on the basement in the other configurations.

In Figure 8 the PSDs of the vertical recordings are shown.

A very sharp peak at 1.46 Hz is apparent at all the locations, while signals are much lower at the other components.

2.5. The motion of the buttresses

The **first experimental campaign** pointed out significant vibrations at the top of the two **buttress**es in radial direction.

So, in the **second campaign**, a detailed analysis was carried out on this aspect.

Three triaxial were deployed along a vertical alignment in proximity of the Valadier's **buttress** (Figures 9, 10).

The results are shown in Figures:

9) tangential values at Valadier buttress VA1, VA4, VA7, the values of PSDs are almost equal to those in the radial direction;

10) radial values at Valadier buttress VA3, VA6, VA9; the values were almost equal to those in the tangential direction, in Figure 9; that this buttress cannot be considered as a rigid constraint for the wall; the PSDs peak at 1.29 Hz with the peaks at higher frequencies.

11) radial values at Stern buttress, at ST1, ST2.

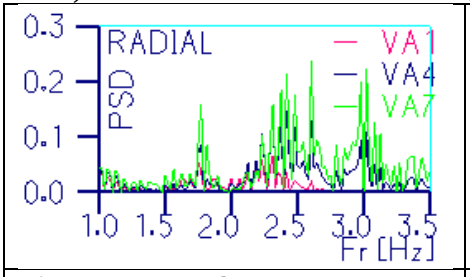

Figure 9. *Tang Val. VA1, VA4, VA7.*

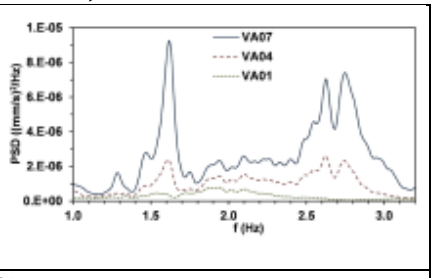

b) Tests.

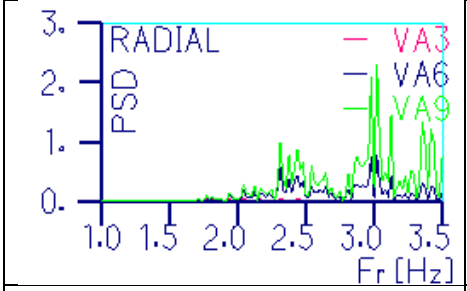

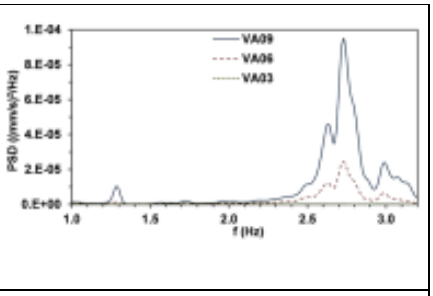

Figure 10. *Radial Val. VA3,VA6, VA9.* b) Tests.

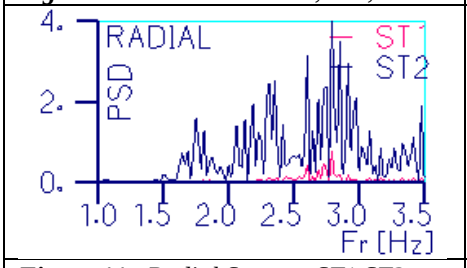

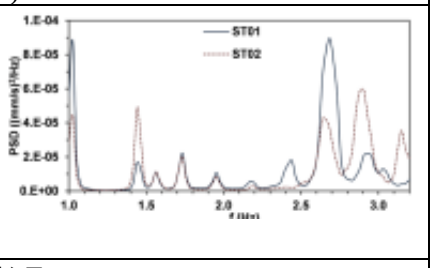

Figure 11. *Radial Stern at ST1,ST2.* b) Tests.

2.6. Tangential motion of the walls

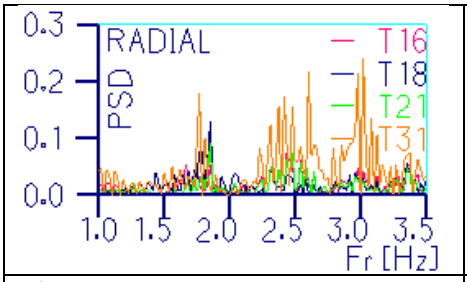

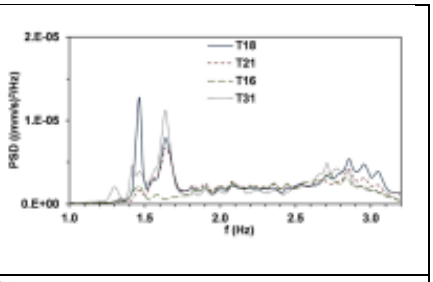

Figure 12. *Tang. T16, T18, T21, T31.* b) Tests.

It is apparent that tangential motion was much higher at the Valadier's **buttress** (T31) than at the Stern's **buttress**.

This occurrence confirms the lower stiffness of the Valadier's **buttress** in comparison with the Stern's **buttress**.

The main resonance frequency at the Stern's **buttress** is at 1.46 Hz, while at the Valadier's higher peak is at 1.61 Hz but also the already pointed out peaks are present.

The PSD of tangential values are shown in Figure 12, for the points T16, T18, T21, T31.

3. Signal processing by Uniroma1 [7], [9]

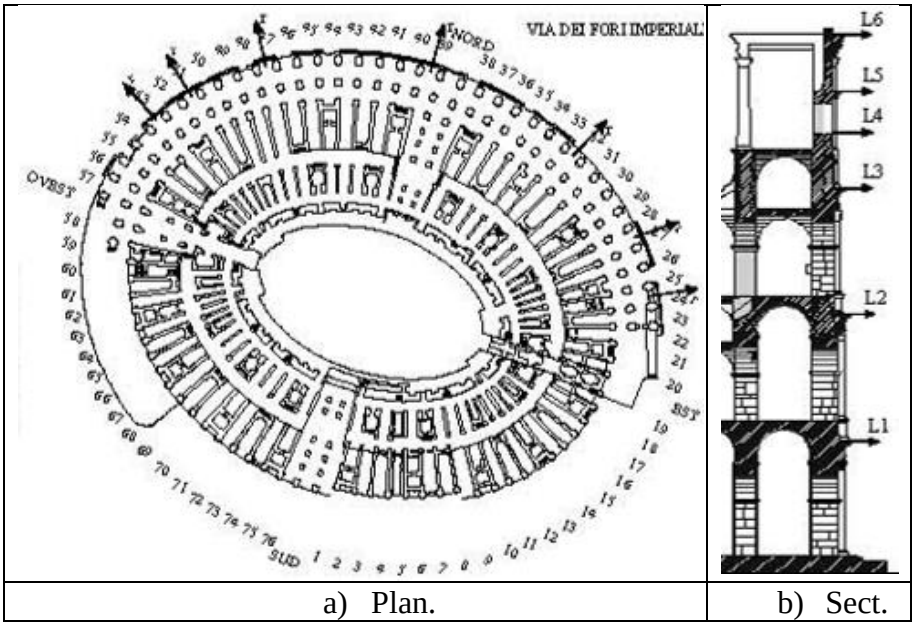

a) Plan. b) Sect.

***Figure** 13. Locations of the triaxial sets and radial accelerometers.*

3.1. Approximate numerical experimental modal comparison

Experimental modal analyses were performed [7]:

a) experimental, obtaining the frequencies of Table 2 at line 1

b) analytical, assuming the usual mechanical characteristics for integer walls of Table 1 at lines 1,2,3, obtaining a large scatter between the frequencies of Table 2, at lines 1 and 2.

That was considered due to the walls' damages, which produce Young moduli reduction

Then, we consider that for simple oscillator is $F=2\,\pi\,(K/M)^{1/2}$

The mean reduction coefficients are:

a) Frequency reduction = (ΣFanal/ΣFexp) = 2.055; as in Table 2 line 3;

b) Young modulus reduction $2.055^2 = 4.22$; as in Table 1, line 4. N. 4 materials are considered. No modal analytical displacements appear up to level L1, as in Figure 13.

Table 1. *Material mechanical characteristics.*

		Travertine	Masonry	Tuff	Concrete	
1	ρ	2400	1800	1800	2400	Kg/m^3
2	Einitial	20,000	5,000	8,000	8,000	MPa
3	ν	0.10	0.20	0.15	0.10	Poi
4	Efinal	4,700	1,200	1,900	1,900	MPa

Table 2*. The first six natural frequencies [Hz]*

		Freq	1	2	3	4	5	6
1		Fexp	1.03	1.30	1.49	1.60	1.66	1.75
2		Fanalysis1	2.32	2.34	3.12	3.17	3.58	3.62
3		Fanalysis2	1.13	1.14	1.52	1.54	1.74	1.76

3.2. Buttresses

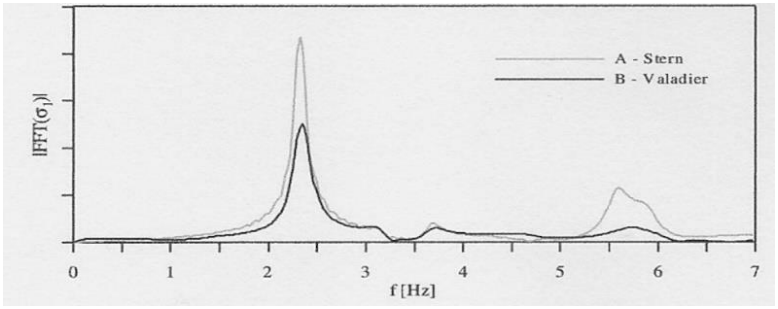

Figure 14a*. FFT of the maximum principal stress at points A and B, by tests [7].*

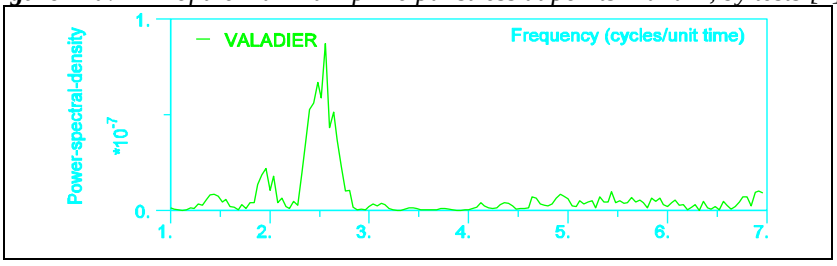

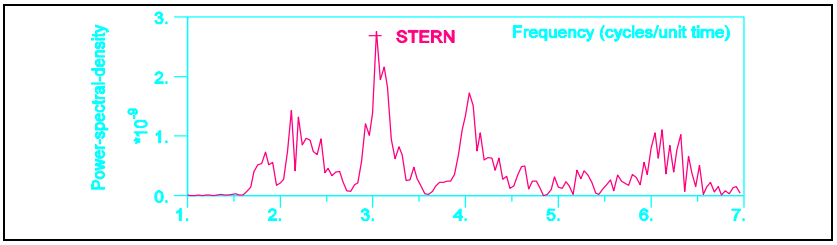

***Figure 14b**. FFT of the maximum principal stress at points A and B, by analysis [8].*

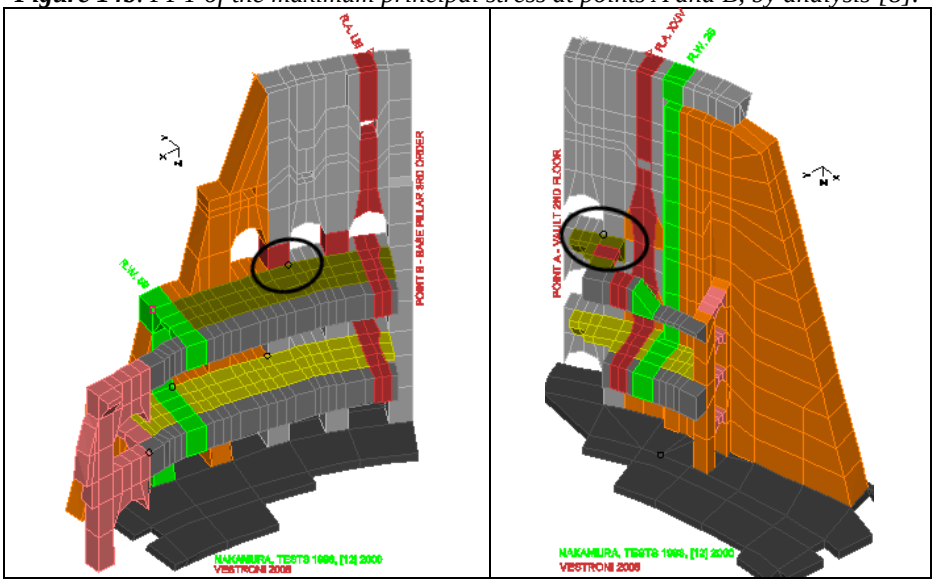

***Figure 15.** Measurement points on: B) Valadier Arcade LIX; A) Stern Arcade XXIV.*

The results showed that the parts of the structure with maximum principal stress, which are the most vulnerable areas of the monument, are:

the vaults of the second order near Stern's buttress, for the compressive stress (Point A),

the pillars of the third order near Valadier's buttress, on account of the flexural actions (Point B).

Both these points are located near the base of the third order, where the internal radial walls finish and the external annular wall is effectively free and behaves as a clamped plate.

The Fourier transforms of the maximum principal stress are shown in Figures 14a and 14b, they confirm that the first and second modes are mainly responsible for the maximum stress.

The amplitude of the response in the second mode is lower than that of the first mode, for buttresses Valadier and Stern respectively.

It is also evident from this analysis that the first two modes can represent two important control parameters for monitoring the health conditions of the structure.

3.3. Predominant frequencies

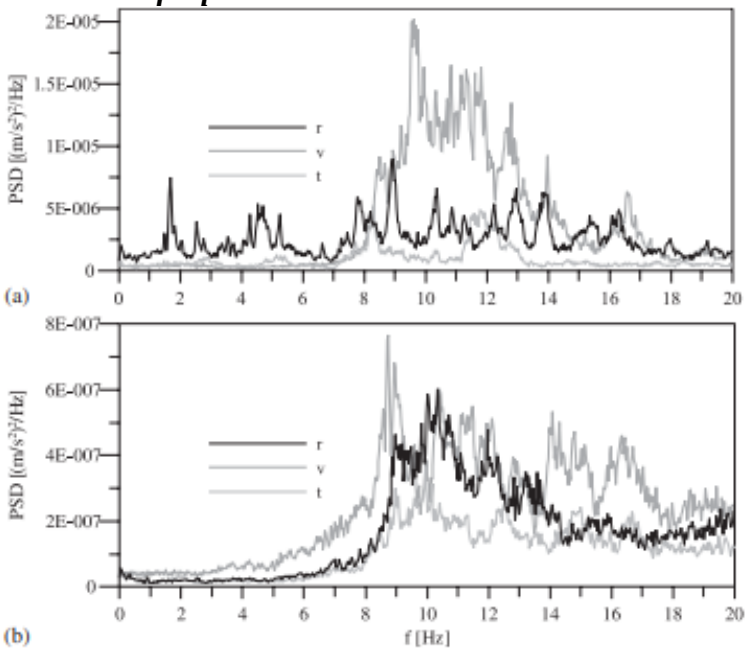

***Figure 15a**. PSDs of triaxial tests at level L4 (a) and base (b) [7].*

3.4. Identification of experimental modal parameters

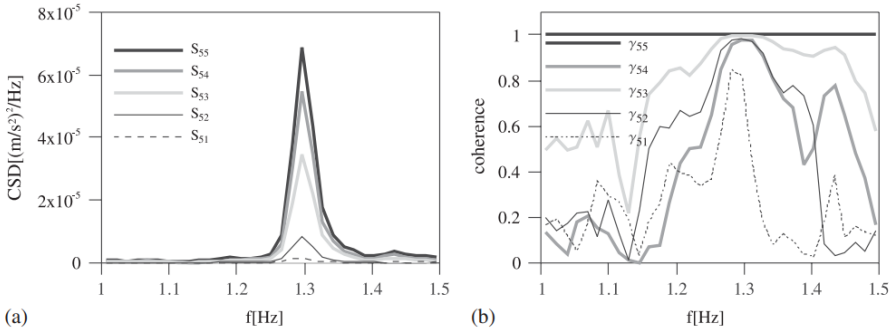

***Figure 15b**. Cross-spectral density magnitudes (a) and coherence (b) of the radial accelerations at arcade LIII, [7].*

3.5. Experimental and analytical model comparison and tuning

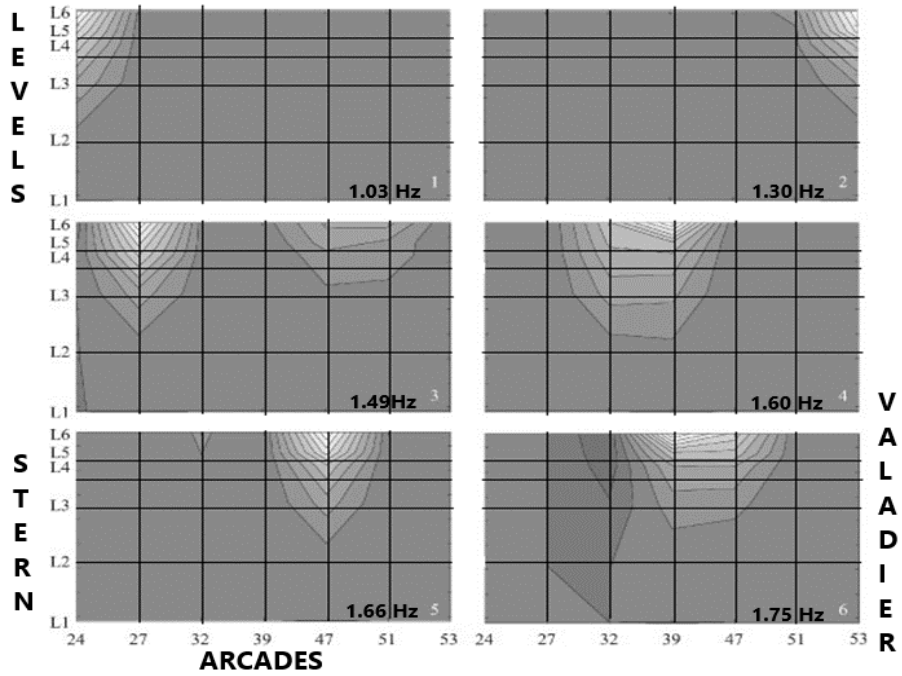

***Figure** 16. Contour plots of the radial components of the first six experimental mode shapes, on the unrolled northern wall [7].*

4. Comparisons of the tests

Some significant differences between two different Authors can be found.

Accurate 5% tests are indispensable for detecting damage to mechanical properties of 20%, and it would be considered that the above doubts could be resolved using other tests already carried out [7] and [8].

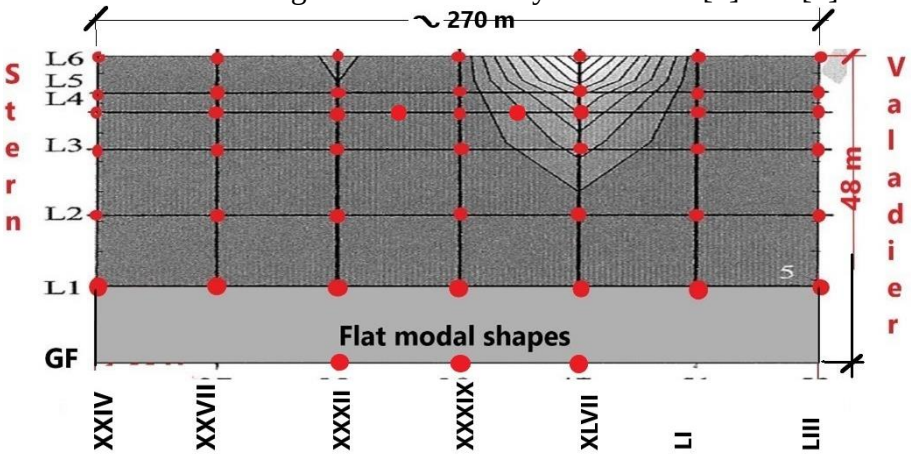

Figure 17. *N. 47 measurement points, for the unrolled northern wall. None at GF with flat modal shapes between GF and L1 [8], [7].*

"Traffic vibrations are induced by the stress waves generated by the vehicle–pavement interaction. Stress waves in the soil reach the foundations of buildings and cause them to vibrate ..Interaction with soil is not taken into account in this study and all degrees of freedom are restrained at the base … so that the soil–structure interaction is deemed of scant significance for the present analysis."

5. Dynamic characterization

With material characteristics derived from the literature, the natural frequencies appear too high.

A monolithic travertine specimen may have Young modulus over 30,000 MPa.

In order to arrive to natural analytical frequencies similar to experimental, it needs medium travertine Young modulus around 5,000 MPa.

But a homogeneous reduction, is not able to accurately reproduce modal shapes similar between tests and analyses.

Such strong reduction of Young moduli implies a variable reduction in all the rings and in all the walls.

5.1 Homogeneization

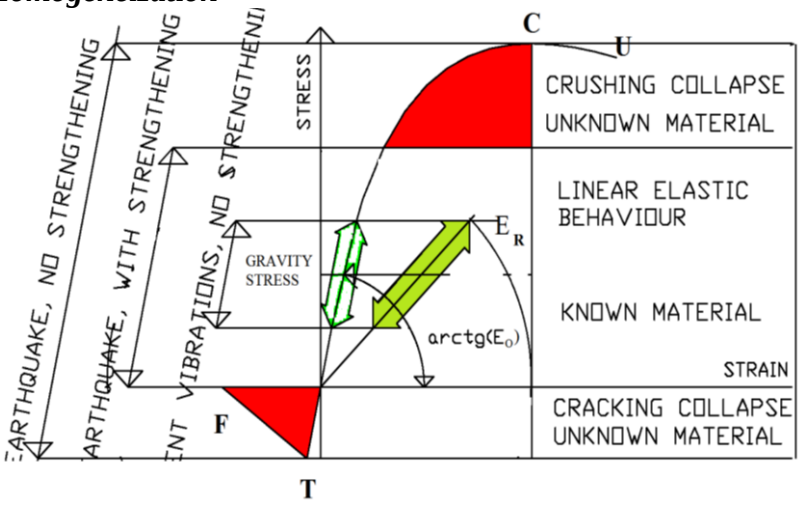

Figure 18. *Uniaxial stress-strain relationship for walls. Stresses' ranges: a) ambient vibrations $\Delta\sigma=\pm1/1000$;*

The model is assumed linear elastic, with the initial Young moduli, as in Figure 18.

The reduction of Young modules is due to the disconnections between bricks and to damages of the walls.

The homogeneized model is adopted, smearing the damages inside each group of F.E.

With exception of buttresses, we tried with more elasticity modules in outer northern wall:

a) unique value;

b) n. 32 for outer northern wall as in Figure 24a;

c) n. 64 for as in Figure 24b.

5.2 Methodology of the characterization

The Young modulus of a travertine brick is over 30,000 MPa, it is reduced of about $(6)^{1/2}$ for a damaged wall.
Such a strong reduction is due to the many stone blocks and to the many damages in time, it is natural to imagine that these damages are diffused with high variability.

5.3 Smeared Crack Band

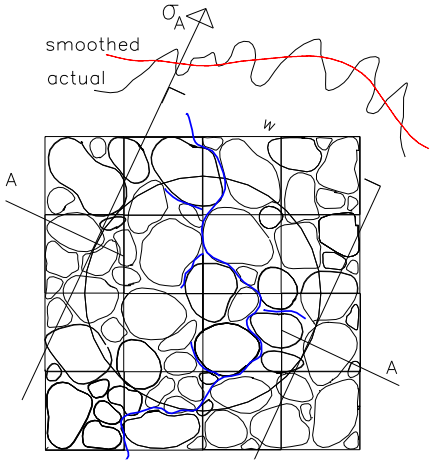

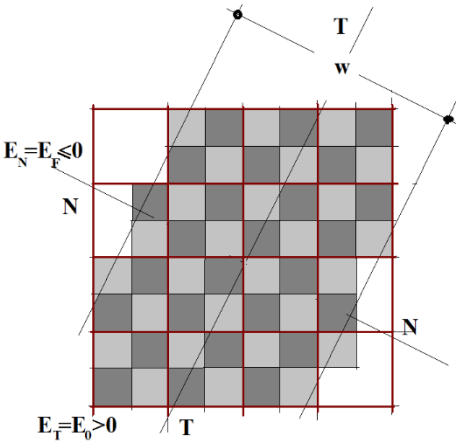

Figure 23.
1) "Crack Band Width", $w=6d_{MAX}$
2) "Smeared Crack Band". Orthotropic Symmetric Matrix

The Mechanics of concrete already consolitated the two methodologies of :

a) "Homogeneization of concrete",

b) "Smeared Crack Band", The principal researchers in this field are K. J. Bathe (orthotropic, hypoelastic) [14], Z. Bažant (plastic-fracturing, endochronic, microplanes, non-orthotropic, fracture, aggregate interlock) [11], Technical University of Delft (Blaweendradt, Hillerborg, Walraven, Reinhardt, Rots, Van Mier) [10].
The "Smeared Crack Band" is adopted since the Mörsch frame of one century ago; but for F.E. model, the "Smeared Crack Band" was better defined by Bazant et alii [12], [13].

5.4 Chess model for northern wall

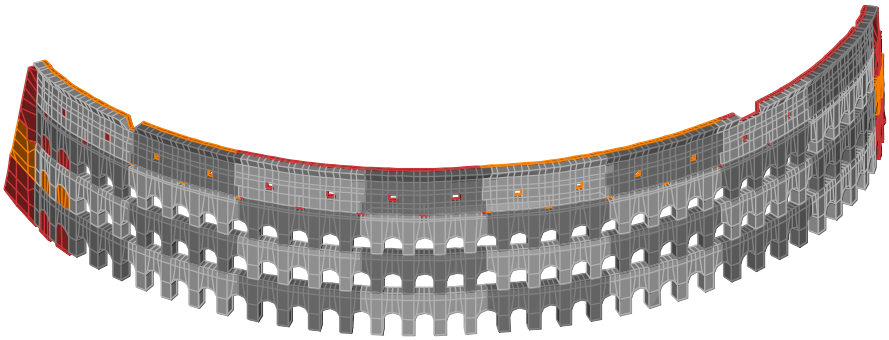

Figure 24a. *Ring4, Travertine wall (n. 32 different elasticity modules). Size 12.00 x 27.00 x (1.50÷3.50) m.*

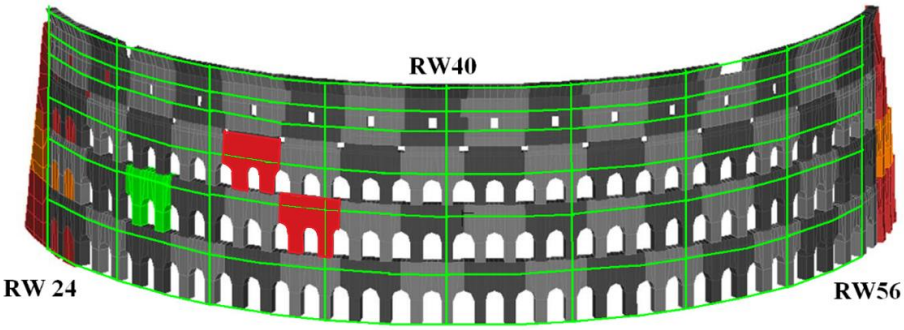

Figure 24b*. Ring4, with (8x16=64) elasticity modules. Arcades 24, 28, 32, 36, 40, 44, 48, 52, 56, 58, at levels (Z=0.00/ 10.55/ 22.29/ 33.84/ 39.00/ 41.51/ 48.02 m)*

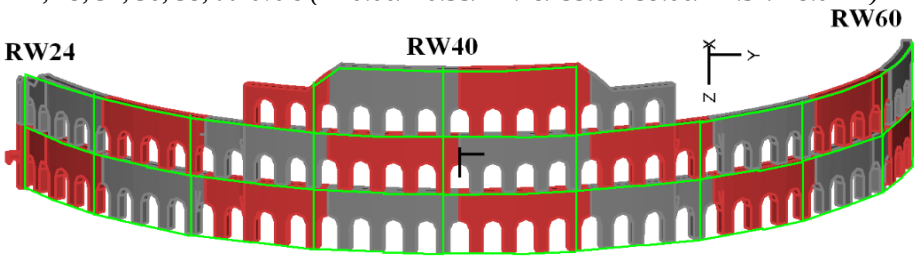

Figure 24c. *Ring between 3 and 4, Z_{SUMMIT}=23.96, 32.08, 37.50, N. (10 x 5)= 50 points. Arcades 24, 28, 32, 36, 40, 44, 48, 52, 56, 60, at levels (Z=0.00/ 12.47/ 23.96/ 32.08/ 37.50 m)*

For the best fitting between test and analysis, for the n. 7 natural modes, for shapes and frequencies, we must use different zones in the walls with different Young moduli, as in Figures 24÷25.

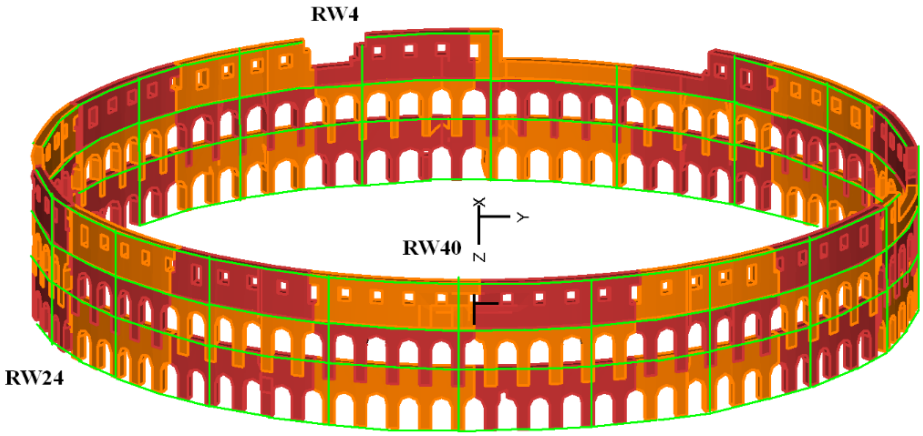

Figure 24d.. *Ring3, Z_{SUMMIT}=24.14, 29.84, N. (20 x 4)=80 points. Arcades 4, 8, 12, 16, 20, 24, 28, 32, 36, 40, 44, 48, 52, 56, 60, 64, 68, 72, 76, 80, For levels (Z=0.00/ 12.47/ 23.96/ 29.84 m)*

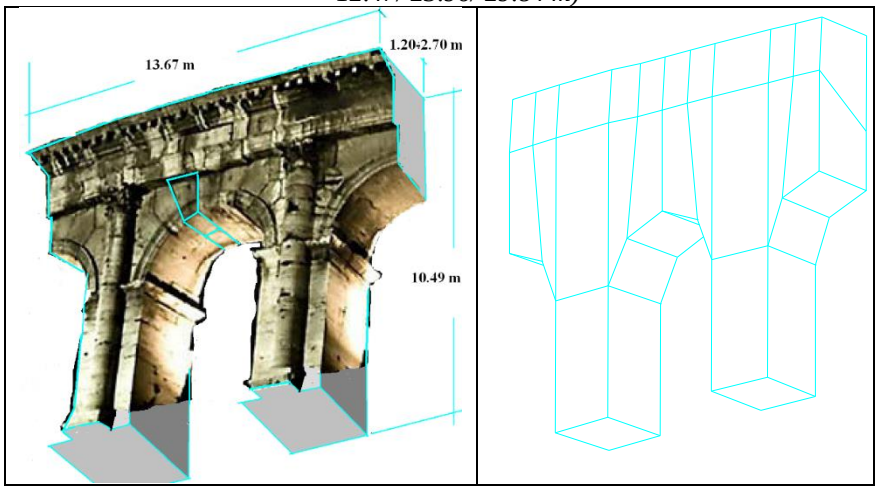

Figure 25. *Wall homogeneization.*

6. Uses of the Modal Assurance Criterion MAC [6]

The historical development of the modal assurance criteria originated from the need for a quality assurance indicator for experimental modal vectors that are estimated from measured frequency response functions. The standard of the late 1970s, when the modal assurance criterion was developed, was the orthogonality check.

Table 3. *MAC coefficients for perfect fitting between analytical and experimental mode shapes.*

a/e	1	2	3	4	5	6
1	1.00	0.0	0.0	0.0	0.0	0.0
2	0.0	1.00	0.0	0.0	0.0	0.0
3	0.0	0.0	1.00	0.0	0.0	0.0
4	0.0	0.0	0.0	1.00	0.0	0.0
5	0.0	0.0	0.0	0.0	1.00	0.0
6	0.0	0.0	0.0	0.0	0.0	1.00

The experimental and analytical radial modal displacements were normalised with their maximum values equal to zero, in the n. 42 test points.

Table 4*. Scatter between frequencies experimental [7] and analysis [8] [Hz].*

	1	*2*	*3*	*4*	*5*	*6*	*7*
Fanalysis	*1.01*	*1.236*	*1.478*	*1.585*	*1.598*	*1.740*	*2.848*
Fexperimental	*1.03*	*1.30*	*1.49*	*1.60*	*1.66*	*1.75*	*2.76*
Scatter %	*1.98*	*5.12*	*0.81*	*0.94*	*3.88*	*0.58*	*3.14*

The accuracy of the characterization may be obtained from the comparison between shapes and frequencies.
The first two modes are clearly identified, as appears from the high value of their MAC coefficients.

6.1. Use of MAC in the present situation by DISS

Table 5*. Modal participation factors* [8]

Mode	1	2	3	4	5	6	7
Γx	264.97	-19.45	-169.48	-11.57	-56.64		
Γy	30.35	-10.81	-80.66	22.94	48.68		
Γz	-8.88	-52.09	29.44	-14.60	-501.41		

We are referred to experimental data by [7] because it furnishes the values of modal shapes, admitting that the level curves are equally distanced.
Beside this, appears some differences with respect to [8], [7].

In an unrolled surface having dimensions ≈250x48 m, all the three components of the modal shape are important, radial tangential and vertical; all these components are obtained by analysis, but the tests consider the radial alone.

The elasticity reduction of Young moduli is due to the disconnections between bricks and to damages of the walls.

The homogenised model is adopted, smearing the damages and the disconnection inside each group of F.E.

The Figures 26÷32 show the comparison between tests and analyses, the former shows the vertical components too, in red.

In order to compare analytical and experimental mode shapes, all the values of the modal assurance criteria (MAC) [6] between analytical and experimental mode shapes were calculated (Table 6).
The first two modes are clearly identified, as appears from the high values of their MAC coefficients.

Table 6. *MAC coefficients for perfect fitting between analytical [8] and experimental mode shapes [6].*

a/e	1	2	3	4	5	6	7
1	0.97	0.10	0.27	0.03	0.01	0.03	0.05
2	0.10	0.90	0.11	0.02	0.00	0.06	0.11
3	0.14	0.12	0.85	0.23	0.49	0.51	0.17
4	0.12	0.05	0.28	0.72	0.64	0.50	0.31
5	0.13	0.02	0.69	0.20	0.71	0.62	0.21
6	0.15	0.09	0.37	0.47	0.45	0.41	0.37
7	0.04	0.08	0.32	0.12	0.37	0.18	0.72

6.2. Accuracy

For shapes, by diagonal of MAC matrix, the scatters are:
S_i=(1-MACii), (i=1, n),

[DSi = 0.03, 0.10, 0.15, 0.28, 0.29, 0.59, 0.28]

For frequencies, the scatters are:

[DFi= 1.98, 5.12, 0.81, 0.94, 3.88, 0.58, 3.14]

We need to minimize the total standard deviation by DSi and DFi.

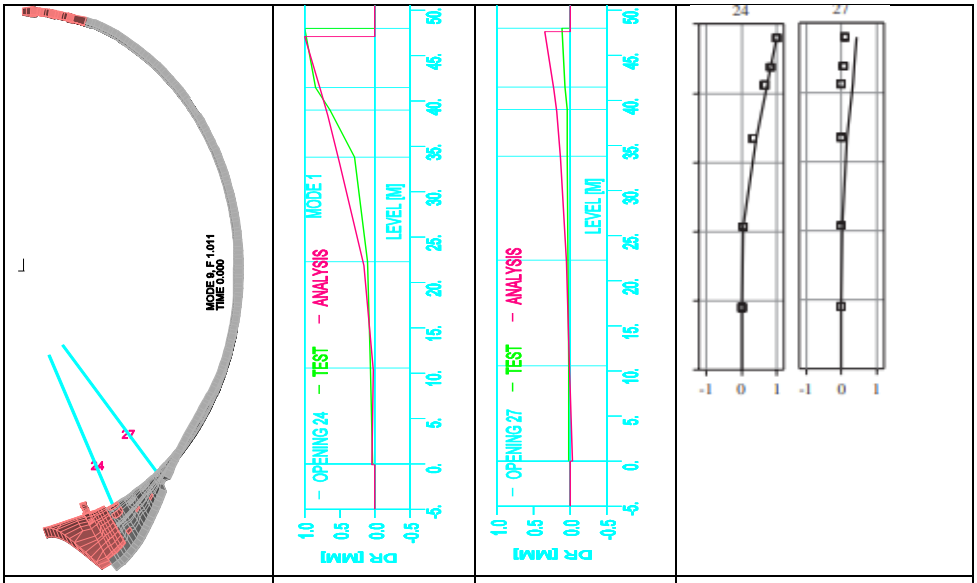

Analysis, Fr=1.01 Hz	*XXIV*	*XXVII*	*[7]*

Figure 26. *Comparison for mode 1: (-------) test; (-------) analysis.*

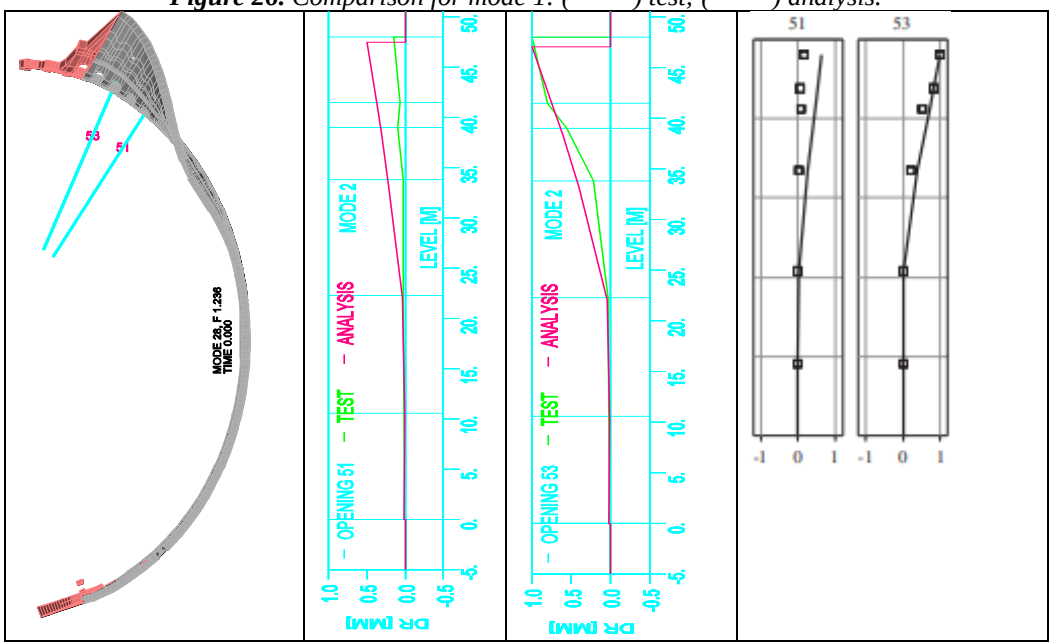

Analysis, Fr=1.236 Hz	LI	LIII	[7]

Figure 27. *Comparison for mode 2: (-------) test; (-------) analysis.*

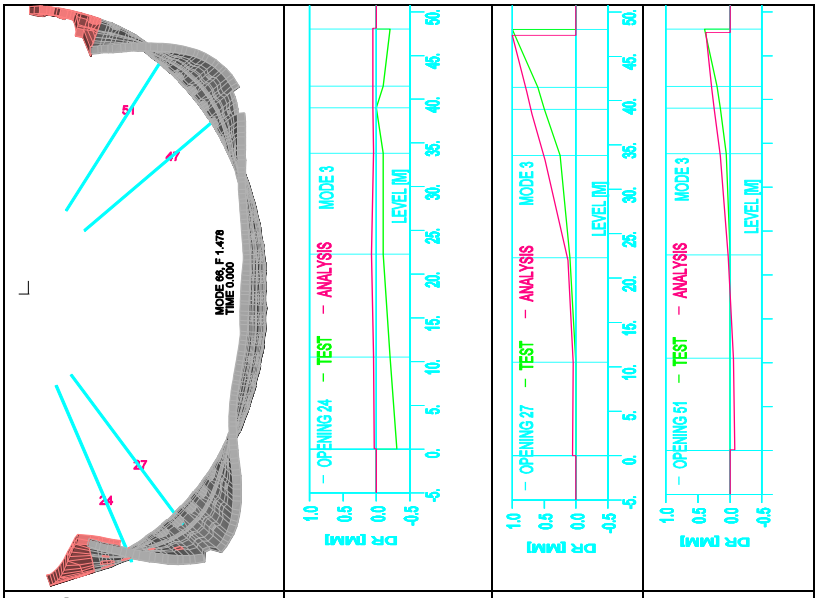

Analysis,Fr=1.478 Hz	*XXIV*	*XXVII*	*LI*

Figure 28. *Comparison for mode 3: (-------) test; (-------) analysis.*

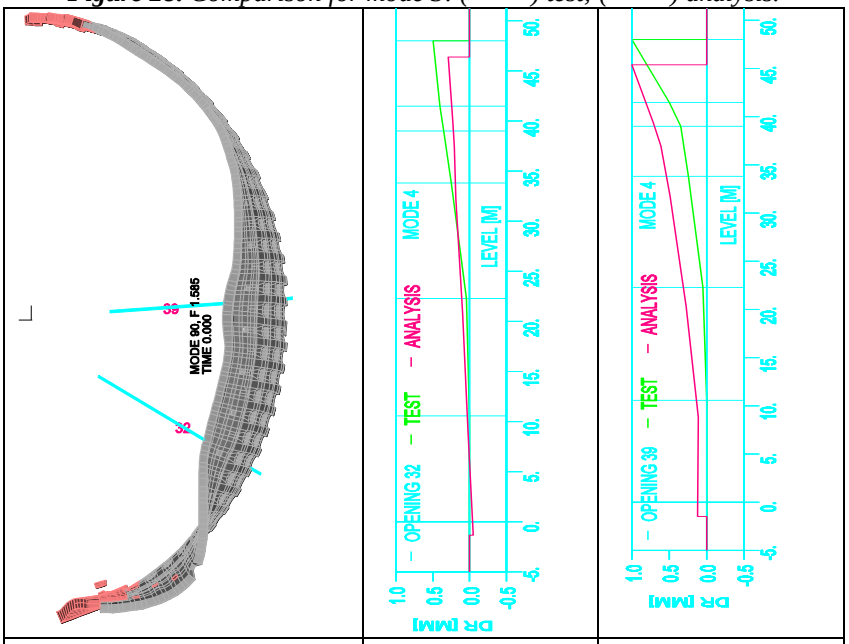

Analysis, Fr=1.585 Hz	*XXXII*	*XXXIX*

Figure 29*. Comparison for mode 4: (-------) test; (-------) analysis.*

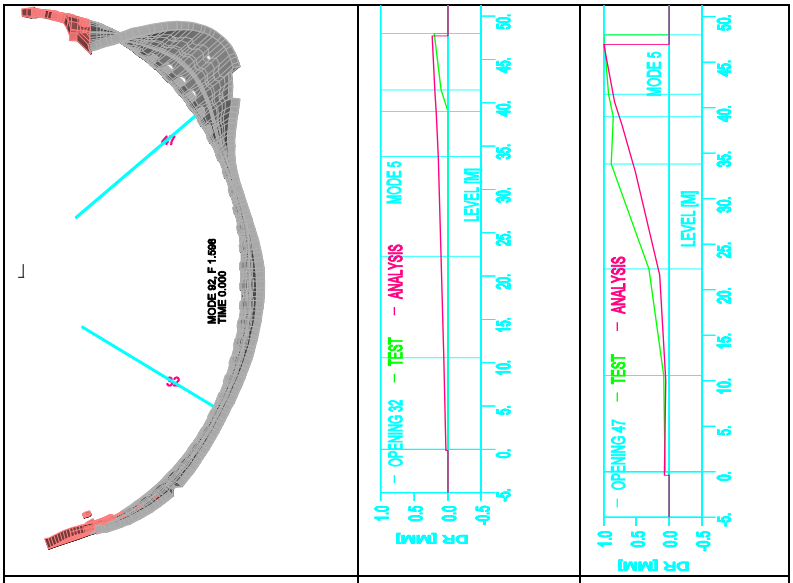

Analysis, Fr=1.598 Hz	*[2], XXXII*	*[1] 1.70 Hz*

Figure 30. *Comparison for mode 5: (-------) test; (-------) analysis. [2], 1.70 Hz*

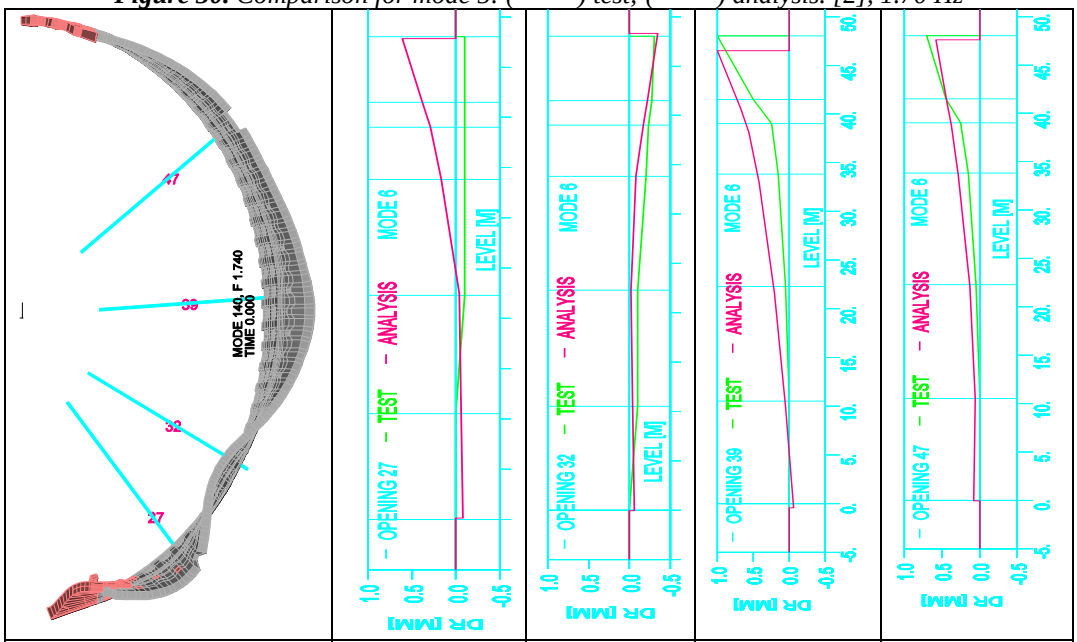

Analysis, Fr=1.740 Hz	*XXVII*	*XXXII*	*XXXIX*	*XLVII*

Figure 31. *Comparison for mode 6: (-------) test; (-------) analysis.*

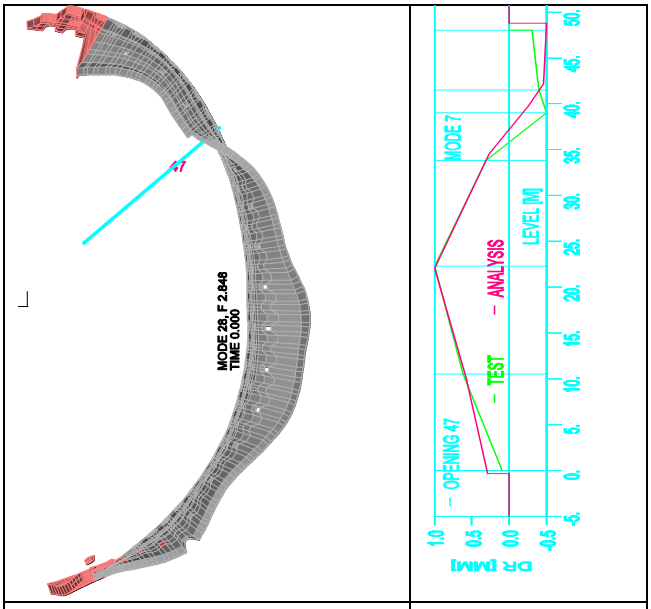

Analysis, Fr=2.848 Hz	*[1], [8] 2.75 Hz*

Figure 32. *Comparison for mode 7: (-------) test; (-------) analysis. [2] 2.80 Hz.*

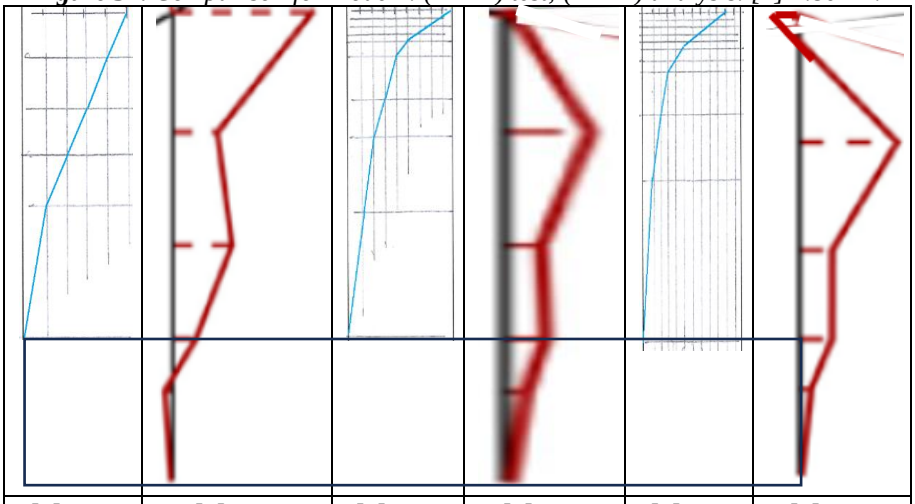

[7] 1.60	[5] 1.61	[7] 1.60	[5] 1.61	[7]1.75	[5] 1.78
XXXII		XXXIX		XXXIX	

Figure 33a*. Mode shapes comparison on arcades XXXII and XXXIX.*

Effectively, the monument is fixed at the level L1 because the tangential and vertical components are disregarded, and the radial component is nihil, why seven instruments are present at the level L1?

Comparisons are made at arcades XXXII, XXXIX and XLVII, and in the frequency range 1.46÷1.78 Hz, as in Figures 33 a, b.:

1) no flexus are present for [7], and flexus is every time present for [5],

2) between GF and L1, every time the diagrams are flat for [7], different from zero for [5].

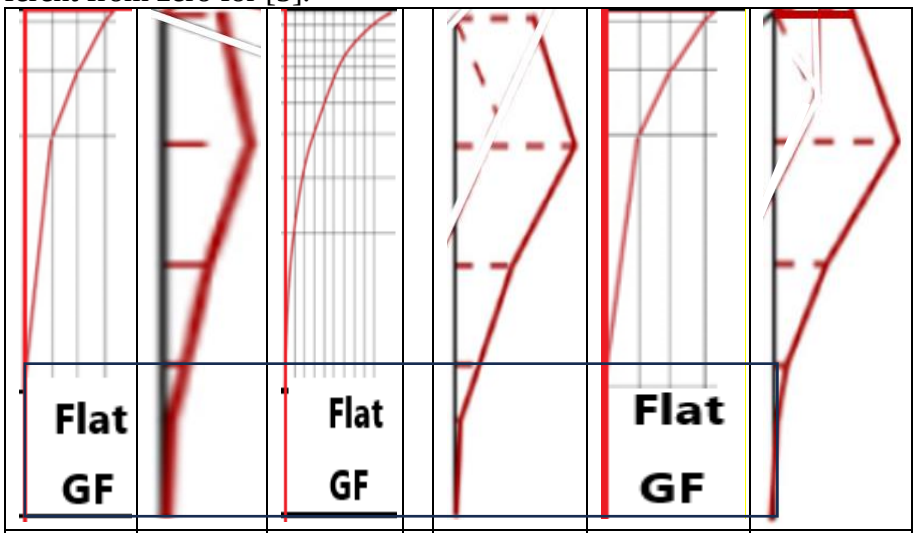

[7] 1.49	[5] .51	[7] 1.66	[5] 1.71	[7] 1.75	[5] 1.78
XLVII			XLVII	XLVII	

***Figure 33b**. Mode shapes comparison on arcade XLVII.*

7. Tests by Nakamura

7.1. Amplification factor [4]

From spectral ratios of each point, where measurements were done simultaneously, different peaks caused by different modes of the structure were found. Figure 34 shows the distribution of amplification factor (A) for simultaneously measured points at ground and upper floor levels at 1.5 Hz frequency.

As we can follow, there are no peaks for the points from 6 to 25 (location of these points are shown in Figures 1÷3). For both first and second floor levels, 1.5 Hz peak with amplification factor about 4.5 in radial (R) and 3.5 in transversal (T) direction starts from the point 25 on the outer wall. This point is the one which is connected with the supporting triangular wall. Peaks continue till point 60 which outer wall ends.
Amplification is high along the radial direction for many points of outer wall. This can be concluded as 1.5 Hz vibration is caused by the effect of outer wall. This can be concluded as 1.5 Hz vibration is caused by the effect of outer wall.
Similarly Figure 35 shows distribution of A for about 3 Hz. For the first floor, amplification factor having the value of 13 in radial component is high especially for the beginning and the ending points of the outer wall which starts from 25 and continues till 60. There are no strongly amplified points at upper floor levels for this frequency.
Amplification in radial direction for the first floor is about three times bigger than the transversal direction for point 25 and 60. This can be concluded as, structure is weak for the effects coming from the radial direction. Although triangularly shaped supporting wall supports the system in transversal direction, the wall is weak to the motion at radial direction. Figure 36 shows that at 4.5 Hz in radial direction, amplification on the first-floor level is high at points 15, 25 and especially at 70 having a value of 16. Amplification at this frequency for the upper floor levels is small.

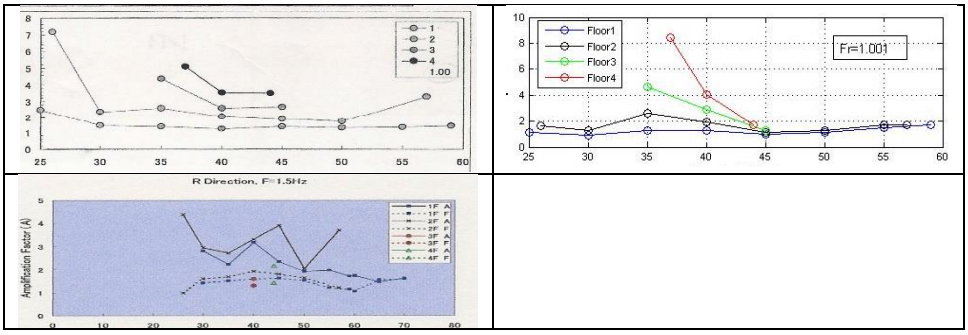

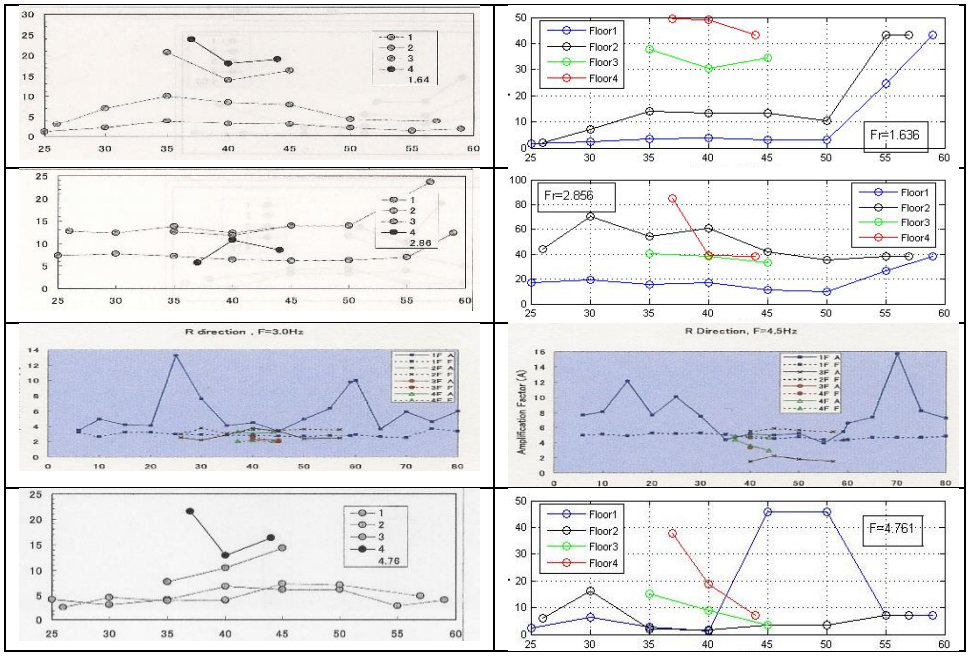

***Figure 34**. Amplitude vs Radial Wall, Ring n. 4.*

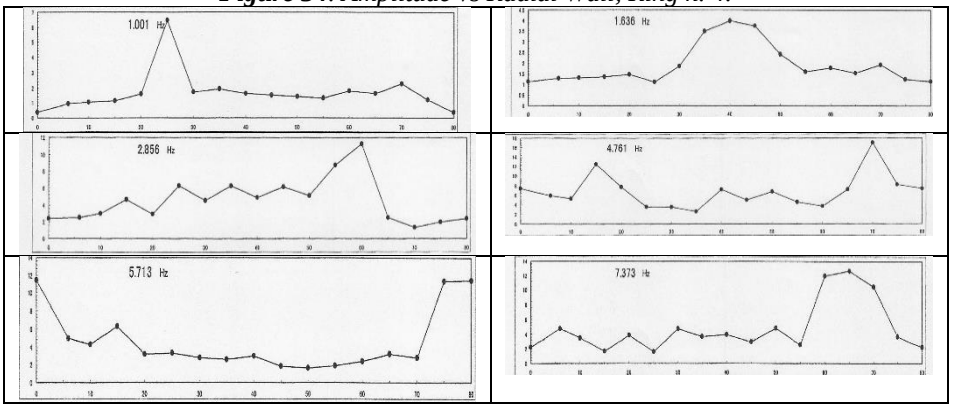

***Figure 35**. Amplitude vs Radial Wall, Ring n. 3, radial direction, by tests.*

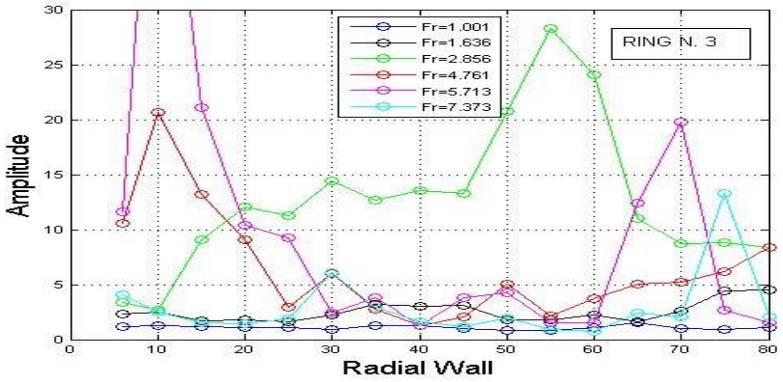

***Figure 36**. Amplitude vs Radial Wall, Ring n. 3, radial direction, by analysis.*

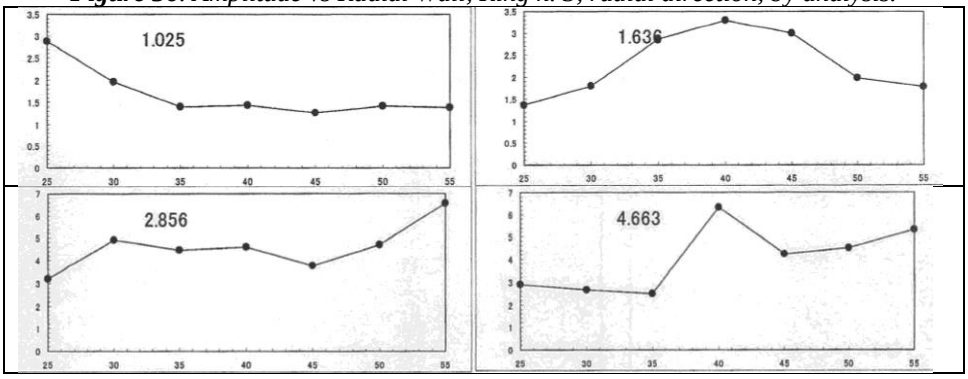

***Figure 37**. Amplitude vs Radial Wall, Ring n. 2, radial direction, by tests.*

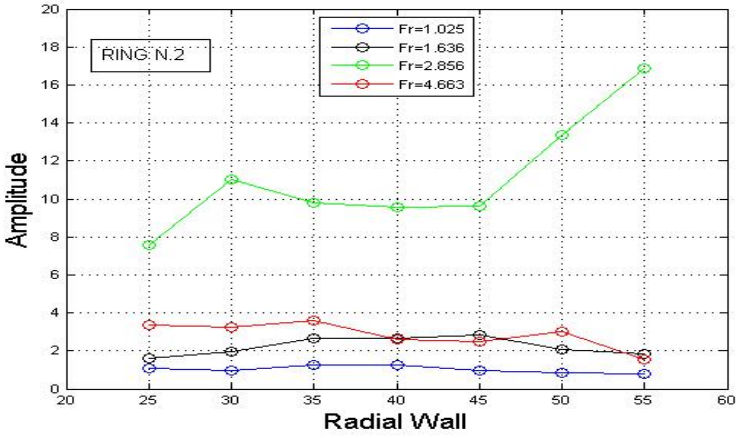

***Figure 38**. Amplitude vs Radial Wall, Ring n. 2, radial direction, by tests.*

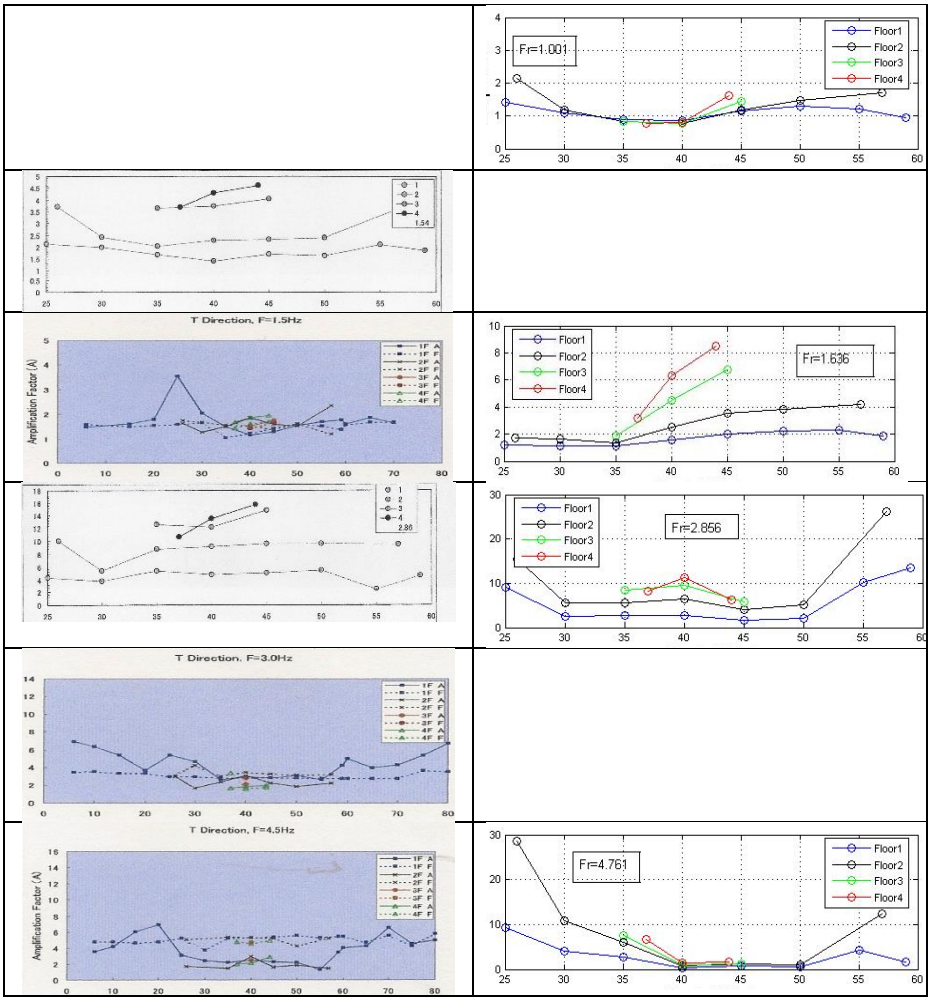

***Figure 39**. Amplitude vs Radial Wall, Ring n. 4. Tangential direction,*

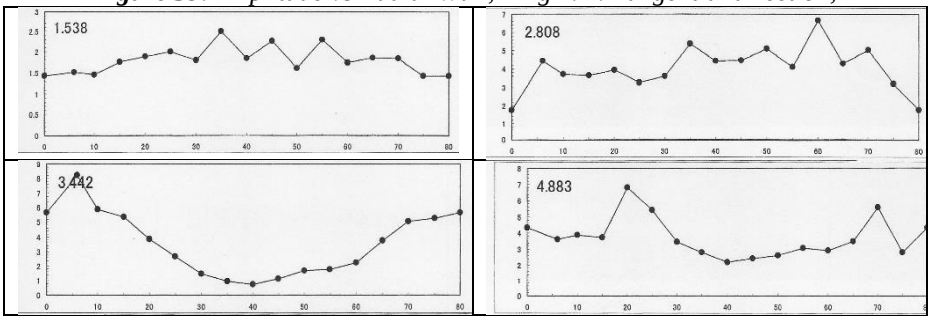

***Figure 40**. Amplitude vs Radial Wall, Ring n. 3Tangential direction, by tests.*

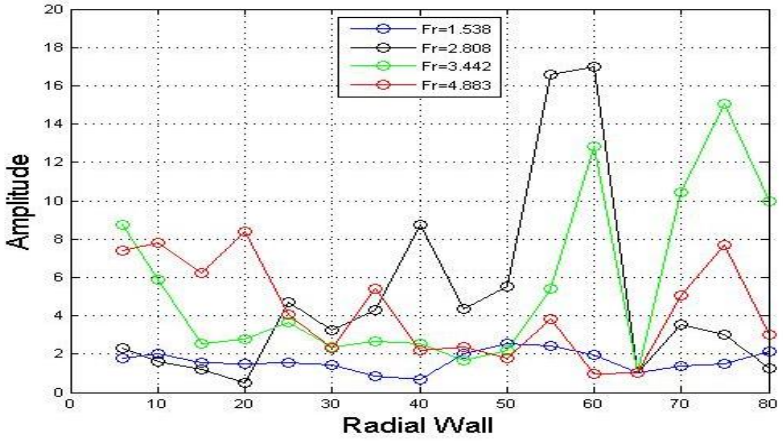

***Figure 41**. Amplitude vs Radial Wall, Ring n. 3. Tangential direction, by analysis.*

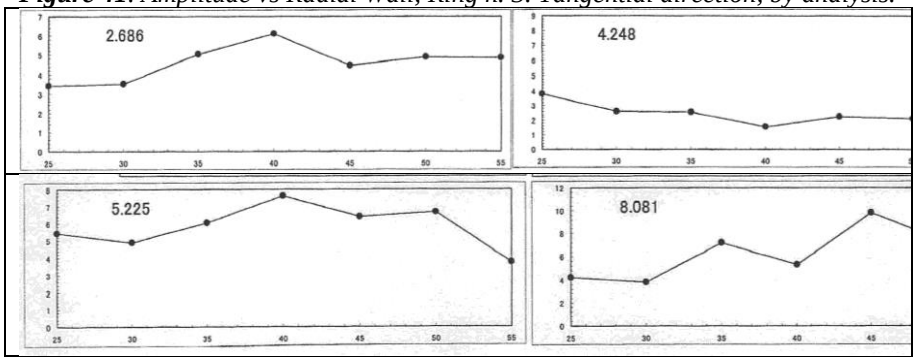

***Figure 42**. Amplitude vs Radial Wall, Ring n. 2, Tangential direction, by tests.*

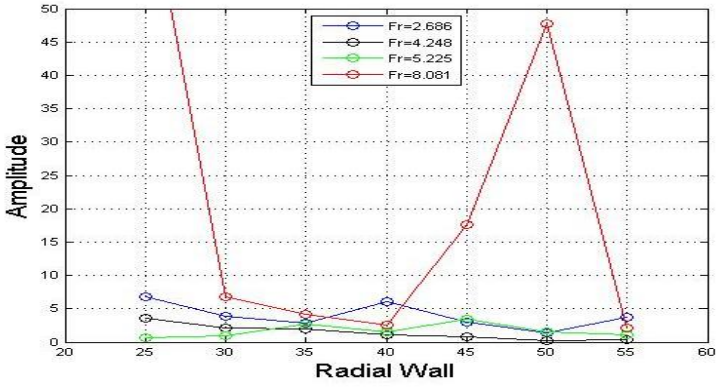

***Figure 43**. Amplitude vs Radial Wall, Ring n. 2, Tangential direction, by analysis.*

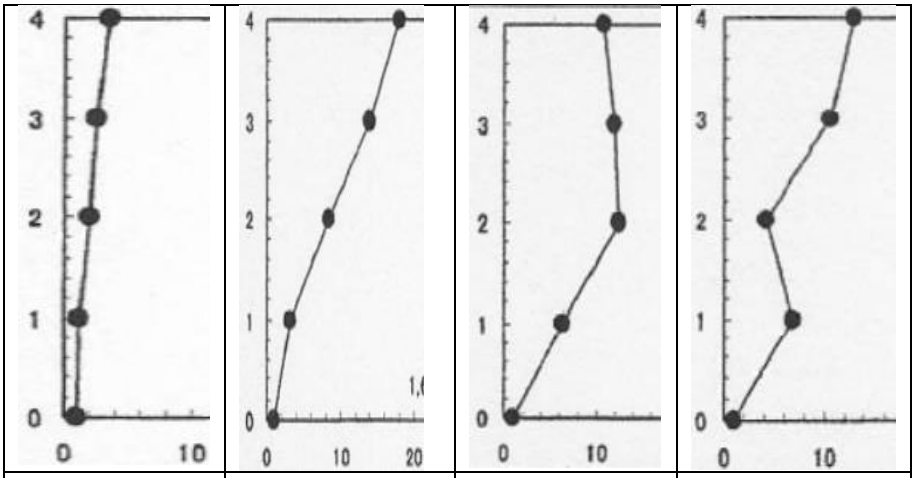

1.01 Hz	1.636 Hz	2.856 Hz	4.761 Hz

Figure 44. *Amplification factors for pillar #40 [4].*

7.2 Vulnerability index

The vulnerability index, K_{Tj} values are also calculated from the equation (10).

Figure 45 shows the distribution of K_{T1} values on the first floor at inner wall through the whole ring, for 1.5 Hz. This distribution shows the vulnerable points. High K values at points 25, 30, 40, 55, 60 in figure 45, also shows that these points have higher risk of damage for inner wall.

Figure 46 shows K_{T1} values again for the first floor but outer. In outer wall, having a value of 110, K value is extremely high at point 25 showing the weakness of this point.

Similarly figure 47 shows the distribution of K_{T2} values for second floor for 1.5 Hz. At this figure, points 26 and 59 have K value as 150 and 60 respectively, again showing the high risks at these points. K_{Tj} values are also calculated for 3.0 Hz. frequency and shown in figure 48, 49 and figure 50 for first and second and fourth floor levels, respectively.

Similar with 1.5 Hz frequency, figure 49 shows high values of K at points 25 and 59. In figure 50, K values are not high for second floor, comparing with 1.5 Hz frequency. And finally Figure 50 shows K_{T4}

values for 3.0 Hz. At this level, point 40 has higher risk than the other points.

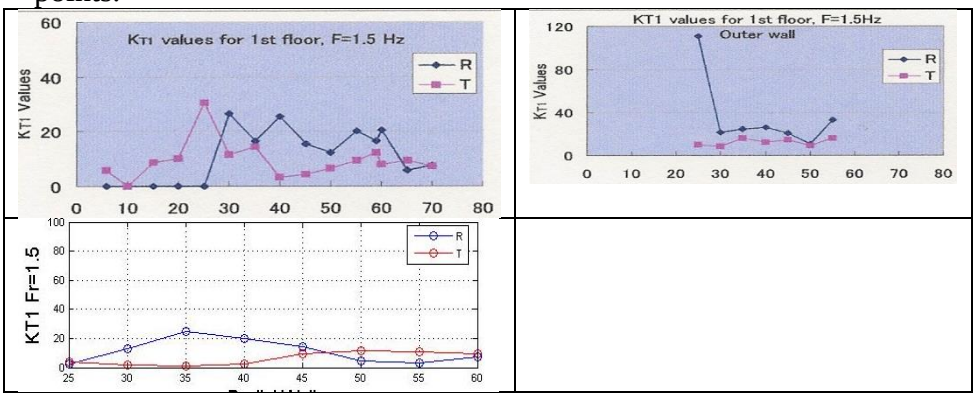

Figure 45. *KT1, 1st floor, inner Ring, F=1.5 Hz.*

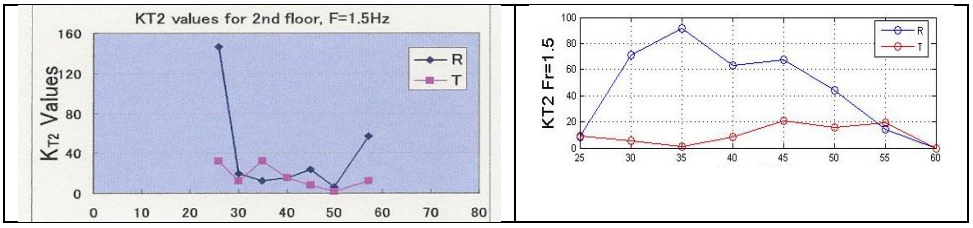

Figure 46*. KT2 Fr=1.5, 2.nd Floor, outer wall*

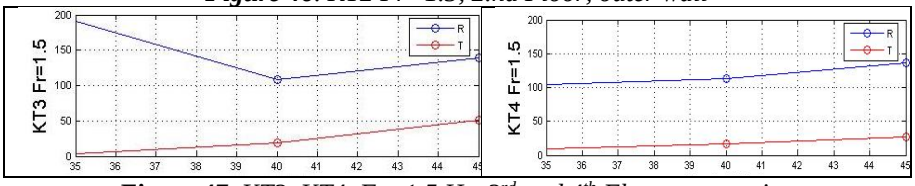

Figure 47*. KT3, KT4, Fr=1,5 Hz, 3rd and 4th Floors, outer ring*

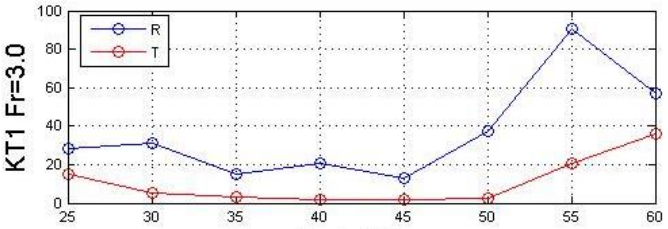

Figure 48*. KT1, Fr=3.0, 1st Floor, outer ring.*

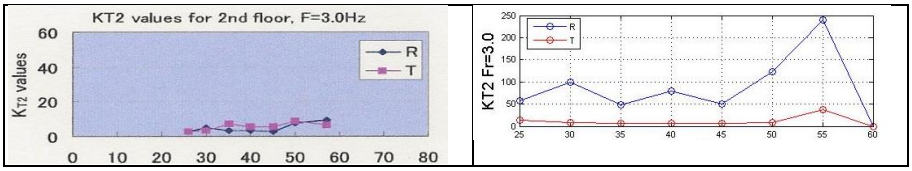

***Figure 49**. KT2, Fr=3.0 Hz, 2nd Floor, outer ring*

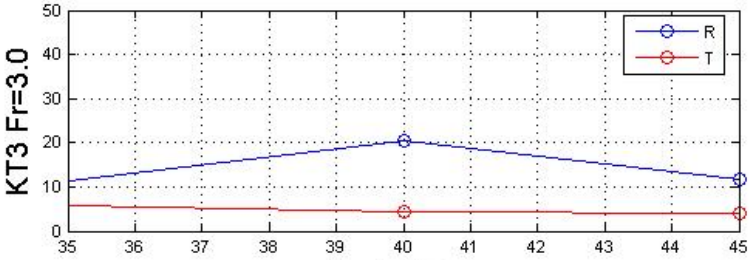

***Figure 50**. KT3, Fr=3.0 Hz, 3rd Floor, outer ring*

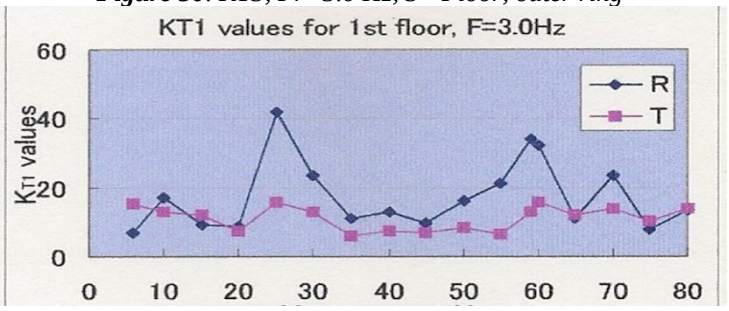

***Figure 51.** KT1, 1st floor, inner Ring, F=3.0 Hz*

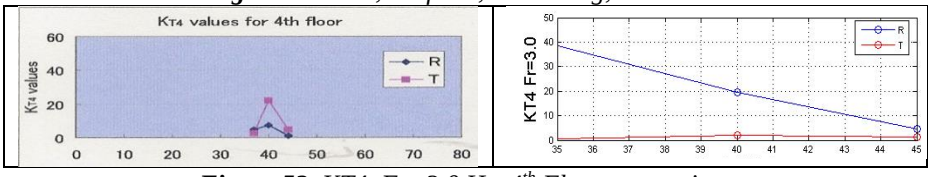

***Figure 52**. KT4, Fr=3.0 Hz, 4th Floor, outer ring.*

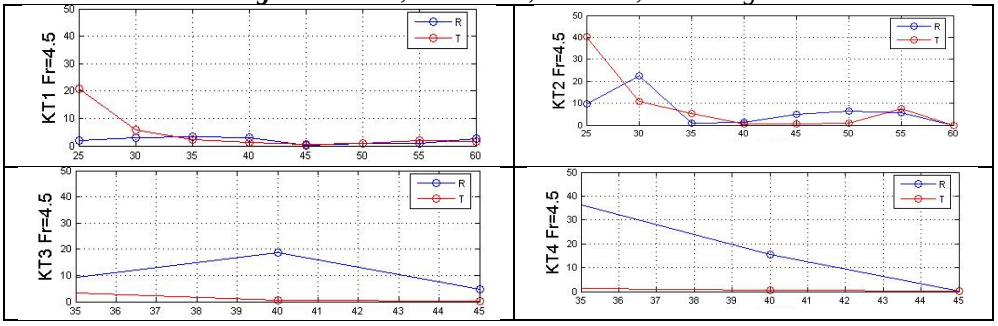

***Figure 53**. KT1, KT2, KT3, KT4, Fr=4.5 Hz, outer ring.*

By Nakamura [4], the maximum acceleration values calculated for vulnerable points that are grasped by K values checked with the acceleration value caused by 1349 earthquake. It successfully explains the damage of outer wall during this earthquake. Maximum acceptable acceleration values for R.A. XXIII, corresponding to Stern's buttress, where the supporting wall has a connection showed that, this point is very weak especially in the radial direction and may have more damage from MM VI-VII intensity earthquake.
Making quick and precise damage estimation possible this type of preparatory study in highly seismic areas is very promising for the future disaster prevention activities.

8. Conclusions

The analysis in the frequency domain made it possible to identify the main mechanical characteristics of the walls through numerical-experimental comparison of the natural vibration modes.

The first two modes involve the two buttresses and the others the entire outer northernmost wall.

The behaviour of the structure is rather complex.

References

[1] Clemente, P., Bongiovanni, G., (1993) *Ambient vibration effects on the Colosseum*, IABSE Symposium on Structural Preservation of the Architectural Heritage, Rome, pp. 107÷114. 1st Campaign

[2] Bozzano, F., Funiciello, R., Marra, F., Rovelli, A., Valentini, G. (1995) "*Il sottosuolo dell'area dell'anfiteatro Flavio in Roma*", 405÷422.

[3] Nakamura, Y., Saita, J., Rovelli, A. and Donati, S. (1998) "*Seismic response of roman Colosseum and its foundation by using microtremor measurement*", The 10th Japan Earthquake Engineering Symposium, pp. 2625-2630. (in Japanese). <1997 measurement>

[4] Nakamura, Y., Gurler, E.D., Saita, J., Rovelli, A., Donati, S.,

(2000) *Vulnerability investigation of roman Collisseum using microtremor,* 12WCEE2000, paper 2660.

[5] Bongiovanni G., Buffarini G., Clemente P., Rinaldis D., Saitta F., "*Dynamic characteristics of the Amphitheatrum Flavium northern wall from traffic-induced vibrations*", Annals of geophysics, 60, 4, 2017, S0439, doi: 10.4401/ag-7178. 2nd Campaign

[6] Randall J. Allemang, *"The Modal Assurance Criterion – Twenty Years of Use and Abuse",* University of Cincinnati, Ohio, Sound and Vibration, August 2003

[7] Pau, A., Vestroni, F., (2008) *Vibration analysis and dynamic characterization of the Colosseum*, Structural Control and Health monitoring, Journal of Structural control, Ed. J. Wiley & Sons, February.

[8] A. Caserta, P. Clemente, Y. Nakamura, A. Rovelli, G. Valente, (2012). *Identification of mean elasticity modules for soil Colosseum interaction*. DISS12.

[9] Vestroni, Pau, De Sortis, (2020)"*Measurements of the Colosseum response to environmental actions*", Eurodyn Conference Paper.

[10] Walraven, J.C., Reinhardt, H.W., "*Theory and Experiments on the Mechanical Behaviour of Cracks in Plain and Reinforced Concrete Subjected to Shear Loading*", Heron, Vol. 26, 1981, N0.1A.

[11] Bazant, Z.P., (1982). "*Crack Band Propagation and Stress-Strain Relations for Fracture Process Zone in Geomaterials*", International Symposium on Numerical Models in Geomechanics, Zurich, pp. 189-197.

[12] Bazant, Z.P., LIN, F.B., (1988). "*Nonlocal Smeared Cracking Model for Concrete Fracture*", Jrn. Str. Eng. ASCE, Vol.114, No.11, pp.2493-2510.

[13] Rots, J.G., Blaauwendraad, J., "*Crack Models for Concrete: Discrete or Smeared? Fixed, Multi-Directional or Rotating?*", Heron, Vol.34, 1989, No.1.

Existing tests for the soil

Abstract

Using environmental vibration recordings, experimental mechanical characteristics were determined, invariant to external actions: 1) for elevation, the natural frequencies and mode shapes of the monument; 2) for the ground, the H/V diagrams. These data will be used in the 3D model to evaluate the elasticity moduli in order to reproduce the same analytical shapes and frequencies. Similarly, numerical-experimental comparisons can be made for PSD diagrams.

1. Introduction

The tests were aimed at determining the natural frequencies and mode shapes of the structure.

For Colosseum, we were exceptionally lucky because the tests in many points are at disposal of researchers.

But, further tests and analyses are needed for:

c) Constantine Arch, cryptoportici and tunnels of Metro B and C;

d) improvement of geometric and mechanical characteristics of foundations and soil;

f) the tests for the map of damping coefficients.

2. Measurement points

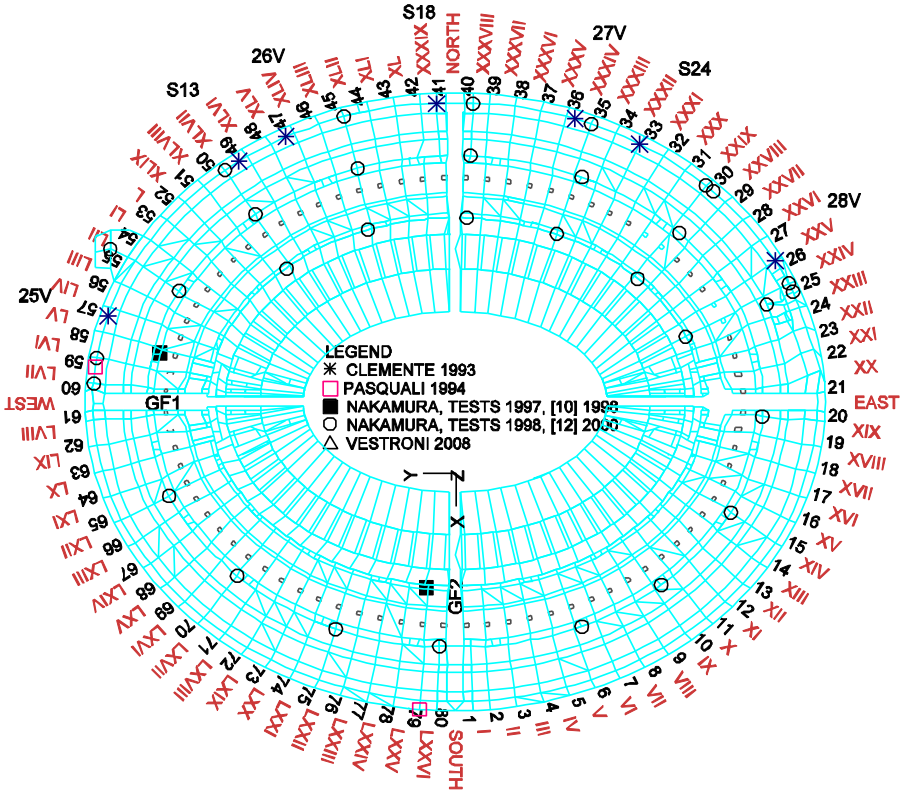

Figure 1. *Measurement points on the ground at Z=0.0 m, a) Pillars with arabian numbers, b) arcade with roman numbers. (n.45 points).*

2.1 Measurement points for [3], [4]

Three components (two horizontal and one vertical) of microtremor are recorded at every measurement points. Sampling interval is 1/100 sec and the length of each record is 40.96 sec. Measurement was repeated three times at each observation point. Figure 2 shows the location of measurements at ground, 1st, 2nd, 3rd,4th floors.

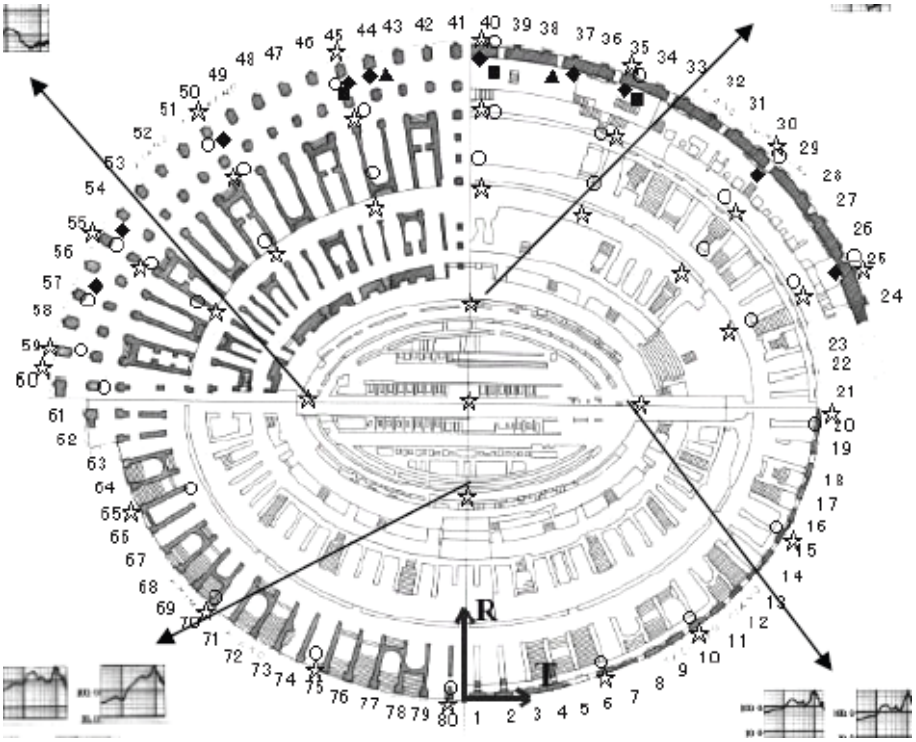

Figure 2*: Location of measurement points. from [4], at ground, 1st, 2nd, 3rd,4th floors with ☆,O,◆,,◙▲, respectively.*

The analysis was carried out under the hypothesis of linearity. Interaction with soil is taken into account. Figures 2 to 7 show the totally 87

microtremor measurement points at GF and BF.

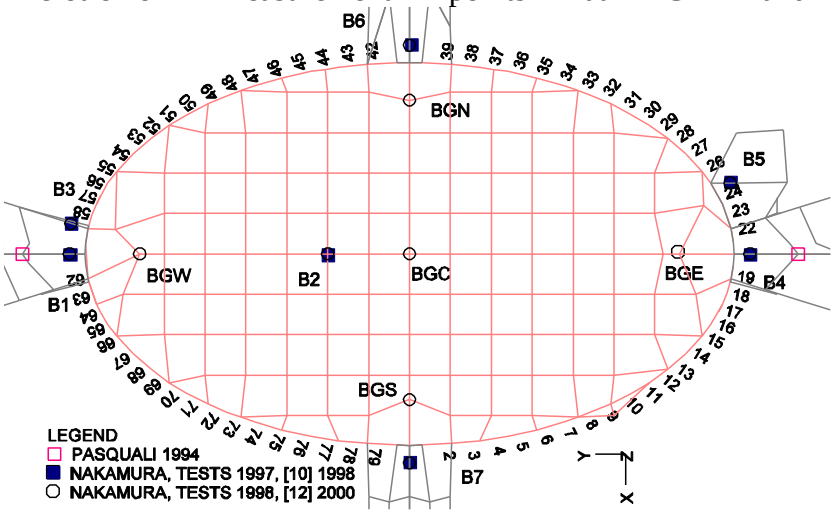

Figure 3*. Hypogeum, Z=-6.50 m. (n.14 points).*

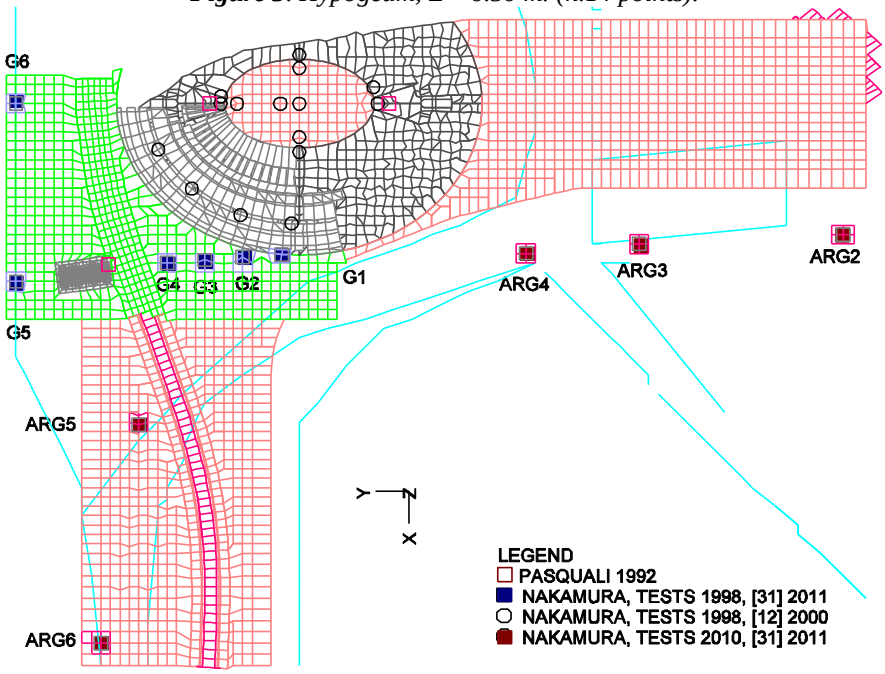

Figure 4. GF and BF *(N.25 points, 11 inside).*

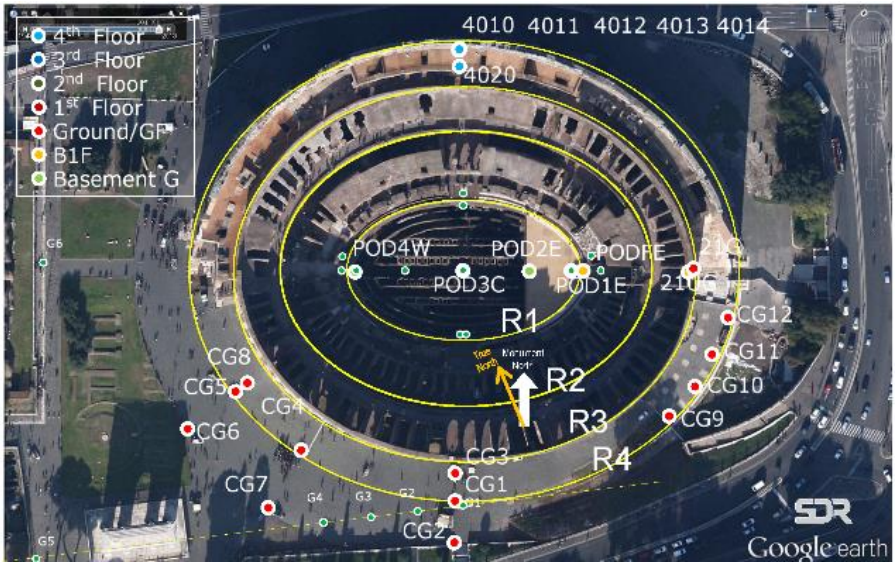

Figure 5*. Measurement points from 1997 to 2013.*

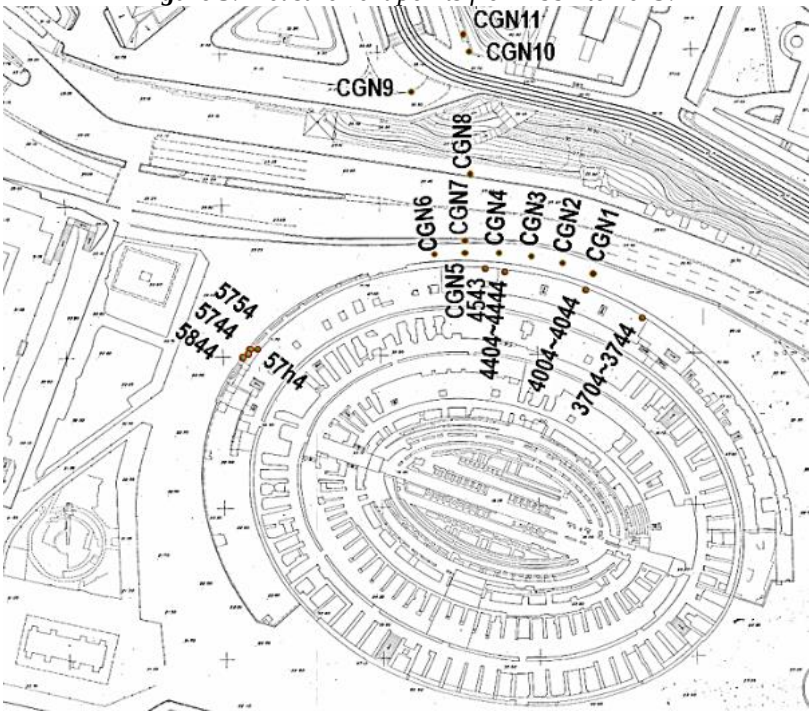

Figure 6. *Measurement points in December 2015, after DISS_15.*

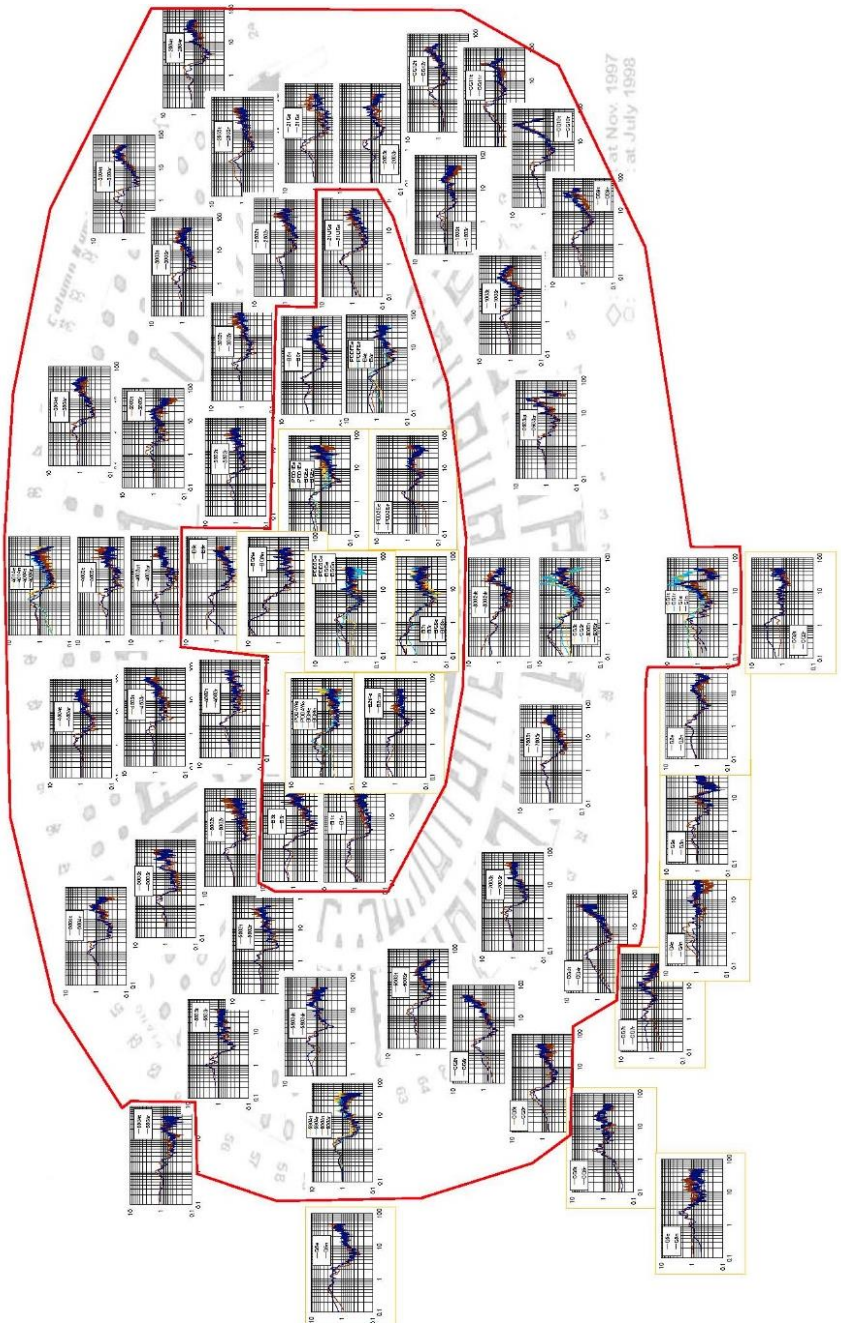

Figure 7. *Map of measuring points on the ground.*

For Colosseum, many tests were performed in different times, since 1987 to 2015. Figure 7 illustrates a top view distribution of test points around 15 to 25 m for CGN1 to CGN6 corresponding to the pillar number #40 to #46. The experimental results are shown in the papers [1 to 5] at n. 87 points, for principal frequencies, amplification factors, diagrams, etc.

3. Tests by Bozzano et al [2]

The three boreholes (Figure 8) from [2] in the southern part of the Colosseum were drilled in correspondence to. the buried "*Fosso Labicano*» valley; during the drilling some specimens were extracted for geomechanically characterisation.

The location of the soundings (Figure 8) was chosen so as to intercept, with the first of them (A), the Holocene valley in correspondence with what was assessed to be the central axis.

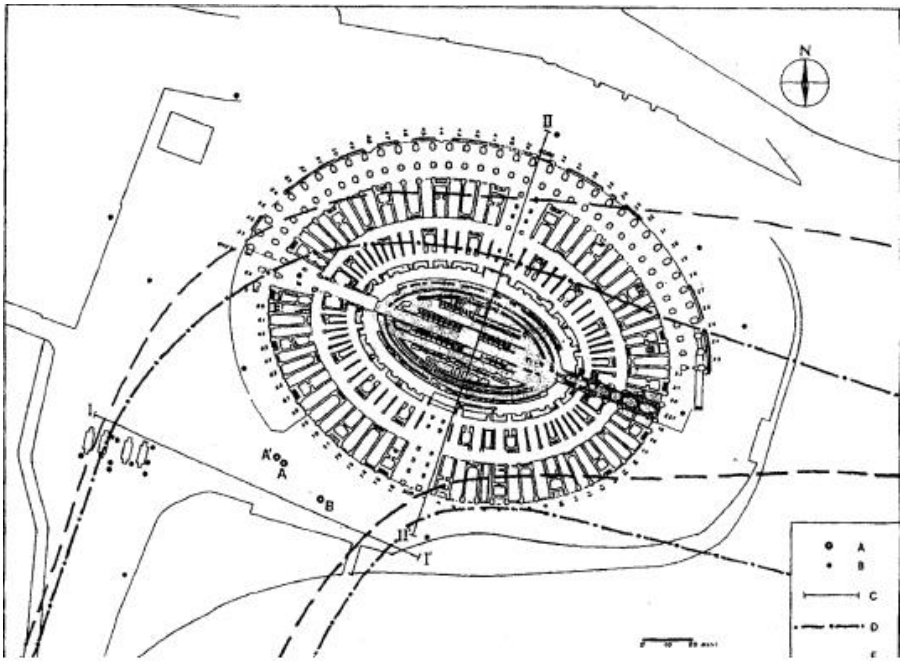

Figure 8. Planimetry of Colosseum area, [2]:
A, A': boreholes drilled for this study.

B: reviewed boreholes:
C: cross section traces of Figure 9.
D: borders of the recent alluvial valley (Holocene deposits):
E: border of the ancient alluvial valley (Middle Pleistocene deposits).

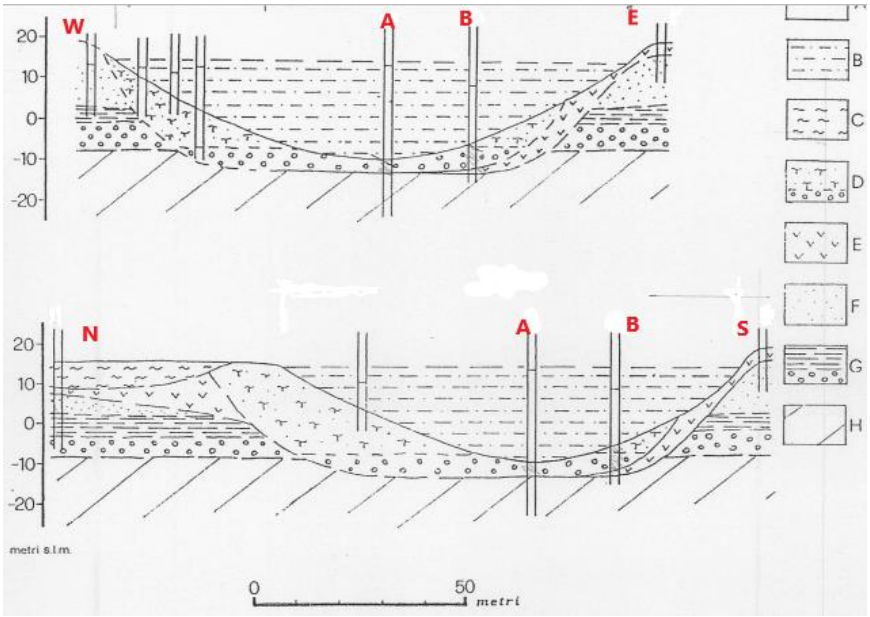

***Figure 9**. Profiles crossing file Labicana valley in Colosseum area, with new boreholes, A and B, (with the central portion of the profile shown in Figure 8):*
A: man-made fill of roman to modern age. [2]
B: silt and clay with rare intercalations of fine gravel (recent alluvial deposits Holocene)
C: sandy-silt with frequent volcanic material: «Aurelia Unit» Middle Pleistocene.
D: yellow silty-sand al/d gravel: «Valle Giulia Unit» (Middle Pleistocene);
E: pvroclastites: «Palatino Pyroclastic Unit (Middle Pleistocene)
F: yellow sandv-silt: Paleotiber Unit 2b (Middle Pleistocene);
G: lacustrine blue clay and gravel: Paleotiber Unit 2b (Middle Pleistocene);
H: Pliocene bedrock consisting of marine clays with thin sand levels.

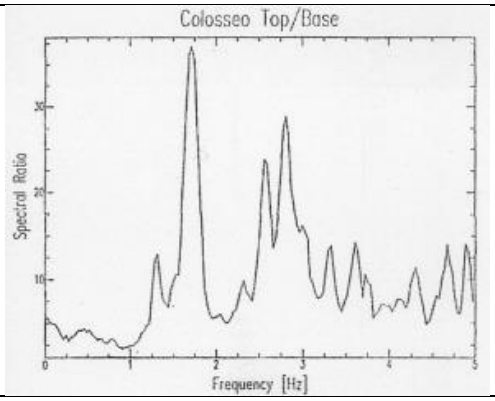

***Figure 10**. Spectral ratio of horizontal motion between the top and the bottom of the monument using ambient noise vibrations. This ratio is representative of the natural modes of the monument: two spectral peaks are evident at 1.7 and 2.8 Hz. The soil amplification is found in the frequency range 2÷3 Hz [2].*

4. Results by [6]

***Figure 11**. Inserting in existing boreholes (up to 47 m) of: Geophone in A); sparker source in B)*

The preliminary results of the investigation are presented below, broken down according to the configuration under investigation:

1. IPOGEO configuration (IPO): recordings acquired at the underground level, located approximately 6 metres below the current apron floor, obtained using the 7 ENEA backhoe loaders (en2, en3, en4, en5,

en6, en7, en8), positioned on the foundation of the monument in the walkable tunnels and at the extrados of the foundation itself, and 1 backhoe INGV (st0), located in the centre of the hypogeum at the same topographical level but on topsoil backfill (Figure 12). All the sensors were oriented according to the vertical direction and according to the NS and EW geographical directions.

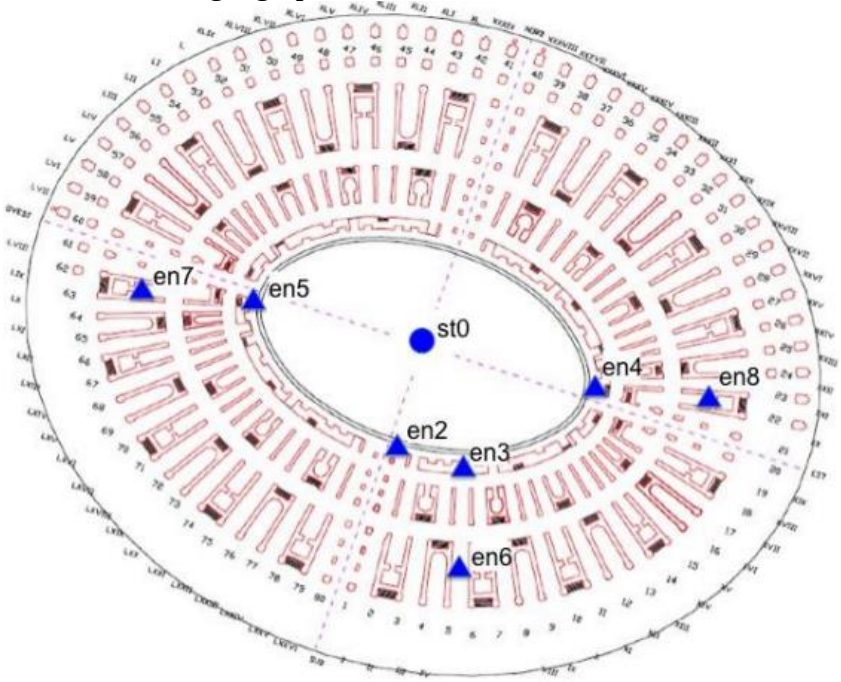

Figure 12. *Location of measuring stations in the IPO configuration. The triangles indicate the position of the ENEA velocimeter triads while the circle indicates the position of the INGV velocimeter triaxial,*

3. COMMODO (COM) configuration: recordings acquired along the Passage of Commodo (excavated within the foundation slab), located approximately 4 metres below the current below the current walking surface of the forecourt, using the 8 INGV backhoe loaders (st00, st01, st02, st03, st04, st05, st06, st07), installed at a distance of approximately 8 metres from each other from each other starting from the NORTH entrance of the corridor itself. The corridor develops in rectilinear manner radial to the monument for the entire width of the

foundation slab. At the end of this section, the corridor is oriented in an East-South-East direction and is still passable for a few metres. The last two stations were installed in this section and are probably positioned outside the foundation (Figure 13). All sensors were oriented in the vertical direction and according to the geographical directions NS and EW.

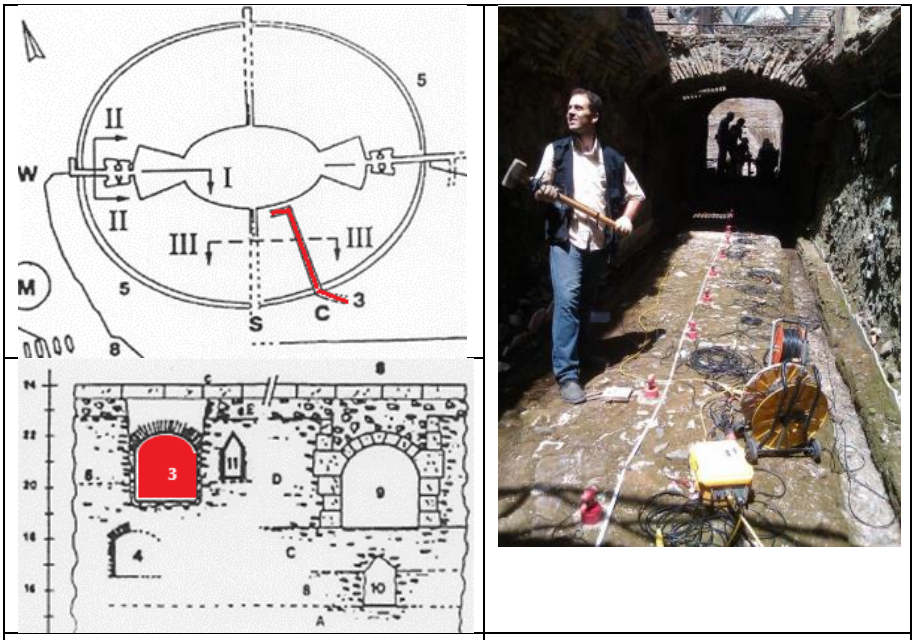

a) Plan and section | *b) acquisition line, length 250 m.*

Figure 13. Commodo Passage, under arcade V.

This was done in order to verify the actual depth, previously estimated on the basis of indirect data, of the incision originated during the erosive phase culminating in the maximum Wurmian regression, and to ascertain the nature of the soils present at the base of the recent alluvium.

The borehole was then drilled down to a depth of 47 metres from the basement, so as to enter at least ten metres into the pIiocene substrate, as in Figure 11.

A second core-destruction borehole (A') was drilled at a distance of 3 meters from the first in order to perform cross-hole measurements of seismic wave velocity in situ.

The third borehole (B) was performed at a position roughly intermediate between the central axis of the valley and its southern side. Its location was chosen in order to provide additional data on the geometry of the buried incision profile and to obtain more information on the soils between the Pliocene substratum and the Holocene.

It was precisely this survey that made it possible to highlight peculiar features with regard to the stratigraphic structure known to date for this area, providing, among other things, important confirmation to the most recent hypotheses on depositional processes in the area [1].

With the aid of the new soundings, the profiles in Figure 11. were reconstructed, representing two sections roughly transversal to the Labicana Valley. The most relevant new element with respect to what was already known or hypothesised is the presence of the Palatine Pyroclastic Unit, with a horizon approximately one metre thick, in direct contact with the eroded Pliocene substrate. The presence of this pyroclastic flow at an elevation of -13 m o.s.l., already identified at higher elevations in two other soundings carried out at the northern and southern edges of the amphitheatre, can be interpreted in two ways. The first hypothesis is that its deposit, as would also appear to be evident from the sub-horizontal flaking of the core samples, is primary and that the deposit was placed in post-historical position.

5. Conclusions

We are interested on tests devoted to 3D DISS model, not to generic tests.

For such model, further dynamic tests are requested inside the monument too, for:

1) completing the map of elasticity modules;

2) producing the map of damping coefficients;

3) permanent recording in 50 points from the depth of 80 m under the place to the monument summit.

References

[1] Marra Rosa (1995): *Stratigrafia e assetto geologico-strutturale dell'area romana, in: La Geologia di Roma. Il Centro Storico'*, Memorie Descrittive della Carta Geologica d'Italia, Annali di Geofisica

[2] Bozzano, F., Funiciello, R., Marra, F., Rovelli, A., Valentini, G. (1995) "*Il sottosuolo dell'area dell'anfiteatro Flavio in Roma*", 405÷422.

[3] Nakamura, Y. (1998). "*Seismic response of roman Colosseum and its foundation by using micro-tremor measurements*", *The 10th Japan Earthquake Engineering Symposium*, pp. 2625-2630 (japanese).

[4] Nakamura, Y., Gurler, E.D., Saita, J., Rovelli, A., Donati, S., (2000) *Vulnerability investigation of roman Collisseum using ambient vibration, 12WCEE2000*, paper 2660.

[5] Y. Nakamura, J. Saita, T. Sato and G. Valente, *Attempts to Estimate the Physical Property of Surrounding Ground and Foundation Concrete of Colosseum using Microtremor*, DISS15

[6] Working Group: (ENEA) (INGV) (Sapienza Università di Roma) (Università dell'Aquila), "*Anfiteatro Flavio rilievo di vibrazioni ambientali: caratterizzazione del sito e della fondazione*", March 2015.

Analysis with multibody model, with the same convoy, and wagons all alike

Abstract

We use a multi-body 'wagon-track' model, which instantaneously provides the forces in the rails created by passing trains. We use the same wagons, the same convoys and the same railway for Metro B and C. It does not matter that the convoys are not exactly the real ones, because we are interested in producing the model vibrations in order to derive analytical H/V diagrams, that are forcing-independent. All time histories can be obtained: a) the motion parameters [s(t), v(t), a(t)] for the convoys; b) the forces [F(t)] at the contact between all 48 wheels and rails. We consider outward and return journey on the Metro B from Colosseum to Circus Maximus, on the Metro C from Colosseum to Amba Aradam, with the prescribed speeds. In addition, we started to realise a further vehicle model to reproduce the dynamic behaviour of the magnetic levitation train based on the Italian UAQ4 technology.

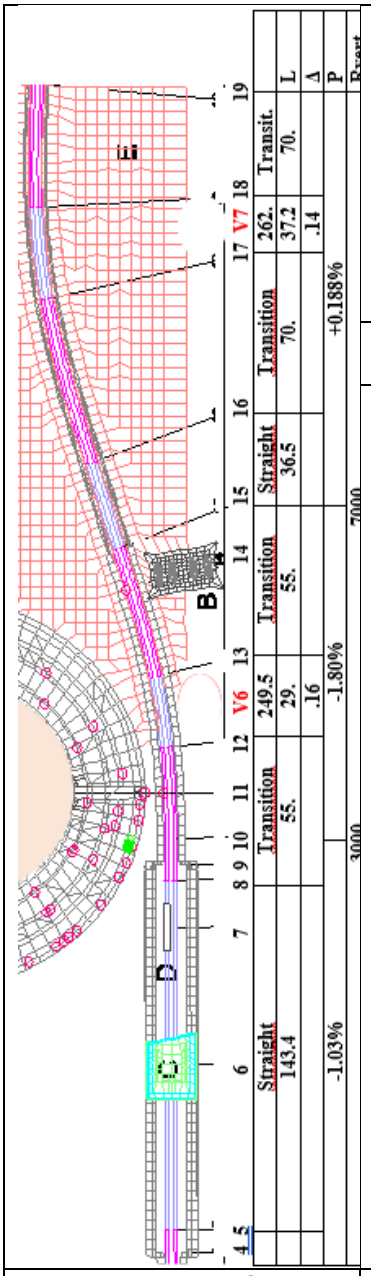

Figure 1. Convoy path

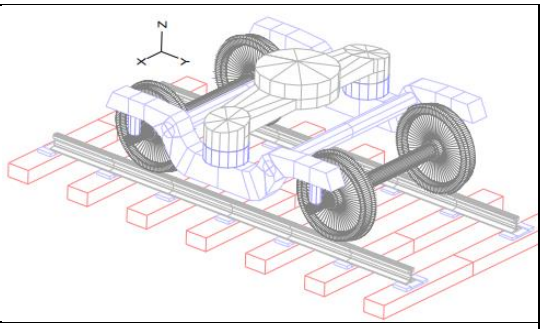

Figure 2. The boogie (roller bearing, frame, wheels), railway, connections, sleepers.

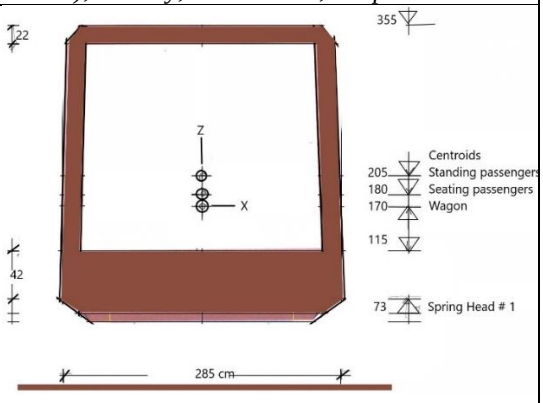

Figure 3. Hollow core wagon section.

1. Introduction

Each convoy is composed of six wagons, two of which are pilot electric railcars, each mounted on two motor bogies and positioned at the ends, and four hauled cars, central to the pilot electric railcars, each mounted on pairs of non-motor bogies.

The pilot electric traction (by Fiat Ferroviaria and Breda-Ansaldo) is equipped with: a) coil-spring primary suspension, without shock absorbers, b) air secondary suspension, and oil and air shock absorbers.

The rubber shock absorbers limit the amplitude of vertical and lateral oscillations between the body and bogies.

The specific data for each individual element were obtained from the documentation provided by the CO.TRA.L. company in Rome [5] and [6].

The convoys constitute a known source of noise for the soil Monument interaction.

Moreover, we have started to perform a further vehicle model with the magnetic levitating train based on the UAQ4 Italian technology; its bogie was obtained by aforementioned simply changing the wheelsets with skates, and the usual rail profile with a new one having L shape.

2. Modifications of standard ERRI vehicle

Table 1. The suspension characteristics of the bogie.

Suspension primary	Stiffness axial	Stiffness transversal	Damping	Allowed displacement
X	3.36×10^5	5000.	1.7×10^4	±20
Y	3.36×10^5	5000.	1.7×10^4	±20
Z	7.47×10^5	5000.	3.0×10^4	±40
Secondary				
X	2.25×10^5	1833.	2.33×10^4	±22
Y	2.25×10^5	1833.	2.33×10^4	±22
Z	3.10×10^5	1833.	0.635×10^4	-45/+40
	N/m	N/m	N/(m sec)	mm

The full vehicle assembly was obtained by changing of design variables for the vehicle Erri model (by Adams/Rail); according to the trains running on Metro B, the configurations of the new wagons are:

1) Car body (with passengers). Mass = 32000.0 kg; I_{XX} = 48000.0 kgm^2; I_{YY} = 830000.0 kgm^2; I_{ZZ} = 830000.0 kgm^2 ; Length = 19.0 m; Width = 2.9 m; Height = 2.9 m

2) Wheeelset. Wheelbase = 2.16 m; Distance between two bogies = 11.0 m

3) Buffer. Length = 1.0 m; Spring stiffness F_X = 160000.0 kg/m; F_Y = 160000.0 kg/m; F_Z = 430000.0 kg/m; T_X = T_Y = T_Z =183.3 kg/m

2.1. The wagon model

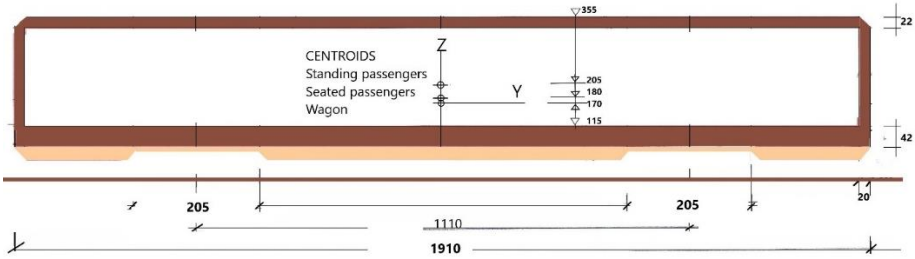

Figure 4. Longitudinal section

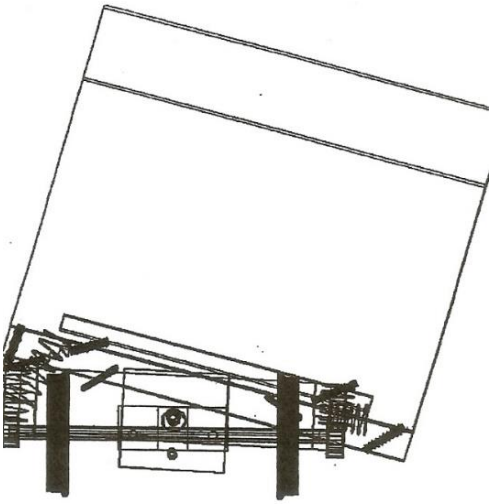

Figure 5a Wagon rolling at 1.4 / 7.5 Hz.

The wagon is a hollow prism 2,85x19.10x(1.15/3.55) m.
For dead load, Zg=170 cm. Pdead=36 t
Irock_x=4.2E+05 kgm2,
Iroll_y=2.4E+04 kgm2
Isnake_z=4.2E+05 kgm2 ,
Plive=3.84 t; Zg=180 cm for 48 seated passengers.
Plive=15.6 t; Zg=205 cm for 195 standing passengers.

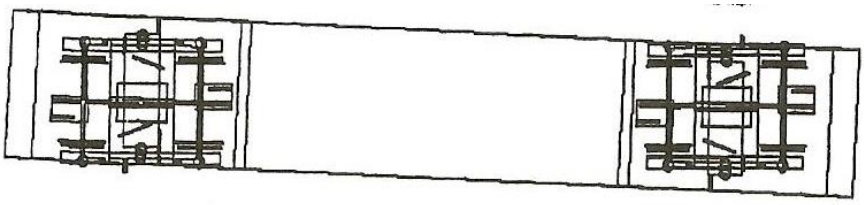

Figure 5b Wagon snaking at 1.19 Hz.

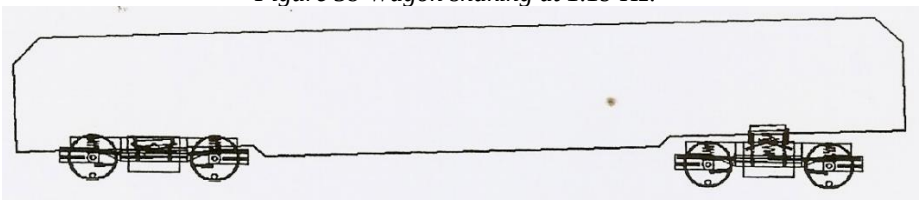

Figure 5c Wagon rocking at 1.34 Hz.

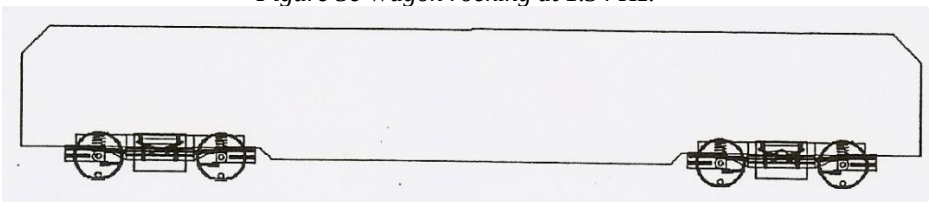

Figure 5d Wagon shuddering at 1.24 / 1.34 / 5.21 / 5.31 Hz.

The principal natural modes are 19: 1. Rolling of the case on the primary suspension; 2. Snaking of the case; 3. Case snubbing; 4. Pitching of the case; 5. Rolling of the case on the secondary suspension; 6. Snaking of bogies in phase; 7. Snaking of the bogies in phase; 8. Swaying of the bogies in phase; 9. Sussing of the trolleys in counterphase; 10. Rolling of the trolleys in phase; 11. Rolling of trolleys in counterphase; 12. Pitching of the trolleys in phase; 13. Pitching of trolleys in counterphase; 14. Lateral oscillation of the trolleys in phase; 15. Lateral

oscillation of the trolleys in counterphase; 16. Pitching of the drive axles in phase; 17. Pitching of the drive axles in counterphase; 18. Rotation of the rear bogie on its vertical axis; 19. Front bogie rotation on its own vertical axis.

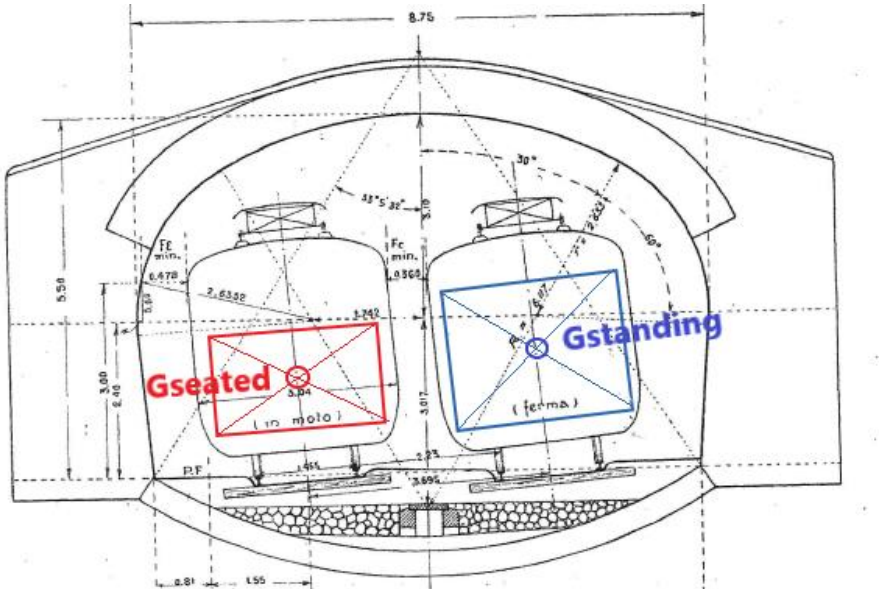

Figure 6. Section of tunnel in the curve V6 having R=249 m, length 139 m and rail rise Δz=16 cm; minimum lateral clearance inside the bend is mm 935, to be reduced by mm 21.

Table 2. Wagon loads.

parts	n	P	n P
Axle	4	12.87	51.48
Fifth wheel	2	4.84	9.68
Frame	2	5.0	10.
Engine	2	9.60+4.90	29.
Ratio axle box	4	22.0	88.
Actuating arm	4	0.25	1.
Axle box	8	0.50	4.
Main shaft	4	0.30+0.73	4.12
Cardanic semishaft	4	0.19+0.21	1.6
Box	1	160.	160.
Seating passengers	48	0.7	33.6
Standing passengers	195	0.7	136.5
Elements	n	kN	kN

2.2. The convoy model

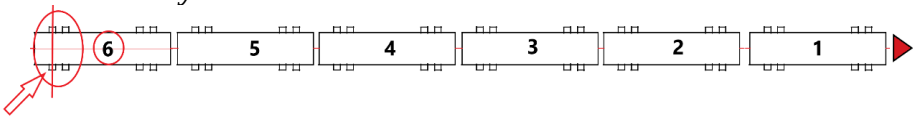

Figure 7. Convoy model, with n. 6x8=48 wheels. Wagon n. 6, rear boogie, second axle, right wheel.

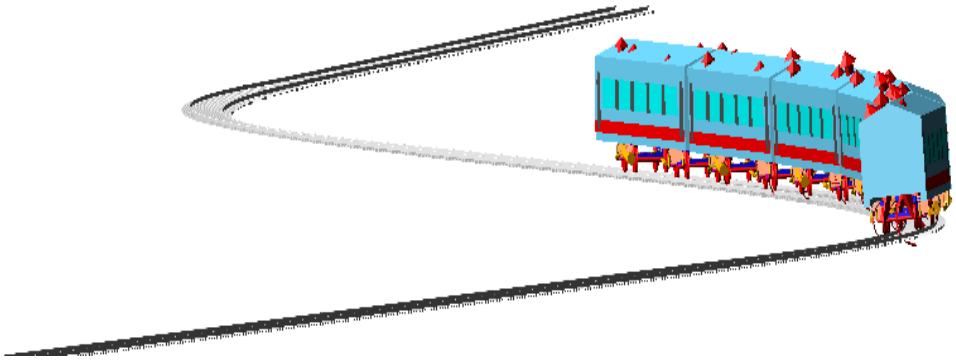

Figure 8. Convoy

3. Velocity profile

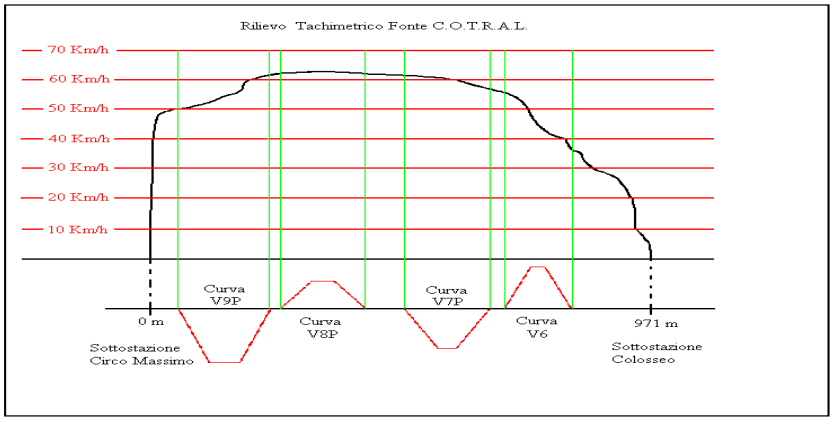

Figure 9. *Production of the relief on the route between the tacho-stop "Circus Maximus" and stop "Colosseo" (Search by experimentation Convention "Sapienza" University of Rome - Met.Ro., year 2001).*

It is defined by the following characteristics:
maximum starting acceleration = 1.0 m/sec^2; minimum stopping deceleration = -1.1 m/sec^2;
velocity at Colosseum, Constantine arch and maximum: 47, 57 and 66 km/h respectively.

4. Irregularities

***Figure 10a**. Measurement of the typical lateral irregularities of a rail.*

The measured typical lateral irregularity of a rail is represented in Figure 10a, and 10b the connected FFT is shown, with s_{max}= 6 mm.
The rail irregularities constitute a casual noise, stationary and ergodic.
We plan to use sinusoidal, smoothed ramp and smoothed dip irregularities together.

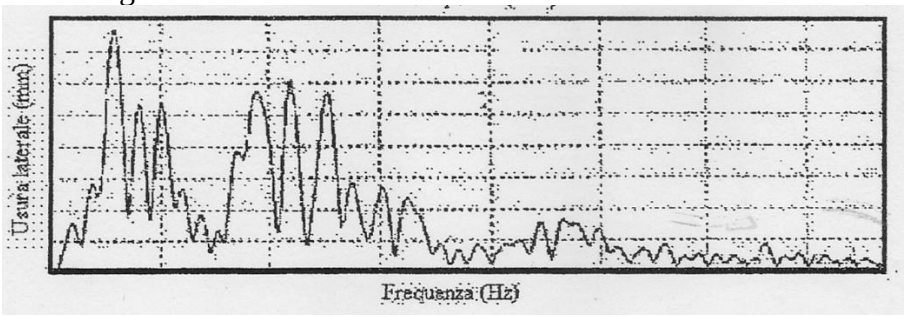

***Figure 10b**. Frequency analysis (FFT).*

To use track irregularities, use the IRREGULARITIES block of the track property file.
The IRREGULARITIES data block contains different information according to the model of irregularities used.

4.1 Measured irregularities using unformatted data block

Measured irregularities are stored in the IRREGULARITIES data block in two different ways, according to the track property file version specified in MDI_HEADER data block.
Measured Irregularities Using Unformatted Data File (FILE_VERSION = 4.0)
This is the format used for old VI-Rail versions. The irregularities data block should look as follow:

1) Specifies the type of model used for the irregularities TYPE = 'MEASURED'

2) Specifies format far the irregularities data file, FORMAT = 'ASCII_YZ'

3) Method used for the interpolation of measured data, INTERPOLATION = 'SPLINE'

4) Scaling factor for the measured data, SCALE = 1.0

5) Length of the undisturbed track section before the beginning of the irregularities, INACTIVE LENGTH = 30.0

6) Abscissa of the track at which the perturbation ends, ACTIVE LENGTH = 4000.0

7) Distance between consecutive measured data, DATA STEP = 0.266

8) Name and path of the unformatted data file containing the irregularities data. You can introduce comments by specifying a "!" as first character of the line. DATA FILE= ‘C:\work\erri.dat’

4.2 Measured irregularities using formatted data file

This is the standard format for the latest Vl-Rail versions. The irregularities data block should look as follows:

9) Name and path of the unformatted data file containing the irregularities data. You can introduce comments by specifying a "!" as first character of the line. DATA FILE= ‘C:\work\erri.idf’
Note: To avoìd numerical problems, VI-Rail automatically introduces a smoothing at the beginning of the section with irregularities. The

actual value of the irregularities is scaled by a (1-cos) function, which reaches the unit value after 1 second from the beginning of the irregularities section.

4.3 PSD irregularities

The higher level of irregularities, connected with the convergences on the four paths, for a time of 40 secs, were found with PSD irregularities, defined by:

10) minimum wavelength, in meters, of the reconstructed signal; this value determìnes the upper of frequency limit of the function, PSD_Ll=10;

11) maximum wavelength, in meters, of the reconstructed signal; this value determines the lower frequency limit of the PSD function, PSD_L2=100. m;

12) number of frequency bands in which the PSD will be divided; the greater the number of frequencies, the more accurate the frequency content of the signal; of course, increasing the number of frequency terms leads to longer computational time, FREQUENCY_TERMS=100;

13) a third order INTERPOLATION=SPLINE;

Beside this, are defined:

14) distance of consecutive data, DATA_STEP= 0.266 m;

15) length of undisturbed track section before the beginning of irregularities, INACTIVE_LENGTH= 23.0 m;

16) abscissa of the track at which the perturbation ends, active length ACTIVE LENGTH = 650.0 m;

Parameters for the generation of the PSD, according to formulas specified in the ORE B176.

For example, the data for the high level ORE irregularities are:

PSD_OC = 0.8246 rad/m,

PSD_OR = 0.0206 rad/m,

PSD_OS = 0.4380 rad/m,

PSD_AV = 1.08E-6 m x rad (high level irregularities)

PSD AA = 6.125E-7 m x rad (high level irregularities)

$\lambda = 2m$ (where $\lambda = 100$ m)

b = 0.70 m (taken from the track base value)
Vertical PSD in, Lateral PSD in, Cant PSD in.

Vertical PSD

$S_{XX} = [{}_{V}A\ {}_{C}\Omega^2\ ] / [\ (\Omega^2 + {}_{R}\Omega^2\ )\ (\ \Omega^2 + {}_{C}\Omega^2\ )]$ m^2 / [rad/m]

Lateral PSD

$S_{YY} = [{}_{A}A\ {}_{C}\Omega^2\ ] / [\ (\Omega^2 + {}_{R}\Omega^2\ )\ (\ \Omega^2 + {}_{C}\Omega^2\ )]$ m^2 / [rad/m]

Cant PSD

$S_{\Phi\Phi} = [{}_{V}A\ {}_{C}\Omega^2\ \ \Omega^2] / [\ (\Omega^2 + {}_{R}\Omega^2\ )\ (\ \Omega^2 + {}_{C}\Omega^2\ )\ (\ \Omega^2 + {}_{S}\Omega^2\ )]$:
rad^2 / [rad/m]

17) toggle the activty of lateral irregularities , LAT_ACTlVE=YES;

18) toggle the activity of vertical irregularities VERT_ACTlVE =YES;

19) toggle the activity of roll! Irregularities, ROLL_ACTlVE= YES;

Note: To avoìd numerical problems, VI-Rail automatically introduces a smoothing at the beginning of the section with irregularities; the actual value of the irregularities is scaled by a (1-cos) function, which reaches the unit value after 1 second from the beginning of the irregularities section.

The coordinates (x, y, z) and the cant angle, are obtained by a simple relationship

$X = X_{ANALYTIC}$

$Y = Y_{ANALYTIC} + Y_{IRREGULARITY}$

$Z = Z_{ANALYTIC} + Z_{IRREGULARITY}$

$CANT = CANT_{ANALYTIC} + CANT_{IRREGULARITY}$

20) the format for this irregularities model, FORMAT= ANA_1;

21) the direction the irregularity has to be applied, DlRECTION=GAUGE, irregularities applied in lateral and vertical direction, cant deficiency irregularities too.

22) the rail side the irregularities have to be applied, RAIL_SIDE=BOTH

23) track abscissa where the irregularities start, STARTING_S = S0 = 2.0 m;

24) shift left rail sinus versus right rail sinus. (valid only for RAIL_SIDE=BOTH and

DIRECTlON=VERTICAL_LATERAL), SHIFT=0.0

25) toggle smoothing of the ramp, SMOOTH=YES; ramp is interpolated using a STEP5 function.

We use all the common analytic irregularities implemented together, for left and right rails independently, in order to obtain the rolling action too:

a) Sinusoidal Irregularities, Figure 11a;

b) Ramp Irregularities, Figure 11b;

c) Dip Irregularities, Figure 11c.

4.4. Sinusoidal irregularities

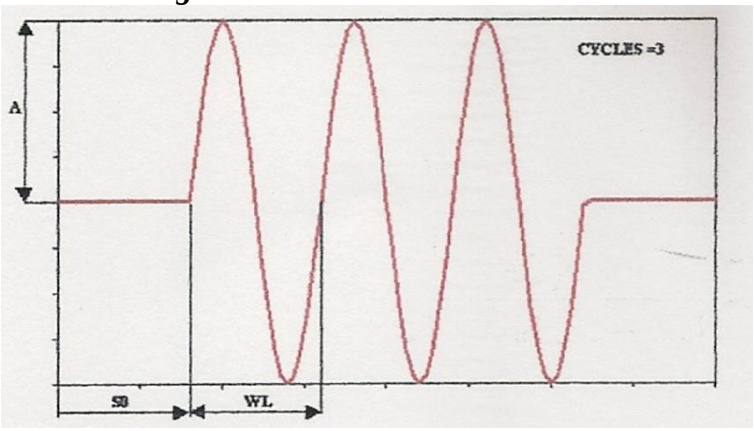

Figure 11a. Sinusoidal irregularities

26) the model of irregularities is TYPE =ANALYTIC_SINUS;

27) sinusoidal irregularities amplitude; when DIRECTION = CANT, the amplitude represents an angular value, A=AMPLITUDE =0.005;

28) sinusoidal irregularities wavelength. WL= WAVE_LENGTH=0.5;

29) number of sinusoidal cycles, CYCLES=3;

The basic formula far the analytic sinusoidal irregularity is:

IRR= A*sin(w), where:

w = (2π/WL) * (abscissa - SO)

4.5. Ramp irregularities

30) the model used for the irregularities, TYPE=ANA-LYTlC_RAMP.

31) ramp irregularities height (H). When DIRECTION = CANT, the height represents an angular value, HEIGHT=0.01 m;

32) ramp irregularities width W= WIDTH=0.5 m;

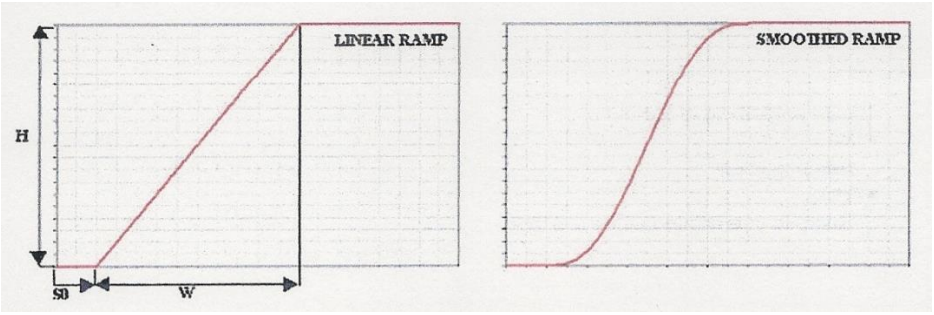

Figure 11b. Ramp Irregularities

4.6. DIP irregularities

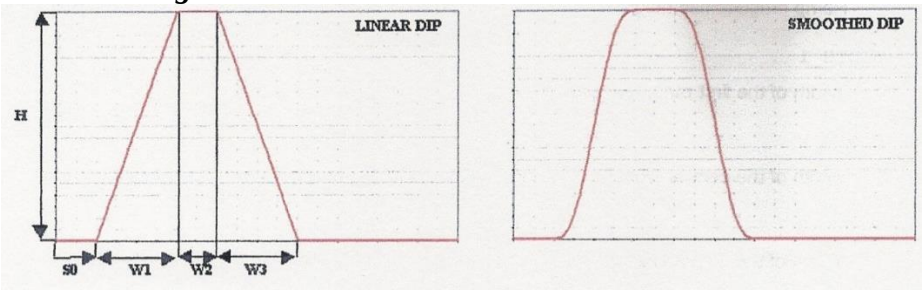

Figure 11c. Dip Irregularities

33) the type of model used for the irregularities; TYPE=ANA-LYTlC_DIP;

34) ramp irregularities height (H). When DIRECTlON = CANT, the height represents an angular value, HEIGHT = 0.01

35) width of the first ramp (ascending) W1= WIDTH_1=1.0 m;

36) width of the central (constant) section W2= WIDTH_2=0.5 m;

37) width of the second ramp (descending) W3= WIDTH 3 = 1.0 m

Ramp is interpolated using a step5 function.

The basic formula for ramp and dip analytic irregularities:

IRR = 0.0 if (S < SO)
IRR = (H/W)*(S-SO) if (SO ≤ S ≤ SO+W) - NOT SMOOTHED
IRR = STEP5 (S ,SO, 0.0, SO+W, H) if (SO ≤ S ≤ SO+W) - SMOOTHED
IRR = H if (S > 80+W)
Where S is the actual track abscissa and IRR is the corresponding irregularity amplitude.

5. Analysis results for the convoy

Figure 12 shows for **W**agon n. 6, wheelset n. 1, left/right, front wheel; track with irregularities

Figure 13 shows the travelled distance s(t), with the contact forces of the left side of the second bogie of the second wagon, expressed with their time histories P(t); so we can know these forces expressed as P(s,t), without and with irregularities.

Figure 14 shows Forces in the buffer n. 5, a) new track; b) track with irregularities PSD with rail side left and right, direction lateral and vertical, factor=0.60.

Figure 15 shows **the** contact of the S1002 wheel and UNI60 rail and exchanged forces

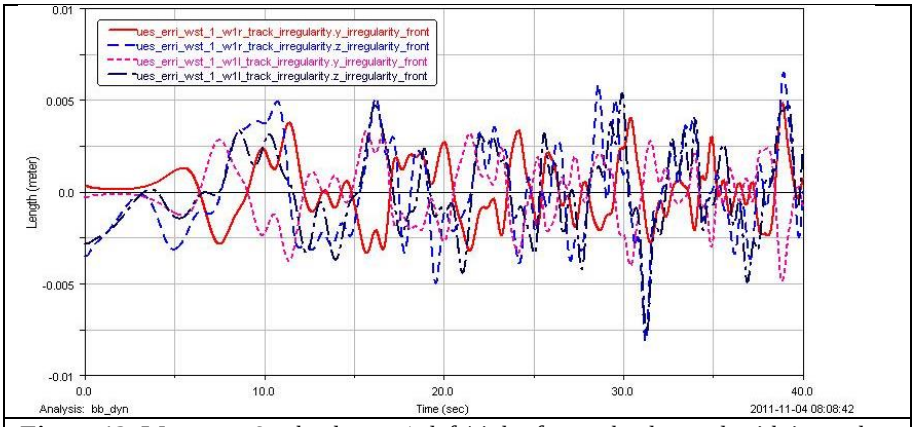

***Figure 12. W**agon n. 6, wheelset n. 1, left/right, front wheel; track with irregularities PSD, rail side left and right, direction lateral and vertical, shift=1.0 m, factor=0.60, S_{MAX}=8 mm.*

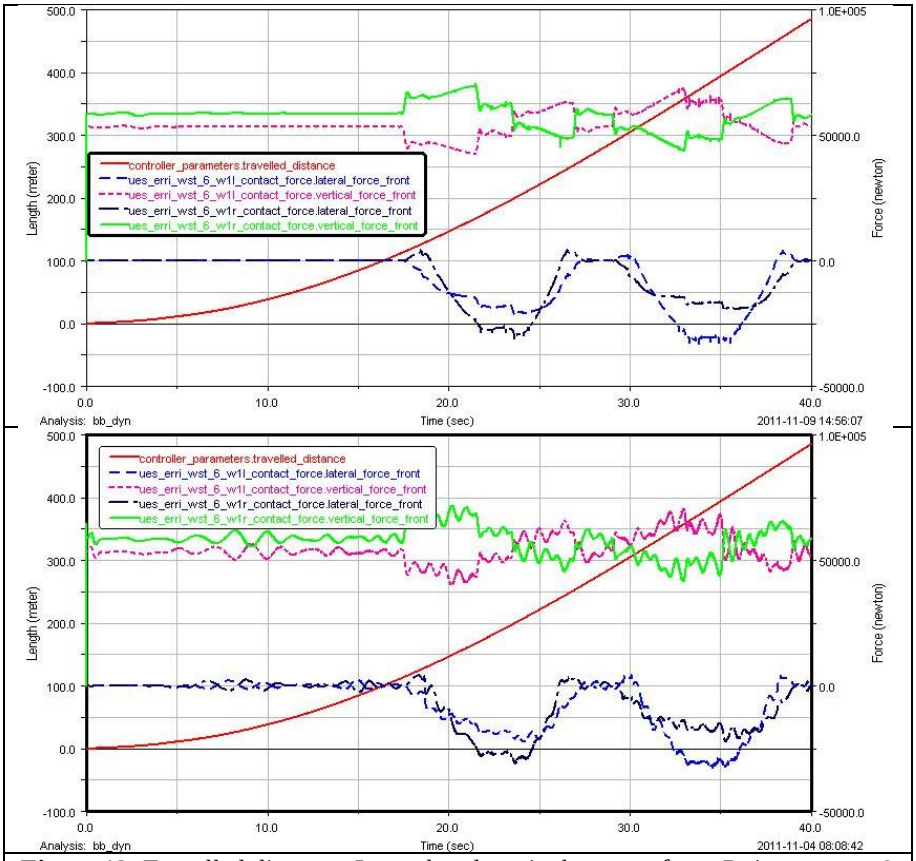

Figure 13. *Travelled distance. Lateral and vertical contact force P_J in wagon n.6, wheelset n.1, front (J=21), left/right, for Metro B, odd rail; a) new rail; b) track with irregularities PSD with rail side left and right, direction lateral and vertical, factor=0.60.*

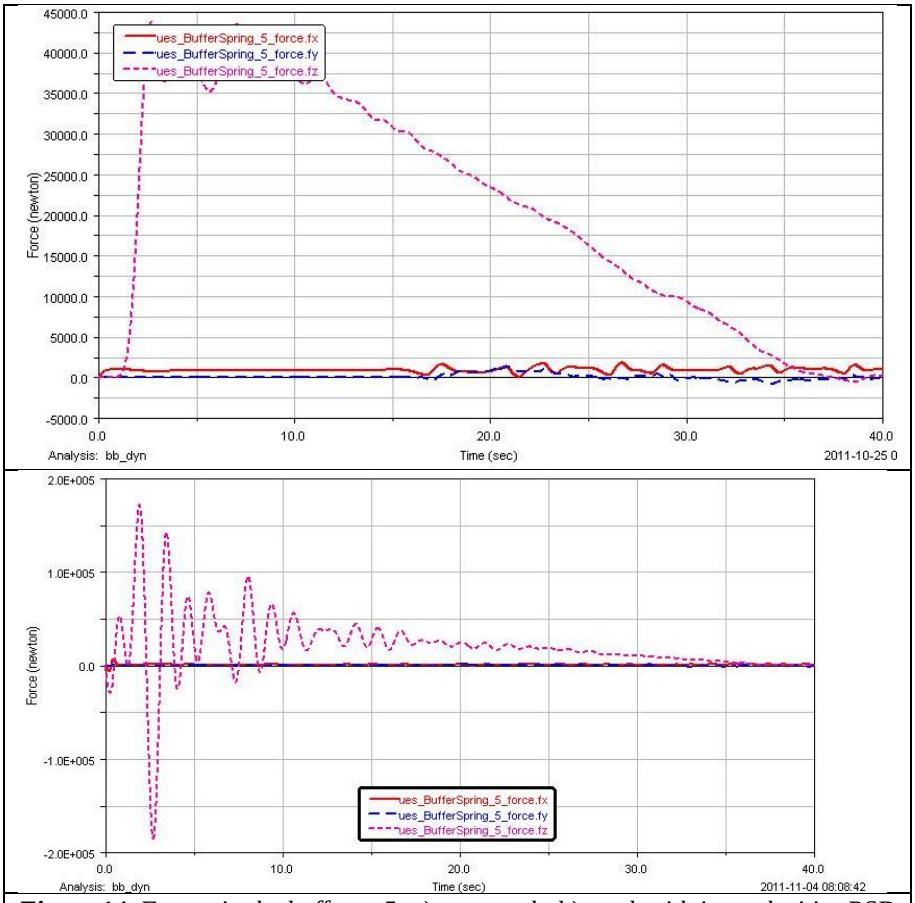

Figure 14. *Forces in the buffer n. 5, a) new track; b) track with irregularities PSD with rail side left and right, direction lateral and vertical, factor=0.60.*

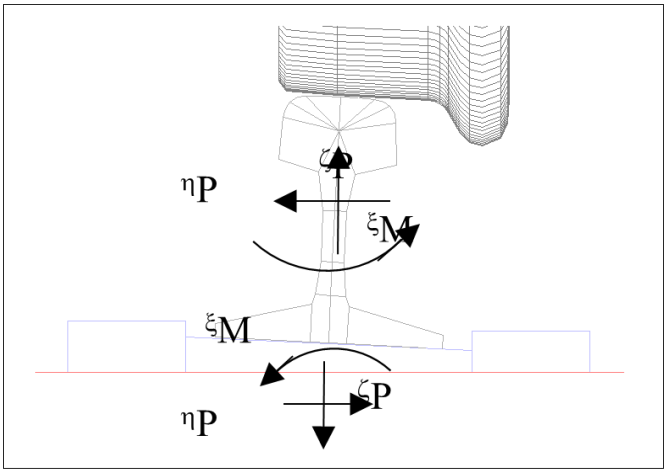

Figure 15. *Contact of the S1002 wheel and UNI60 rail and exchanged forces*

The train velocities are 47, 57 and 66 km/h in correspondence of Colosseum, Constantine arch and Antiquarium respectively.

6. Magnetic levitating train

This system is a guided train using superconductors and super magnets for lifting and guiding. It is a unique and patented technology, that is comprehensively tested in the laboratory.
UAQ 4 is the only magnetic levitating vehicle with 100% resistance free motion, except aerodynamic drag. The energy consumption is almost zero.
The system significantly minimizes environmental impact as it reduces vibrations, noise and pollution.
The system can operate at both low speed in urban environment and high speed for long distance trips.
We plan to introduce these irregularities in the code by PSD and spline interpolation over coordinates x, y, z and can't angle of each rail.

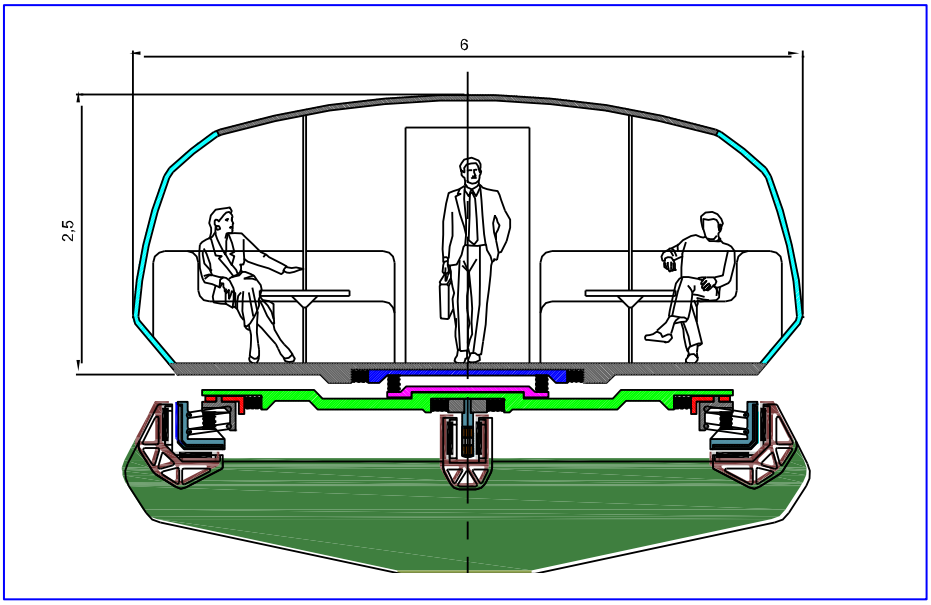

Figure 16. *The cross section of the wagon.*

Figure 17a*. The model. View n.1*

Figure 17b*. The model. View n.2.*

The UAQ4 work principles are: a) self-stabilizing magnetic lift and guidance; b) no drag forces during the motion; c) high operative gap.
Magnetic guideway:
A=64800mm2
Elastic module=207000MPa
Ix=3.97050E+009mm4
Iy=1.98530E+009mm4

Iz=1.98530E+009mm4
Lift spring stiffness: klev=67500N/mm
Pre-load:6400N
Guide spring stiffness: klev=56250N/mm

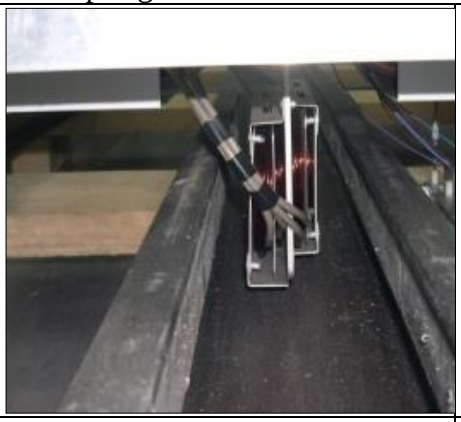

Figure 18a. Propulsion system

Figure 18b. The scaled boogie demonstrator

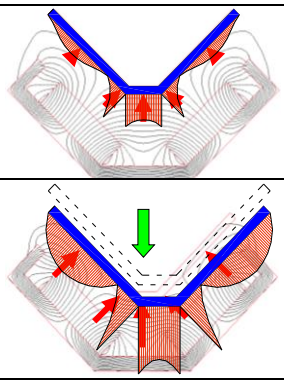

Figure 19a

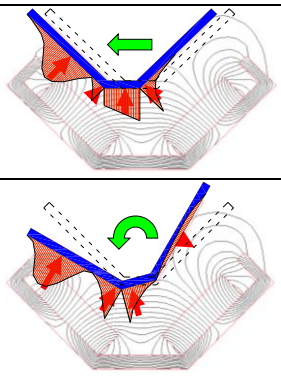

Figure 19b

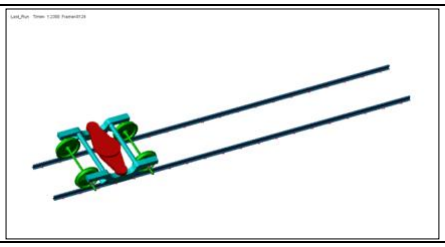

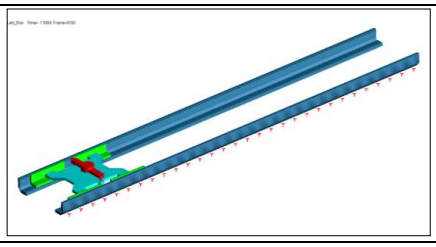

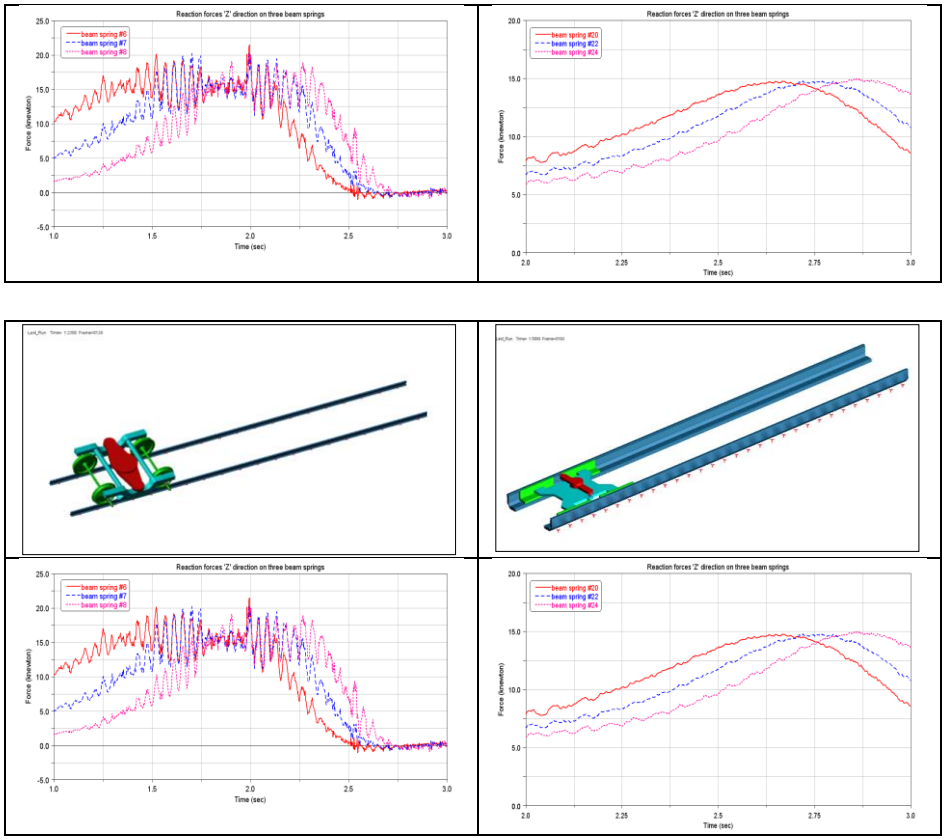

Figure 20 *The forces in three elastic springs*

Concerning the vehicle/track interaction

1. Traditional train

The dynamic interaction between wagon and track produces peaks and ripples of forces due to wheel/rail contact

The numerical results are in according with the experimental data

2. Maglev train

After preliminary analysis the resulting force Vs. time profile show a drastic mitigation/removing of ripples

The numerical model is partially carried out and it must be completed and defined by experimental data

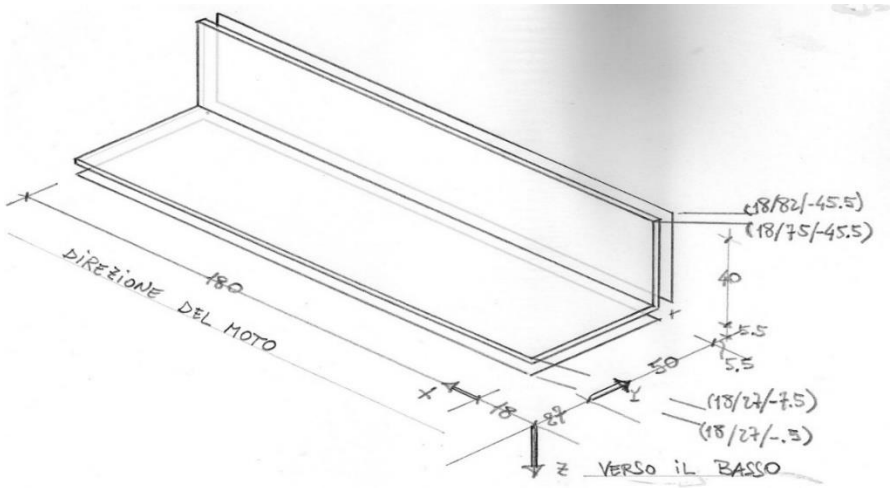

Figura 21 *– Axonometric view of a skate.*

6.1. Planned magnetic levitating skate

We intend to use a traditional Erri bogie, in order to modify it with:
1) Skates instead of wheelsets;
2) Frame flat in the bolster plane;
3) Lowered Primary suspention.
The stiffnesses, dampings, width, heights and depths stay the same of traditional ERRI bogie.
The skate has L shape as in Figure 21; it is connected to two independent fictitious elements, by six springs each one.
The fictitious elements slip without friction on the rail L shaped; the pressure between the skate and the fictitious elements is defined in Figure 22, both levitating and stabilizing.
By integrating, the forces in the six springs may be obtained.

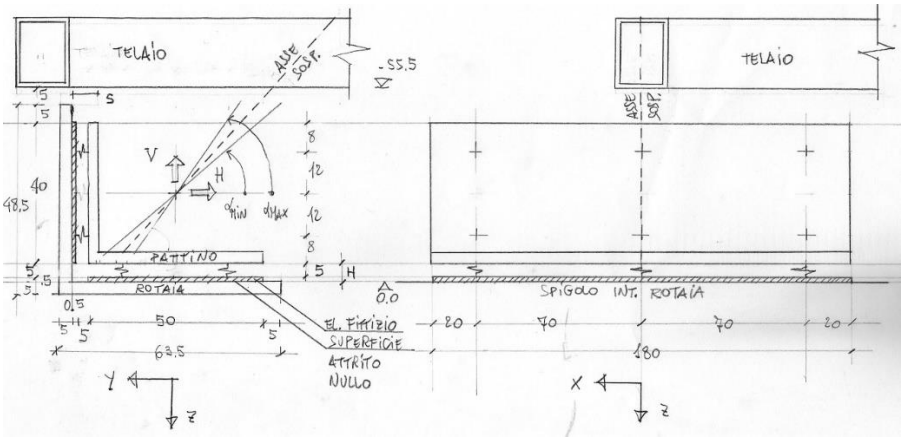

Figure 21 *skate, ficticious element and rail* (S_{mean}=5.5 cm, H_{mean}=5.5 cm).

Figure 22. *Levitating and stabilizing pressure [kg/m^2] on the skates vs gap [m]*

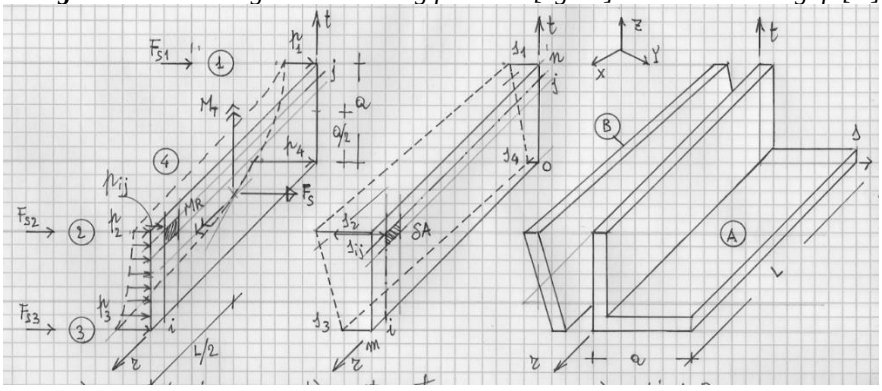

Figure 23*. The skate, with: a) pressures; b) displacements; c) skate and its fictitious elements.*

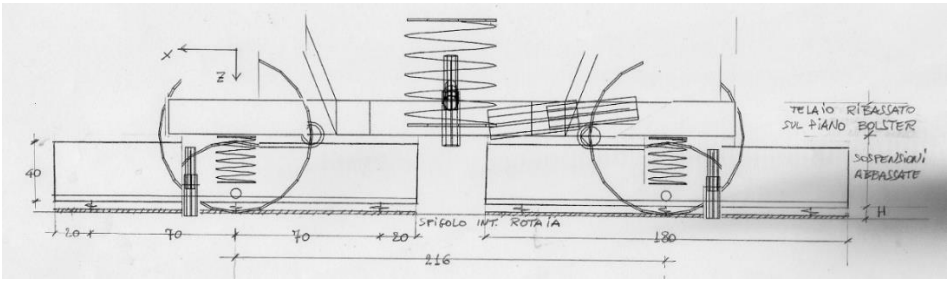

Figure 24. L*ateral view of the bogie, flat frame on the bolster plane*

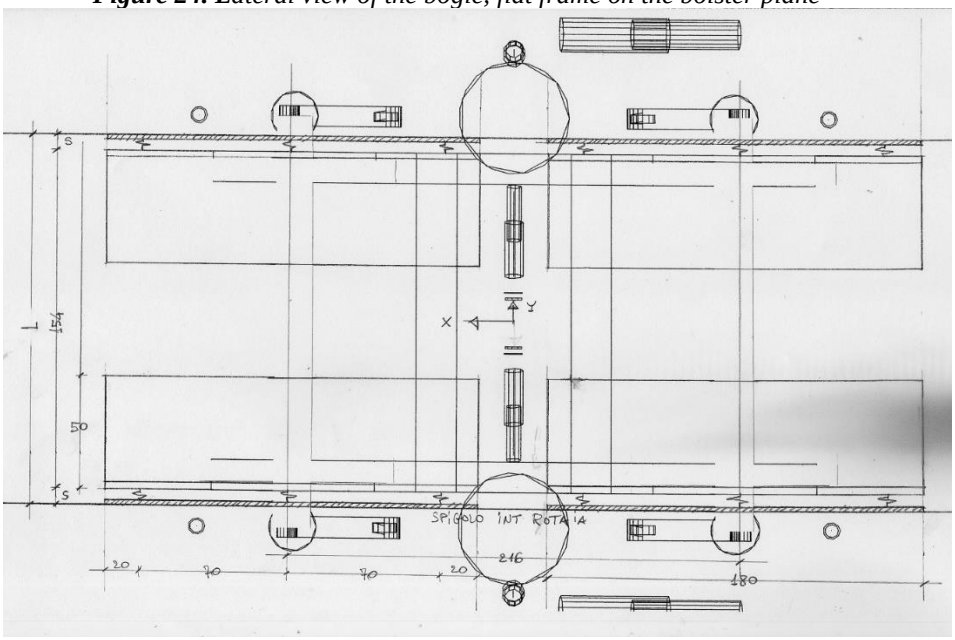

Figure 25. *Plan of the bogie (S_{mean}=5.5 cm), L=165 cm.*

7. Conclusions

The analyses were performed with a multi-body model for Metro B and C, with the same convoy going to and from the same carriage.

Such traffic is plausible but not rigorous; but it is perfect for producing the dynamic noises in the interaction model to obtain the analytical H/V diagrams.

We obtained the motion characteristics s(t), v(t) and a(t) for all nodes and the tensor characteristics ε(t) and σ(t) for all finite elements of the model.

References

[1] Perrone, V., "la ferrovia Metropolitana a Roma", Trasporti pubblici, nn. 4÷10 1952, nn. 1÷2, 9, 11 1953, nn. 5, 7÷8 1954.

[2] M. Bruner, (2001), "Analisi della marcia di un veicolo di Metropolitana", Tesi di laurea, Dpt Trasporti, Università di Roma "La Sapienza".

[3] Crisi, F., D'Ovidio, G., Valente, G., *"Metodologia di analisi delle vibrazioni strutturali dovute al traffico ferroviario: caso di studio dell'area archeologica del Colosseo"*, March 2009, Ingegneria Ferroviaria.

[4] F. Crisi, G. D'Ovidio, G. Valente, "Vibrations analysis in the archaeological area of Rome by rail traffic"**,** 4th VI-grade User's Conference - Udine, 18-19 October 2011.

[5] "Carrello Motore: descrizione, revisione generale e manutenzione", Pubblicazioni Tecniche CO.TRA.L., Roma.

[6] Estratti de "Disegni Tecnici Carrello Motore" Pubblicazioni Tecniche CO.TRA.L. Roma.

Dynamic characterization of soil by H/V model

Abstract

Since 1998, microtremor measurements were performed in about one hundred points in the ground of Colosseum area.

The train vibrations are used to obtain the analytical time histories in the same points, and the corresponding analytical H/V diagrams.

The comparisons between experimental and analytical H/V diagrams are used to obtain the best map of Young moduli of soil and foundations.

1. Introduction

In the soil-monument interaction, the trains' vibrations obtained from analysis are used to evaluate the analytical H/V diagrams to compare with experimental one.

2. The H/V technique

As well know, the horizontal motion shows larger value than the vertical motion on the soft ground, the same motions are similar on the hard ground. The horizontal to vertical spectral ratio of micro-tremor was confirmed is stable not depended on the measured time and season [4]. The characteristic of H/V for microtremor is summarized as follows. The first peak near F_0 consists of S-wave mainly. The first trough near 2 F_0 is caused by Rayleigh wave.
Around F_0 there is almost no energy of Rayleigh waves, so the dispersion curves are unstable near F_0. Rayleigh wave are growing from F_0, and reach the first peak near the 2 F_0. It is verified that the H/V spectral ratio of both microtremor and strong motion is useful for estimation of at least fundamental frequency F_0 and its amplification factor. Consequently, the excellent papers of Nogoshi and Igarashi (1971) and Suzuki (1933) have no relation to the H/V technique directory. Tests are used for the dynamic characterization in order to obtain the mechanical characteristics in the ground [1], [2], [7].

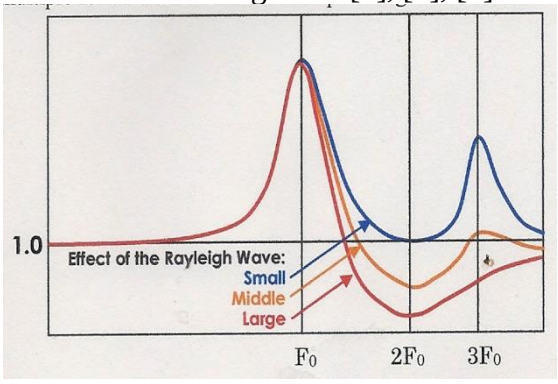

Figure 1. *Image of H/V Spectral Ratio*

***Figure 2**. Map of H/V diagrams in the Colosseum (in filigree) and on the ground, in two orthogonal directions*

Table 1. *Predominant frequencies, amplification factors, from H/V diagrams in the Colosseum and in the surroundings, in two orthogonal directions.*

QTS	lower range > 0.8Hz			higher range > 10Hz			foundation h = 6m		QTS	lower range > 0.8Hz			higher range > 10Hz			foundation h = 6m	
R or X	F	A	Kg	F	A	Kg	Vs_upper	Vs_lower	T or Y	F	A	Kg	F	A	Kg	Vs_upper	Vs_lower
	Hz		μ /Gal	Hz		μ /Gal	km/s	km/s		Hz		μ /Gal	Hz		μ /Gal	km/s	km/s
B4r	1.15	1.82	2.9	32.3	1.30	0.1		774	B4t	1.12	1.54	2.1	20.3	1.03	0.1		488
B5r	1.27	2.32	4.2	19.7	2.06	0.2		472	B5t	1.20	2.10	3.7	18.9	1.56	0.1		455
B6r	1.42	1.80	2.3	36.9	1.26	0.0		885	B6t	0.95	1.54	2.5	49.7	1.11	0.0		1194
B3r	1.07	2.20	4.5	26.0	2.58	0.3		623	B3t	1.10	2.05	3.8	22.9	1.92	0.2		550
B1r	1.22	1.81	2.7	29.7	1.09	0.0		714	B1t	1.44	1.83	2.3	32.2	1.12	0.0		773
B7r	1.15	1.60	2.2	24.3	1.52	0.1			B7t	0.98	1.70	3.0	27.1	1.55	0.1		
B2r=n	1.15	1.80	2.8	33.5	1.25	0.0			B2t=e	1.15	1.76	2.7	12.0	1.43	0.2		
BGEn	0.88	2.23	5.7	41.4	2.54	0.2			BGEe	1.12	2.24	4.5	23.5	1.44	0.1		
BGCn	1.34	1.97	2.9	10.3	1.39	0.2			BGCe	1.22	2.33	4.5	43.3	1.09	0.0		
BGWn	0.81	1.75	3.8	33.3	0.79	0.0			BGWe	0.95	2.00	4.2	25.1	0.81	0.0		
BGNn	0.90	3.20	11.4	25.4	1.48	0.1			BGNe	1.17	2.90	7.2	41.4	1.50	0.1		
BGSn	1.17	1.67	2.4	19.0	1.65	0.1			BGSe	0.78	1.77	4.0	35.7	1.37	0.1		
PODFEs	1.22	1.88	2.9	27.5	1.12	0.0		659	PODFEe	1.51	1.86	2.3	21.3	1.33	0.1		512
POD1Es	1.22	2.01	3.3	10.2	0.93	0.1			POD1Ee	1.61	1.80	2.0	32.4	1.45	0.1		
POD2Es	1.54	1.31	1.1	11.5	1.12	0.1			POD2Ee	1.76	1.58	1.4	44.6	1.13	0.0		
POD3Cs	0.78	1.60	3.3	10.5	1.50	0.2			POD3Ce	1.68	1.21	0.9	41.9	1.55	0.1		
POD4Ws	1.25	2.20	3.9	45.9	1.00	0.0			POD4We	1.32	1.57	1.9	46.4	1.73	0.1		
G1n	1.42	2.09	3.1	16.3	5.52	1.9	391	2157	G1e	1.37	2.30	3.9	17.7	1.95	0.2	425	830
G2n	1.17	2.26	4.4	49.7	1.69	0.1			G2e	1.12	2.39	5.1	49.7	2.00	0.1		
G3n	1.05	1.50	2.1	29.8	1.50	0.1			G3e	1.42	2.20	3.4	11.2	1.82	0.3		
G4n	1.34	2.80	5.8	11.7	1.78	0.3			G4e	1.44	3.23	7.2	13.9	1.71	0.2		
G5n	2.25	2.69	3.2	16.9	1.60	0.2			G5e	2.54	2.69	2.9	22.1	2.19	0.2		
G6n	1.25	2.48	5.0	37.4	2.04	0.1			G6e	1.22	2.19	3.9	45.9	2.84	0.2		
CG1r	0.95	2.57	6.9	15.4	10.69	7.4	370		CG1t	2.10	3.79	6.8	27.8	6.05	1.3	666	
CG2r	1.00	3.79	14.3	44.8	2.57	0.1			CG2t	1.66	1.93	2.2	41.9	2.44	0.1		
CG3r	1.15	3.04	8.1	15.5	11.19	8.1	371		CG3t	1.25	2.65	5.6	25.9	6.41	1.6	621	
CG4r	1.54	2.42	3.8	40.1	4.51	0.5	963		CG4t	1.27	3.06	7.4	47.0	4.82	0.5	1127	
CG5r	1.54	2.06	2.8	23.1	1.71	0.1	555	951	CG5t	1.78	2.62	3.9	49.7	1.95	0.1	1194	2324
CG6r	2.08	1.90	1.7	16.3	2.08	0.3			CG6t	1.90	2.13	2.4	21.0	2.16	0.2		
CG7r	1.12	2.20	4.3	12.5	3.21	0.8			CG7t	2.00	2.05	2.1	10.9	2.44	0.5		
CG8r	1.39	2.13	3.3	48.9	4.99	0.5	1174		CG8t	1.39	2.47	4.4	40.9	5.53	0.7	982	
CG9r	0.95	2.28	5.5	35.7	4.61	0.6	857		CG9t	1.07	2.41	5.4	38.4	2.81	0.2	922	2587
CG10r	1.10	2.51	5.7	33.2	10.11	3.1	797		CG10t	1.54	2.69	4.7	33.3	10.29	3.2	798	
CG11r	1.61	2.08	2.7	31.2	1.83	0.1	749	1373	CG11t	1.68	2.27	3.0	33.0	2.89	0.3	791	2284
CG12r	1.51	1.94	2.5	30.4	2.96	0.3	730	2162	CG12t	1.93	2.21	2.5	33.7	3.03	0.3	809	2446
4014n	1.27	2.33	4.3	20.1	2.16	0.2	482	1041	4014e	1.25	2.43	4.8	30.0	1.71	0.1	720	1231
21Gs	1.20	3.08	8.0	22.9	1.75	0.1	548	960	21Ge	1.20	2.87	6.9	22.9	3.68	0.6	549	2023
21UGs	1.20	2.46	5.1	30.4	1.86	0.1		729	21UGe	1.20	2.63	5.8	38.6	2.00	0.1		928
2502r	1.46	1.58	1.7	19.7	1.92	0.2	472	908	2502t	1.49	1.92	2.5	26.3	2.35	0.2	632	1487
3002r	1.39	1.76	2.2	37.7	1.75	0.1	905	1588	3002t	1.34	2.11	3.3	22.9	2.94	0.4	548	1611
3502r	1.05	1.64	2.6	24.1	1.71	0.1	578	987	3502t	1.17	1.96	3.3	29.4	2.47	0.2	707	1745
4002qr	1.03	1.94	3.7	40.4	1.76	0.1	970	1706	4002qt	1.05	1.89	3.4	23.9	2.37	0.2	572	1358
4502r	1.12	2.17	4.2	45.4	2.03	0.1	1089	2208	4502t	1.03	1.97	3.8	38.5	1.26	0.0	924	1169
5002r	1.05	2.32	5.1	46.7	1.47	0.0	1121	1647	5002t	0.95	1.94	4.0	43.6	2.86	0.2	1046	2994
5502r	0.98	1.81	3.4	36.5	1.81	0.1	876	1589	5502t	0.98	1.87	3.6	37.7	2.45	0.2	904	2212
GF2r	1.15	1.84	2.9	19.6	2.46	0.3	471	1158	GF2t	1.12	1.93	3.3	19.6	3.68	0.7	471	1732
0603qr	1.46	1.99	2.7	28.3	4.68	0.8	679	3173	0603qt	1.20	1.94	3.1	24.7	3.36	0.5	594	1996
1003r	1.22	2.19	3.9	21.1	2.71	0.3	507	1375	1003t	1.05	1.92	3.5	19.6	1.92	0.2	469	900
1503r	1.44	1.99	2.7	17.4	1.66	0.2	418	693	1503t	1.81	1.58	1.4	17.6	1.17	0.1	421	491
2003r	1.20	1.61	2.2	18.6	1.70	0.2	445	755	2003t	1.46	1.77	2.1	20.5	1.05	0.1	492	517
2503r	1.15	1.89	3.1	36.4	1.79	0.1	874	1567	2503t	1.15	2.77	6.7	36.4	2.07	0.1	874	1811
3003r	1.00	1.65	2.7	20.1	1.68	0.1	482	807	3003t	1.37	2.19	3.5	21.9	2.57	0.3	527	1355
3503r	1.17	1.25	1.3	20.4	1.43	0.1	489	698	3503t	1.25	1.78	2.6	12.5	1.06	0.1	300	318
4003r	1.05	1.64	2.6	25.2	1.84	0.1	606	1117	4003t	1.81	2.11	2.5	23.6	3.56	0.5	567	2017
4503r	1.05	1.93	3.6	49.7	2.77	0.2	1194	3301	4503t	1.15	1.55	2.1	34.0	1.76	0.1	816	1434
5003r	1.29	2.06	3.3	23.9	2.53	0.3	574	1450	5003t	1.76	1.91	2.1	48.1	2.82	0.2	1155	3254
5503r	1.00	2.58	6.6	14.9	1.33	0.1	357	477	5503t	1.56	1.98	2.5	48.2	1.36	0.0	1156	1569
GF1r	1.07	2.06	3.9	14.1	2.02	0.3	339	684	GF1t	1.15	1.88	3.1	32.3	1.85	0.1	774	1432
6503r	1.17	1.78	2.7	20.6	1.25	0.1	495	620	6503t	1.15	2.34	4.8	15.9	1.48	0.1	383	566
7003r	1.49	1.78	2.1	16.8	1.49	0.1	404	601	7003t	1.46	2.52	4.3	41.4	1.81	0.1	993	1796
7503r	1.49	1.96	2.6	37.0	1.70	0.1	888	1512	7503t	1.46	2.26	3.5	27.2	2.26	0.2	653	1476
8003r	0.78	2.60	8.7	32.3	4.45	0.6	774	3445	8003t	0.78	2.50	8.0	27.6	2.64	0.3	663	1751
2504r	1.22	1.83	2.7	25.1	2.24	0.2	602	1345	2504t	1.73	2.21	2.8	24.3	1.93	0.2	584	1127
3004r	0.95	1.72	3.1	28.1	2.36	0.2	673	1587	3004t	1.17	2.27	4.4	32.2	2.50	0.2	772	1926
3504r	1.12	1.69	2.5	30.3	1.89	0.1	727	1374	3504t	1.12	1.95	3.4	32.7	1.46	0.1	784	1142
4004r	1.10	2.07	3.9	27.5	2.89	0.3	661	1912	4004t	0.88	2.04	4.7	28.2	2.03	0.1	677	1371
4504r	1.03	1.75	3.0	30.2	1.79	0.1	725	1301	4504t	1.81	1.72	1.6	29.6	1.69	0.1	710	1197
5004r	0.95	1.75	3.2	19.8	1.82	0.2	475	865	5004t	0.98	1.95	3.9	26.0	1.64	0.1	625	1025
5504r	1.12	1.23	1.3	20.0	1.02	0.1	480	491	5504t	1.00	1.50	2.2	22.4	1.05	0.0	537	565
5904r	1.00	1.83	3.3	33.1	1.46	0.1	793	1159	5904t	1.05	1.94	3.6	33.3	1.98	0.1	800	1582
6004r	0.88	1.75	3.5	33.3	1.60	0.1	800	1283	6004t	1.39	2.02	2.9	20.0	1.15	0.1	481	555

2.1. H/V by tests

For Colosseum, many tests were performed in different times, since 1987 to 2015. Figure 2 illustrates a top view distribution of test points around 15 to 25 m for CGN1 to CGN6 corresponding to the pillar number #40 to #46. The experimental results are shown in the papers [1], [3], [5], [6], [7] at n. 87 points, for principal frequencies, amplification factors, diagrams, etc. Figure 1 shows the typical shape of the H/V spectral ratio. Table 1 lists the peak frequency and the amplification factor at the low frequency range of QTS. This table also includes the peak frequency and the amplification factor at high frequency range estimated as the S wave multiple reflections in the foundation concrete, and indicates S wave propagation velocity estimated from those values. The later discussion will be progressed based on the peak frequency and the amplification factor at high and low frequency range of QTS targeting a range over 0.8 Hz with high reliability.

2.2. Physical property of surrounding ground and foundation concrete of colosseum using microtremor [7]

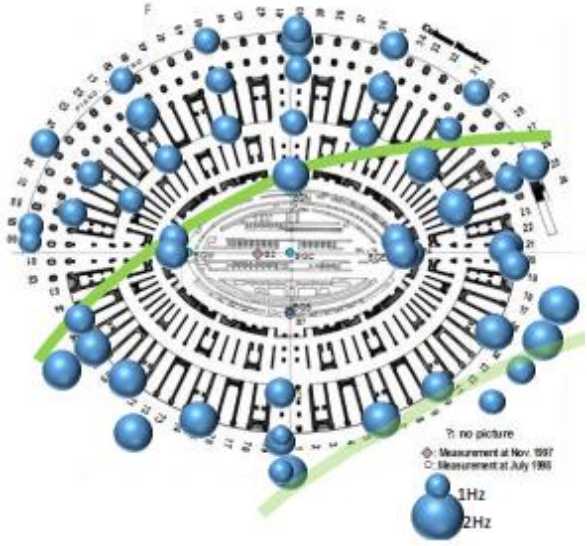

***Figure 3a**. Lower predominant. frequencies.*

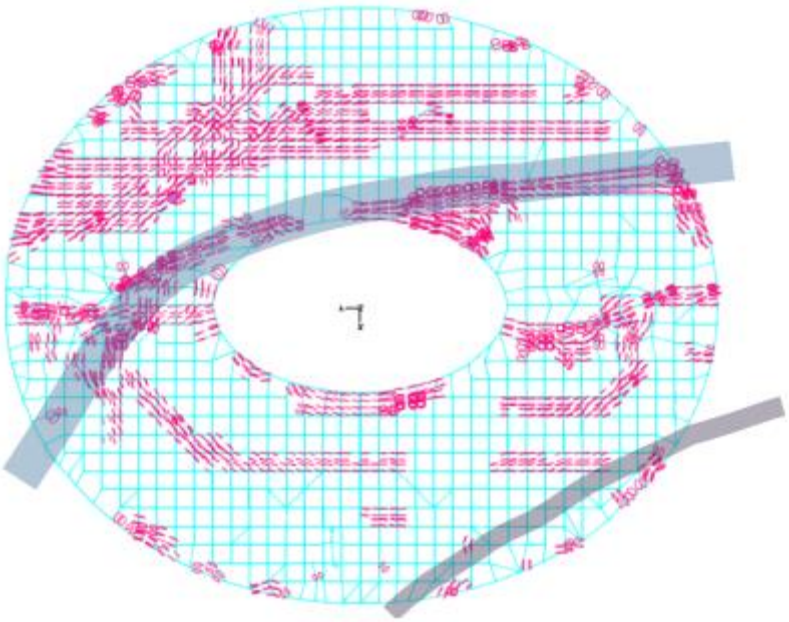

Figure 3b. *Crack estimation by FEM analysis*

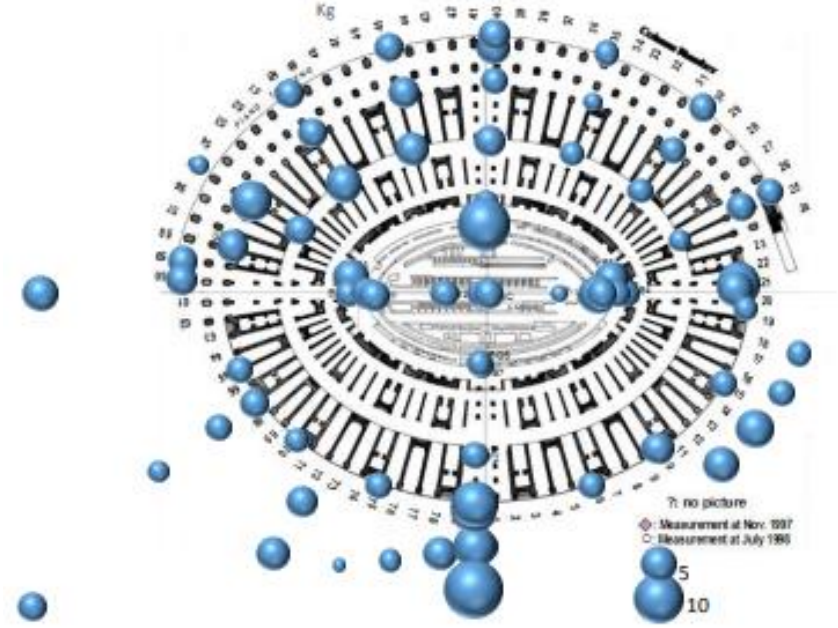

Figure 3c*. Distribution of Kg-value*

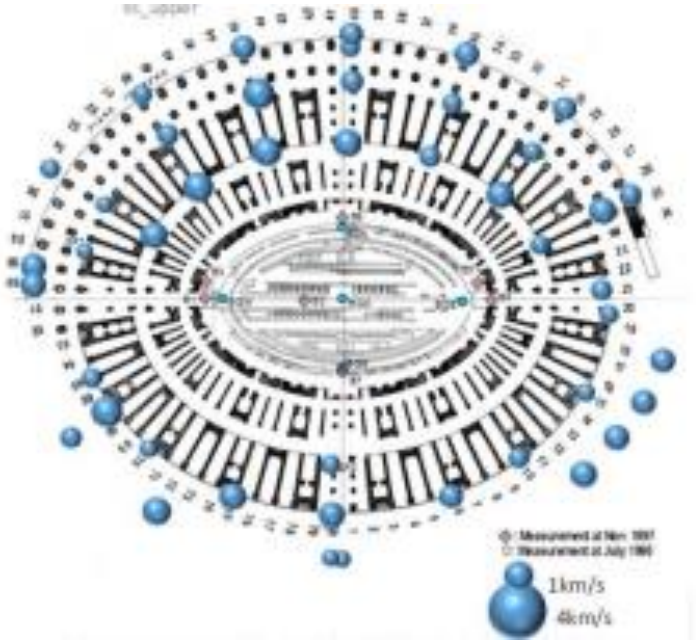

Figure 3d)

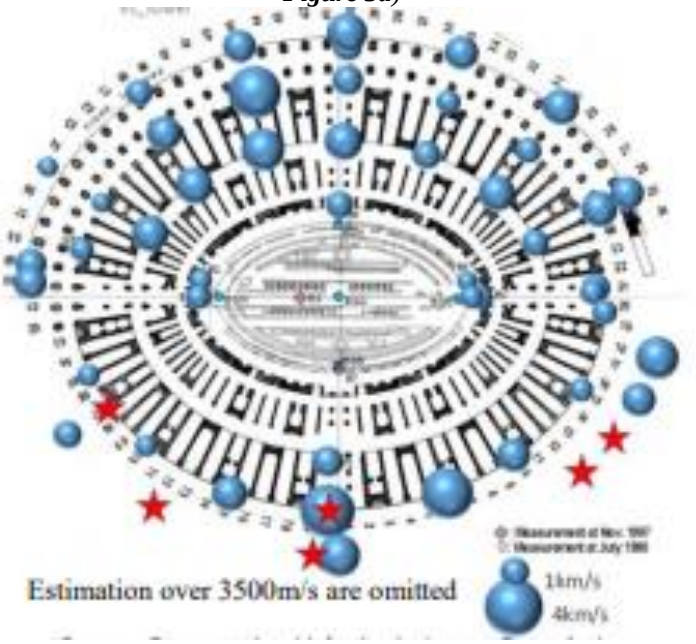

Figure 3d, e *Distribution of S wave velocity in foundations*

Figure 3a shows the predominant frequency as a size of bubble on the measured location. A tendency can be roughly grasped from these figures. That is, the predominant frequency is around 1.1 Hz and about 1.4 Hz at north and south side, respectively. The border is shown as green bold line on Figure 3a and it is impressive that this border seems to correspond to the location of the main estimated crack (see Figure 3b) or the northern border of southern deposit layer.
Figure 3c shows the distribution of Kg value of all the measurement points corresponding to the measured location and the size of bubble indicates the value of Kg value. Kg values are almost less than 5 and do not exceed 10 for all the points on the foundation. On the whole, large Kg value is observed at the points on the ground and also relative large Kg value is observed even at the points on the foundation around hypogeum at east side or southern side. The largest earthquake motion attacked Rome is considered as about 200 Gal of maximum acceleration or MMI VIII, and it will cause almost no ground deformation except on the ground in the southern side.
Figures 3d,e show a distribution of the estimated value corresponding to a size of bubble at the measured location.
Figures 3d,e show the estimated shear wave velocity on the foundation plane with a diameter of bubbles. A star means the abnormal value more than Vs = 3000 m/s. Although it is necessary to notice that this is tentative result because of the missing measured data, the shear wave velocity becomes large in north-west part of both the upper and lower foundation and also becomes large in south part of the lower layer.

Colosseum was constructed on a flat elliptic ring foundation with a hole at arena.

This foundation consists of two layers made by roman concrete with 12 m thickness.

SDR conducted microtremor measurement at totally 71 points at ground floor and surrounding ground of Colosseum till December 15, 2013.

This paper describes the attempt to estimate the physical property of the foundation concrete and surrounding ground of Colosseum using past microtremor measurement data.

Mainly with the vibration of radial direction, some impressive results was obtained such as that the distribution of the predominant frequency on the foundation corresponds to the distribution of clacks at the lower concrete foundation estimated by numerical analysis.

And more, estimation of S wave propagation velocity of upper and lower concrete of Colosseum foundation was attempted, because a possibility of capturing the multiple reflection phenomena in Colosseum foundation from QTS devised to obtain SH wave multiple reflections.

According to the comparison of the SH wave velocity estimated by the result of the measurement at northern ground of Colosseum, the estimation seems to give a certain value for the ground mentioned above.

However, the propagation velocity of the foundation has been not verified yet, we would like to confirm it in near future with direct measurement of them.

This method is a simple and the measurement for this method is possible to conduct repeatedly and precisely.

The authors will progress the validation of the estimation result with comparing to the other research one considering the estimation error and statistical scatter.

2.3. Test-analysis comparison for H/V [5]

Figure 4 shows the H/V analytical diagrams corresponding to the tests carried out by Authors at 9 check zones, as follows:

a) check points 1÷7, (from B1to B7) of hypogeum;
b) check points 8÷12, (BGC, BGE, BGN, BGW, BGS) of hypogeum;
c) check points 13÷17 (PDFE, PD1E,PD2E, PD3C, PDW4), hypogeum;
d) check points 18÷23, (from G1 to G6) on the ground at SW;
e) check points 24÷35, (from CG1 to CG12) at S of Colosseum;
f) check points 36÷46, at the ground, on the ring n.2;
g) check points 47÷62, on the ground, on the ring n.3;
h) check points 63÷71, on the ground, on the ring n.4;
i) check points 72÷76, (from ARG2 to ARG6) over Holocene.

j) check points 77÷87, (from CGN01 to CGN11) North side.
Da DISS12

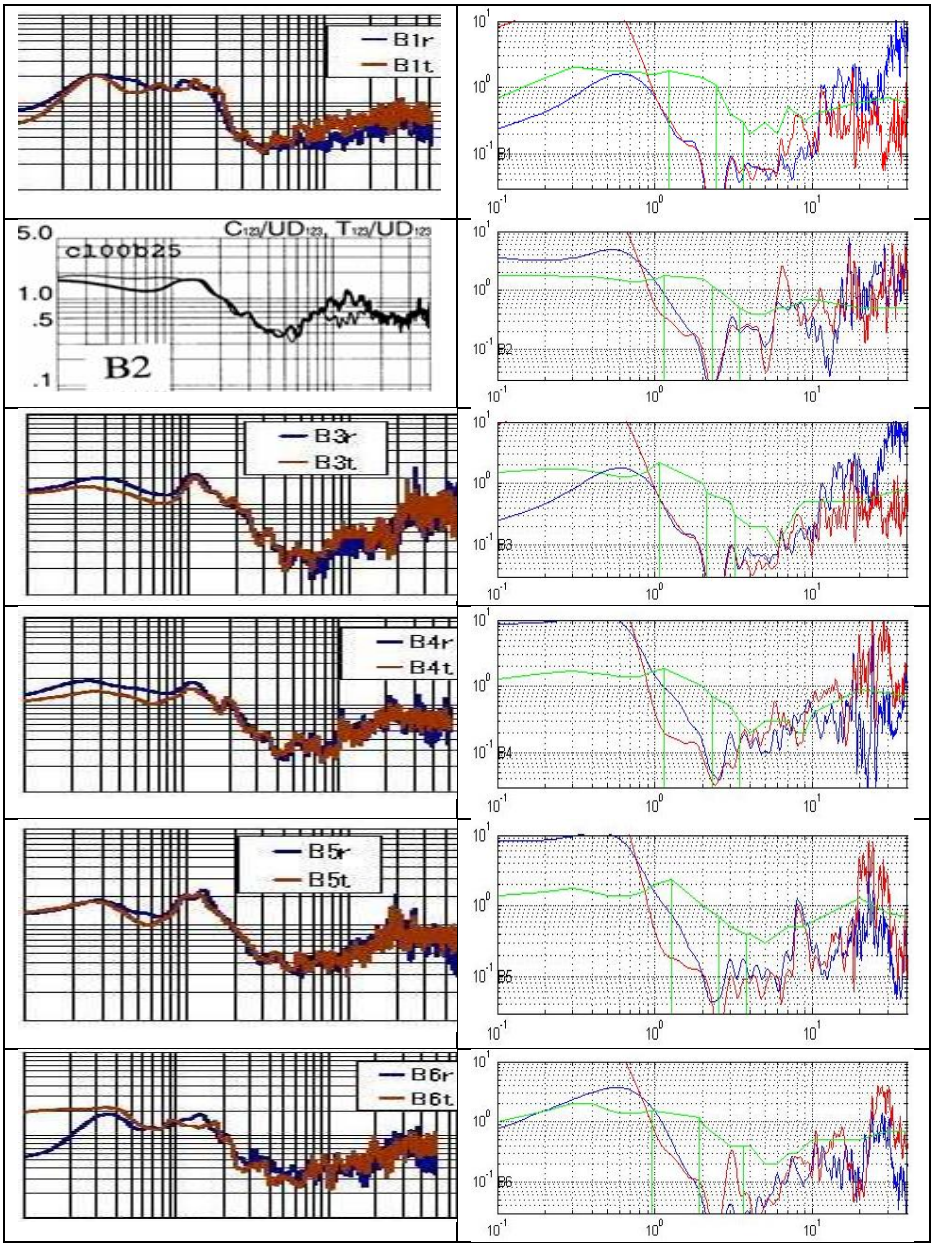

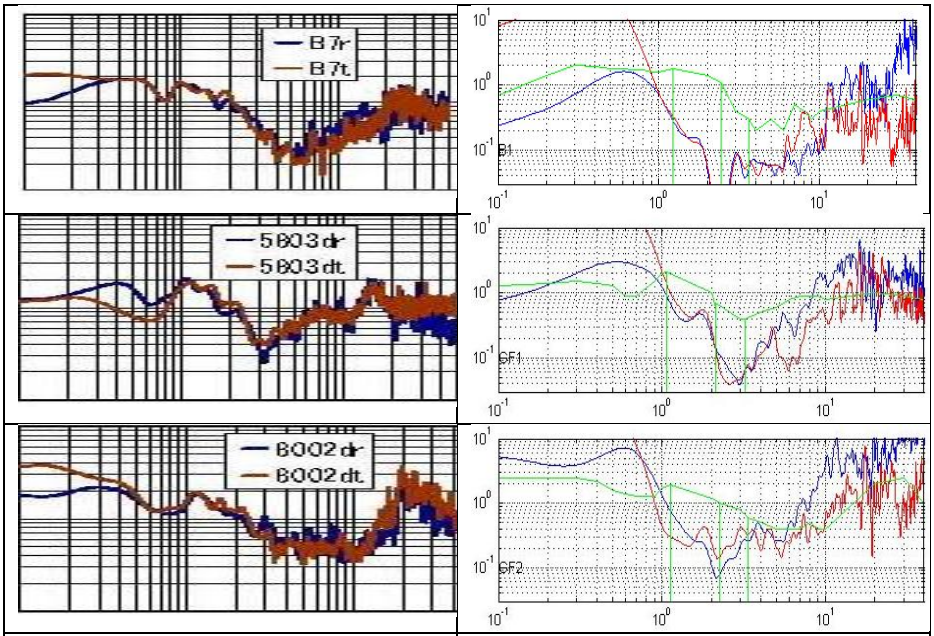

a) Hhypogeum and Ground Floor

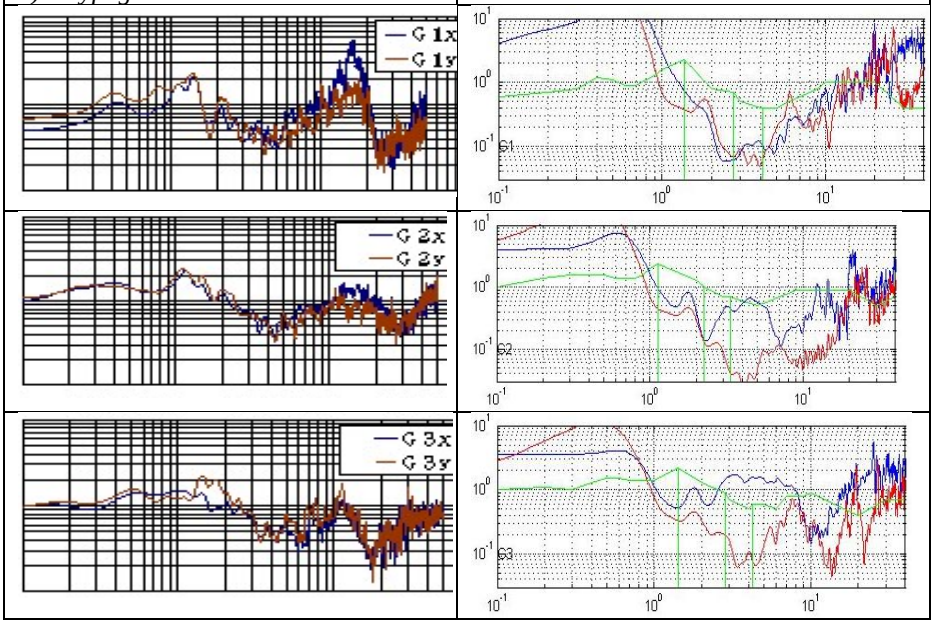

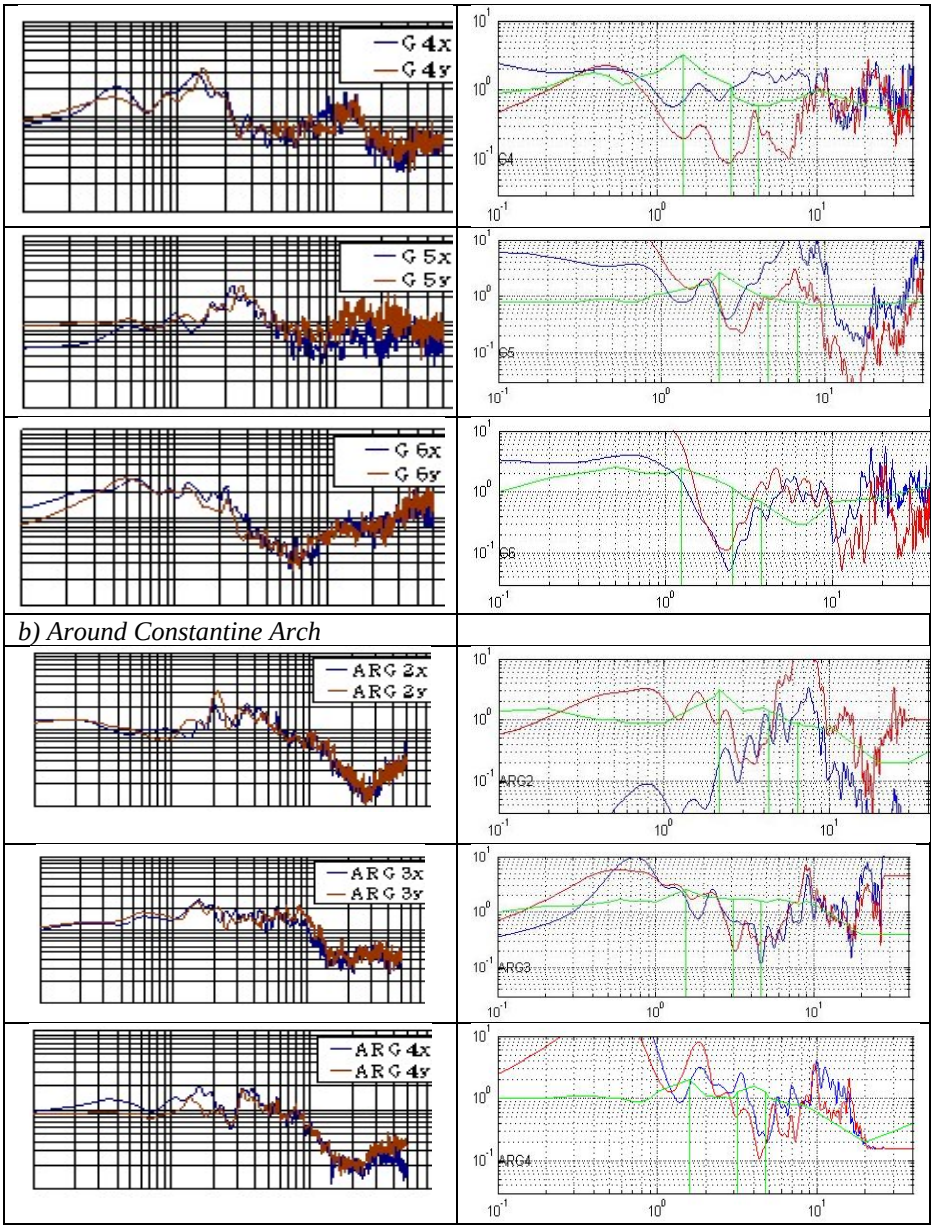

b) Around Constantine Arch

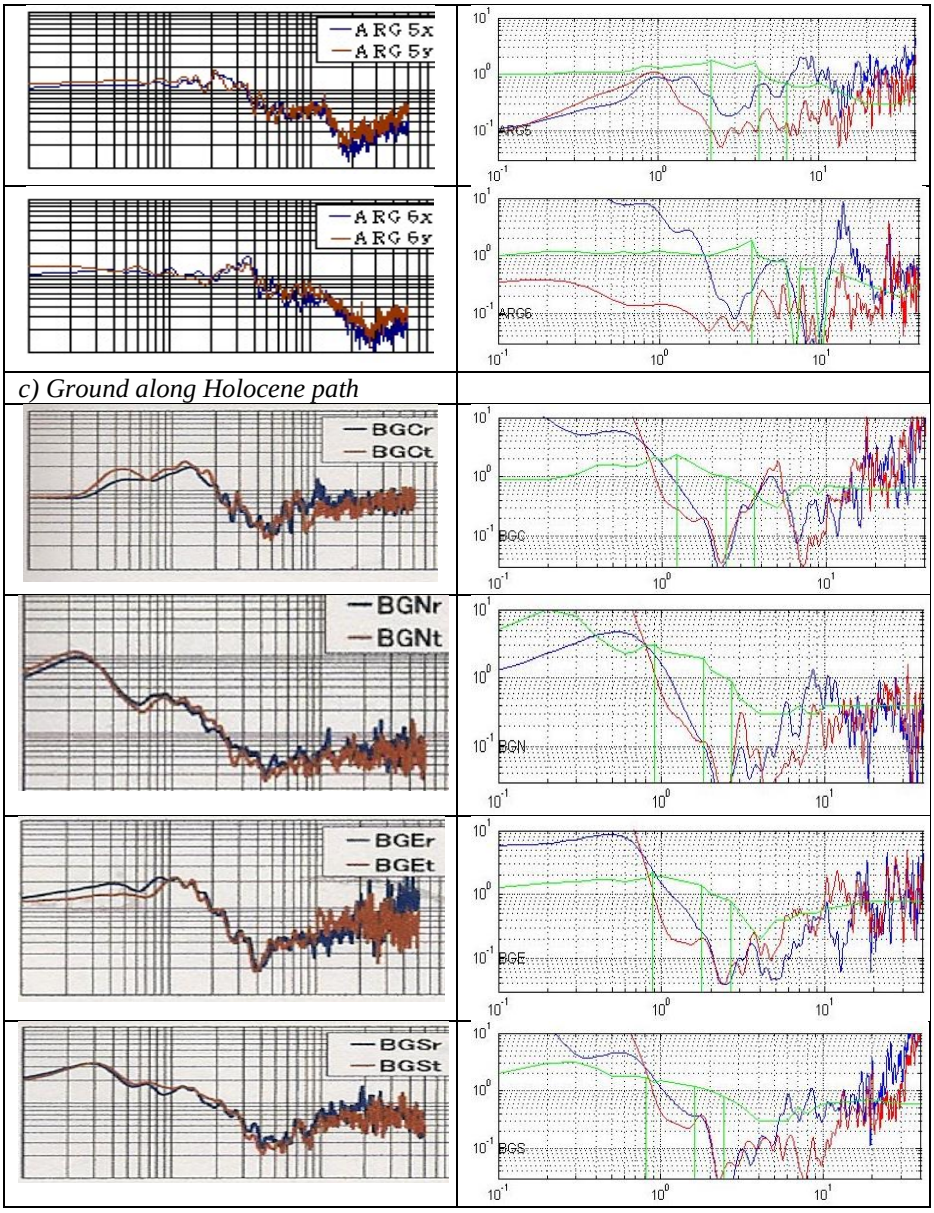
ARG 5x
ARG 5y
ARG5
ARG 6x
ARG 6y
ARG6
c) Ground along Holocene path
BGCr
BGCt
BGC
BGNr
BGNt
BGN
BGEr
BGEt
BGE
BGSr
BGSt
BGS

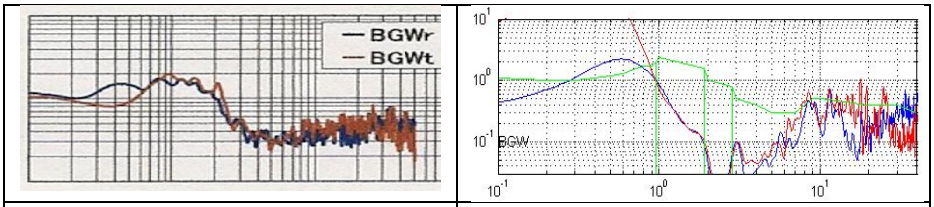

d) Hypogeum

Figure 4. *QTS of n.25 points. Blue EW or radial; Red NS or tangential. Green principal frequency and mean experimental values. Test on left, Analysis on right.*

We use the following notations: E-W or radial in blue line, N-S or tangential in red line.
The vertical lines represent the principal frequencies obtained by tests.
The values at the bottom of each diagram are:

the point number and name,

the two lower and higher principal frequencies by tests.

3. Results from [8]

3.1 Hypo configuration

The spectra were calculated in the frequency band frequency band 0.2-20 Hz, over time windows of 45 seconds duration, and "smoothed" with a Konno-Omachi with parameter b=40 (Konno & Omachi, 1998).

The windows were selected with the criteria described above, from simultaneous recordings of 30 minutes length.

The windows were selected with the criteria described above, from simultaneous recordings of 30 minutes length.
Figure 5 shows the spectral H/V ratios obtained at the stations.

Overall, the spectral shape of these ratios does not change substantially from station to station. Characteristics homogeneous between the curves are:

the presence of a first H/V peak at a frequency of approximately 0.3 Hz;

the presence of a second H/V peak at a frequency of approximately 1 Hz;

H/V values below unity in the frequency band between 2 and 15 Hz

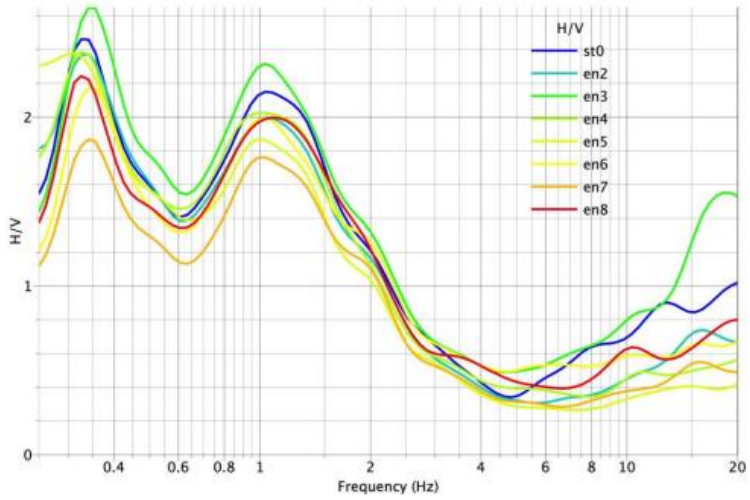

Figure 5*. Spectral H/V ratios calculated at stations.*

3.2 COM configuration

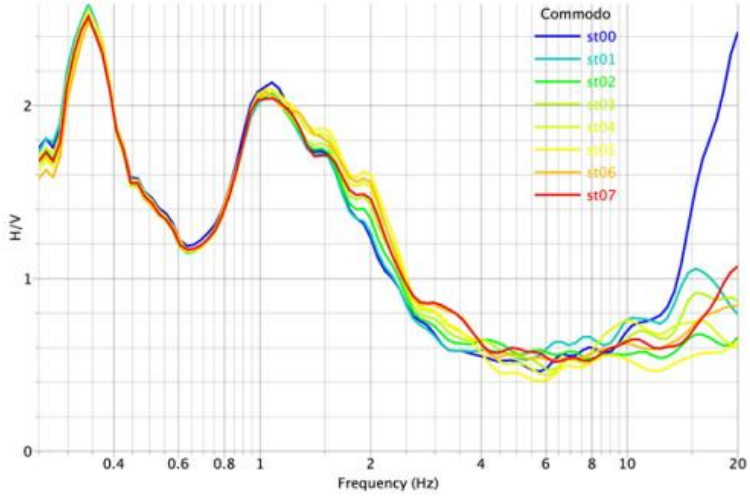

Figure 6. *H/V spectral ratios calculated at stations.*

The logistical characteristics of the Passage of Commodo,not accessible to visitors and separated from the rest of the monument by a lockable gate, made it possible to leave the stations in continuous recording even during the night hours. This made it possible to analyse both

daily variations in the level of ambient vibrations and the influence of these variations on the H/V spectral ratios.
The analyses performed by processing the data recorded during daytime hours are presented below.
Subsequently, a comparison between daytime data and night-time data will be presented for two stations in the configurations, night-time data.

Figure 6 shows the spectral H/V ratios obtained at the stations. Overall, the spectral shape of these ratios does not change substantially from station to station. Characteristics homogeneous between the curves are the presence of:

a first H/V peak at a frequency of approximately 0.3 Hz;

a second H/V peak at a frequency of approximately 1 Hz;

H/V below unity in the frequency band between 2 and 15 Hz.

The only exception is station st0 where a peak is evident at a frequency of about 25 Hz.

This peak could be associated with a disturbance of an electromagnetic nature.

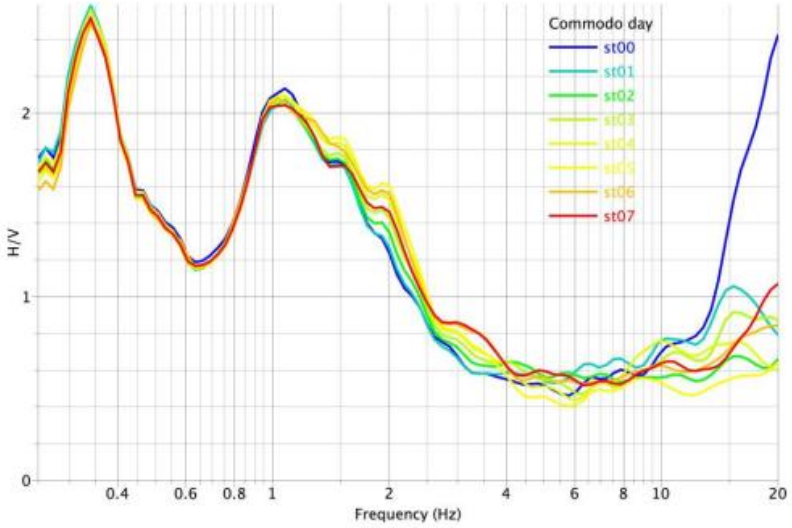

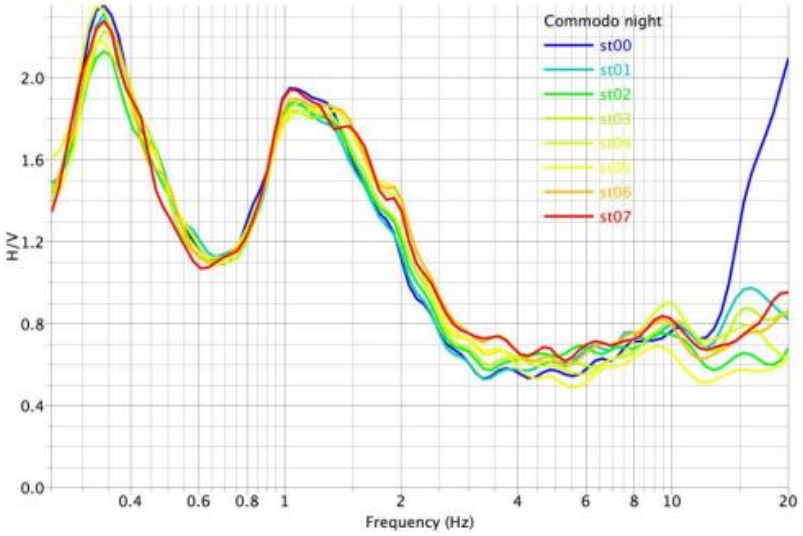

Figure 7*. Comparison of diurnal (top) and nocturnal (bottom) H/V spectral ratios*

However, it is interesting to observe how the differences shown at spectral level by stations st06 and st07 disappear in the H/V ratios, confirming that the amplifying effect is observed on all the

In Figure 7, the comparison of the H/V ratios obtained for all analysed stations does not shows no particular differences either between night and day or between station and station. This observation suggests the hypothesis that the H/V ratios can be calculated without paying particular attention to the external stress conditions.

3.3 Configuration FOR

The locations of the measuring stations are shown in Figure 8

In the dataset the recordings obtained taken into account in the dataset are also the recordings obtained at the underground level with the INGV velocimeter backhoe.

This measurement station remained operational during the entire day of 24/06/2014. All analyses were conducted using simultaneously recorded data.

Figure 8 shows the spectral H/V ratios. Overall, the spectral shape of these ratios do not change substantially from station to station. Homogeneous characteristics between the curves are:

the presence of a first H/V peak at a frequency of approximately 0.3 Hz;

the presence of a second H/V peak at a frequency of approximately 1 Hz;

H/V values below unity in the frequency band between approximately 2 and 15 Hz.

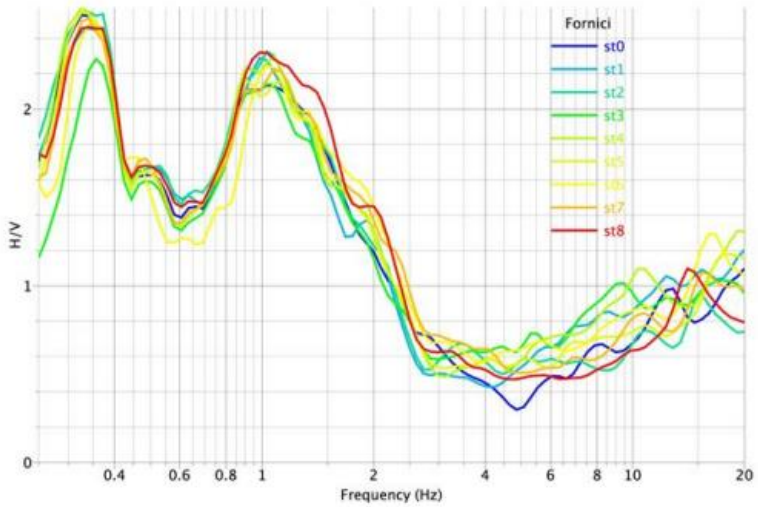

Figure 8. *Spectral H/V ratios calculated at stations*

The circles indicate the position of the INGV velocimeter backhoe loaders: red indicates positions at the current ground level while blue indicates positions at the underground level.

3.4 VER configuration

In order to provide a cognitive contribution regarding the dynamic behaviour of the elevation structure of the monument, the subject of a report prepared ad hoc.

INGV velocimeter terns were positioned along a vertical alignment in correspondence of the first arcade following the Buttress Valadier.

The stations were oriented on the horizontal plane according to the radial and tangential directions with respect to the centre in plan of the monument and were placed on the three walkable levels of the building (Figure 10).

The measuring stations recorded the signals over a time interval of more than 5 hours; this duration guarantees the statistical robustness of the results of the analysis conducted.

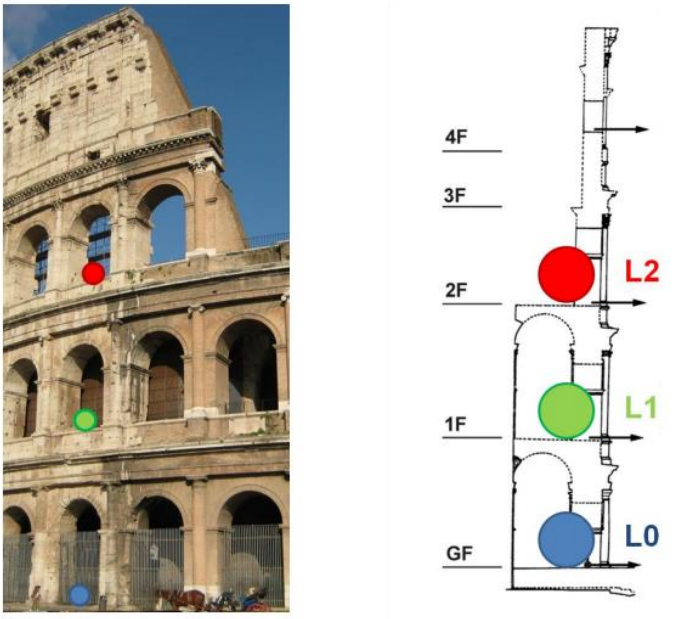

***Figure 9**. Location of the VER vertical.*

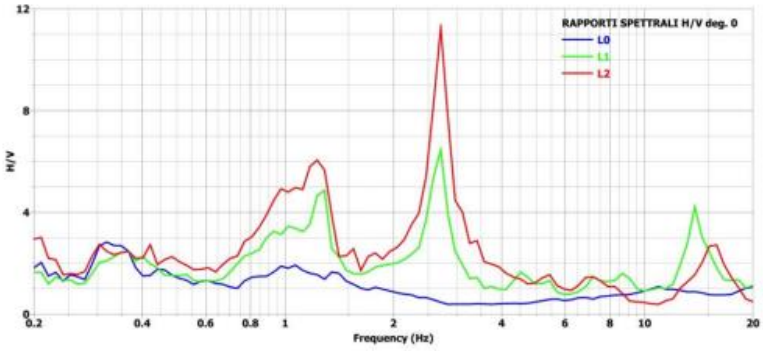

***Figure 10**. H/V ratios calculated at levels L0, L1 and L2 with 0° rotation.*

3.5. Tomography in the Commodo passage

The geophonic configuration used for seismic tomography is based on 59 sensors with spacing of 1 meter. Due to the nature of the passage's pavement, the sensors were placed on bases
support bases capable of ensuring, with their weight, coupling with the ground. The irregularities present in the pavement hindered the correct levelling of the sensors.
This was remedied by using sand for correct levelling (Figure 11). As an active source, a beating mass weighing 5 kg was used, which impacted on an aluminium plate.

The trigger was provided by a piezoelectric device attached to the source.

The source was moved along the line of receivers using a 2 m step with the first point of beat made at -1 m from the first receiver.

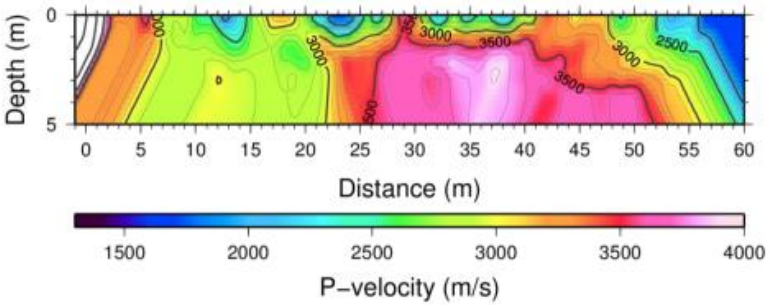

Figure 11. *Results of tomographic inversion of first arrival times. Path of the seismic rays (top). Number of seismic rays in the cells with which the model was discretized (middle). Final tomographic model obtained from the inversion of the first arrival times (bottom).*

Subsequent strikes were performed at an intermediate distance between the geophones of the spread.

At each energisation point, the measurement was repeated for three times in order to reduce the noise level on the recordings by summing the waveforms recorded to the same source-receiver pair (stack technique).

The sampling step was set at 0.125 ms (8000 Hz) with a recording duration of 1 second.

4. Conclusions

An attempt to estimate the mechanical properties of the Colosseum's surrounding soil using the H/V method for numerical-experimental comparison has been presented in this paper.

The proposed method allows to perform a real and in-depth structural characterization.

The results obtained are promising, as an acceptable degree of approximation between numerical and experimental data has been reached; however, further investigations are needed to calibrate the model.

References

[1] Yutaka Nakamura, Jun Saita, Antonio Rovelli, Stefano Donati, (1998). "*Seismic Response of Roman Colosseum and its Foundation by using Micro-tremor Measurements"* (in Japanese), The 10th Earthquake Engineering Symposium.

[2] Nakamura, Y., Gurler, E.D., Saita, J., Rovelli, A., Donati, S., (2000) *Vulnerability investigation of roman Collisseum using ambient vibration*, *12WCEE2000*, paper 2660.

[3] Nakamura, Yutaka, E. Dilek Gurler, Jun Saita, Antonio Rovelli, Stefano Donati. (2000). "*Vulnerability Investigation of Roman Colosseum using Microtremor*", 12th World Conf. on Earth. Eng., New Zealand.

[4] Yutaka Nakamura, (2012). *A modified estimation method for amplification factor of ground and structures using the H/V spectral ratio*, DISS_12

[5] Arrigo Caserta, Paolo Clemente, Yutaka Nakamura, Antonio Rovelli, Gianfranco Valente, (2012). "*Identification of mean elasticity modules for soil Colosseum interaction*", Proc. DISS_12, L'Aquila.

[6] Heinz-Jürgen Beste, Cinzia Conti, Gino D'Ovidio, Yutaka Nakamura, Luciana Orlando, Rossella Rea and Gianfranco Valente, (2013). "*The importance of defining the underground geometry for dynamic analysis of Colosseum*", Proceedings of the workshop DISS_13.

[7] Y. Nakamura, J. Saita, T. Sato and G. Valente, (2015). "*Attempts to Estimate the Physical Property of Surrounding Ground and Foundation Concrete of Colosseum using Microtremor*", DISS_15.

[8] Working Group: (ENEA) (INGV) (Sapienza Università di Roma) (Università dell'Aquila), (2015). "*Anfiteatro Flavio rilievo di vibrazioni ambientali: caratterizzazione del sito e della fondazione*".

Analysis of soil-Colosseum interaction

Abstract

A complete DISS FE 3D analysis was performed for the Colosseum, with Constantine Arch, a 600x600x80 m soil sod with anthropogenic, Holocene, Pleistocene, Gravel, Pliocene, station, Metro B and C tunnels. Elasticity moduli obtained from numerical-experimental comparisons for soil and elevation are used. Analyses were performed for: i) train action; j) Gabor wave; k) subsidence; l) foundation cracking due to the differential viscous effect between Holocene and Pleistocene and the loss of the southern elevation, with the nonlinear behaviour of concrete. We consider weak actions that produce linear elastic material behaviour. All the present analyses are qualitative, since: m) the six wagons are the same for each of the four convoys, for Metro B and C; n) the Young's moduli are approximated; o) the damping coefficients are approximative. The proposed model is oriented to deal with all types of structural events that the monument may suffer.

1. Introduction

These problems however are overcome in the investigative method we propose here, based on the analysis of ground-structure interaction using a geophysical model which ensures structural continuity between the ground, the foundations and the building.
This analysis methodology is applied, in a case study, to an archaeological area of Rome comprising the Colosseum and the Arch of Constantine affected by the B Line of the underground transport system (line B).
The evident greater cracks of Colosseum are introduced as disconnections of the 3D FE model.
The result is the map of the mean elasticity modules of the monument, taking into account the greater existing cracks in the 3D FE mesh; it is very different from the elasticity modules of the material; for travertine of the northern wall, the mean elasticity modulus is around 5,000 MPa, instead for a single specimen of the material is around 40,000 MPa.
For 2000 years, the soil transmitted all the vibrations to the monument, by ambient vibrations too.
The reliability was demonstrated by linear dynamic analyses performed for the aforementioned actions.
The final objective is to bring to perfection the proposed methodology up a small tolerance everywhere, in order to allow a researcher to check deterministically and not intuitively on PC the effect of:

a) traffic and materials variations, on the surface and inside the tunnels,

b) eventual seismic improvement.

Further tests and analyses are needed for:

c) Constantine Arch, cryptoportici and tunnels of Metro B and C;

d) improvement of geometric and mechanical characteristics of foundations and soil;

e) further cars and trains' models;

f) the map of damping coefficients.

Therefore, for each analysis, it is necessary to make the choice of models consistent with the objectives that are proposed; if the

elasticity modules are obtained from the numerical-experimental comparison with one of the models subsequently proposed, then they can be used with difficulty in the analysis of different actions with different models.
Some researchers, from the geotechnical and geophysical areas, have proposed a preliminary reconstruction of the stratigraphy beneath the Colosseum: while the northern part of the monument rests on a more rigid Pleistocene stratum, in its southern area there is a softer alluvial deposit, in a well-bounded depression of fluvial origin, already transformed from palaeo-tever to Labic ditch until the Holocene.
They find a significant amplification of the motion and its duration at the surface, and attribute the greatest damage, in the southern area of the Colosseum, to past earthquakes.
The same authors, basing themselves on the insufficiency of the experimental investigations existing at the time, have some uncertainty for the alluvial soil, and hope for the future, in addition to in-depth experimental tests, a complete 3D study, with the integration of step-by-step time, dynamic dissipation, any seismic action, the interaction between the soil and the monument, and all material nonlinearities.
The true place level is +23.26 m o.s.l. The tunnel of Metro C has: internal diameter 10. m, external 11. m, depth of the axis 20.76 m, it is developed parallel to greater axis of the monument, at North side, the distance between the tunnel axis and the monument axis is 120. m. The elliptical ring foundation has: depth 12.0 m, internal diameters d = 52.80 m and d = 83.70 m, external diameters d = 161.80 m and d = 193.20m.
In most cases monumental sites and structures were built without accounting of the soil characteristics, so they are very vulnerable to earthquakes and also to traffic-induced vibrations.
These represent continuous actions that affect buildings but are also a suitable and free source of excitation for experimental dynamic analysis of structures.
The same strengths $F_{iX}(t)$, $F_{iY}(t)$, $F_{iZ}(t)$ are then transferred into the corresponding nodes of the “soil-structure” model and act as input for the analysis of the structural vibrations of the constructions (buildings, monuments, etc.) included in the same model.

As a result, the analysis provides the values of the spatial components (X, Y, Z) for the movement characteristics *s(t)*, *v(t)* *a(t)* for all the nodes, and the tensors $\varepsilon(t)$, $\sigma(t)$ for all the elements for both models. Therefore, the proposed analysis methodology can be used to calculate the strengths acting on the soil, and to extract the vibration characteristics of all the elements of the soil-structure interaction.

2. The soil monument interaction

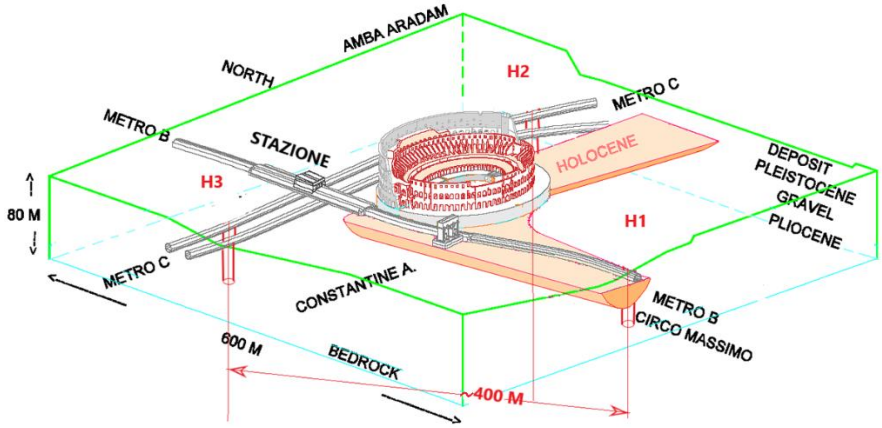

Figure 1. *3D FE model of the area.*

The soil-structure interaction is derived from the literature of the disciplines of Geophysics and Geotechnics; for seismic analysis, the problem of transparency to the dynamic energy on the soil boundary [13], [9], [11], [2], [4], [5], [8], [12], [10].

The ground is represented as a semi-indefinite continuum which, for the analysis, is limited to a finite portion, confined to a sufficient distance from the structure, where tension and/or deformation changes due to loads become negligible.

Furthermore, it is necessary to impose boundary conditions that guarantee the continuity of displacements and stresses across the geometric boundary of the ground; such an edge is also called non-reflecting, or silent; it must be indifferent to the frequency of the incident wave, and therefore suitable for transient analysis in the time domain.

There are several techniques [8] to impose this condition on the subsurface geometry:

superposition boundary, fictitious material damping, viscous dampers, doubly asymptotic approximation, paraxial boundary, extrapolation algorithm.

Dynamic damping is constant in the model according to Rayleigh law ($C=\alpha M+\beta K$) and is 5 % for the first two vibration modes.

The "soil-structure interaction" model with FE is contained in a "pool", with infinitely stiff walls, with the "bedrock" situated 80 m under the intradox of the Colosseum foundations.

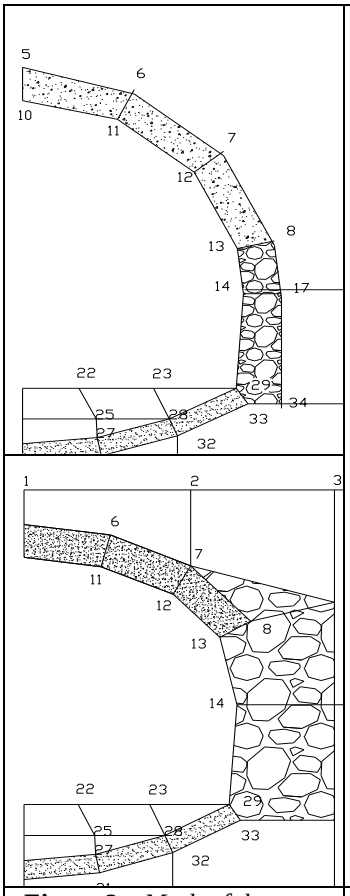

***Figure 2a**. Mesh of the current tunnel, and lowered (between sections 9-15).*

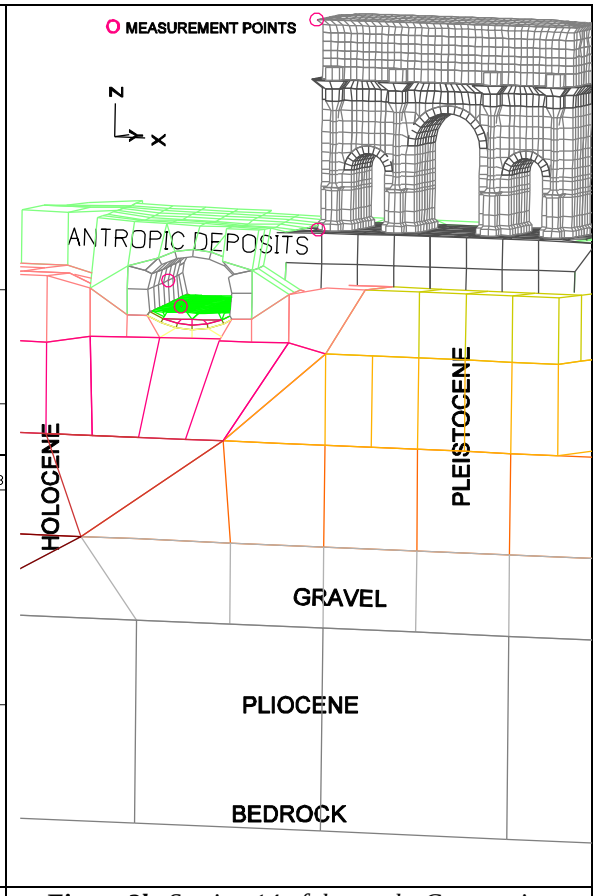

***Figure 2b.** Section 14 of the mesh: Constantine arch, stratigrafy.*

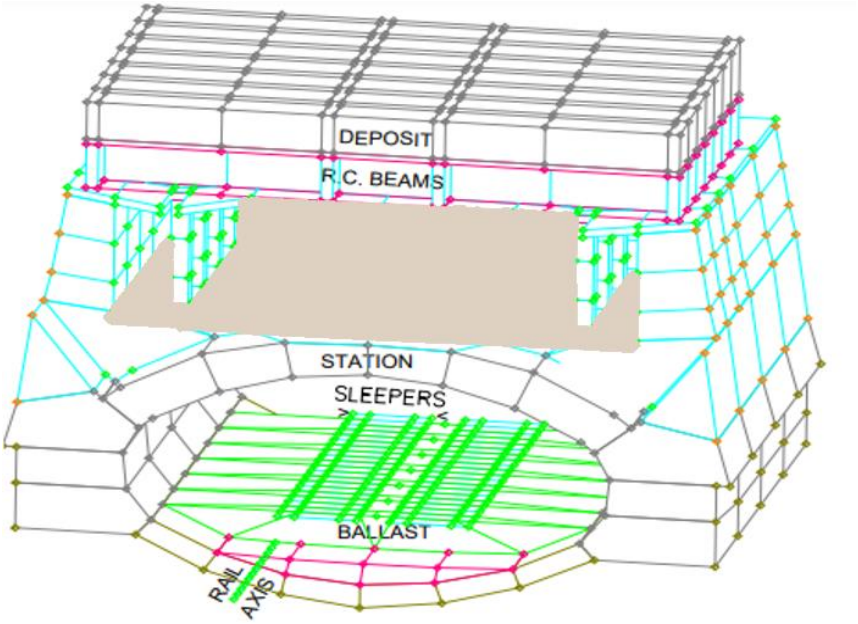

Figure 2c. *Station FE; station tunnel of Metro B.*

In order to avoid the effect of waves rebounds, a damping pool was created on the boundary of soil model [2], with Rayleigh coefficient χ=0.85 between frequencies 1÷10 Hz, as in Figure 2d.

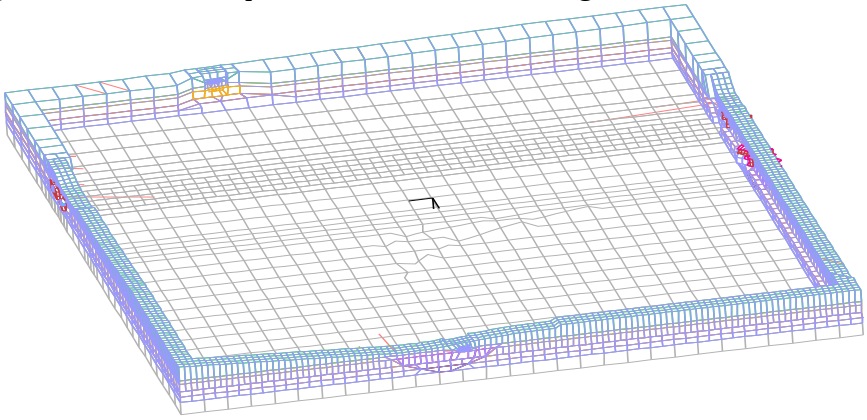

Figure 2d*. The damping pool (absorbing boundary). Rayleigh=85%, for fr=1÷6 Hz.*

3. Trains action

The strengths between wheels and rails are the input for the model which of "soil-structure" interaction to evaluate the structural vibrations.
The characteristics of motion *s(t)*, *v(t)* and *a(t)* for all of the nodes, and the tensorial characteristics $\varepsilon(t)$ e $\sigma(t)$ for all of the finite elements (EF) of the model are obtained in the paths A/R for the Metro:

B, between the stations of Colosseum and Circo Massimo;

C, between the stations of Colosseum and Amba Aradam.

Let us consider the i-th wheel (i=1÷24) on the right rail; from the simulation with multi-body model we obtain:

$$^{IR}s(t), \quad \text{continuous abscissa, i-th wheel, right rail R} \tag{1}$$

$$^{IR}P_X(t),\ ^{IR}P_Y(t),\ ^{IR}P_Z(t), \text{ loading of the i-th wheel / rail R} \tag{2}$$

3.1. Reactions at the crossing between rails and sleepers

As in Figure 3a, between the j-th sleeper (j=1÷850) and the right rail, three elastic linear supports are considered in the directions x, y, z. The constant coefficients (^{JR}K) are derived from the analysis of the model in Figure 3a, as the ratio between applied forces (^{JR}R) and the corresponding displacements ($^{JR}\delta$) according the following relations:

$$^{JR}K_X = {}^{JR}R_X / {}^{JR}\delta_X \tag{3}$$

$$^{JR}K_Y = {}^{JR}R_Y / {}^{JR}\delta_Y \tag{4}$$

$$^{JR}K_Z = {}^{JR}R_Z / {}^{JR}\delta_Z \tag{5}$$

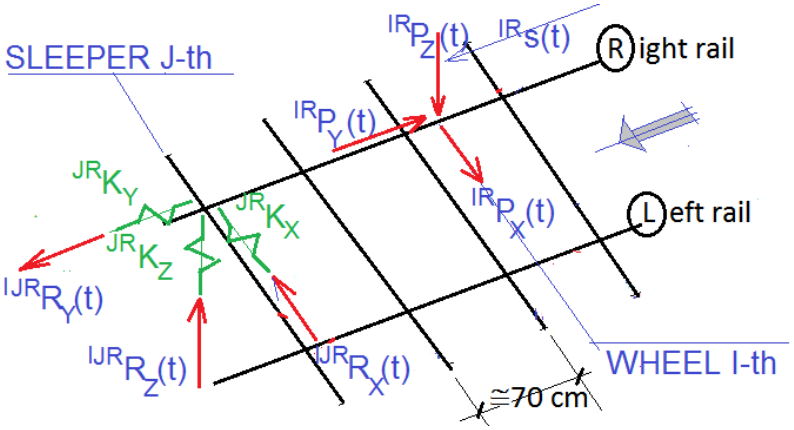

***Figure 3a**. Train-track detail model.*

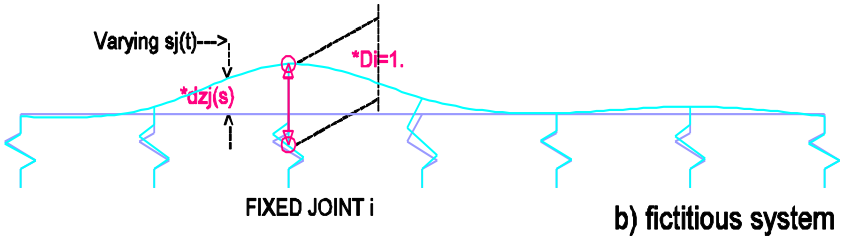

***Figure 3b.** Elastic beam: a) deformation, reactions; b) IL of reaction.*

For one single load ${}^{IR}P_Z(t)=1$ and for whatever the travelling distance ${}^{IR}s(t)$, it is obtained the reaction at the crossing (JR):

$$ {}^{IJR}\underline{\mathbf{R}}_Z(s)= *dzj(s) \qquad (6)$$

With reference to Figure 3b, it results that the fictitious displacement *dzi at abscissa si(t) correspond to the reaction at support j produced by load Pzi=1.
The static "Influence-Functions" depend on abscissa (s) alone, as in Figure 3a:

$$ {}^{IJR}\underline{\mathbf{R}}_X(s), \quad {}^{IJR}\underline{\mathbf{R}}_Y(s), \quad {}^{IJR}\underline{\mathbf{R}}_Z(s), \qquad (7)$$

They evaluate the reaction components at fixed crossing point (JR), produced by unity values of the loading: [$^{IR}P_X(t)=1$, $^{IR}P_Y(t)=1$, $^{IR}P_Z(t)=1$].
For the strengths of the single wheel [$^{IR}P_X(t)$, $^{IR}P_Y(t)$, $^{IR}P_Z(t)$], moving with $^{IR}s(t)$, by the "Influence-Functions" we evaluate the reaction components [$^{IJR}R_X(t)$, $^{IJR}R_Y(t)$, $^{IJR}R_Z(t)$] at fixed crossing point (JR). The total reaction components in the crossing between the right rail and the j-th sleeper are:

$$\begin{aligned} {}^{JR}R_X(t)&=\Sigma\ {}^{IJR}\underline{\mathbf{R}}_X(s)\ {}^{IR}P_X(t),\\ {}^{JR}R_Y(t)&=\Sigma\ {}^{IJR}\underline{\mathbf{R}}_Y(s)\ {}^{IR}P_X(t)\\ {}^{JR}R_Z(t)&=\Sigma\ {}^{IJR}\underline{\mathbf{R}}_Z(s)\ {}^{IR}P_X(t) \qquad (i=1\div 24) \end{aligned} \qquad (8)$$

These reactions [$^{JR}R_X(t)$, $^{JR}R_Y(t)$, $^{JR}R_Y(t)$], with changed sign are applied to the second model, and the obtained outputs are: a) values of the spatial components (X, Y, Z) for the movement characteristics [s(t), v(t), a(t)] at all the nodes; b) tensors [ε(t), σ(t)] at all the elements. These outputs are used for the dynamic identification obtaining the map of elasticity modules for soil, foundations and monument. The second 3D FFEE model of soil-structure interaction may be analysed under other loading conditions like: strengths for surface traffic, accelerations at bedrock for earthquakes, etc

The contact strengths in the train model are function of space and time; they are transformed in the strengths in the rail sleeper connection in Figure 4 function of the time alone.

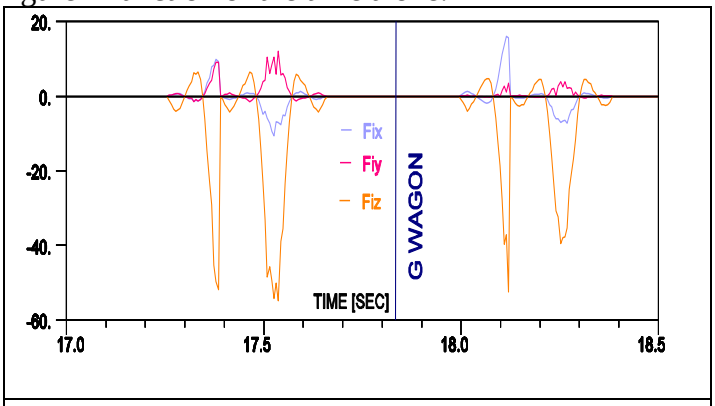

Figure 4. *Typical Force in rail-sleeper connection.*

The transit of trains is reproduced by imposing the tachimetric measurements that is defined by the following characteristics:

- maximum starting acceleration a = 1.0 m/sec^2;
- minimum stopping deceleration d = -1.1 m/sec^2;
- for trains from Colosseum to Circo Massimo stations, velocities at the axes of Colosseum, Constantine arch and Antiquarium: 47.0, 57.0 and 66.0 km/h, respectively.

The simulation of train transits was performed by imposing the following severe traffic assumptions:

a) The tracks of B and C lines are simultaneously travelled in both directions by four trains with 6 wagons full loaded;
b) Different starting times of Metro B and C trains as shown in Table 2;
c) Simultaneous arrival of the middle points of the four convoys on the principal diameters of Colosseum, according to the Table 2, at time $^{AXES}t_{MAX}$= 25.280 secs.

Passage of Metro B from Colosseum to Circo Massimo

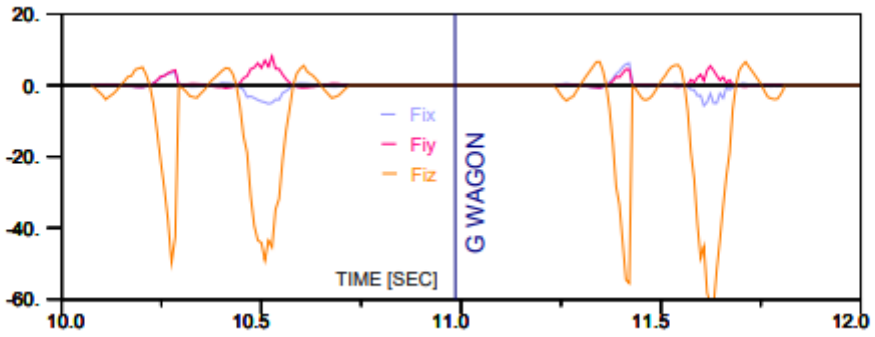

Figure 17. Strengths FiX(t), FiY(t), FiZ(t) in the connection rail-sleeper in the section 11 (Colosseum) in the time interval 10÷12 sec, FiZMAX= 49÷62 kN.

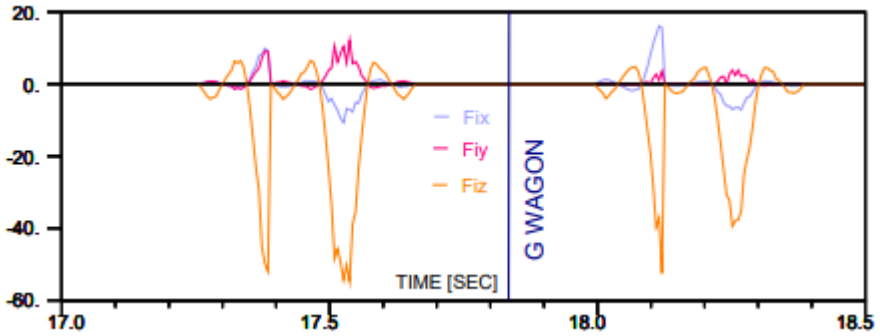

Figure 18. Strengths FiX(t), FiY(t), FiZ(t) in the connection rail-sleeper in the section14 (Constantine arch) in the time interval 17÷18.5 sec, FiZMAX= 40÷57 kN.

Figures 17 and 18 highlight 4 peak values for strength FiZ(t) corresponding to the transit of 4 wheels on the left side of the wagon in sections 11 and 14, respectively; the passage 16 of different parts of the wagon is observed in the following time succession:

1) the anterior boogie,
2) the centre of gravity,
3) the posterior boogie. Table 4. Transit of the wagon's centre of gravity through sections 11, 14 and 21.

***Table 4**. Transit of the wagon's centre of gravity through sections 11, 14 and 21.*

Sec.	Monument	T [sec]	Displacement [m]			Velocity [m/sec]		
			s_X	s_Y	s_Z	v_X	v_Y	v_Z
11	Colosseum	10.98	0.52	54.7	-0.68	0.37	9.8	-0.14
14	Constantine a.	17.83	18.8	146.0	-2.18	5.0	14.5	-0.15
21	Antiquarium	31.82	57.8	375.0	-2.25	1.33	18.5	0.03

3.2. Paths for metro B and C

Figure 5a shows the stopped n. 4 convoys at Colosseum station on Metro B and C, at different times, starting an arriving too.

Table 1 regards the time and space of the n. 4 convoys, from the starts to the principal diameters of Colosseum to their arrivals, running separately.

Table 2 concerns the time and space of the n. 4 convoys, in order to arrive synchronously, in axis of the n. 2 principal diameters of Colosseum, as in Figure 5b, at time $^{AXES}t_{MAX}$= 24.945 secs.

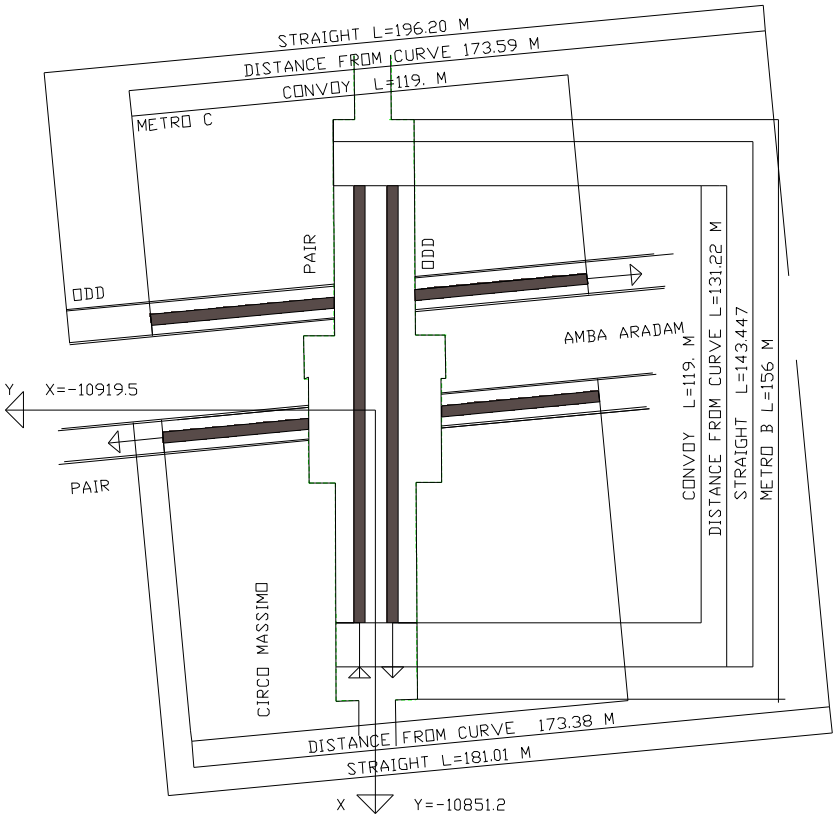

Figure 5a*. Placement of stopped trains at Colosseum station, for Metro B and C, at different times:* $^{B}t_{COL\_MAX}$=4.585 sec, $^{B}t_{MAX\_COL}$=35.065 sec, $^{C}t_{COL\_AMB}$= T=4.66 sec, $^{C}t_{AMB\_COL}$=35. sec.

Table 1 *– Separate paths on the four rails.*

Metro	From	To	Start	Diameters	Arrival	Δt
B	Colos-seum	Circo Massimo	T=0	T=17.090	T=40.	8.115
			s=0	s=109.19	s=497.00	
B	Circo Mass.	Colosseum	T=0	T=25.200	T=40.	3.460
			s=0	s=390.086	s=499.276	
C	Colos-seum	Amba Aradam	T=0	T=17.005	T=40.	8.165
			s=0	s=108.51	s=497.02	

C	Amba Aradam	Colosseum	T=0	T=25.280	T=40.	0.
			s=0	s=429.055	s=537.565	

Table 2 *– Synchronous paths of the four rails.*

	Synchronous space and time		
	Start	On axes	Arrival
COL_MAX	T=8.250	T=25.280	T=44.585
	s=0.	s=109.51	s=496.092
MAX_COL	T=0.065	T=25.280	T=35.065
	s=480.949	s=109.51	s=0.
COL_AMB	T=8.250	T=25.280	T=44.66
	s=0.	s=108.52	s=496.11
AMB_COL	T=0.0	T=25.280	T=35.
	s=481.109	s=108.52	s=0.

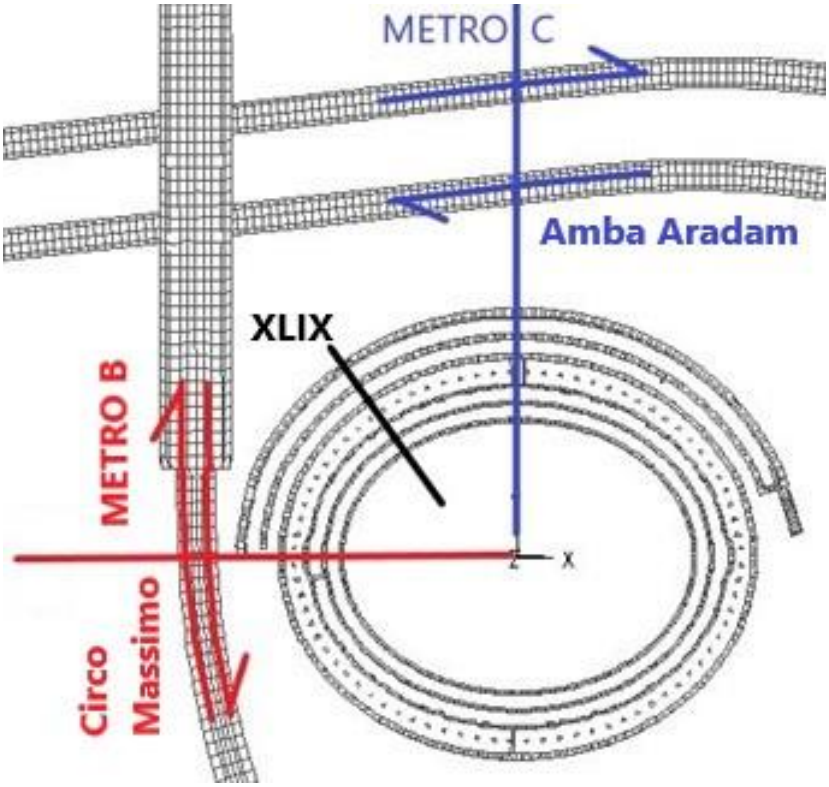

Figure 5b. *Interested paths. Synchronous placements of the four trains, centred on the principal axes, at distances* ${}^{X}d_b$*=109.19 m,* ${}^{Y}d_c$*=108.51 from the station, at time* ${}^{B}t_{COL\_MAX}$= ${}^{B}t_{MAX\_COL}$= ${}^{C}t_{COL\_AMB}$= ${}^{C}t_{AMB}$

3.3. Analysis of trains action on the soil

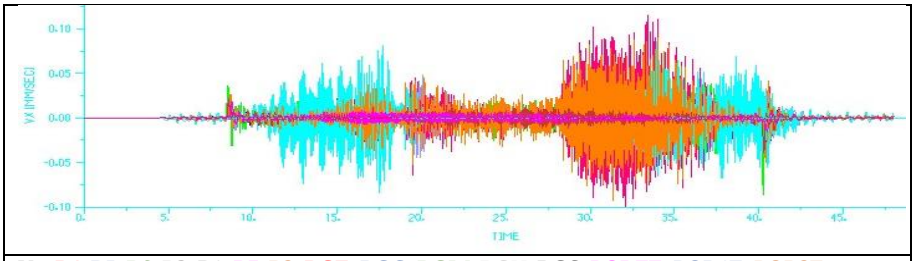

Vx: **B4,** **B5,** **B6,** **B3,** **B1,** **B7,** **B2,** **BGE,** **BGC,** **BGW,** **BGN,** **BGS,** **PODFE,** **POD1E,** **POD2E,** **POD3C,** **POD4W,** **G1,** **G2,** **G3,** **G4,** **G5,** **G6,** **CG1,** **CG2,** **CG3,** **CG4,** **MAGENTA** **CG5,** **CG6,** **CG7,** **CG8,** **CG9,** **CG10,** **CG11,** **CG12,** **4014,** **21G,** **21UG,** **2502,** **3002.**

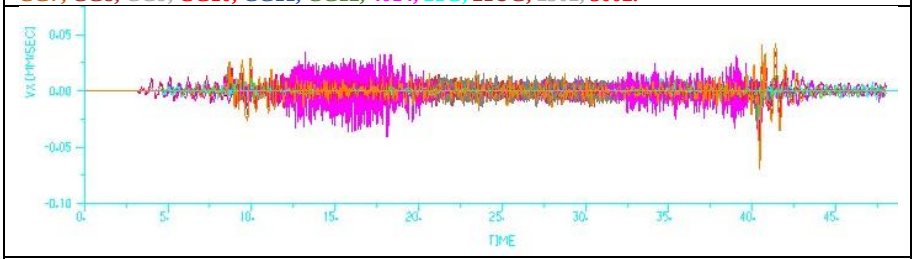

Vx: **3502,** **4002,** **4502,** **5002,** **5502,** **GF2,** **0603,** **1003,** **1503,** **2003,** **2503,** **3003,** **3503,** **4003,** **4503,** **5003,** **5503,** **GF1,** **6503,** **7003,** **7503,** **8003,** **2504,** **3004,** **3504,** **4004,** **4504,** **5004,** **5504,** **5904,** **6004,** **ARG2,** **ARG3,** **ARG4,** **ARG5,** **ARG6,** **4011,** **4012,** **4013,** **4014.**

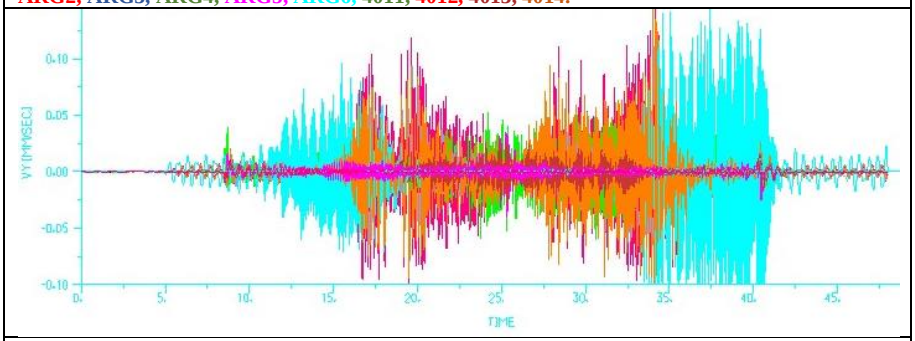

Vy: **B4,** **B5,** **B6,** **B3,** **B1,** **B7,** **B2,** **BGE,** **BGC,** **BGW,** **BGN,** **BGS,** **PODFE,** **POD1E,** **POD2E,** **POD3C,** **POD4W,** **G1,** **G2,** **G3,** **G4,** **G5,** **G6,** **CG1,** **CG2,** **CG3,** **CG4,** **MAGENTA** **CG5,** **CG6,** **CG7,** **CG8,** **CG9,** **CG10,** **CG11,** **CG12,** **4014,** **21G,** **21UG,** **2502,** **3002.**

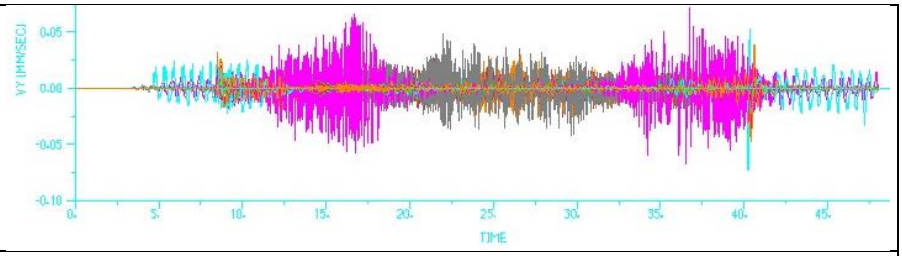

Vy: **3502, 4002, 4502, 5002, 5502, GF2, 0603, 1003, 1503, 2003, 2503, 3003, 3503, 4003, 4503, 5003, 5503, GF1, 6503, 7003, 7503, 8003, 2504, 3004, 3504, 4004, 4504, 5004, 5504, 5904, 6004, ARG2, ARG3, ARG4, ARG5, ARG6, 4011, 4012, 4013, 4014.**

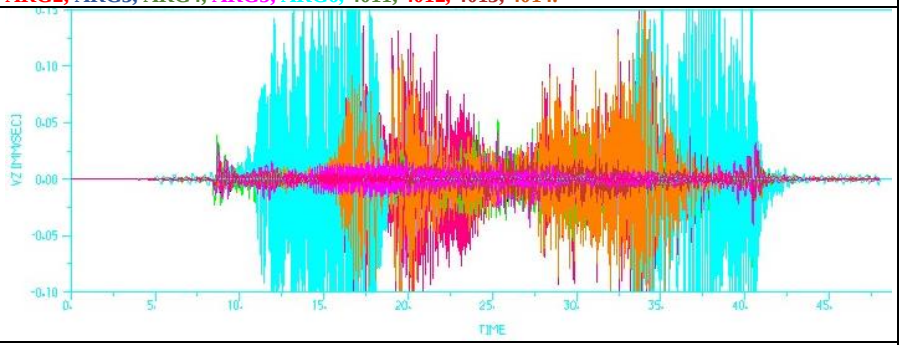

Vz: **B4, B5, B6, B3, B1, B7, B2, BGE, BGC, BGW, BGN, BGS, PODFE, POD1E, POD2E, POD3C, POD4W, G1, G2, G3, G4, G5, G6, CG1, CG2, CG3, CG4, MAGENTA CG5, CG6, CG7, CG8, CG9, CG10, CG11, CG12, 4014, 21G, 21UG, 2502, 3002.**

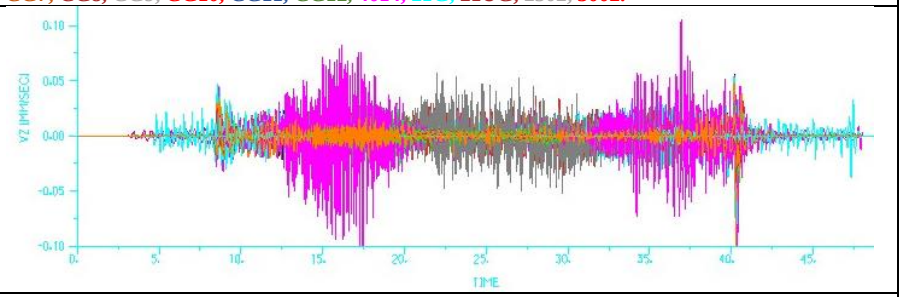

Vz: **3502, 4002, 4502, 5002, 5502, GF2, 0603, 1003, 1503, 2003, 2503, 3003, 3503, 4003, 4503, 5003, 5503, GF1, 6503, 7003, 7503, 8003, 2504, 3004, 3504, 4004, 4504, 5004, 5504, 5904, 6004, ARG2, ARG3, ARG4, ARG5, ARG6, 4011, 4012, 4013, 4014.**

Figure 6. Effects on the soil due to Metro B and C.

3.4. Analysis of trains action on the monument

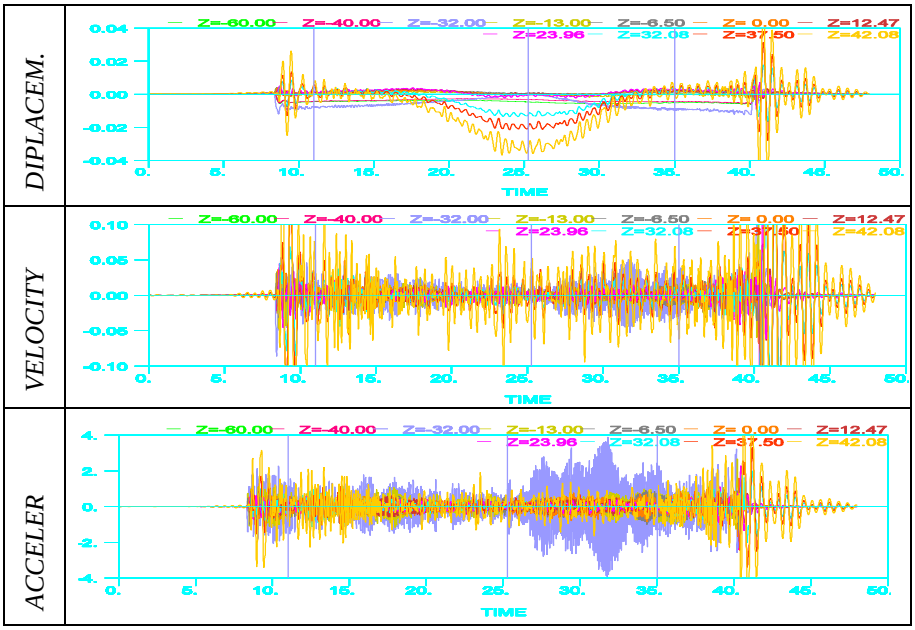

Figure 7*. Colosseum arcade XLIX. Peak radial displacements, velocities and accelerations values due to the Metro B and C traffic trains [mm, sec].*

Figure 7 shows the time histories of displacement peak values (S_{peak}), velocities (V_{peak}) and accelerations (A_{peak}).

Figure 8 shows the time histories of the effective values of displacements (S_{eff}), velocities (V_{eff})and accelerations (A_{eff}).

Figure 9 shows the time histories of the maximum radial displacements, velocities and accelerations values on radial access XLIX, on the external surface of northern travertine wall.

The comparison of the Colosseum section structural behaviour (horizontal radial vibrations) due to the above two traffic assumptions are listed in Tables 3, 4 and shown in Figure 9.

At Colosseum section summit, the following maximum values appear: V_{peak} = 0.0463 mm/sec, A_{peak} = 0.889 mm/sec^2, V_{eff} = 0.0218 mm/sec, A_{eff} = 0.467 mm/ sec^2.

From Table 4, with reference to the B Metro train transits, the further and simultaneous C Metro train transits produce, the following value increases:

- at level of Z=-32 m (C Metro), up to 84% and 89% for velocity and acceleration, respectively,
- at level of Z=42.08 m (summit of Colosseum section), up to 24% and 45% for velocity and acceleration respectively.

Since the Metro C line is deeper 25.5 m than Metro B one, its effects are damped for the greater deep and the obstacle of Colosseum station.

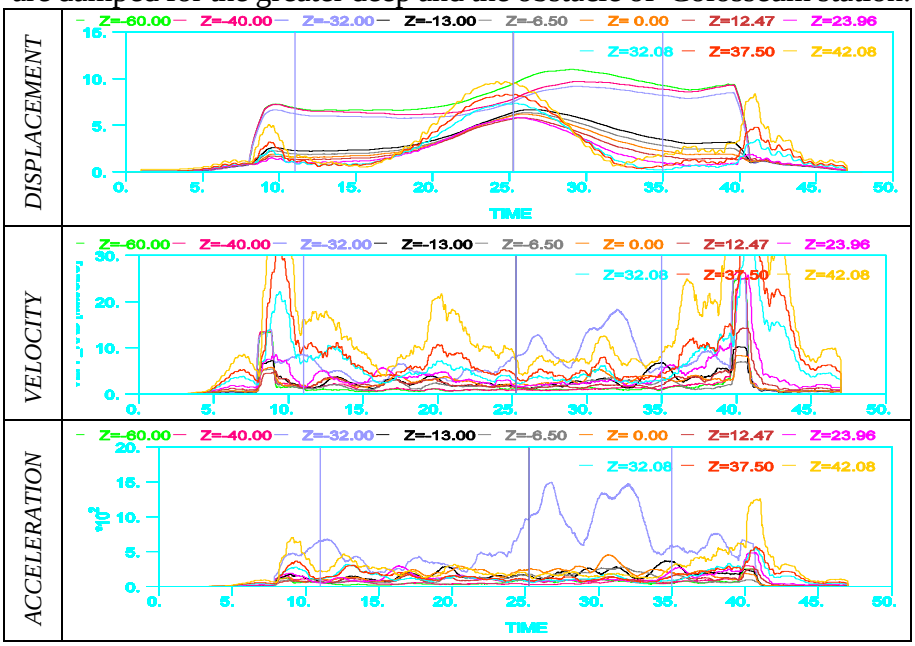

***Figure 8**. Colosseum section XLVII. Effective radial displacements, velocities, accelerations, for trains on Metro B, C, [mm, sec].*

***TABLE 3a**. Comparison between horizontal radial vibrations due to the transits on Metro B, or on Metro (B+C). Peak values.*

	level	*B*	*B+C*	*B*	*B+C*	*B*	*B+C*
		a)	Peak	values			
bedrock	-70.0	0.7	11.3	2.4	4.3	89.9	224
	-40.0	0.8	10.	4.5	4.5	156	244
Metro C	-32.0	1.3	9.7	14.0	35.5	1311	3349
	-13.0	2.5	6.9	7.5	11.6	489	702
Metro B	-6.50	2.6	6.5	6.2	7.0	335	465
Greenfield	0.00	2.8	6.4	6.2	11.2	303	797
	12.47	3.0	6.0	6.7	9.1	274	325
	23.96	3.3	6.3	10.9	12.0	409	498

	32.08	3.6	8.0	16.9	23.5	393	591
	37.50	4.7	9.2	20.4	26.1	451	592
summit	42.08	5.9	11.8	38.7	46.3	775	889
	m	μ	μ	μ/sec	μ/sec	μ/sec^2	μ/sec^2

***TABLE 3b**. Comparison between horizontal radial vibrations due to the transits on Metro B, or on Metro (B+C). Effective values.*

	level	*B*	*B+C*	*B*	*B+C*	*B*	*B+C*
		b)	***Eff.***	***values***			
bedrock	-70.0	0.6	11.1	1.2	1.7	50.	119
	-40.0	0.6	9.8	2.1	2.2	95	100
Metro C	-32.0	1.0	9.3	8.2	19.9	673	1941
	-13.0	2.3	6.8	3.8	7.1	229	376
Metro B	-6.5	2.5	6.4	2.8	3.6	169	288
Greenfield	0.0	2.7	6.3	2.4	5.4	145	451
	12.47	2.8	5.9	3.5	4.1	156	165
	23.96	3.0	5.9	4.6	5.7	236	294
	32.08	2.8	7.6	8.4	11.6	207	313
	37.50	3.5	8.5	12.5	12.3	215	306
summit	42.08	4.1	10.1	20.7	21.8	321	467
	m	μ	μ	μ/sec	μ/sec	μ/sec^2	μ/sec^2

***TABLE 4.** Percentage differences between running of Metro B alone and Metro (B+C), for peak and effective values.*

	level	S_{peak}	V_{peak}	A_{peak}	S_{eff}	V_{eff}	A_{eff}
bedrock	-70.00	178	48	81	181	30	76
	-40.00	174	7	38	175	5	4
Metro C	-32.00	159	84	89	163	81	88
	-13.00	98	48	37	102	60	48
Metro B	-6.50	88	23	37	90	24	51
Green-field	0.00	81	63	92	82	76	104
	12.47	70	25	18	74	14	7
	23.96	64	13	19	67	22	23
	32.08	69	37	44	86	31	43
	37.50	71	26	32	87	16	35
summit	42.08	72	24	31	90	6	45

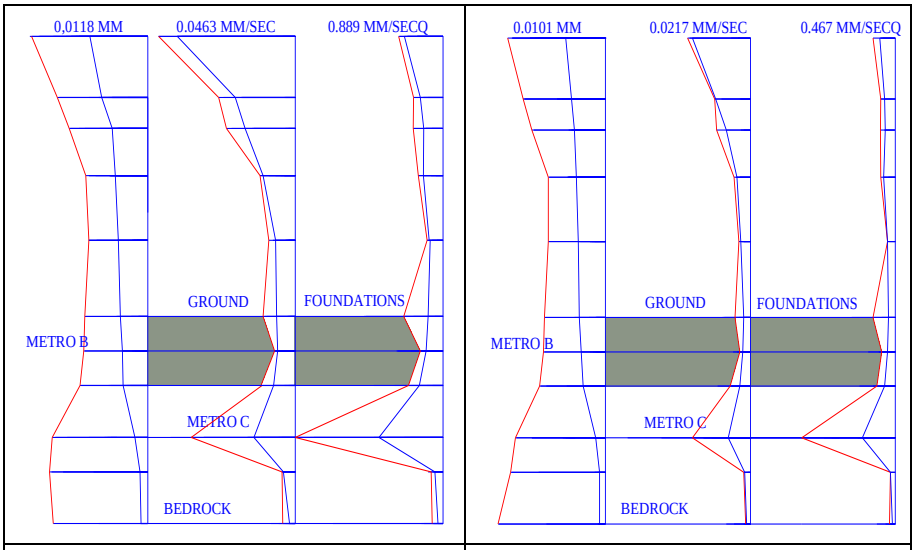

a) peak values | *b) effective values*

***Figure 9**. Maximum radial values on Colosseum section due to train traffics on: 1) Metro B (__); 2) Metro B+C (__) .*

The analysis of Colosseum area structural vibration phenomena due to the metro train transits has been performed by using 3D models of soil-structures and trains.

The calculation assumptions have considered the traffic actions due to existing line (Metro B) and also those due to the imminent opening of further underlining line (Metro C).

The results of structural vibrations for one of Colosseum section due to Metro B severe train transits combination show that at summit the following maximum values appear: V_{peak} = 0.0463 mm/sec, A_{peak} = 0.889 mm/sec^2, V_{eff} = 0.0218 mm/sec; A_{eff} = 0.467 mm/sec^2.

The further simultaneous C Metro train transits, within a severe traffic scenario, will produce the following vibration values increases:

- at Z=-32 m (Metro B level), up to 84% and 89% for velocity and acceleration, respectively,
- at Z=42.08 m (summit of Colosseum section), up to 24% and 45% for velocity and acceleration, respectively.

***TABLE 5**. Comparison between maximum vibrations on arcade XLIX, due to Metro B or Metro B+C, for peak and effective values, at levels from bedrock to summit.*

	level	*B*	*BC*	*B*	*BC*	*B*	*BC*
		a)	Peak	values			
bedrock	-70.0	0.7	11.3	2.4	4.3	89.9	224
	-40.0	0.8	10.	4.5	4.5	156	244
Metro C	-32.0	1.3	9.7	14.0	35.5	1311	3349
	-13.0	2.5	6.9	7.5	11.6	489	702
Metro B	-6.50	2.6	6.5	6.2	7.0	335	465
Greenfield	0.00	2.8	6.4	6.2	11.2	303	797
	12.47	3.0	6.0	6.7	9.1	274	325
	23.96	3.3	6.3	10.9	12.0	409	498
	32.08	3.6	6.0	16.9	23.5	393	591
	37.50	4.7	9.2	20.4	26.1	451	592
summit	42.08	5.9	11.8	36.7	46.3	775	889
		b)	***Eff.***	***values***			
bedrock	-70.0	0.6	11.1	1.2	1.7	50.	119
	-40.0	0.6	9.8	2.1	2.2	95	100
Metro C	-32.0	1.0	9.3	6.2	19.9	673	1941
	-13.0	2.3	6.8	3.8	7.1	229	376
Metro B	-6.5	2.5	6.4	2.8	3.6	169	288
Greenfield	0.0	2.7	6.3	2.4	5.4	145	451
	12.47	2.8	5.9	3.5	4.1	156	165
	23.96	3.0	5.9	4.6	5.7	236	294
	32.08	2.8	7.6	6.4	11.6	207	313
	37.50	3.5	6.5	12.5	12.3	215	306
summit	42.08	4.1	10.1	20.7	21.8	321	467
	m	μ	μ	μ/sec	μ/sec	μ/sec^2	μ/sec^2

Table 6. Percentage differences on arcade XLIX, between Metro B alone and Metro (B+C), for peak and effective values. for maximum values on full arcade XLIX, for peak and effective values.

	level	S_{peak}	V_{peak}	A_{peak}	S_{eff}	V_{eff}	A_{eff}
bedrock	-70.00	178	48	81	181	30	76
	-40.00	174	7	38	175	5	4
Metro C	-32.00	159	84	89	163	81	88
	-13.00	98	48	37	102	60	48
Metro B	-6.50	88	23	37	90	24	51
Greenfield	0.00	81	63	92	82	76	104
	12.47	70	25	18	74	14	7
	23.96	64	13	19	67	22	23
	32.08	69	37	44	86	31	43

	37.50	71	26	32	87	16	35
summit	42.08	72	24	31	90	6	45

The effective values have been calculated according to the well-known formula (DIN [14]):

$$x_{eff}(\tau) = [\int x(t)^2 \, dt / \Delta t]^{1/2} \; ; \text{ in the interval } [\tau - \Delta t/2, \tau + \Delta t/2] \quad (9)$$

where Δt=1.28 sec (adopted in [5]) depends on the vibration's amplification for the monuments due to the trains transit in frequency range of 20÷70 Hz (found by [6]).

Along the vertical on arcade XLIX, the radial values are represented:

Table 5. Comparison between maximum vibrations on arcade XLIX, due to Metro B or Metro B+C, for peak and effective values, at levels from bedrock to monument summit;

Table 6. Percentage differences on arcade XLIX, between Metro B alone and Metro (B+C), for peak and effective values. for maximum values on full arcade XLIX, for peak and effective values.

The comparison of the Colosseum section structural behaviour (horizontal radial vibrations) due to the above two traffic assumptions are listed in Tables 5 and 6 and shown in Figure 7.

At Colosseum section summit, the following maximum values appear: V_{peak} = 0.0463 mm/sec, A_{peak} = 0.889 mm/sec^2, V_{eff} = 0.0218 mm/sec, A_{eff} = 0.467 mm/ sec^2.

From Table 5, with reference to the B Metro train transits, the further and simultaneous C Metro train transits produce, the following value increases:

- at level of Z= -32 m (C Metro), up to 84% and 89% for velocity and acceleration, respectively,
- at level of Z= +46.08 m (summit of Colosseum section), up to 24% and 45% for velocity and acceleration respectively.

Since the Metro C line is deeper 25.5 m than Metro B one, its effects are damped for the greater deep and the obstacle of existing Colosseum station.

3.5. The buttresses

The pillars of the buttresses are the more stressed; for the vertical actions, it is interesting the modulus of the ratio between the increase for

Metro passage and the gravity values; these ratios are very low, as in the analysis, for the pillars # 24, 25, 30, 58, 59, on the outer ring, at the first three levels, the followings are obtained:

a) the ambient vibrations $\Delta\sigma_G$ in the directions x, y, z , in Figure 8 for pillars # 28, 29 and 30 near Stern Buttress, and for pillars # 58 and 59 near Valadier buttress;

b) the Table 7 with the gravity stress σ_G, and the ambient vibrations $\Delta\sigma_G$, and the scatters

$$|\Delta\sigma_{GZ} / \sigma_{GZ}|_{MAX}.$$

Table 7. *Gravity stresses, and their variations for ambient vibrations.*

		σ_G			$\lvert\Delta\sigma_G\rvert_{MAX}$ x 10. E+05			$\lvert\Delta\sigma_{GZ}$
#	Order	x	y	z	x	y	z	$/\sigma_{GZ}\rvert_{MAX}$
				STERN				
24	1	-.006	-.078	-1.80	6.13	1.38	21.0	.012
24	2	-.005	.007	-1.39	1.81	3.86	20.0	.014
24	3	-.017	-.018	-1.00	1.41	3.93	15.0	.015
25	1	-.085	-.078	-2.18	4.98	5.60	14.0	.006
25	2	-.084	-.029	-1.52	2.34	1.36	13.0	.009
25	3	-.059	-.018	-1.05	3.30	1.74	15.0	.014
30	1	-.120	-0.17	-1.45	2.40	2.30	15.0	.010
30	2	-.032	-.095	-1.17	3.30	3.22	17.0	.014
30	3	-.044	-.040	-0.95	2.01	2.24	20.0	.021
				VAL.				
58	1	-0.12	-.084	-0.81	6.80	6.55	76.4	.093
58	2	-.087	-.035	-0.48	4.16	4.93	35.0	.072
58	3	-.049	-.006	-0.21	7.30	1.63	37.6	.175
59	1	-0.13	-.083	-0.86	6.50	6.32	70.3	.082
59	2	-0.11	-.005	-0.42	5.40	3.45	25.6	.060
		MPa	MPa	MPa	MPa	MPa	MPa	%

4. Lowering of the southern foundations

4.1 Smeared Crack Band

The “Smeared Crack Band” is adobted since the Mörsch frame of one century ago; but for F.E. model, this model was better defined by Bazant et alii [3], [6], [7].

4.2. Concrete nonlinear model

The usual "Concrete Mechanics" could arrive to size of 50x50x50 cm with different mechanical characteristics and orthotropic matrix too, defined by crack orientation in the single Gauss point in the single FE. We start from integer concrete for the concrete foundations of 2000 years ago; and we admit to know all nonlinear material characteristics: ε_C, ε_U, σ_C, σ_U, σ_T, G_F, E_0, shown in Figure 10a.

The foundations were analyzed, subjected to all actions happened in 2000 years by: a) building of foundations, b) building of elevation, c) viscosity of all materials, d) missing southern side.

The following elasticity modules are used, for each principal direction, and in each integration point:

E_0= uniaxial initial tangent modulus, and for low stresses;

E_T= uniaxial tangent modulus in the direction for compressive high stresses;

$E_T = E_F < 0$ uniaxial tangent modulus for $\varepsilon_T < \varepsilon < \varepsilon_F$;

$E_T = 0$ uniaxial tangent modulus for $\varepsilon > \varepsilon_F$;

σ_C = maximum uniaxial compressive stress;

σ_T = maximum uniaxial tensile stress;

G_F = fracture energy.

Crack and tensor depictions are shown in Figure 10.

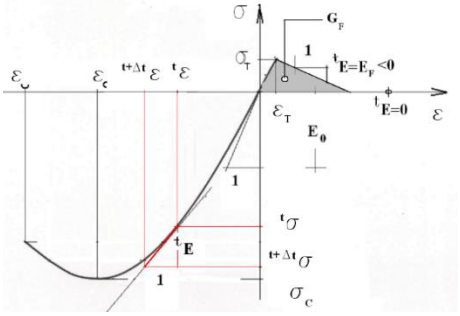

***Figure 10a**. Uniaxial stress-strain relation in the concrete model.*

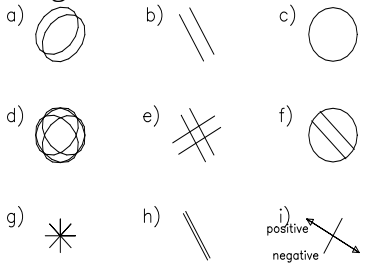

***Figure 10b.** Crack and tensor depictions: a) b) and c) one crack. d) e) and f) two cracks.*

4.3 Nonlinear static Analysis of foundations with concrete model

"La platea di fondazione ..potrebbe presentare al suo interno una frattura accentuata..Quaranta centimetri di dislivello nella parte sud del Colosseo" (Corriere della Sera ***29 luglio 2012*** *).*

The incremental static analysis is performed.

$$M({}^{t+\Delta t}\ddot{u} - {}^{t}\ddot{u}) + {}^{t}K({}^{t+\Delta t}u - {}^{t}u) = ({}^{t+\Delta t}P - {}^{t}P)$$

with C=0, M=const, ${}^{t}K$=variable.

We take into account different phases:

a) foundations construction; initially, for undamaged concrete we assume two different constant modules for the two layers, upper ${}^{0\_UPPER}E_{CONCR}$=12000 MPa, lower ${}^{0\_LOWER}E_{CONCR}$ =24000 MPa, corresponding to the maximum values obtained by identification;

b) monument construction;

c) viscous effect development; at viscous effects exhausted, the final analysis, was performed for the full dead load enclosing the elevation, half elasticity modules for concrete, 0.75 elasticity modules for the soil:

${}^{\infty}\gamma = 2.\ {}^{0}\gamma$, ${}^{\infty}E_{CONCR} = 0.5\ {}^{0}E_{CONCR}$, ${}^{\infty}E_{SOIL} = 0.75\ {}^{0}E_{SOIL}$

d) missing of southern walls.

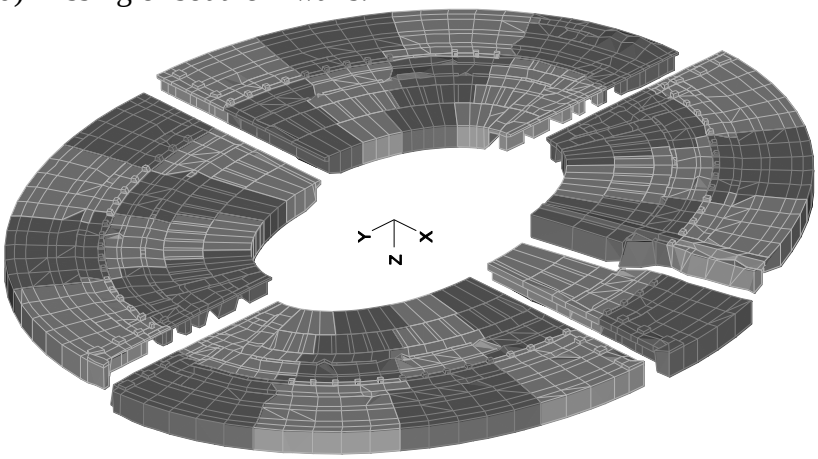

Figure 11*. The mesh of upper concrete layer, with the n.5 tunnels (E, S, W, N and Commodo at SSE). Z=1.00÷7.00 m*

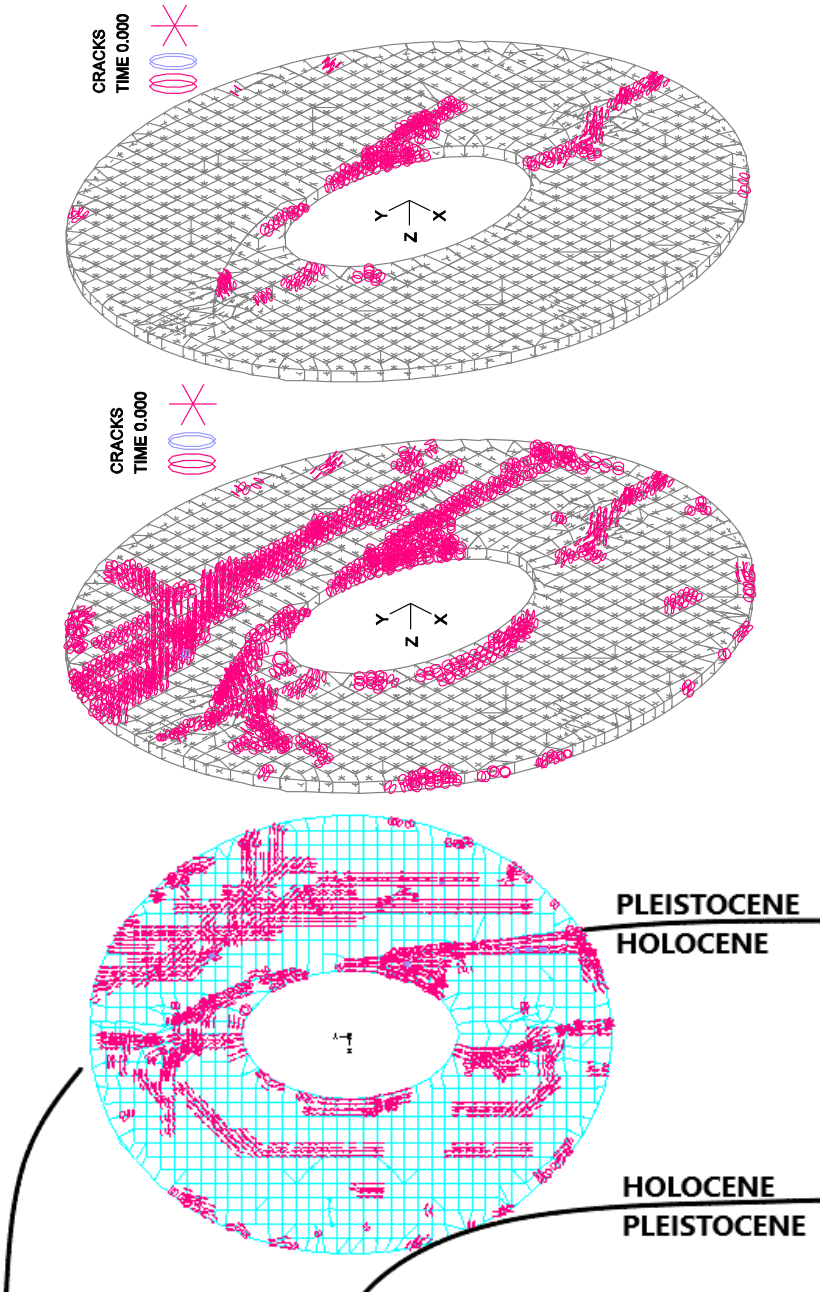

***Figure 12**. Cracks of lower layer foundations, at phases: 2) full t=0; 3) full t=∞; 4) partial t=∞, estimated principal disconnection by tests.*

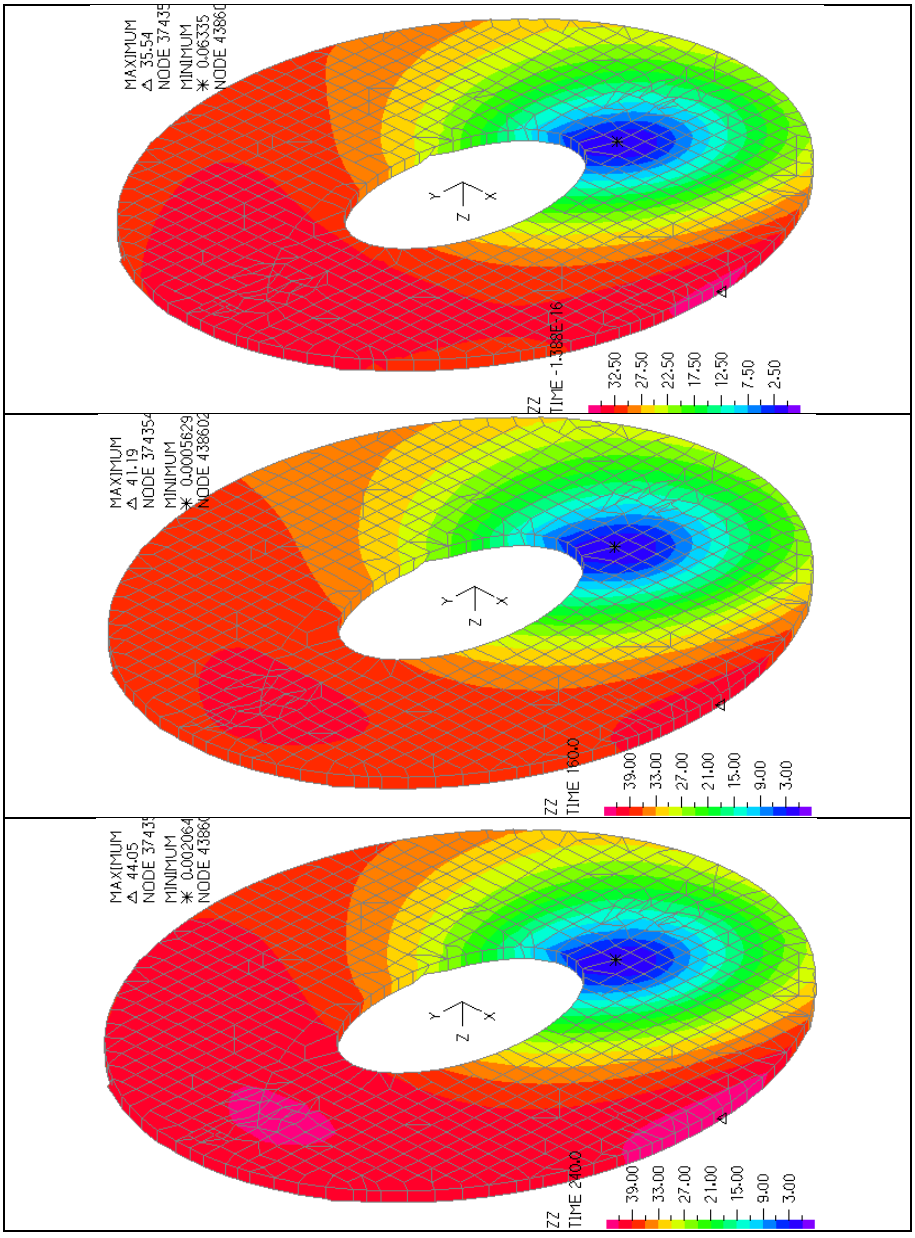

Figure 13. *Vertical displacements of foundations, for phases: 1) full t=0; 3) viscosity t=∞; 4) partial load t=∞. "La platea di fondazione ..potrebbe presentare al suo interno una frattura accentuata..Quaranta centimetri di dislivello nella parte sud del Colosseo" (Corriere della Sera 29 luglio 2012).*

And such analytical cracking agrees with the separation in two parts by your dynamic analysis. For foundations, we perform the static non-linear analysis with load increments. For lower layer of foundations, we start with Young elasticity moduli by characterization.

5. Analysis of soil colosseum interaction subjected to accelerations at the bedrock 80 m under the ground level

At the bedrock level of our model, we apply the three acceleration components at 80 m under ground level, accelerations ${}^{x}\ddot{u}_{G,}\ {}^{y}\ddot{u}_{G,}\ {}^{z}\ddot{u}_{G,}$
Then we will analyse the most significant time interval 0÷54 secs, when the principal actions happened.
Amplifications: Rx = 1.40, Ry =1.42, Rz=2.85
In nonlinear analysis the incremental F.E. equations used are:

$$M({}^{t+\Delta t}\ddot{u}-{}^{t}\ddot{u}) + C({}^{t+\Delta t}\mathring{u}-{}^{t}\mathring{u}) + K({}^{t+\Delta t}u-{}^{t}u)= -M({}^{t+\Delta t}\ddot{u}_G-{}^{t}\ddot{u}_G)$$

$C=\alpha M+\beta K$, Rayleigh damping matrix, with $C_1=C_2=5\%$
K=constant, corresponding to reduced elasticity modules according to "Smeared Crack Band" model, obtained by identification; M=const.

6. Ground vibrations

Table 8. *Peak accelerations on the ground, felt by pedestrians.*

Dx	A_H	A_V	A_{TOT}		A_H	A_V	A_{TOT}		*Sc*		*Section*
0.	13.03	7.91	33.57		3.38	4.53	12.21		36.37		Station
12	21.90	34.78	66.49		4.01	14.92	15.17		22.82		
24	22.77	36.13	65.24		3.32	2.56	4.57		7.00		
100	40.42	60.27	61.17		1.71	1.32	2.15		3.51		Valad.
192	47.23	65.41	71.74		0.29	0.25	0.37		0.52		Const.
240	38.58	81.52	84.90		0.19	0.13	0.20		0.24		MAX
m	Metro B+C [mm/sec^2]				Metro C [mm/sec^2]				%		

Table 9. *Peak velocities on the ground, felt by pedestrians.*

Dx	V_H	V_V	V_{TOT}		V_H	V_V	V_{TOT}		*Sc*		*Section*
0.	.220	.292	.869		.057	.175	.404		46		Station
12	.356	.269	1.353		.089	.157	.337		25		
24	.393	.262	1.407		.076	.134	.204		14		MAX
100	.335	.528	.546		.068	.053	.089		16		Valad.
192	.347	.494	.535		.023	.008	.023		4		Const.
240	.270	.527	.543		.016	.006	.016		3		
m	Metro B+C [mm/sec]				Metro C [mm/sec]				%		

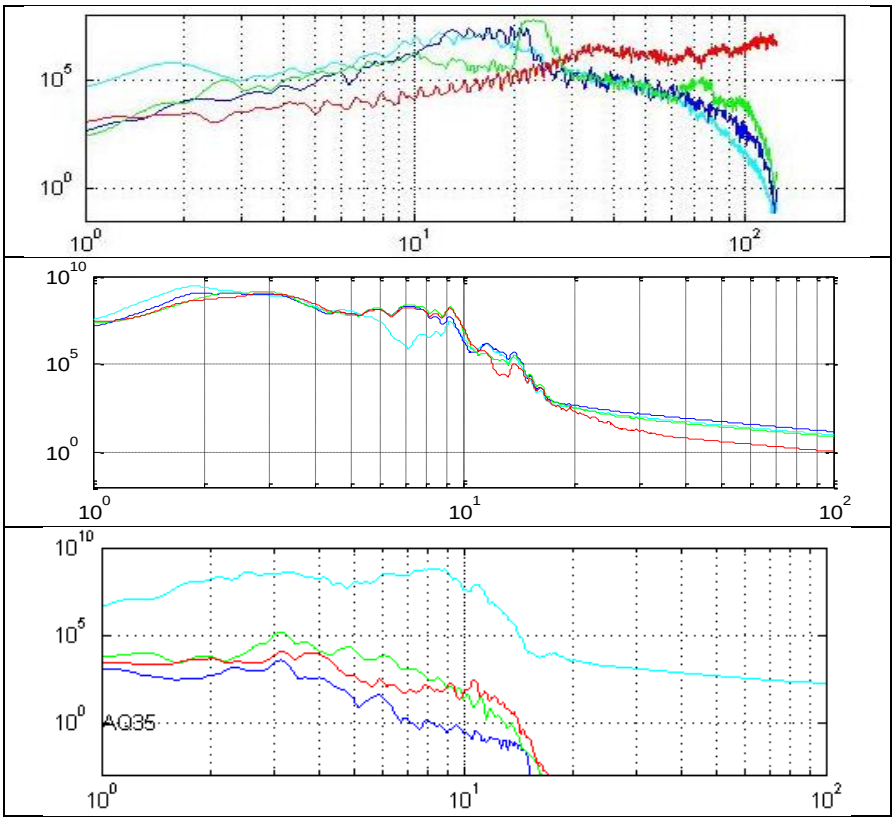

Figure 14. *FFT of A_{TOT} felt by pedestrians, due to Metro (B+C). Station cyan, Valadier blue, Constantine green, Max red.*

About the vibrations on the ground, in axis with Metro (B+C), as in Figures 14 and 15, when the two trains arrive both in axis with greater ellipse diameter, at distance Dx from the step of the station to the end of Constantine arch:

a) the Table 6 and 7 show the maximum velocities and accelerations, in horizontal and vertical directions, with

$a_H = [\ (a_X)^2 + (a_Y)^2]^{1/2}$; $a_{TOT} = [\ (a_X)^2 + (a_Y)^2 + (a_Z)^2]^{1/2}$; $a_V = a_Z$; (2)

and analogous equations for velocity components;

b) the last numerical column of Table 6 shows the percentage increasing of Metro C accelerations with respect Metro B vibrations, which is less of 3% in proximity of the monuments.

c) the values A_{TOT} are shown in Figure 17, they arrive to a maximum value around 0.01 g, with fundamental frequencies of 5÷30 Hz,

d) the Figure 15 shows the maximum radial accelerations on the RA XLVII, and on the ground over the tunnel of Metro B.

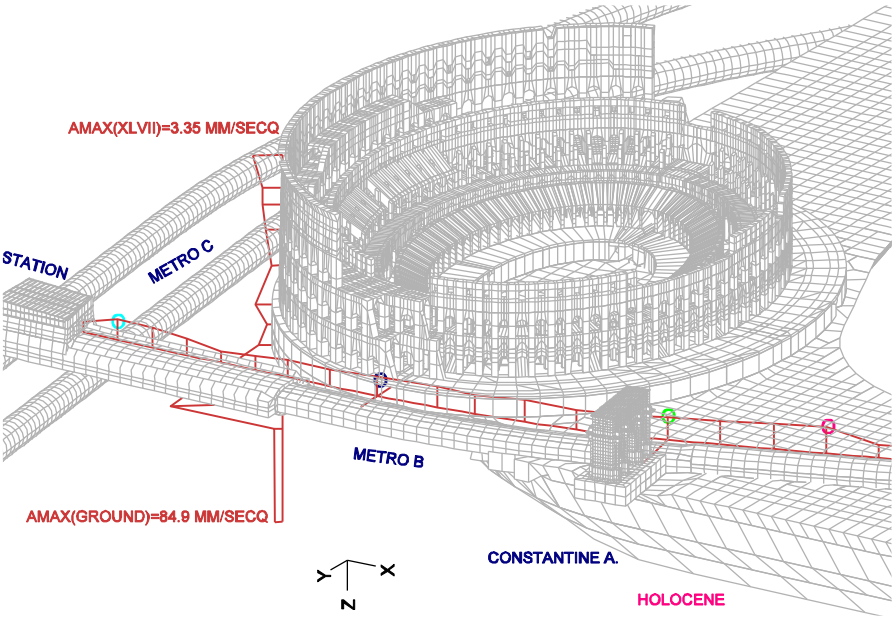

Figure 15. *Peak of A_{TOT} on: a) RA XLVII, b) axis of Metro B, felt by pedestrians. Station cyan, Valadier blue, Constantine green, Max red.*

The lower limit of vibrations perceptible to people is set by observation and experiment at approximately 0.00l7g or l cm/sec (from National Information Service for Earthquake Engineering, University of California, Berkeley, "The Nature of Ground Motion and its Effect on Buildings*", Christopher Arnold, A.I.A., 1982).*

Whole-body vibrations in the range of 3-10 Hz are particularly critical because large body organs within the rib cage and abdomen resonate within this frequency range and it is within this general range that the inherent vibration isolation capability of the body is least effective (*Grether, W. F., "Vibration and Human Performance," Human Factors, Vol.13, No. 3, 1971, pp. 203-216*).

Man is sensitive to mechanical oscillations ranging in frequency from well below 1 Hz up to at least 100 kHz. Guignard, J. C., Journal of Sound and Vibration, Volume 15, Issue 1, 03/1971.
The maximum accelerations overcome this threshold of human perceptibility; instead the maximum velocities are near the limit of perceptibility for pedestrians.
The analyses should be deepened for different convoys passages, besides the proposed four convoys simultaneously centred on the two diameters; however, in order not to feel any vibration by pedestrians, from the analysis the reduction factor is requested $\chi \cong 85/17=5$.
If we consider a single point centred on the axis of Metro B, the simultaneous passage of two convoys is a rare event, instead for one convoy alone the interval time is around few minutes; so we could be satisfied of the reduction factor requested $\chi \cong 2.5$, for a single convoy.

Table 8. Maximum horizontal and total accelerations

	X, N		Y, E		Z		Ah		Atot	
	t	f	t	f	t	f	t	f	t	f
C1	.064	0.277	40.364	0.397	40.576	0.918	40.364	0.404	40.576	0.925
C2	1.680	0.146	40.342	0.194	40.944	0.208	40.428	0.196	40.436	0.251
Station	40.108	7.796	40.084	12.431	40.096	29.07	40.084	14.194	40.096	29.137
Valadier	23.908	20.12	23.664	32.878	25.332	46.613	23.664	34.634	25.332	50.567
Constantine	30.296	33.528	21.384	33.385	32.500	61.680	30.296	36.102	32.584	65.392
Max	35.024	36.778	35.944	23.938	37.064	41.029	35.024	37.507	37.568	44.708
Bedrock	11.028	0.1								
47MetroC	30.524	2.1								
47MetroB	32.164	0.75								
47Ground	12.572	0.77								
47Top	12.692	2.34								
	sec	mm/sec^2								

If we consider a single point centered on the axis of Metro B, the simultaneous passage of two convoys is a rare event, instead for one convoy alone the interval time is around few minutes; so we could be satisfied of the reduction factor requested $\chi \cong 2.0$, for a single convoy.

7. Action of unidirectional Gabor wave in the 2d and 3d models

The geophysicists performed the 2D analysis [11] in Figure 16, for a horizontally incident plane shear Gabor wave acting at the bedrock.

The horizontal soil displacements above the Holocene valley, have an amplification of up to 7 times that of the bedrock, to which they remain higher for 10 periods.

The same Gabor action was applied in x-direction in a 3D model. Displacements in the orthogonal y- and z-directions are also derived from this analysis, as shown in Figures 17÷19.

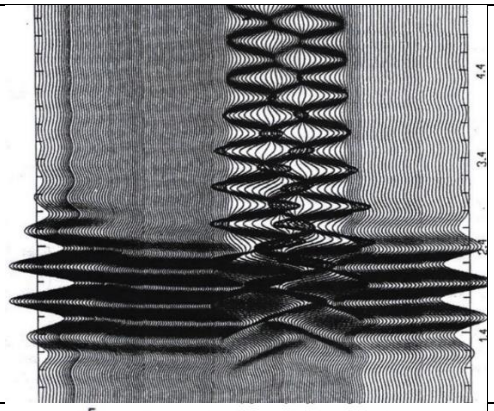

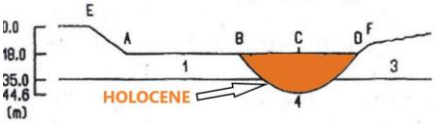

Figure 16a. Action in EW direction.

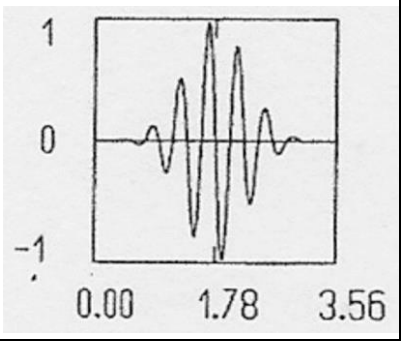

$s(t) = \exp\{-[\omega_P(t-t_S)/\gamma]^2\} \cos[\omega_P(t-t_S)+\psi]$

$\omega_P = 2\,\pi\, f_P$ sec^{-1},

$t_S = 0{,}45\,\gamma / f_P$, $t \in < 0.2\, t_S >$

we are referring to the constant values

$\gamma = 9.50$ $f_P = 2.40$ sec^{-1},

$\psi = 1.57080$; $t_S = 1.78035$ sec.

Figure 16b. Gabor wavelet.

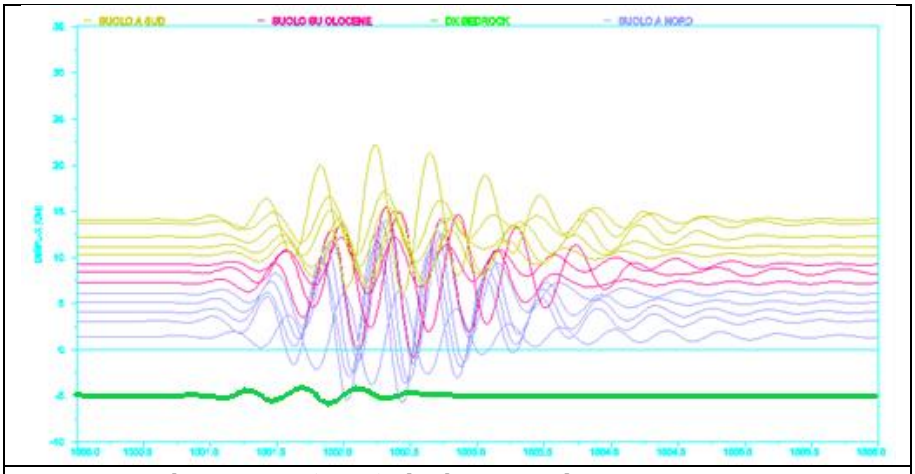

Figure 17. Gabor Forcing (green), displacements direction x.

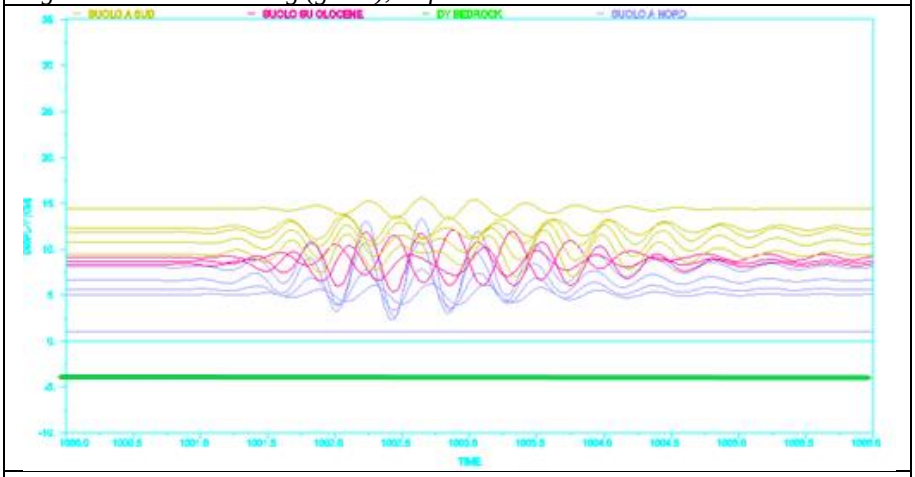

Figure 18. Gabor Forcing (green), displacements direction y.

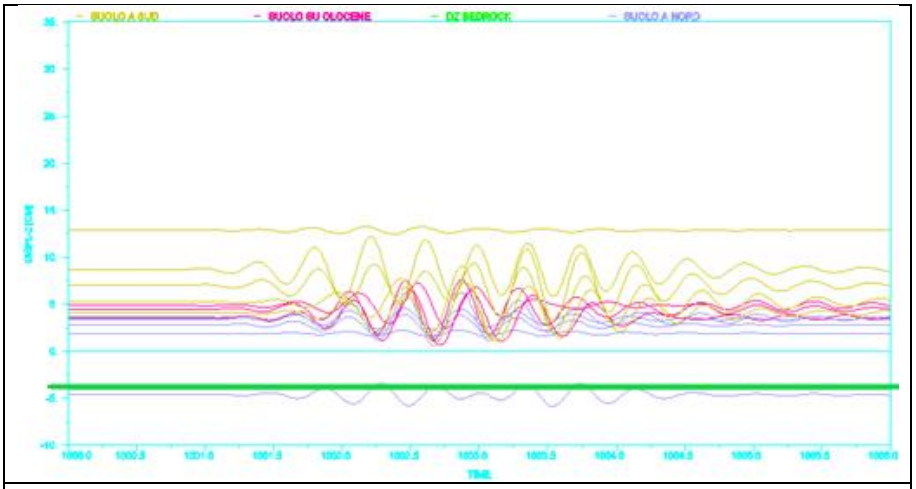

Figure 19. Gabor Forcing (green), displacements direction z.

8. **Tunnel excavation**

Firstly, we consider the two circumferences connected at their lower points, with displacements converging to the centre of the final circumference, that has no more relative displacements between their points, but it is free to move for the geotechnical stresses. The displacement δ is obtained by imposing the volumetric variation $\Delta V=1\%$

$\Delta V=(\delta^2 /4 - R_I \delta) / (R_I)^2$; $\delta = 55.14$ mm

The excavation happens with a TBM shield having depth 10.0 m and weight 10000 kN and excavation pressure of 225 kPa; from Est to West. The following phases are repeated 116 times on depths of 5.0 m: a) excavation, b) advancing of TBM shield, c) contraction, d) concrete covering. For each phases the structural model varies 3 times for a total of 116 x 3 = 348 times.

8.1 Mechanism

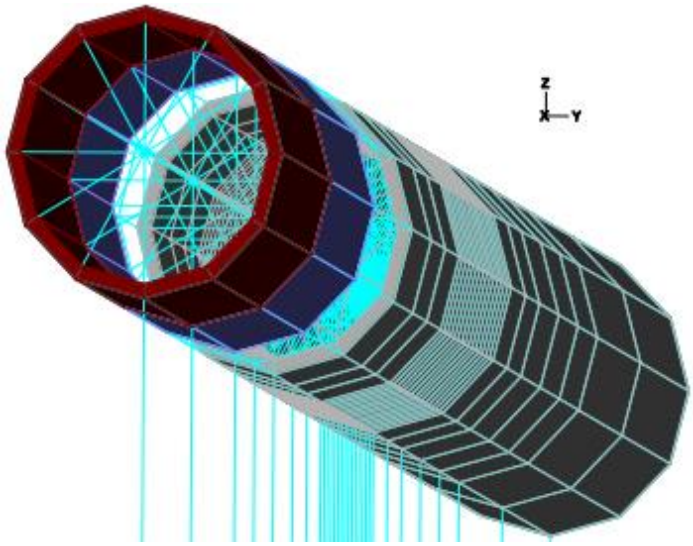

Figure 20. *a) TBM shield in blue, b) concrete covering in gray ,c) soil excavation in red, transversal contraction is applied on the light blue section between a) and b).*

8.2. Tunnel deformations

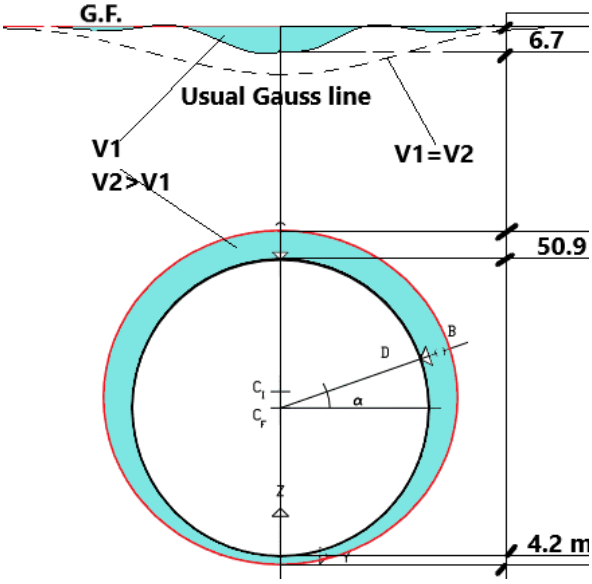

Figure 21. *Contraction of cross section.*

The tunnel excavation produces:
a) at the greenfield δ_Z= -6.65 mm;
b) at the summit of the tunnel δ_Z=-50.90 mm;
c) at the bottom of the tunnel δ_Z=+4.24 mm;
d) total external diameter contraction δ = 50.90 + 4.24 = 55.14 mm ;
e) monument $|\delta_Z|$=0.12 mm; σ_1=19.9 kPa;
f) foundations $|\delta_Z|$=0.13 mm; σ_1=9.7 kPa;
g) transversal contraction of the tunnel A=0.9503 m^2 ;
h) subsidence contraction at the greenfield A=0.3036 mq.

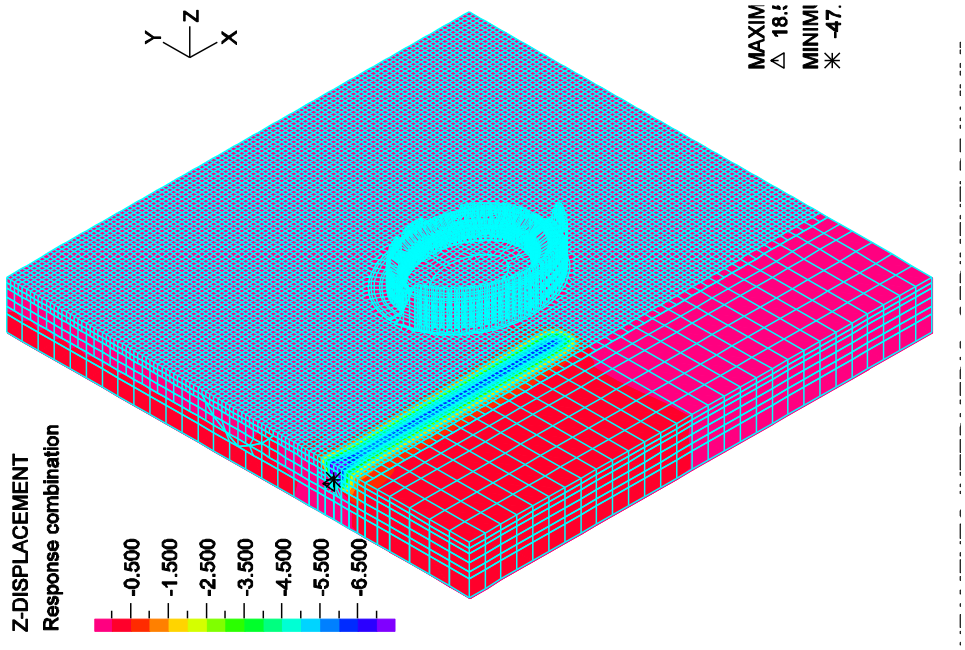

Figure 22.. *Vertical displacements at Z=0 for intermediate advancement.*

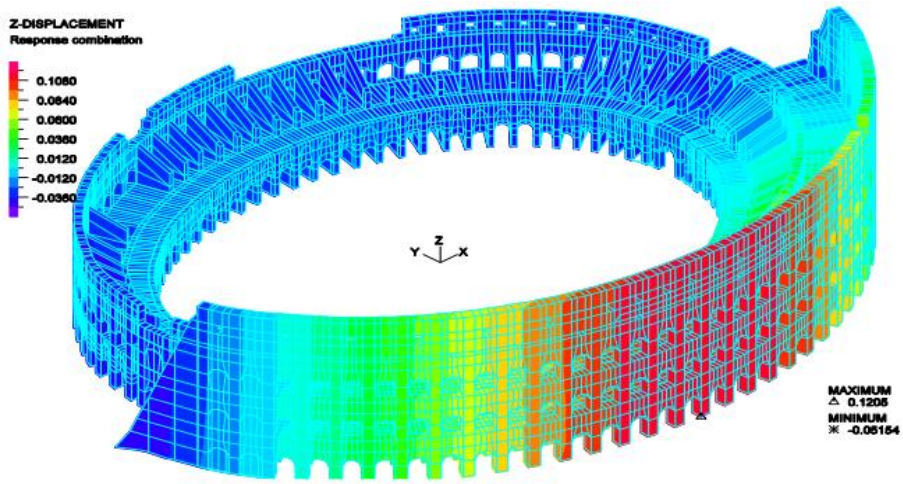

***Figure 23**. Vertical displacements for the monument, for total advancement..*

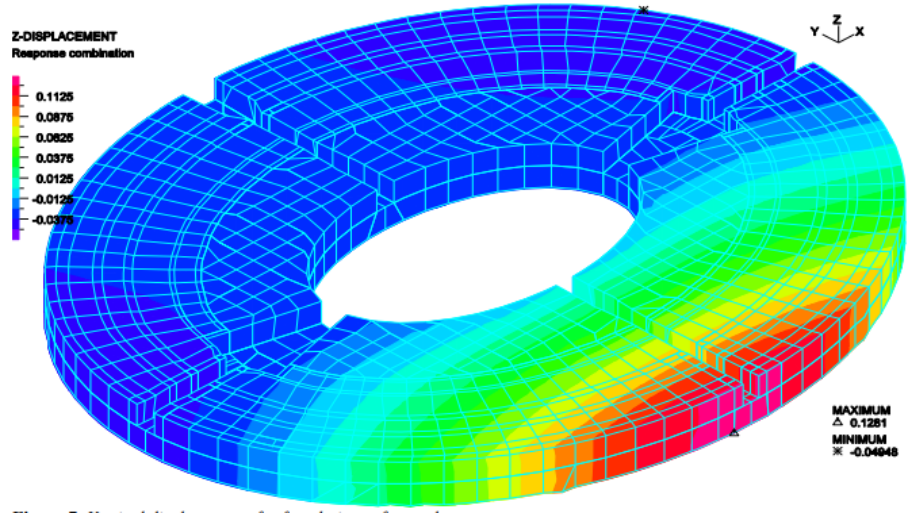

***Figure 24.** Vertical displacements for foundations, for total advancement..*

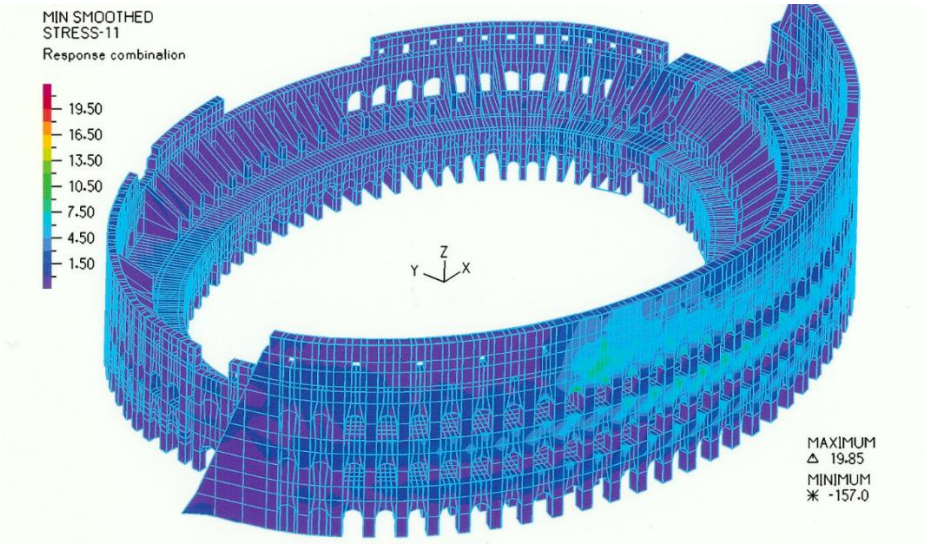

Figure 25. *First principal stress for the monument, for total advancement.*

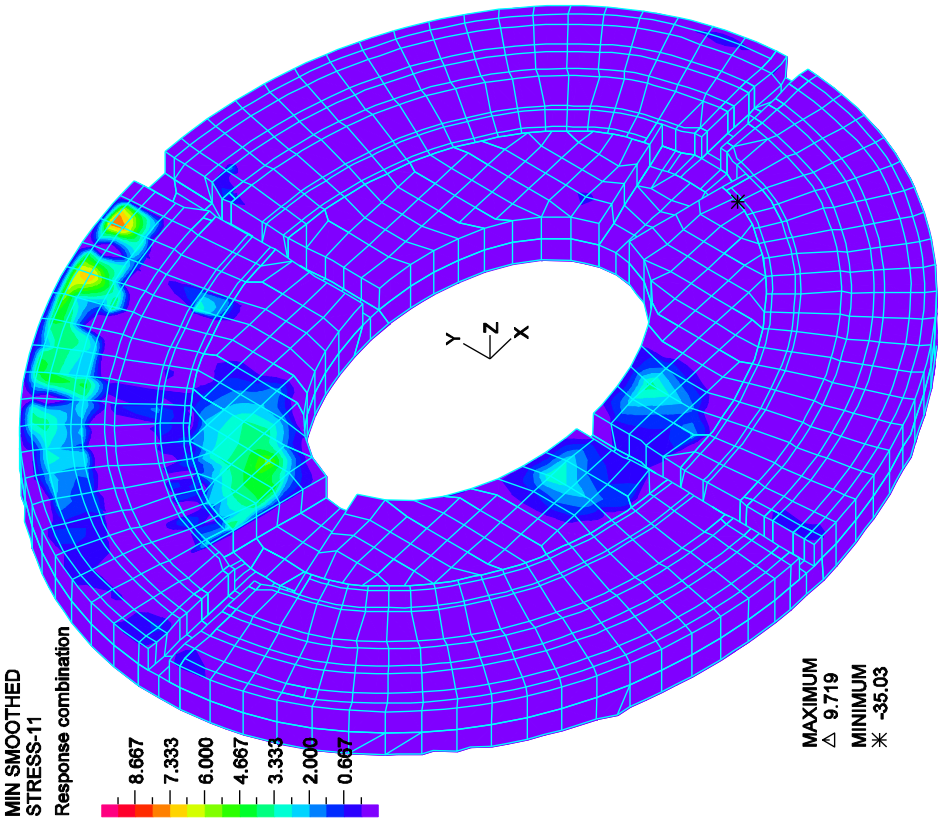

Figure 26. *First principal stress for the foundations, for total advancement.*

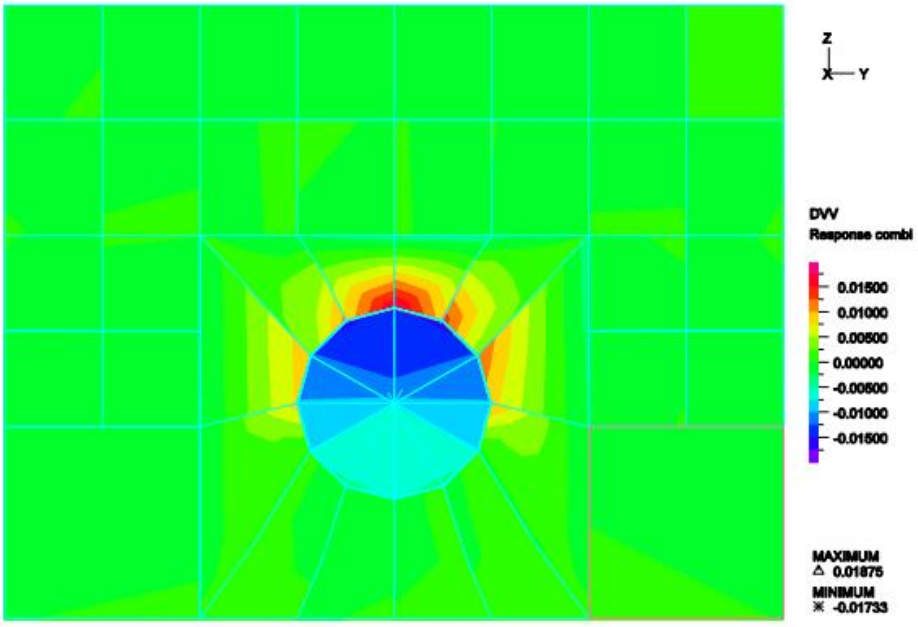

Figure 27. *Total volumetric variation around the tunnel.*

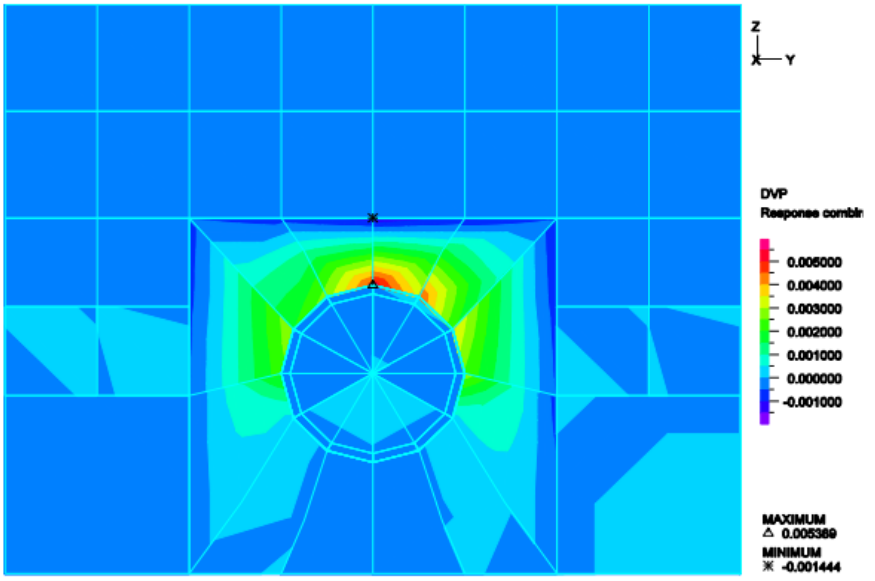

Figure 28. *Plastic volumetric variation around the tunnel.*

9. Conclusions

The structural events of the Colosseum provide a great scientific opportunity:

1) the foundations of the Colosseum on a bend of the paleo-Tiber, later filled by the Holocene layers;

2) the Metro B with its upper arch at ground level, which passes only a few metres from the monuments.

For the Colosseum soil interaction, the great uncertainties of the mechanical characteristics of the monument's walls produce great difficulties; the average spread elasticity moduli of the damaged walls reach a reduction in the ratio of 1:8 with respect to an intact specimen, due to invisible internal cracks and disconnections of the blocks.

Researchers recognise three different phases in the study of ancient monuments: diagnosis, safety assessment and intervention planning; they describe the best procedures in detail, so much so that it is impossible not to share them, but it is only a programme of intent, which cannot be solved analytically before the third millennium.

What is needed is an analytical tool with less engineering precision.

Geophysicists have already noted the amplifications of accelerations from the ground to the top of the monument, due to the effect of ambient noise, certainly transmitted through the ground.

The tunnels excavation produces subsidence at the greenfield Z= -20.82 mm o.s.l.

In the short term, environmental vibrations are not dangerous for the monument, while for the long term there is no experience.

References

[1] Perrone, V., "*la ferrovia Metropolitana a Roma*", Trasporti pubblici, nn. 4…10 1952, nn. 1-2, 9, 11 1953, nn. 5, 7-8 1954.

[2] Reynolds, A.C. 1976. "*Boundary conditions for the numerical solution of wave propagation problems*", *Geophysics*, 43, 1099-1110.

[3] Bazant, Z.P., "*Crack Band Propagation and Stress-Strain Relations for Fracture Process Zone in Geomaterials*", International

Symposium on Numerical Models in Geomechanics, Zurich, 13-17 September 1982, pp. 189-197.

[4] Virieux, J. 1984. "*SH-wave propagation in heterogeneous media: velocity-stress finite-difference method*", *Geophysics*, 49, 1933-1957.

[5] Wolf, J. P. 1985. *"Dynamic Soil-structure interaction*", Prentice Hall.

[6] Bazant, Z.P. and Pfeiffer,P.A., "*Shear Fracture Test of Concrete", Materiaux et Constructions*, Vol.19, N.110, 1986.

[7] Bazant, Z.P., "*Mechanics of distributed cracking*", Mechanics Review, vol.39, no 5, May 1986, pp.675-705.

[8] Wolf, J. P. 1986. *"Soil-structure interaction analysis in time domain*", Prentice Hall.

[9] Moczo, P., Bard, P.Y. 1993. "*Wave diffraction, amplification and differential motion near strong lateral discontinuities"*, Bulletin Seismological Society America, 83, 85-106.

[10] Zhou, T., Dravinski, M. 1994. "*Resonance prediction of deep sediment valleys through an eigenvalue method*", Geophysic Journal International, 117, 749-762.

[11] Moczo, P., Rovelli, A., Labàk, P., Malagnini, L., (1995) *Seismic response of the geologic structure underlying the Roman Colosseum and a 2-D resonance of a sediment valley*, Annali di geofisica, pp. 939÷956.

[12] Wolf, J. P., Chongmin, S. 1996. "*Finite Element Modelling of unbonded media*", Wiley & Sons.

[13] Moczo, P. 1989. "*Finite Difference Technique for SH-waves in 2-D media using irregular grids – application to the seismic response problem*", Geophysic Journal International, 99, 321-329.

[14] DIN 4150/3 (1999) *Erschütterung im Bauwesen – Einwirkungen auf bauliche Anlagen* (in German).

Interaction of soil and Constantine Arch

Abstract

This paper presents the results obtained by using a novel methodology for the dynamic analysis of soil structure interaction due to trains' transit on Constantine Arch monument, in the archaeological area of Rome. The FE model of Constantine Arch is inserted in the full 3D FE model comprising Colosseum, tunnels of Metro, soil layers up the bedrock. The trains actions produce the vibrations of the "soil-structure" interaction to determinate the structural vibrations of the Arch. The numerical results are related to the experimental dynamic tests already carried out on the monument.

1. Introduction

The prevention of damage from traffic vibrations requires a technical approach which becomes more complex with the increasing cultural value of the affected buildings and monuments and the expected time of conservation.
Deciding upon the right course of action for the conservation and structural safeguarding of the building patrimony subject to vibration noise requires calculation instruments that allow the monitoring of structural vibrations up to seismic collapse.
The problems however are overcome in the investigative method we propose here, based on the analysis of soil structure interaction using a geophysical model which ensures structural continuity between the ground, the foundations and the building [3,4,5,6].
This analysis methodology is applied, in a case study, to an archaeological area of Rome comprising the Arch of Constantine [2] affected by the B Line of the underground transport system.

2. The construction

2.1. The construction of foundations

During the excavations to the south of the Meta Sudans, a number of structures were identified that appear to be components definitely pertaining to the western portion of the foundations of the Arch of Constantine, closest to the Palatine slope.
The first section of the foundation was identified in the autumn of 1987 in a small trench located almost in the centre of the western side of the Arch (Figure 1).
A 2.10 m long, 90 cm thick on average and 2.90 m high cement foundation in hollow reinforced by wooden elements, such as a vertical quarter-circle post 25 cm wide and 20 cm thick at the most, and horizontal boards at least 5 cm thick, was laid.
The casting is made of mortar with large elements (30-40 cm) of white and coloured marble, travertine and to a lesser extent basalt.

The alignment of the foundation is irregular, but parallel to the Arch of Constantine; the outcrop level is 20.17 m above sea level, with different dates, starting from the Flavian age.
Important investigations were carried out in 1987, 1989, 1992, 1993.
Along the western side of the Arch, towards the Palatine, there is a section of cement foundation 2.30 m long, with an average thickness of 20 cm and a height of 4.80 m, which presents the height of the prominence at 20.05 m above sea level.
Reinforcements testified by a large 45° inclined prop, of which the hollow imprint with a rectangular section of approx. 20x25 cm remains in the Constantinian concrete.
The alignment of the northern section on the western side of the Arch of Constantine is very irregular, and is not parallel to the elevation of the monument.
As one descends in depth this irregularity diminishes, up to a statue of Julio-Claudian age.

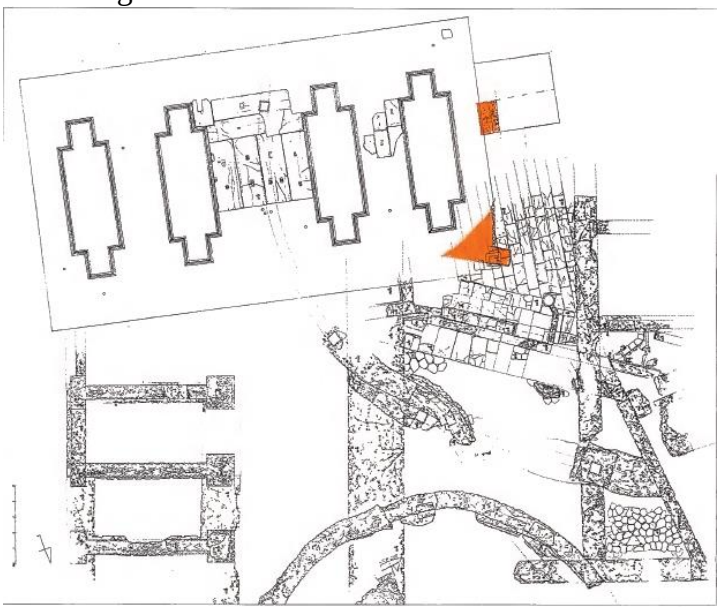

Figure 1. *Planimetry of area I of the excavation of the meta Sudans[2].*

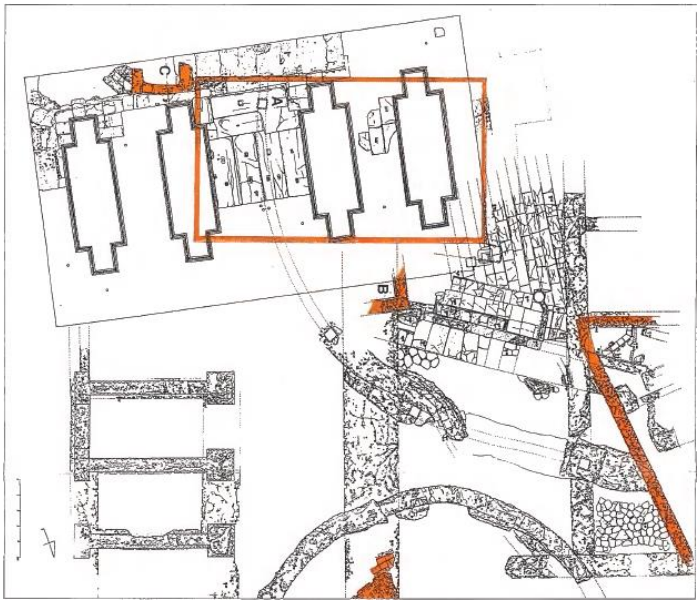

***Figure 2**. Planimetry of area I of the excavation of the meta Sudans. In the central-western area, the hypothesised impact of the Domitian monumental arcade[2].*

***Figure 3**. Planimetry of area I of the excavation of the meta Sudans. In the southern side, the hypothesised impact for the Neronian structures[2].*

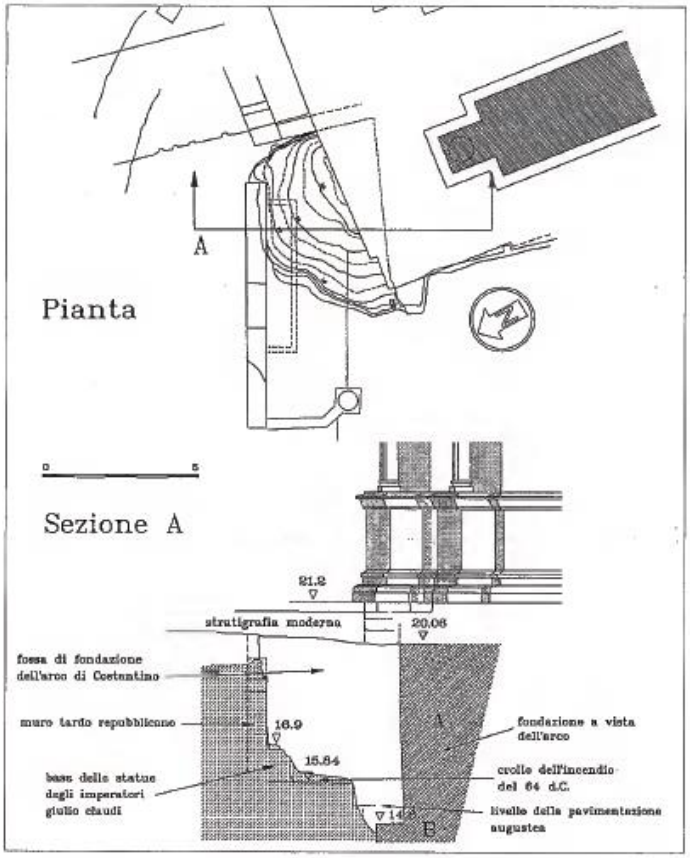

Figure 4. *Schematic reconstruction in plan and N-S section, view from the west [2].*

This brick reinforcement at the height of m 20.06 o.s.l. towards the Colosseum, for m 1.90 ca., but it is presumable that it actually measures m 7 ca. (figure 1).
Its alignment, due to force majeure, is not orthogonal to the Arch, followed by a height of 1.70 m, it is not perfectly vertical, but slightly inclined northwards, towards the Meta Sudans.
The limited portion of foundations currently known is not sufficient to establish the exact sequence of building operations that led to the construction of the curtain wall.

The most probable construction hypothesis is derived from the deep facing curtain wall in "*opus listata"*, the localised widening of the foundation pit, the protrusion of the spur towards the west and the imperfect verticality of the brick curtain wall, pushed northwards by the pressure of the subsequent cement casting behind it.
In order to realise this exposed section, it was necessary to widen the foundation pit on the corner, creating a large pit (Figures 4, 5); with the profile (Figure 4, Section A) that narrows in depth, closing at 14.35 m a.s.l. in brickwork and marble pieces.

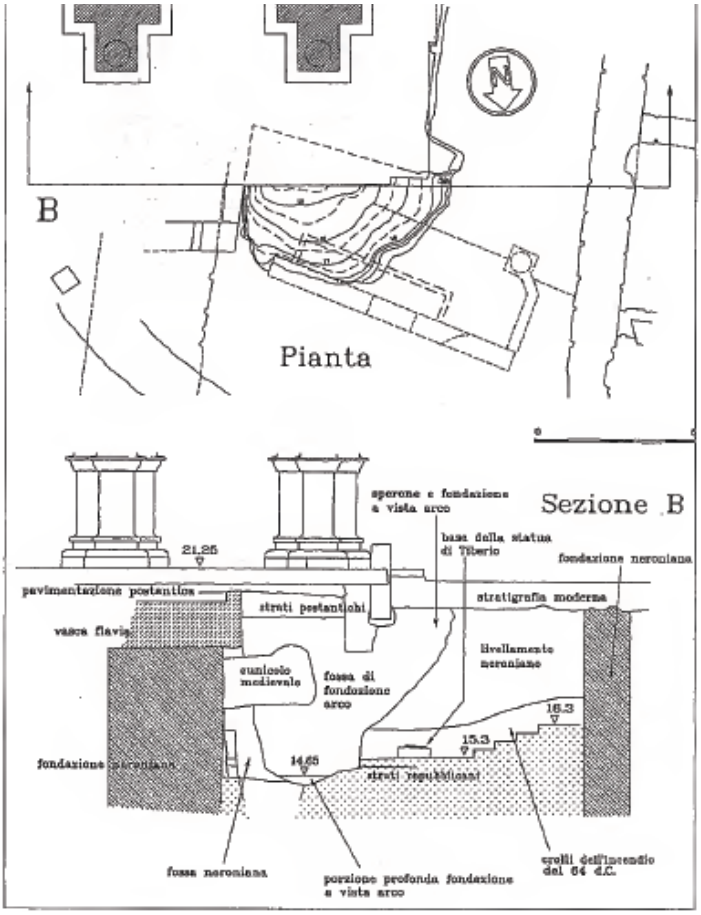

Figure 5*. Schematic reconstruction in plan and section E-W, view from the N [2].*

Within a very complex stratigraphy, the north-western corner of the trench (figure 5) is first crossed by very ancient levels not reached in the present excavation, then marble and travertine solids (from the sacred area of the Julio-Claudian period) to the collapses of the fire of 64 and then an interruption due to the ground level for the creation of the Domus Aurea.
And it is precisely in the thick Neronian sands that the angle of the hollow loses shape and evidently needs correction.
The large semicircular reservoir, with a maximum diameter of 6.30 m and at least as deep, necessary for the construction of the exposed section, presents finds.
With over ten thousand fragments, essentially ceramic, white and polychrome marble, moulded or decorated.
It should be noted that the finds were scarce in the superficial levels of the fill, being mostly concentrated in the portion of the fill below approximately 19.50 metres above sea level.
Finally, it should be noted that the ceramic finds represent only 16.1 % of the total ceramic nucleus; among them, however, are not only types datable between the 3rd and early 4th century, but also many much earlier types, so that the strictly dated materials are only 1.2 % of the total.
The north-west corner would consist of the concrete section that briefly supported a Domitian monumental archway (Figure 2).
The following were found:

1) a sewer drain that (figure 2) collected rainwater, central arcade of the Arch of Constantine.

2) a basin (figure 2, B), E-W side not less than 2.50 m, on the axis of the arcade, obstructed the path of the triumphal pump, north of the western arcade.

3) a hydraulic structure, with an underground cistern of a small fountain on the southern side of the present arch (figure 2, C), on the eastern arcade

4) a possible existence of a Domitian monument in the area later occupied by the Arch of Constantine, straddling the road axis that existed from the Archaic to the Constantinian period.

The foundations developed from the Arch of Constantine to the present day (Figure 3).
It has a great irregularity, for an adaptation of the foundation system to the pre-existing structural situation.
For the structures of the Domus Aurea, we realise how they form a kind of mesh that was largely reused by the later monument (figure 2).
We do not know of the underlying structures of the Arch the scarce 40% of the perimeter and more or less 10% of the surface, and the solution adopted in two of the four corners is totally unknown to us.
There have only been essays of limited size, in the face of such a complex monument and such a c

2.2. Building Technique and Masonry Installation

Archaeometric analyses confirmed that marbles of different quality appear in the upper and lower parts of the monument, as well as in the pylons (Adriano) and plinths (a Constantinian addition).
In particular, the presence of blocks belonging to buildings in pseudo-isodomic marble in the masonry of the staircase that occupies the western pylon, in the entablature, in the plinths and in the pylons, is noteworthy.
Two building techniques coexist in the Arch of Constantine:

1) brickwork in the interior of the attic with marble ashlar facing in the façade; solid opus quadratum in the piers.
2) marble opus quadratum (the core of the piers is travertine)

The presence of "Constantinian" cement to the marble blocks of the barrel vaults remains to be clarified by some core drilling carried out in the floor ballast of the attic, which proves the homogeneity and continuity of the same material between the middle and upper parts of the monument, while its dating to the beginning of the 4th century is guaranteed by its contemporary relationship with the brick walls of the attic rooms.
This datum provides a decisive element for the unity of the entire construction, which can only be challenged if one assumes that in the Constantinian age the marble blocks of the extensive band running from the archivolts of the arcadees to the attic were removed from the interior (except for the stairwell of the western pylon, which is all

marble), leaving only the ashlars of the façade in place, and that the void was filled with the same cement with which the top of the building was being constructed.
The study of the piers and plinths that support the detached order of the columns and that frame the main arcade and the two minor arcadees on the main sides of the arch (exemplified in figure 6a-b) allows us to verify the hypothesis that sees the column pedestals as a late antique addition to a pre-existing second-century construction with only semi-pillars and therefore less projecting plinths than those documented today.
Now, since the latter are linked to the structure of the piers, it follows that they were built together.

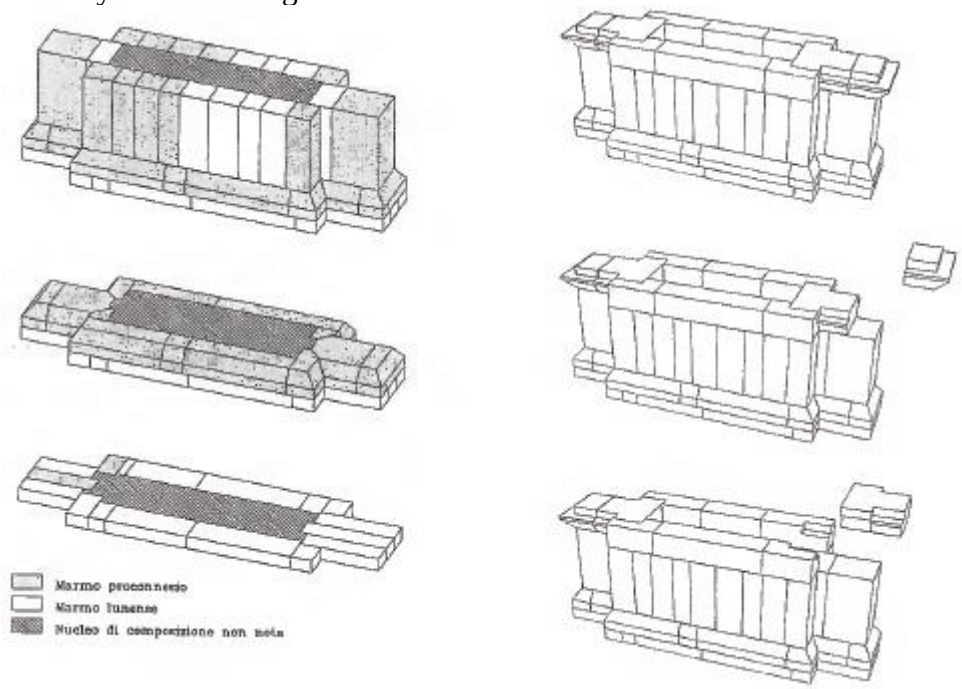

Figures 6 *Arch of Constantine. East pier:*
a) reconstruction of the laying of the first three rows; in dotted lines the lunense blocks, in white those in proconnesio marble;
b. laying of the rows (dab. by M. Fano) [2].

In fact, the first row (three blocks arranged at the top) and the fourth row (two blocks arranged in shear, which contain the crowning

cornice) penetrate the masonry behind, while the second row (two blocks arranged in shear), on which the plinth is built, is generally set against it.
The shape of the first block of the fourth row, which fits interlocking into the pier structure, is quite peculiar (Figure 6b).
Not all four pylons have the blocks arranged like the ones we have shown in figure 6 and which refer to the east pylon (towards the Caelian).
It must also be kept in mind that the number of modern restorations and repairs makes the lower part of the arch difficult to read.
Nevertheless, the variations found between pylon and pylon are not substantial.

2.3 Constantinian intervention

The Constantinian intervention consisted only of the enlargement of the plinths and the insertion of the decorated block between the second and fourth rows, it must be explained why the first (Adriano) row on which the pedestal rests already had the size later documented by the '*Constantinian*' plinths in this age.
The unity of the construction is confirmed by the presence of irregularities in the construction of the architectural apparatus and the marble blocks of the masonry; these not only affect the attic, where they are largely due to modern restoration, but also the lower part of the monument.
Little, for instance, had been known about the extent and quality of the restoration carried out in 1732-33 on the top of the attic until the dismantling of this part of the building.
In this way, the architectural partitions, marked by the plinths, column shafts and the attic prominences, should have been even more evident.
Some concluding remarks
Constantinian craftsmen would have:

1) built the attic from scratch, with prior dismantling of a similar pre-existing structure;

2) moved the columns forward by inserting the projecting part of the entablature and the decorated plinths;

3) carried out chiselling of the original apparatus for the installation of the pillars,

4) inserted the slabs of the great Trajan's frieze into the masonry of the central passage with the consequent dismantling of the row above and the impost frame of the vault of the arcade itself

5) lowered and reworked the archivolts and keystones of all three archways;

6) lowered and reworked the masonry for the Victories and Rivers of the spandrels

7) inserted Constantinian reliefs of the Sun and Lucy on the short sides of the Arch with the consequent dismantling and reassembly of much of the surrounding masonry, as well as the string-course cornice below the attic

8) inserted busts in the side passages; in an extensive remodelling (not otherwise specified) of the stairwell of the western pier; in the inspection of the foundations and the construction of a reinforcement on the NW corner

9) removed the floor and consequently replaced the floor at a lower level

10) replaced the stone core in the middle part of the building (from the archivolts of the archways to the attic cornice) with concrete

11) reworked the architrave and masonry blocks of the frieze;

12) reworked the plinth that runs around the arch, whose mouldings are identical to those on the added part of the plinths, which is by unanimous admission Constantinian.

The "*tampering*", therefore, would not have been limited to "*a few key points*" and would have concerned not only conspicuous parts of the body of the building with the disassembly and reassembly of entire building blocks.

2.4 The geometric survey

The paper drawings were kindly given by Soprintendenza Archeologica di Roma [8] (Figures 7÷11).

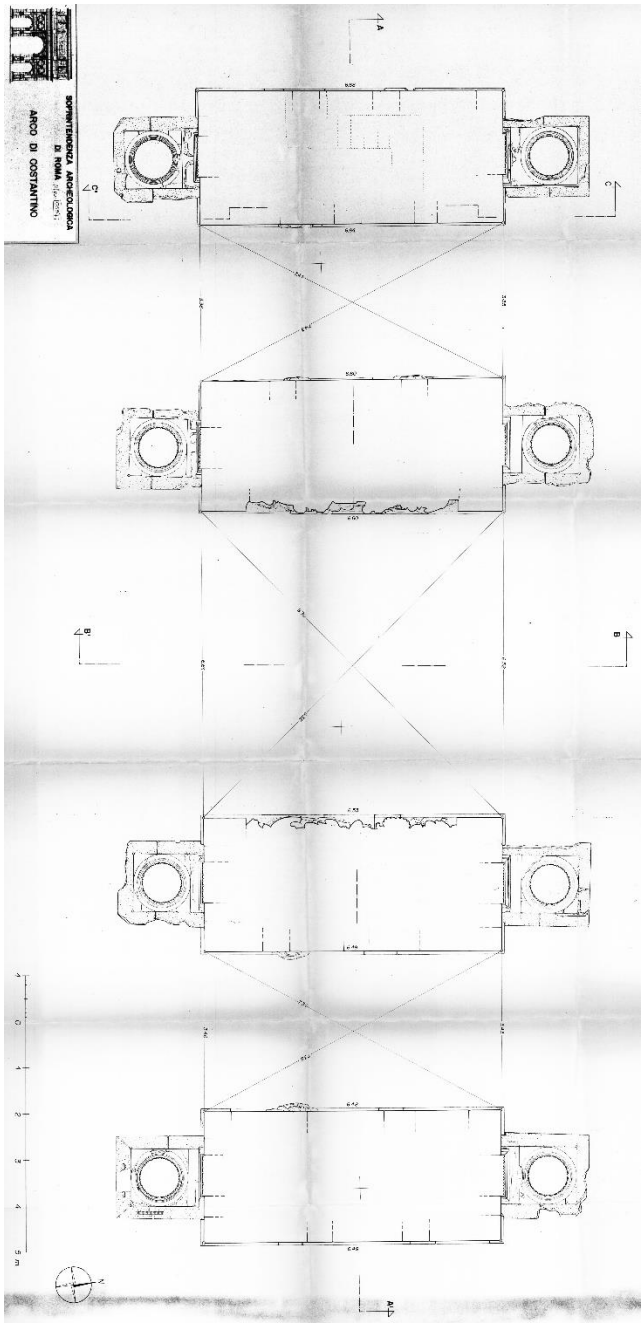

***Figure 7**. Plan at level Z=+26.00 m, [8].*

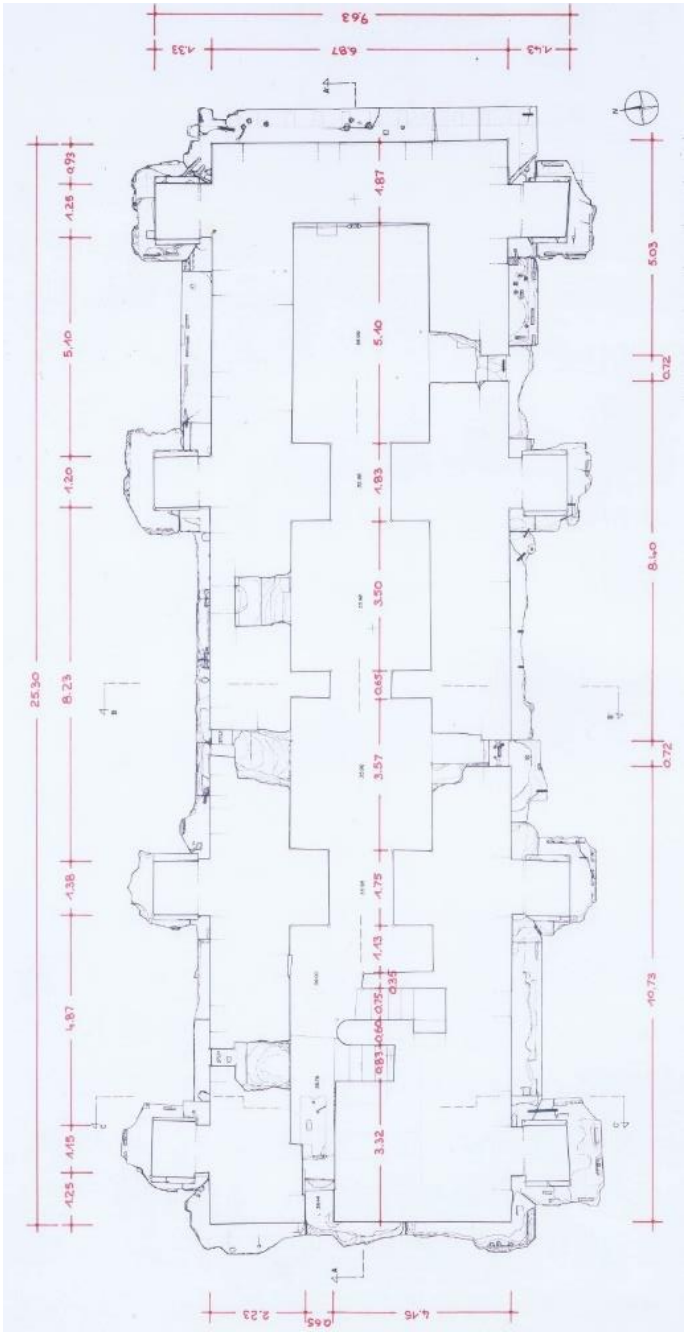

***Figure 8**. Plan at level Z=+37,20 m, [8].*

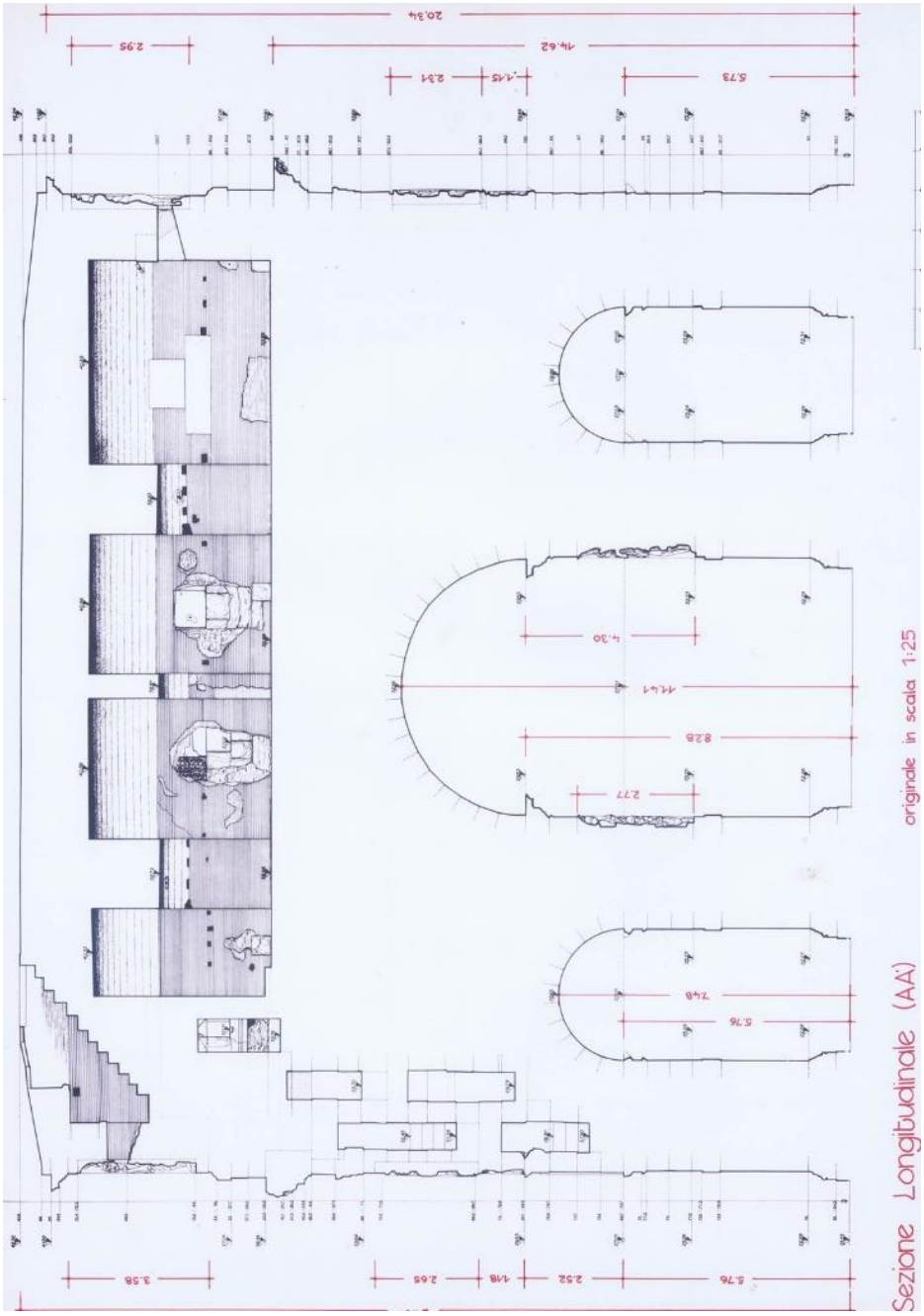

***Figure 9**. Longitudinal vertical section A-A'[8].*

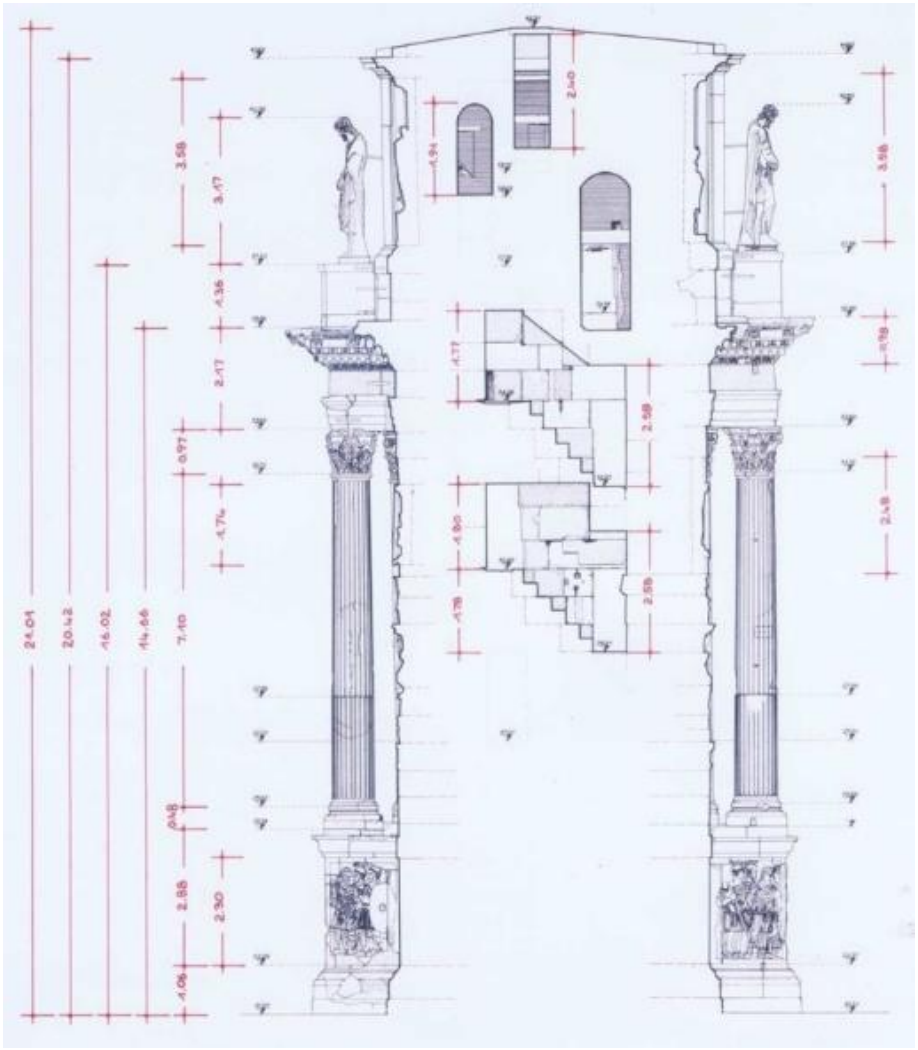

Figure 10*. Vertical section C-C'[8].*

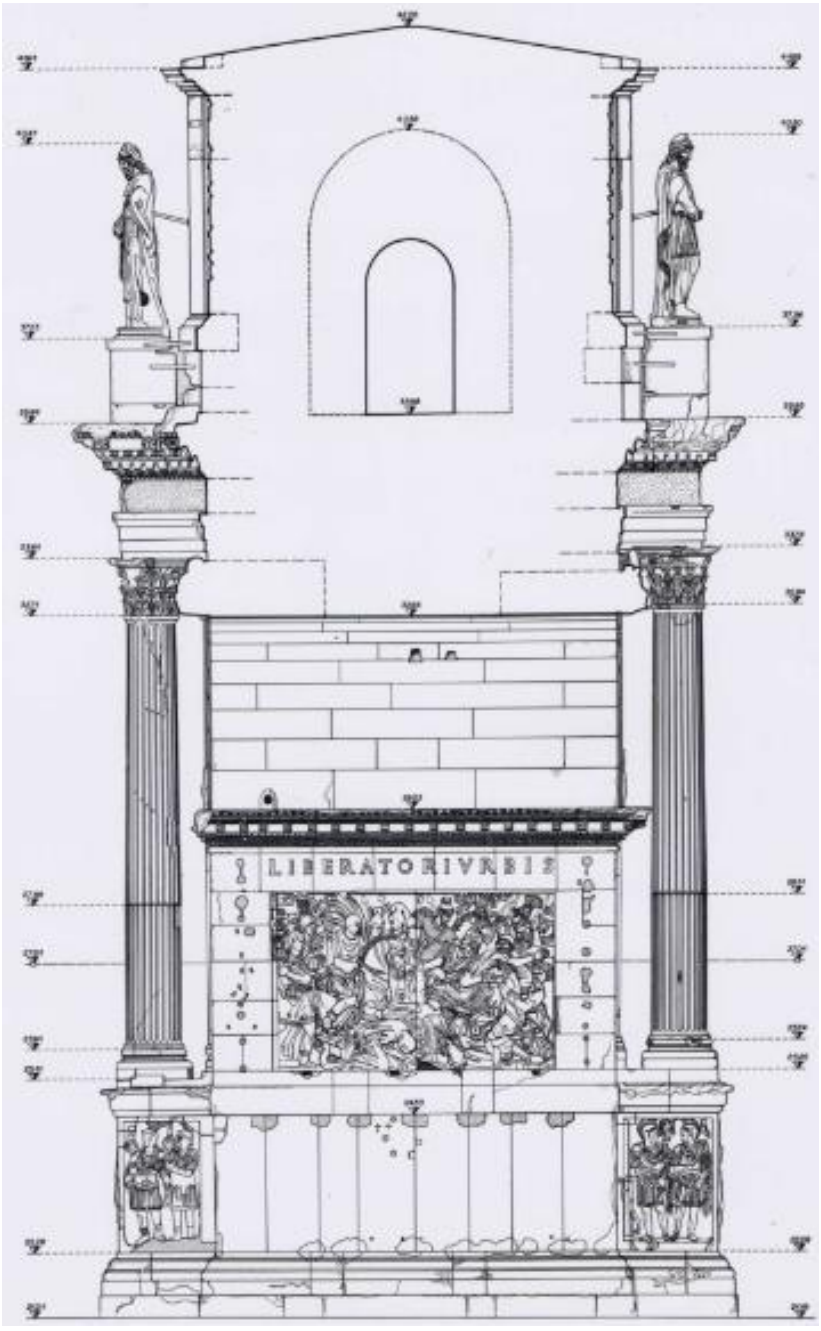

Figure 11. *Vertical levels [8].*

The main monument dimensions are approximatively:
length 25.30 m; depth of pillars 6.60 m;
total height 22.00 m; height of the attic floor Z=24.78 m;
width of the arcades from E to W 3.45, 6.60, 3.37 m;
impost of arches of arcades E to W 5.83, 8.33, 5.83 m

3. Analysis method

The study area covers the archaeological zone (approximately 36 hectares) on which the Colosseum and the Arch of Constantine stand; this area is affected by the underlying Metro line and station.
The soil underlying the study area presents different stratifications: anthropic, Holocene, Pleistocene, Pliocene gravel and deposits.
The path of the Metro line skims the foundations of the Colosseum and the Arch of Constantine through a double inverse curve with a ratio of about 250 m.
The FE "*soil-structure interaction*" model faithfully reproduces the study area, the metro, the monuments and the infrastructure of the metro line (including sleepers, ballast, etc.), as shown in Figure 13.

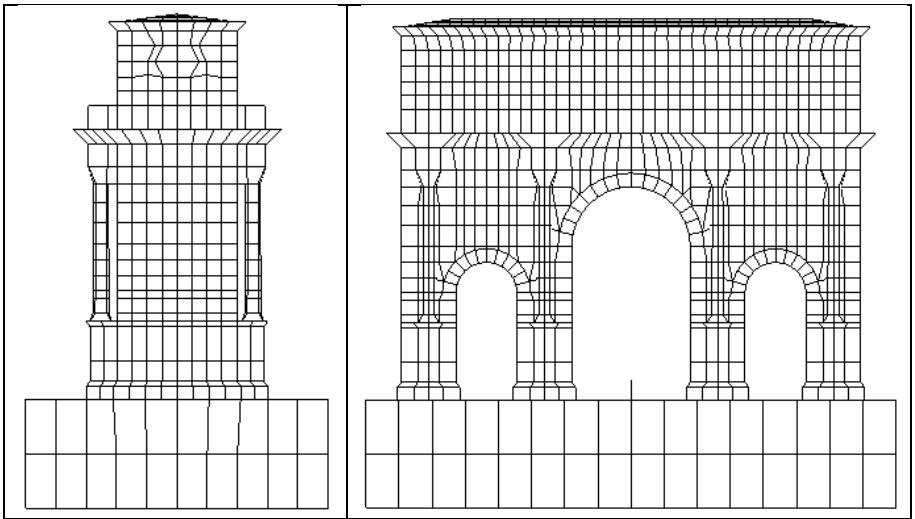

f) XZ direction | *g) YZ direction*

Figure 12. *Orthogonal projections of the FE mesh.*

This model for Constantine Arch alone is made up of about 8,700 nodes, n.6 Young moduli and 850 FE.
The corresponding drawings are shown in figures 12 and 13.
Then, this model is connected to the total model of soil-Colosseum interaction.
The 3D "wagons-track" model faithfully reproduces a rail convoy with Fiat-Ferroviaria / Breda-Ansaldo engines used between 1985 and 1990, to which the vibrations measurements are referred and the Plano-altimetric route of the Metro line in the study area [5].

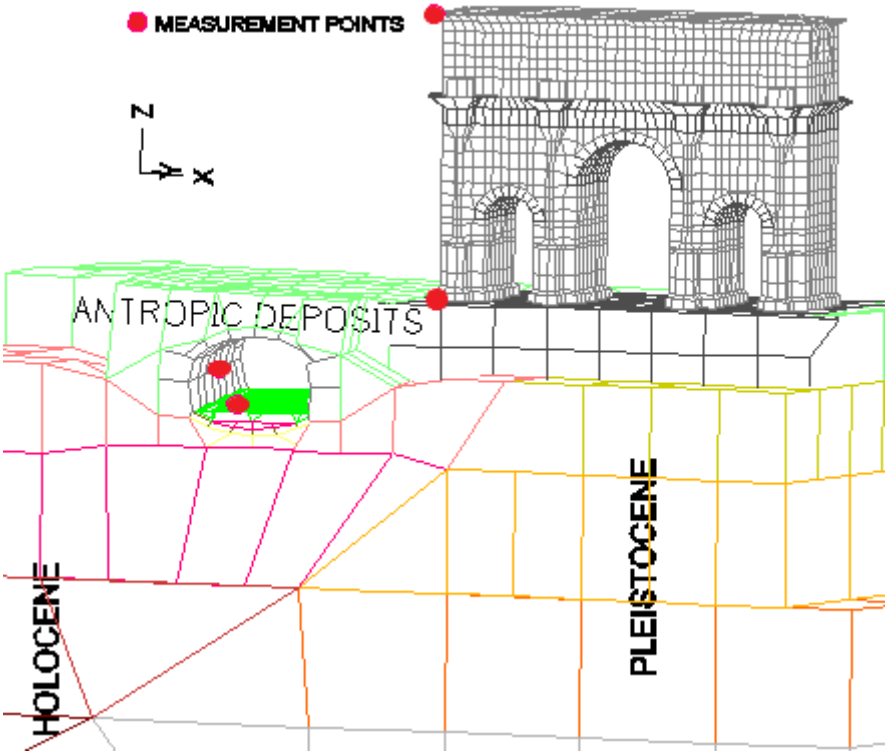

Figure 13. *FE model of Constantine arch, close to the subway. Measurement points.*

4. Analysis of vibration measurements

The measurements were performed by ISMES, in archaeological area happened on between 1991 and 1993. On between the Colosseum station and Constantine arch, the tunnel has: a) lowered upper arch having

its extrados in contact with the pavement of the square above, b) reverse lower arch, c) wooden sleepers. In 1994, the subsequent analysis of vibration measurements was the object of studies by Pasquali [2], at the top and on the basement of Constantine. He represented the spectrograph at 1/3 of eight for the Arch of Constantine in various sectors and levels, as in Figure 14. It must be observed that the graphs shown here are related to effective values and not maximum. He discovered an amplification of the vibrations for the Colosseum and the Arch of Constantine for the passage of trains in frequency domains between 20÷70 Hz. For Constantine arch, the own frequencies are between 2.4 and 3.8 Hz. The train velocities are about 67 km/h in correspondence of Constantine arch. With the actual armament and trains, and regarding Figure 15, the rule UNI 9916 defines the following velocity limits:

a) perceptible v=0.1 mm/sec;

b) in the night v=0.15 mm/sec

c) during the day v=0.2 mm/sec;

d) for the monuments v=2.5 mm/sec; the maximum effective velocity of Constantine arch is v=0.06 mm/sec.

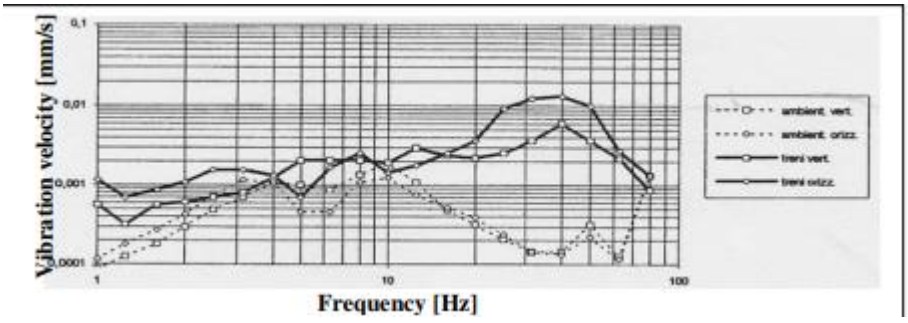

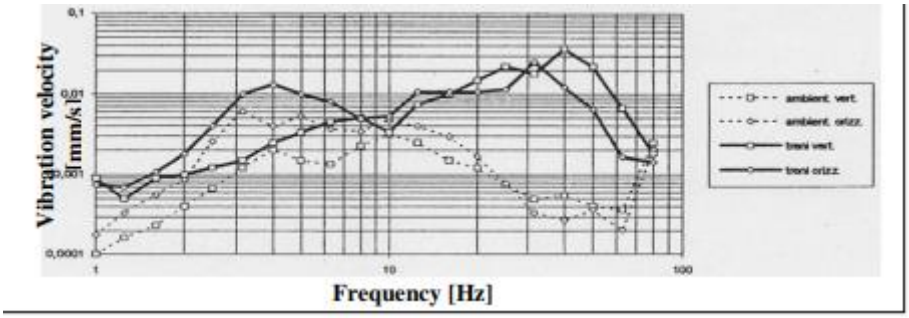

***Figure 14**. Constantine arch, typical response at ground and roof floors.*

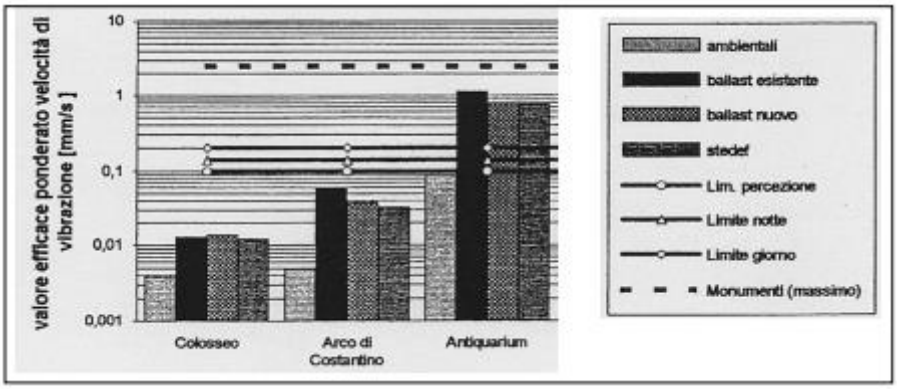

***Figure 15**. Maximum effective velocities, and their limits*

5. Analysis results

The numerical analysis was performed with the transit of one wagon alone, and a supposed map of elasticity modules. Figure 16 represents the velocity components (VX, VY, VZ) on the top and at the basement of Constantine arch.

Figure 17 shows the vertical absolute and relative displacements, between the rail and the wall, in the cross section of the tunnel corresponding to the Colosseum and Constantine arch; the corresponding measured values were 1.2 mm and 1.5 mm respectively; these measurements was carried out for a convoy transit.

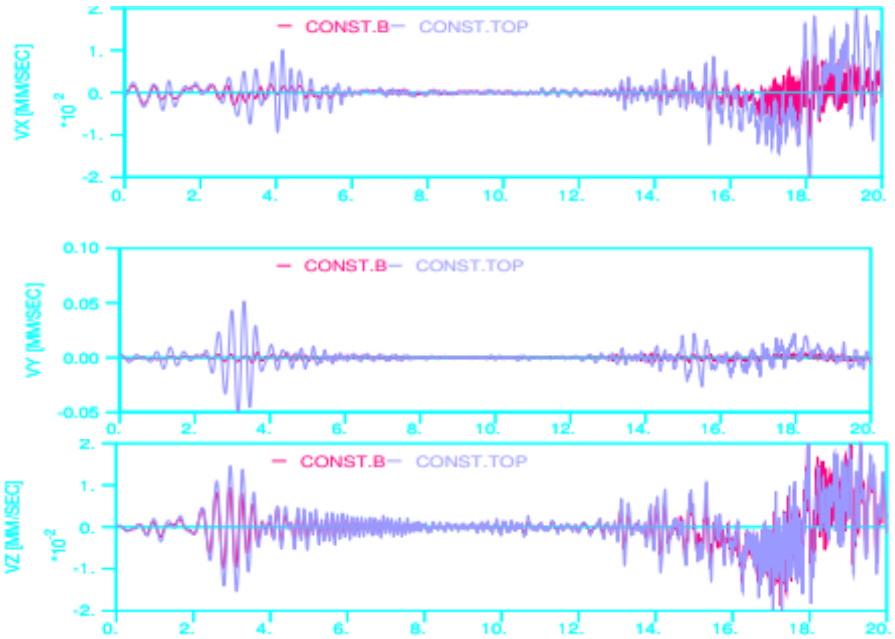

Figure 16. *Velocity components on the top and on the basement.*

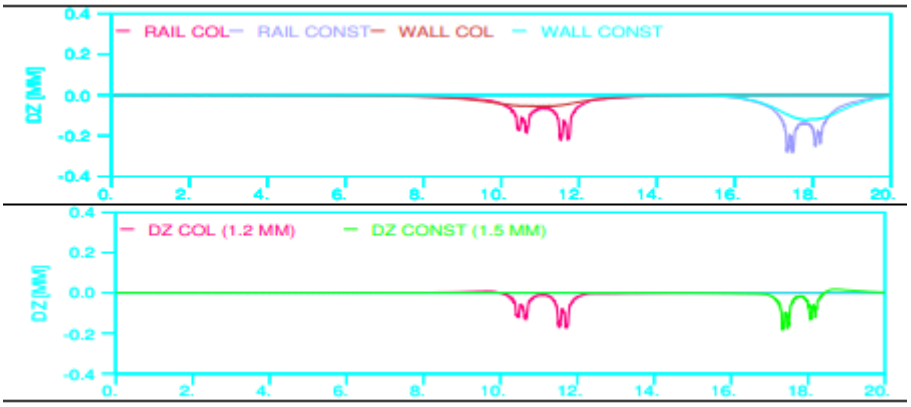

Figure 17. *Absolute and relative vertical displacements inside the tunnel.*

6. Conclusions

References

[1] Pasquali C., *Esperienze e risultati delle campagne di misura per la*

Metropolitana di Roma, Giornate Impatto vibro-acustico e ambientale delle ferrovie Metropolitane. 1994

[2] Pensabene P,. Panella C., *Arco di Costantino tra archeologia e archeometria*, L'Erma editrice. 1999

[3] G. Valente, G., M. Cerone, M., A. Rovelli, A.. "*Indagine preliminare per l'identificazione dinamica del Colosseo*", XI Congresso nazionale "L'Ingegneria Sismica in Italia", ANIDIS, Genova, Italia 2004.

[4] F. Crisi, F. Dell'Isola, G. D'Ovidio, G. Valente, *Vibrations analysis of Colosseo due to trains' transit*", 2.nd EMAS, pp. 191÷198, Hammamet, Tunisia, 2008.

[5] Valente, G., D'Ovidio, G., Crisi, F., "*An Analysis Methodology for Studying the Structural Vibrations Caused by Rail Traffic: a Case Study of the Archaeological Area Around the Colosseum in Rome*", Rivista di Tecnica ed Economia dei Trasporti "Ingegneria Ferroviaria" N° 3, pp. 213÷228, CIFI, Roma 2009.

[6] A. Caserta, M. Cerone, F. Crisi, A. Delladio, G. D'Ovidio, A. Govoni, F. Marra, Y. Nakamura, A. Rovelli, G. Valente, "*Methodology for analysing dynamic soil-structure interaction connected to rail traffic*", Workshop DISS_10. L'Aquila, Italy, March 19th 2010.

[7] F. Crisi, G. D'Ovidio, G. Valente, *Vibration Analysis on Constantine Arch monument due to the metro train transit*, Proceedings of 14th International Conference. Transport Means. 2010.

[8] Soprintendenza Archeologica di Roma, "*Rilievi e disegni coopera tiva Modus 1986*"; their digital developments were found in internet, by Arch. Paolo Rolli.

.

Structural Health Monitoring by soil-Colosseum interaction, with numerical accuracy

Abstract

A full 3D DISS FE model was developed for the Colosseum area, with a 600x600x80 m sod of soil having the anthropogenic, Holocene, Pleistocene, Gravel and Pliocene layers, with station, Metro B and C tunnels, Arch of Constantine. Weak actions are considered to produce linear elastic behaviour of the material. Elasticity's moduli for elevation are obtained by dynamic characterization. A multi-body "wagon-track" model is used to obtain the forces on the rails created by the passage of trains; they produce model vibrations for analytical-experimental comparison of soil H/V diagrams. INGV catalogues report the most disastrous event in Rome in 1349, over 7.5 MCS, from which in the outer ring derived a first southern breach. There were other seismic events, up to No. 9 events with magnitude Mw > 5 during the 2016-2017 Central Italy seismic sequence: at distances of about 100 km between epicentres and the Colosseum. Traffic vibrations may be another risk, in the long term. Specialists in the field agree on the importance of "Structural Health Monitoring" (SHM), but its applicability must be ensured, with processing that goes beyond random vibration diagrams. To reveal any damage, modal analysis will be carried out periodically for environmental vibrations, and occasionally after heavier actions such as earthquakes. Changes in modal shapes and frequencies mean that damage has occurred. Damaged areas are those indicated by characterization with greater change in mechanical characteristics. One could be convinced that proposed SHM is feasible and indispensable for the monitoring of structural problems in the monument, such as those already addressed in the past (reinforcements, excavations, differential ground subsidence), arriving to a permanent monitoring.

1. Introduction

The soil-structure interaction is derived from the literature of the disciplines of Geophysics and Geotechnics (Moczo et al. 1995). The ground is represented as a semi-indefinite continuum limited to a finite portion, confined to a sufficient distance from the structure, where tension and/or deformation changes become negligible; the transparency to the dynamic energy is solved by an adsorbing boundary.
SHM Monitoring is both experimental and analytical, in the frequency domain, it is little pursued because it requires delicate processing to locate the damage, although not visible, as in the red zone of Figure 14.

2. Health damage by events like happened in the centuries

2.1. Health damage by earthquake, from a perspective of longevity

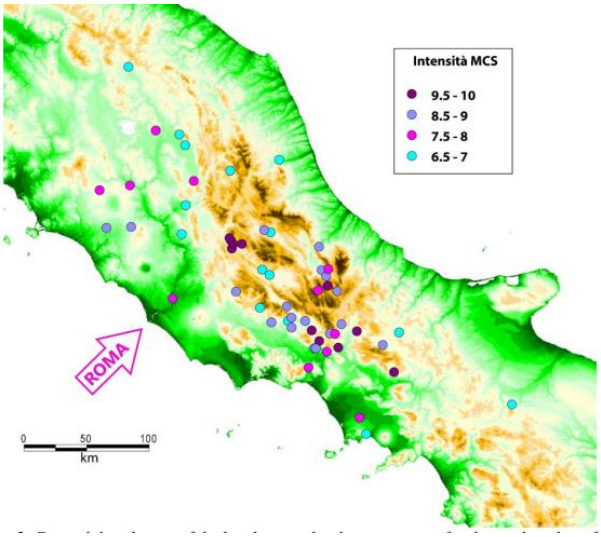

Figure 1. Distribution of the intensities for the earthquakes of 1349, (7.5÷8 MCS for Rome).

The sure notices about monument damages by earthquakes are on the years 422, 443, 508, 801, 1349, 1703

and 1812. For the 508 event, Decio Mario Venanzio Basilio said *"abominandi terrae motus"*.
The past maximum intensity happened in 1349, Petrarca said "*cecidit aedificarum veterum neglecta civibus, stupenda peregrinis moles",* and the probabilistic return period is very long. The past maximum intensity was very high, and its probabilistic return period is very long (Tertulliani et al. 2011).

2.2 Strengthenings

#24

#57

Figure 2. Buttresses by: a) Stern (1806) from pillar #24; b) Valadier (1823) up to pillar #57.

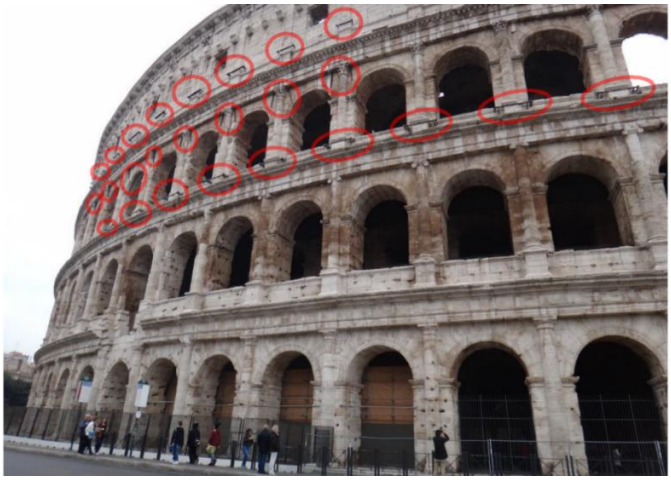

Figure 2c. Fasteners by Canina for 60 Cm out plumb (1830-1850).

2.3 Escavation of Metro B (1939).

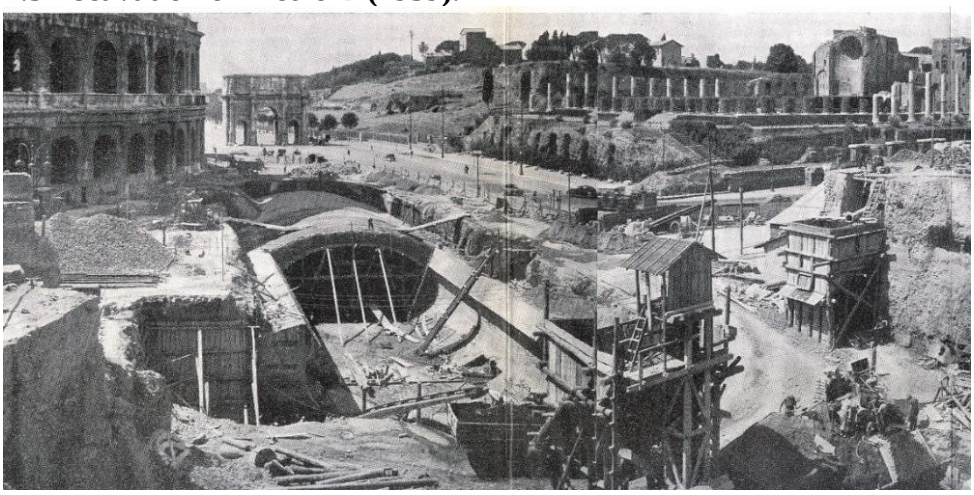

Figure 3a. Metro B excavation between Colosseum and Constantine arch (Perrone, 1952-1953-1954).

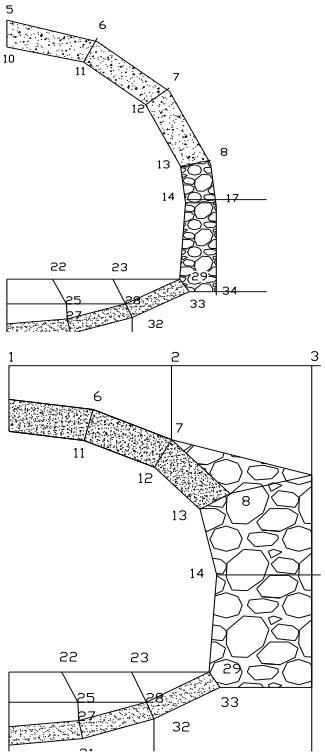

Figure 3b. Mesh of the current tunnel and lowered (sections 9-15).

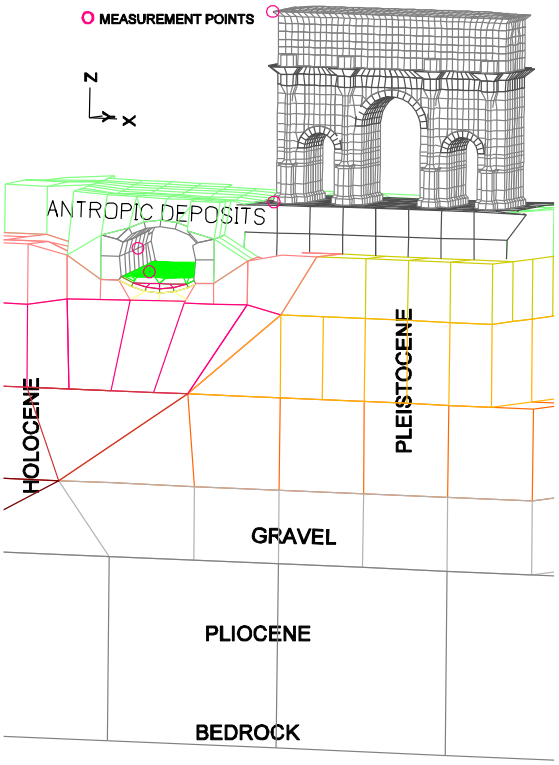

Figure 3c. Section 14 of the mesh: Constantine arch, stratigraphy.

2.4 Tunnel excavations

The tunnel excavation (Valente 2006) produces:
a) at the greenfield δ_Z = -6.65 mm;
b) at the summit of the tunnel δ_Z=-50.90 mm;
c) at the bottom of the tunnel δ_Z=+4.24 mm;
d) total external diameter contraction δ = 50.90 + 4.24 = 55.14 mm;
e) monument $|\delta_Z|$=0.12 mm; σ_1=19.9 kPa;
f) foundations $|\delta_Z|$=0.13 mm; σ_1=9.7 kPa;
g) transversal contraction of the tunnel A=0.9503 m^2 ;
h) subsidence contraction at the greenfield A=0.3036 m^2 .

Referring to Figure 4, the displacement δ is obtained by imposing the volumetric variation ΔV=1%.

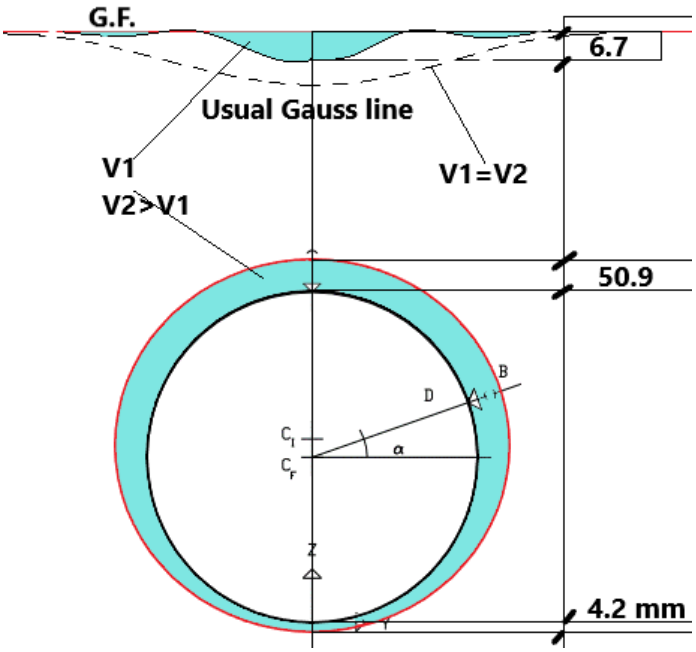

Figure 4. Contraction of cross section [mm].

2.5 Six pillars strengthened with steel bars and epoxy resins injections (1978-1979)

In 1978, the travertine facing were stripped, and the pillars from #16 to #21 were seen to be seriously damaged (Bulian 1980): large widespread cracks could be seen, due to crushing, and the section was considerably smaller than the original one. An intervention based on the use of epoxy resins, was chosen, for the ability to be injected at low pressure, with an excellent degree of diffusion, even capillary lesions, so as to "regenerate" it even in depth.

Figure 5b. Support of the arcades. Reinforcement of n. 6 pillars with steel and Epoxy resin injections through holes

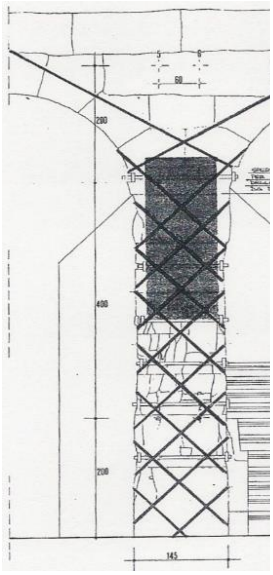

Figure 5c. Single pillar.

2.6 Nonlinear static analysis of foundations with concrete model

Table 1. *Loading sequence*

Phases	t	E_{CONCR}	E_{SOIL}	Load	Colosseum
2	0	E		foundation	Full
3	∞	0.5 E	0.75 E	Found+ el(N+S)	Full
4	∞	0.5 E	0.75 E	Found+ el(N+S/3)	Partial, Figg. 7, 8.

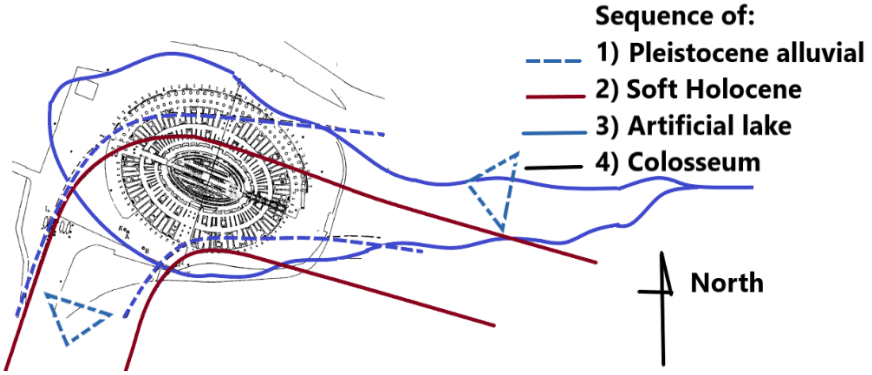

Figure 6. *From (Benevolo 1988) and (Bozzano et al. 1995).*

Figures 7 and 8 agree between them.

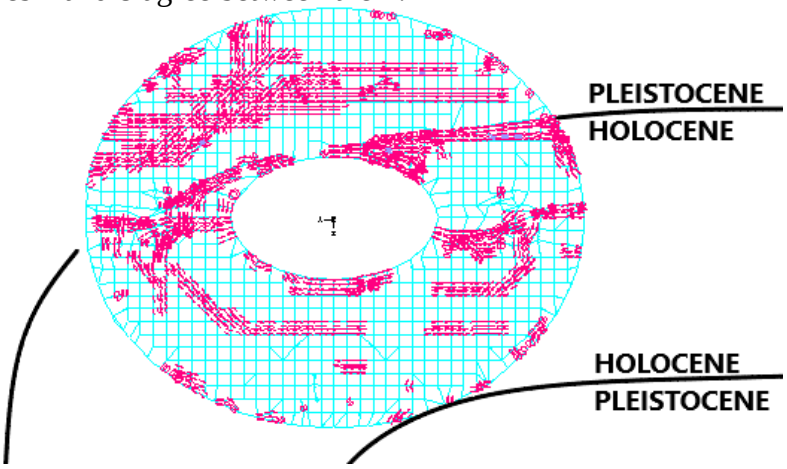

Figure 7. Final cracks of lower foundations layer, by analysis

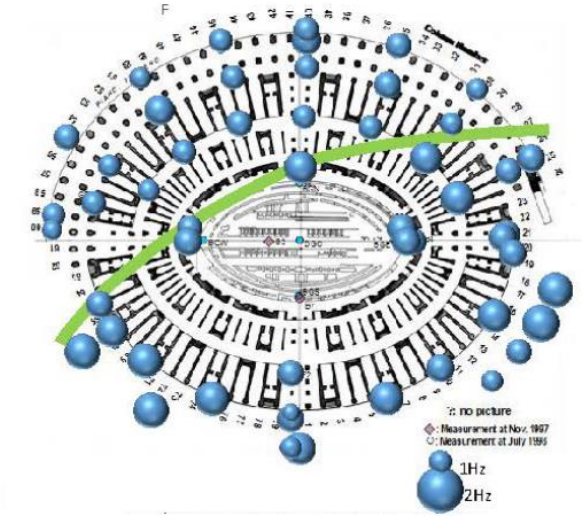

Figure 8. Predominant frequency distribution of the foundation of Colosseum, by tests.

The soil layers underlyng Colosseum are represented in Figure 6.
*"La platea di fondazione ..potrebbe presentare al suo interno una frattura accentuata ..Quaranta centimetri di dislivello nella parte sud del Colosseo" (*Corriere della Sera ***29 luglio 2012*** *).*

Figure 7 shows the crack patterns, for the phases 2), 3) and 4) respectively (Alaggio et al. 2015**)**.
We perform an incremental analysis taking into account different phases, as in Table 1:

a) initially, for undamaged concrete we assume two different constant modules for the two layers, upper ${}^{0\_UPPER}E_{CONCR}$=12,000 MPa, lower ${}^{0\_LOWER}E_{CONCR}$ =24,000 MPa, the maximum values obtained by identification

b) monument construction;

c) viscous effect development; at viscous effects exhausted, the final analysis, was performed for the full dead load enclosing the elevation, half elasticity modules for concrete, 0.75 elasticity modules for the soil:

$$ {}^{\infty}\gamma=2.\ {}^{0}\gamma\ , \quad {}^{\infty}E_{CONCR}=0.5\ {}^{0}E_{CONCR}, \quad {}^{\infty}E_{SOIL}=0.75\ {}^{0}E_{SOIL} $$

d) missing of southern walls.

2.7. Action of unidirectional Gabor wave in the 2d and 3d models

The geophysicists performed the 2D analysis (Moczo 1995), as in Figure 9, for a horizontal incident plane shear Gabor wave acting at the bedrock.
The horizontal soil displacements above the Holocene valley, have an amplification up
to 7 times that of the bedrock, to which they remain higher for 10 periods.
The same Gabor action was applied in x-direction in a 3D model (Cerone et al. 2004). Displacements in the orthogonal y- and z-directions are also derived from this analysis.

$$ s(t) = \exp\{-[\omega_P(t-t_S)/\gamma]^2\}\ \cos[\omega_P(t-t_S)+\psi] $$

$$ \omega_P = 2\ \pi\ f_P\ \sec^{-1}, $$

$$ t_S = 0{,}45\ \gamma\ /\ f_P\ , \quad t \in < 0.2\ t_S > $$

we are referring to the constant values

$$ \gamma=9.50 \qquad f_P = 2.40\ \sec^{-1}, \quad \psi=1.57080\ ;\ t_S = 1.78035\ \text{sec} $$

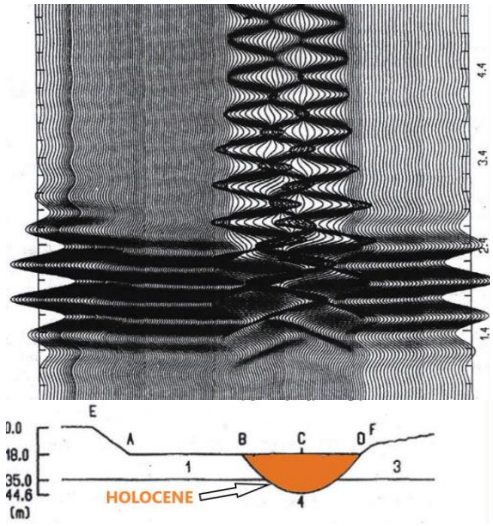

Figure 9a. Action in EW direction.

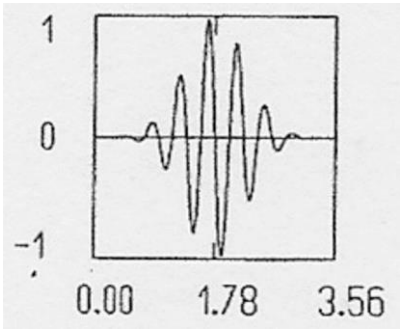

Figure 9b. Gabor wavelet.

3. APPROXIMATE METHOD

They are: a) intuition in structural design (Croci, 1970), b) transfer of functions through the soil (Pasquali 1994), c) shaking table (Costley et al. 1994), d) Limit Equilibrium Method (LEM) (Giuffrè et al. 1999) (Como 2012), e) model fixed at the basis (Pau et al. 2008), f) rules that allow personal discretion. Their approximations are so rough that the comparisons with tests are unuseful.

3.1 The intuition

The intuition method is the true ten-line reasoning (Croci, 1970); it is the more brilliant; it is the best for speed and economy; it does not rest confused from many simplifying hypotheses; it was the unique opportunity before seventies of the last millennium, and so it is still today for the majority of monuments. But anyone can have an intuition, even non-graduate. Which is the best intuition?

3.2. Scale models and shaking table

In 1996, a full-scale prototype for a two-storey unreinforced masonry (URM) building was subjected to static actions, in Pavia, Italy. The same structure in a 3/8th model (Costley et al. 1994), for bricks and

mortar too, was tested on a shaking table at Urbana in Illinois, subjected to the Nahanni earthquake which occurred in NW Canada on December 23rd 1985, recorded at a time interval of dt=0.005 sec, applied with the same amplitude and scaled time interval dt=0.0031 sec. It is impossible to reproduce the existing damages in the model, as cracks' system. The models introduce further errors due to the use of too many scales: geometric, time, dynamic, mechanical, granulometric (logarithmic too).

3.3. Hazards with Limit Equilibrium Method (LEM, proposed in the 18th century)

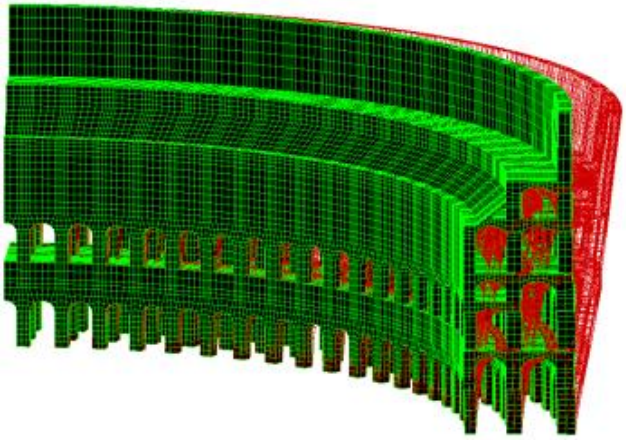

Figure 10. Broadening of the outer wall at collapse, λ=0.122.

It seems a metaphysical method (Giuffrè et al. 1999), because it considers too many uncontrolled hypotheses, which are: 1. horizontal static loads, 2. monotone loads,3. constant acceleration along the height, 4. null tensile strength, 5. structure fixed to the base, 6. generation of macro elements by cutting planes, 7. transformation of the problem from 3D to 2D, 8. the only conditions of equilibrium are imposed, 9. introduction of plastic hinges.
Figure 10 shows the broadening of the wall at collapse (Como 2012), where the collapse multiplier is given with three significant digits λ=0.122, when the approximation is over ±100%.

3.4. Approximate numerical experimental comparison with modal analysis

Modal analyses were performed (Pau et al. 2008):

a) experimental, obtaining the frequencies of Table 3 at line 1

b) analytical, assuming the usual mechanical characteristics for integer walls of Table 2 at lines 1,2,3, obtaining a large scatter between the frequencies of Table 3, at lines 1 and 2.

That was considered due to the walls' damages, which produce Young moduli reduction

Then, we consider that for simple oscillator is $F=2\,\pi\,(K/M)^{1/2}$

The mean reduction coefficients are: a) Frequency reduction = $(\Sigma Fanal/\Sigma Fexp) = 2.055$; as in Table 3 line 3; b) Young modulus reduction $2.055^2 = 4.22$; as in Table 2 at line 4.

N. 4 materials are considered. No modal analytical displacements appear up to level L1, as in Figure 11.

Table 2*. Material mechanical characteristics.*

		Travertine	Brick	Tuff	Concrete	
1	ρ	2400	1800	1800	2400	Kg/m^3
2	Einitial	20,000	5,000	8,000	8,000	MPa
3	ν	0.10	0.20	0.15	0.10	Poisson
4	Efinal	4,700	1,200	1,900	1,900	MPa

Table 3*. The first six natural frequencies*

	Frequencies	1	2	3	4	5	6	
1	Fexperimental	1.03	1.30	1.49	1.60	1.66	1.75	Hz
2	Fanalysis1	2.32	2.34	3.12	3.17	3.58	3.62	Hz
3	Fanalysis2	1.13	1.14	1.52	1.54	1.74	1.76	Hz

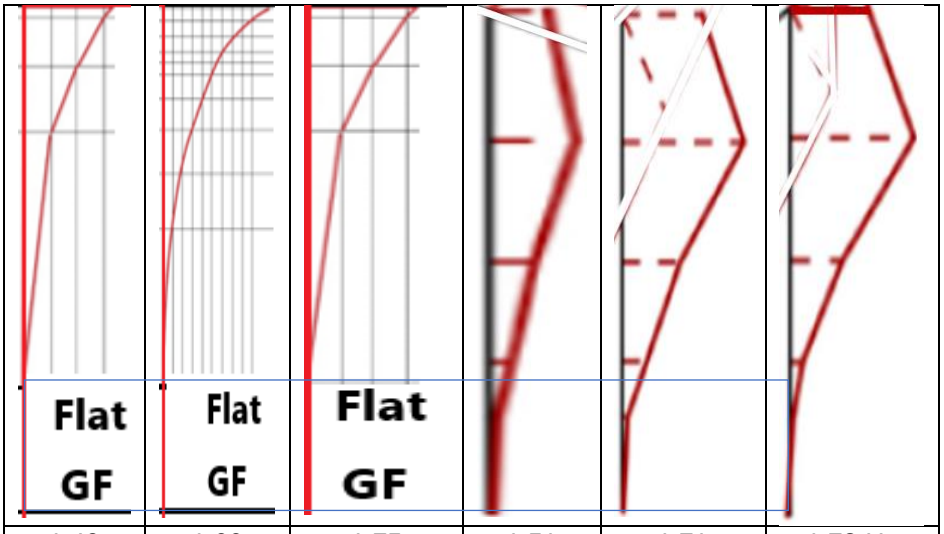

1.49	1.66	1.75	1.51	1.71	1.78 Hz
(Pau al. 2008)			(Bongiovanni et al., 2017)		

Figure 11*. Mode shapes comparison on arcade XLVII.*

Figure 11 concern the comparison of experimental results at arcade XLVII, the modal displacements are:

a) nihil between GF and the level L1 with Z1=10.55 m, without flexus over L1 for (Pau al. 2008);

b) different from zero between GF and the level L1 with Z1=10.55 m, with various flexus over L1 for (Bongiovanni et al., 2017).

3.5. Rules that allow personal discretion

Such mechanics is so complex that it cannot be addressed with empirical formulas and tables or be governed by legislation; therefore, it is a tool for specialist research only.

4. The scientific method leads to numerical analysis, with accurate errors control

The scientific method for natural sciences, is the typical way to reach a knowledge of objective, reliable, verifiable and shareable reality; the reproducibility principle of the experiments is valid.

We proceed with the following cyclical steps: a) Observation, b) Experiment, c) Correlation, d) Physical mathematical model, e) Verification and assurance.
Our solution is numerical with controlled accuracy, around 5%, between tests and analyses.
For this purpose, FFEE models (Zienkiewicz,1971) and nonlinear analysis (Bathe et al. 1979) are available.

4.1. Linear elastic model for small vibrations

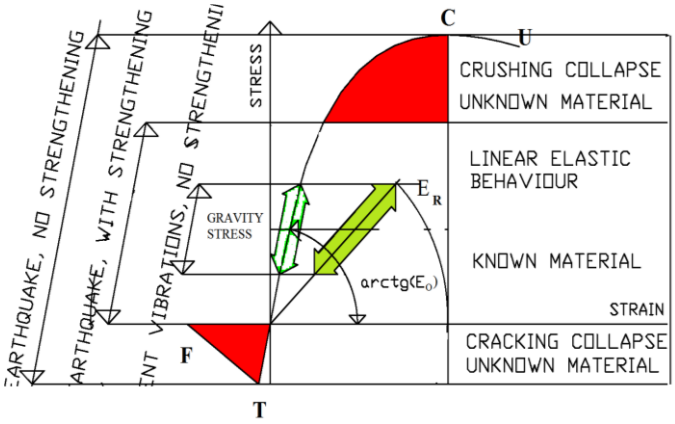

Figure 12. Uniaxial stress-strain relationship for walls. Stresses' ranges: a) ambient vibrations $\Delta\sigma=\pm 1/1000$; b) earthquake with strengthening $\Delta\sigma<\pm 20\%$; c) earthquake without strengthening $\Delta\sigma=(\sigma_T \div \sigma_C)$.

Traffic vibrations may be another risk, in the long term. Specialists in the field agree on the importance of "Structural Health Monitoring" (SHM), but its applicability must be ensured, with processing that goes beyond random vibration diagrams.

4.2. Homogeneization of damaged walls

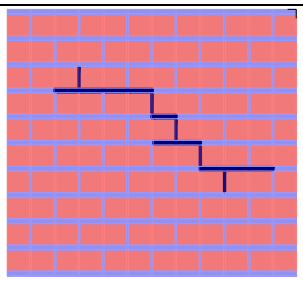

a) regular bricks.

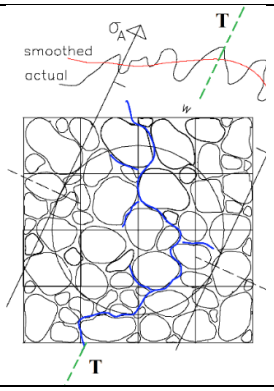

"Crack Band Width"

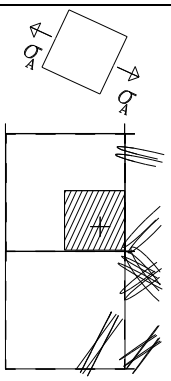

F.E. mesh

Figure 13

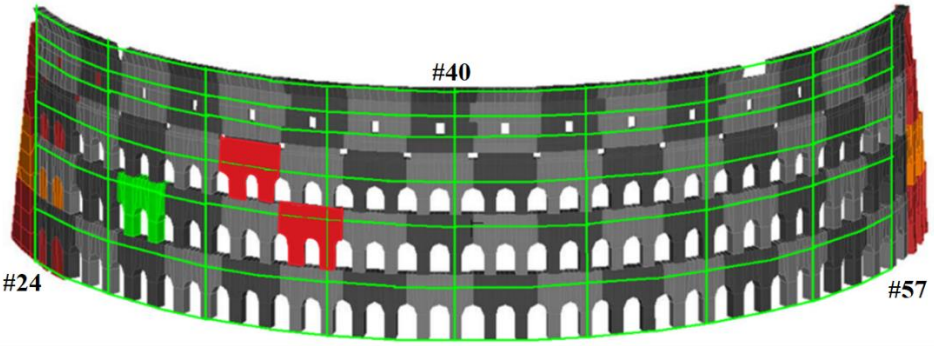

Figure 14. Ring 4, with n. 64 different Elasticity moduli. N. 2 zones with greater damages in red, by SHM.

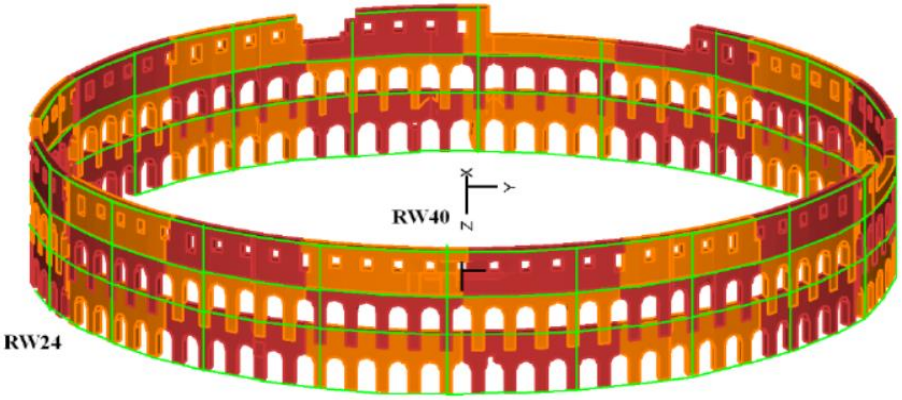

Figure 15. Ring3, Z_{SUMMIT}=24.14, 29.84.

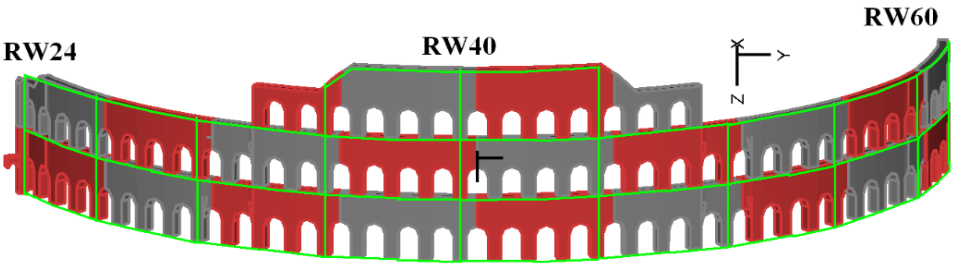

Figure 16. Ring2, Z_{SUMMIT}=23.96, 32.08, 37.50.

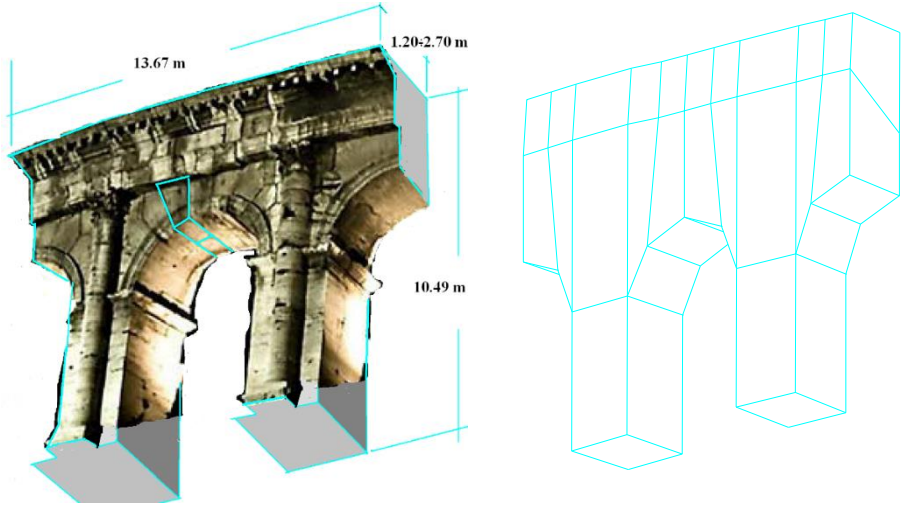

Figure 17. Arcade homogeneization.

Since ’60 years, it was: 1) defined theoretically the geometric and constitutive laws discretization, 2) foreseeable that the fast electronic and informatic developments would have allowed the solution of complex problems with 500,000 dof. The “Smeared Crack Band” is adopted since the Mörsch frame of one century ago; but for F.E. model, the “Smeared Crack Band” was better defined by (Bazant 1992).
The principal evident disconnections were introduced in the mesh, according to existing survey (Cerone et al. 2000). The damages are not known inside a large depth of a wall.
Finally, only the isotropic linear elastic behaviour may be assumed, with zones having different elasticity moduli. The very good analytical-

experimental fitting testifies the reliability of the proposed method. But, for an ancient concrete wall, the knowledge for integer material of mechanical characteristics is not allowable, surely pre-existing crackings there are: a) crack band width for concrete, b) disconnections of bricks.

4.3. Homogeneization of soil

Seismic wave lengths have very large values, for example:

(a) crustal waves have wavelengths less than 5 km;

(b) volume waves can be P-type or S-type. The corresponding wavelength is 2-20 km;

(c) surface waves propagate with a velocity of 3-4 km/s, which corresponds to a wavelength of 60-80 km.

Thus, the soil model to be adopted is geophysical rather than geotechnical, with large clods
having homogenized mechanical properties in large volumes.

Many tests were performed in different times (Nakamura 2012), since 1987 to 2015. Figure 18 shows the typical shape of the H/V spectral ratio. The characteristic of H/V for microtremor is summarized as follows. The first peak near F_0 consists of S-wave mainly. The first trough near 2 F_0 is caused by Rayleigh wave. Around F_0 there is almost no energy of Rayleigh waves, so the dispersion curves are unstable near F_0. Rayleigh wave are growing from F_0, and reach the first peak near the 2 F_0. Tests are used for the dynamic characterization in order to obtain the mechanical characteristics for the analysis by H/V, in the ground.

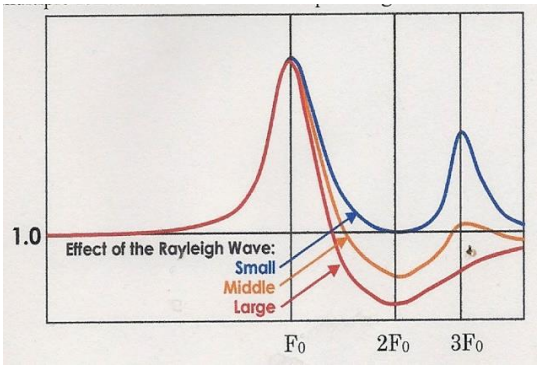

Figure 18. Image of H/V Spectral Ratio.

5. SHM

5.1. Permanent monitoring for dynamic thermal and rainy actions

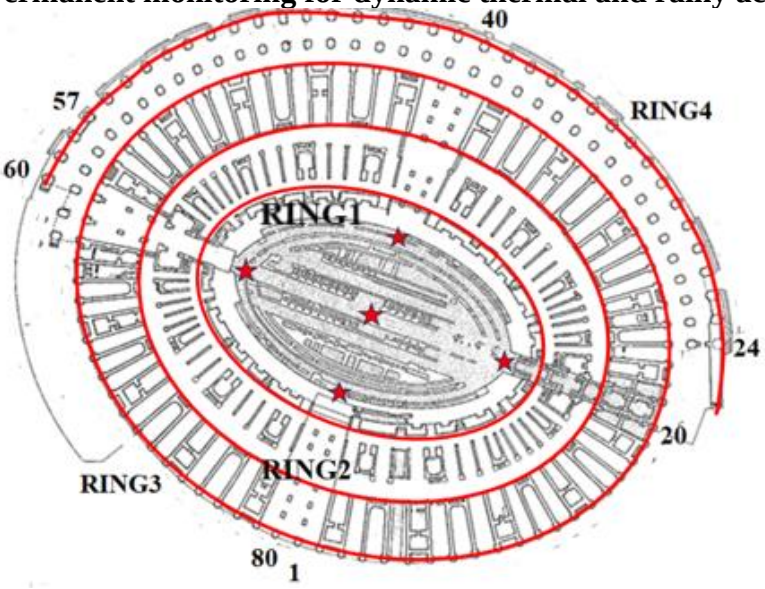

Figure 19. *Measurement points at hypogeum. Rings from 1 to 4. Pillars numbering*

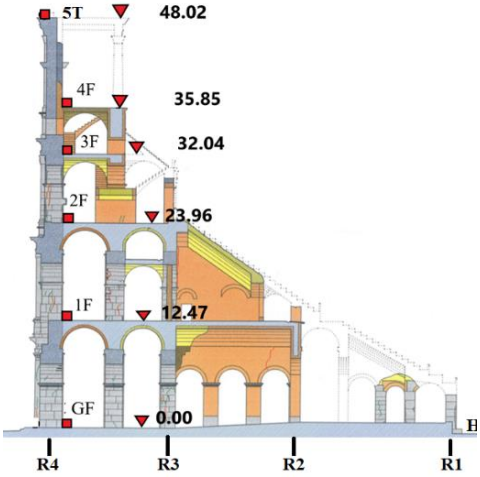

Figure 20. *Floor levels (Hypogeum, GF, 1F, 2F, 3F, 4F, 5T)*

To complete the present study, perhaps it would be appropriate to record simultaneous dynamic monitoring network in elevation and in three holes (type H1, H2, H3 in Figures 19÷21. We put the measurement points: a) at interval of 5 pillars, b) for hypogeum and all the floors, GF, 1F, 2F, 3F, 4F, 5T, c) for rings 3 and 4. One point in the monument is defined by three coordinates: the pillar number, the ring number, the floor level.

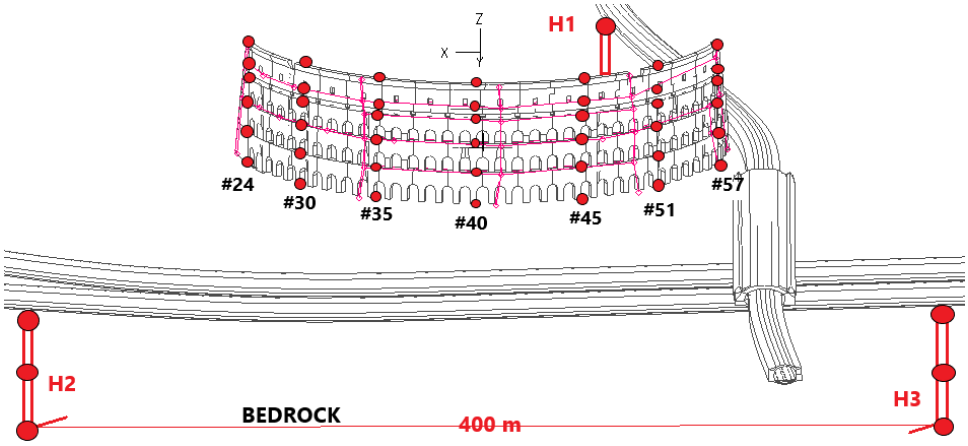

Figure 21. N. 42 instruments on northern wall, n. 9 instruments in n. 3 boreholes from the tunnels.

5.2 Automatic modal evaluation program

The natural evolution to today's artificial intelligence makes it likely that such SHM methodology is fully feasible, reliable and even automatable, with a simple click.

6. Conclusions

Researchers show interest in recordings of monument vibrations, as they consider them indispensable for SHM control.

In analogy to musical instruments that produce a series of certain sound frequencies, a series of dynamic frequencies and fundamental modal forms can be extracted from the random vibrations of the monument subjected to environmental actions, which are independent of actions and only change if the masonry has suffered structural damage.

Well, wanting to verify the production of any damage to the masonry, by comparing the recordings before and after a certain action, two types of monitoring are feasible: 1) the only experimental "Vibration Monitoring", examining only two simple random diagrams, which can never check the eventual production of the damage;
2) the "SHM Monitoring" which can locate the non-visible damage, is highly advocated but not trivial because very precise modal, experimental and numerical analyses must be performed.
To achieve SHM, what must be taken care of is: the positioning of the instruments, the processing of the recordings in the frequency domain, the numerical model (www.diss-co.it).
The SHM methodology can control every structural problem, even those similar to the past: c) Stern, Valadier and Canina reinforcements, d) differential foundation failures, e) amplification of vibrations in the south above the Holocene, f) neighbouring excavations, g) reinforcement with epoxy resins in the south-east pillars, h) environmental vibrations, i) seismic prevention and protection, l) conservation and restoration.
For total control, permanent recording instruments should be spread: m) in the north wall, from Stern to Valadier, from the base to the top, n) in the inner rings, o) perhaps in the ground, from the Metro tunnels.
Because of the importance of the monument and the fascinating scientific topic, it would be useful and interesting to investigate SHM further, even with an investigative service conference between researchers, which would lead to the best possible SHM control.

7. References

Alaggio R., Di Fabio F., Di Egidio A., Dominici D., D'Ovidio G., Luongo A., (Macerola L., Massimi V., Nakamura Y., Tallini M., Totani G., Valente G. (2015). *A methodology for the 3D DISS model of Colosseum*, Proceedings DISS15.

Bathe K.J., Ramaswamy S. (1979). *On Three-Dimensional Nonlinear Analysis of Concrete Structures*, Nuclear. Engineering and Design, Vol. 52 pp.385-409

Bazant Z.P., (1982). *Crack Band Propagation and Stress-Strain Relations for Fracture Process Zone in Geomaterials*, International Symposium on Numerical Models in Geomechanics, Zurich.

Benevolo L., (1988). *The History of the City*, MIT press,

Bongiovanni G., Buffarini G., Clemente P., Rinaldis D., Saitta F., (2017). "*Dynamic characteristics of the Amphitheatrum Flavium northern wall from traffic-induced vibrations*", Annals of geophysics, 60, 4, S0439, doi: 10.4401/ag-7178.

Bozzano F., Funiciello R., Marra F., Rovelli A., Valentini G. (1995). *Il sottosuolo dell'area dell'anfiteatro Flavio in Roma*.

Bulian G., (1980). *Resine epossidiche per il consolidamento di sei pilastri dell'Anfiteatro Flavio*, L'industria tecnica delle costruzioni, A. N. C. E, n° 99.

Cerone M., Carluccio G., D'Ercole F., Di Lorenzo A., Fumagalli F., Ricciardi M. A., Sardo A., Scadile M., Terziani M. V., D'Angelo C. (2000). *Analisi e Documentazione dei dissesti strutturali ed individuazione delle situazioni a rischio*, CISTEC, le tre Università di Roma.

Cerone M., Rovelli A., Valente G., (2004). *Indagine preliminare per l'Identificazione Dinamica del Colosseo,* XI Congresso nazionale "L'Ingegneria Sismica in Italia", ANIDIS, Genova.

Como M., (2013). *Statics of Historic Masonry Constructions*, Springer Series in Solid and Structural, Berlin Heidelberg

Costley A.C., Abrams D. P., Calvi G. M. (1994). *Shaking table of an unreinforced brick masonry building*, Proceedings of the 5th National Conference on Earthquake Engineering, Chicago, pages 127-135.

Croci, G. (1990). *Studies and research on the Colosseum* (in italian),

Quaderni del Dipartimento di Ingegneria Strutturale e Geotecnica,

Rome, Italy

Giuffrè A., Carocci C., Ceradini V., De Benedictis R., De Felice G., Pugliano A., Zampilli M.; e con Baggio C., Boschi E., Guidoboni E., Mariotti D., Trovalusci P. (1999) *Sicurezza e conservazione dei Centri Storici - Il Caso Ortigia*, Laterza.

Moczo P., Rovelli A., Labak P., Malagnini L., (1995). *Seismic response of the geologic structure underlyng the roman Colosseum and a 2-D resonance of a sediment valley*, Annali di Geofisica, 939-956.

Nakamura, Y., (2011). *The H/V Technique and Example of its Application for L'Aquila and Rome Area*, *Proceedings of the workshop DISS_10, L'Aquila, 19 March 2010,* Aracne Editor.

Nakamura Y., Saita J., Sato T., (2015). *Dynamic Characteristics of the Colosseum at the Pillar #40 Comparing the Results of Microtremor Measurement in 1998 and 2013*", Proceedings DISS_15, www.diss-co.it.

Pasquali C., (1994) "*Esperienze e risultati delle campagne di misura per la Metropolitana di Roma*", Giornate Impatto vibro-acustico e ambientale delle ferrovie Metropolitane.

Pau A., Vestroni, F., (2008). *Vibration analysis and dynamic characterization of the Colosseum, Structural Control and Health monitoring*, Journal of Structural control, Ed. J. Wiley & Sons.

Perrone V., (1952-1953-1954). *La ferrovia Metropolitana a Roma*", Trasporti pubblici.

Tertulliani A., Rossi A., Castelli V., Meletti C., D'Amico V., (2011). *Spunti e contrappunti di sismologia storica: 1349 annus horribilis*", DBMI04, INGV, GNGTS.

Valente G., (2006). *Influence of a tunnelling for Metro C to Colosseum in Rome*, 1st EMAS, Hammamet.

Zienkiewicz, O. C. (1971). *The finite element method*, McGraw Hill.

ISBN 978-88-940114-5-6